Thermal modelling of the green roof substrate

Kantitut Tubsuwan

Submitted for the degree of Doctor of Philosophy

Heriot-Watt University

School of Energy, Geoscience, Infrastructure and Society

Royal Academy of Engineering Centre of Excellence in Sustainable Building Design

May 2017

The copyright in this thesis is owned by the author. Any quotation from the thesis or use of any of the information contained in it must acknowledge this thesis as the source of the quotation or information.

Abstract

This research aims to improve the accuracy of a green roof thermal simulation by linking the moisture transfer in the substrate with the conduction heat transfer. The improved simulation is divided into two phases, which are the absorption and evaporation. For the absorption, this research applies the Sharp Front theory to predict the position of the boundary between the saturated and dry zones. The theory of evaporation from a porous medium is used to predict the moisture content in different substrate layers during evaporation. After the moisture content in each layer is determined, this moisture content data can be converted into thermal conductivity, and the time dependent effective thermal resistance can be calculated, which is used in the conduction heat flux calculation for the thermal simulation. Having developed the simulation of heat conduction through the substrate as a result of absorption and evaporation, the results are applied to a case study building to compare a green roof substrate in three moisture conditions (dry, saturated, and the varying simulated moisture content).

The results confirm that it is possible to include the effect of water absorption and evaporation from a green roof substrate in the thermal simulation of building performance using the two theories. The improved simulation makes it possible to model an intensive green roof, where the depth of the substrate is likely to produce a greater distribution of moisture content in service. The simulation is an improvement over previous models and the case study shows that, assuming the substrate to be dry (as in existing models), underestimates the heat loss, whilst assuming it is saturated slightly overestimates the heat loss.

The small, but significant, effect of moisture variation in service is important for designers of green roofs. If it is not taken into account it would be preferable to assume that the roof is continuously saturated as this gives a conservative estimate of the heat loss from a building.

Dedication

This thesis is dedicated to my family and friends who always support me through this long journey.

Acknowledgement

Firstly, I would like to express my sincere gratitude to my supervisor Prof. Phil Banfill for the continuous support of my Ph.D. study, for his patience, motivation, and immense knowledge. His guidance helped me in all the time of research and writing of this thesis. I could not have imagined having a better supervisor and mentor for my Ph.D. study.

Beside my supervisor, I would like to thank Heriot Watt University for support me via the James Watt scholarship. Without this support, I will not able to start this research. For laboratory works, I would like to express my gratitude to Mr Graham G Sorley and Mr Alastair M MacFarlane for their immense technical support.

Last but not least, I would like to thanks my Thai friends in the Edinburgh who always stay by my side and make this city feel like home. Finally, I would like to thank my family for supporting me spiritually throughout this study and my life in general.

Declaration of Statement

ACADEMIC REGISTRY
Research Thesis Submission

Name*:*	Kantitut Tubsuwan		
School:	School of Energy, Geoscience, Infrastructure and Society		
Version: *(i.e. First, Resubmission, Final)*	Final	Degree Sought:	Ph.D.

Declaration

In accordance with the appropriate regulations I hereby submit my thesis and I declare that:

1) the thesis embodies the results of my own work and has been composed by myself
2) where appropriate, I have made acknowledgement of the work of others and have made reference to work carried out in collaboration with other persons
3) the thesis is the correct version of the thesis for submission and is the same version as any electronic versions submitted*.
4) my thesis for the award referred to, deposited in the Heriot-Watt University Library, should be made available for loan or photocopying and be available via the Institutional Repository, subject to such conditions as the Librarian may require
5) I understand that as a student of the University I am required to abide by the Regulations of the University and to conform to its discipline.
6) I confirm that the thesis has been verified against plagiarism via an approved plagiarism detection application e.g. Turnitin.

* *Please note that it is the responsibility of the candidate to ensure that the correct version of the thesis is submitted.*

Signature of Candidate*:*		Date:	

Submission

Submitted By *(name in capitals):*	
Signature of Individual Submitting:	
Date Submitted:	

For Completion in the Student Service Centre (SSC)

Received in the SSC by *(name in capitals):*			
Method of Submission *(Handed in to SSC; posted through internal/external mail):*			
E-thesis Submitted (mandatory for final theses)			
Signature:		Date:	

Table of Content

List of Figure

List of table

Chapter 1: Introduction

1.1 Introduction

The green roof is a sustainable construction that contributes to mitigating the current world energy crisis and climate change. From its long history, dating back to Babylon's hanging gardens (Ascione *et al*., 2013), it was improved and used for energy conservation by German engineers during the 19th century (Newton *et al*., 2007). Benefits of green roofs include improved storm water management, noise reduction, reduction of air pollution and a reduced carbon footprint of the building, achieved by transferring the green space up to the roof (Newton *et al*., 2007). This roof is a common choice for engineers and architects when designing a sustainable building.

For building energy saving purposes, a green roof delivers both heating and cooling benefits by its thermal insulation for the former and a foliage canopy shading effect for the latter. Additionally, researchers found that green roofs can provide passive cooling by the plant and soil evaporation; a process which has been studied and presented via many different theories. The majority of these models involve thermal energy balance from solar radiation, latent heat of evaporation, sensible heat loss or gain, and conduction heat transfer. The first three energy terms are reasonably well supported by theories and assumptions (Frankenstein and Koenig, 2004a, Frankenstein and Koenig, 2004b) and have been used in many green roof thermal modules (Sailor, 2008, Lazzarin *et al*., 2005, Tabares-Velasco and Srebric, 2012).

However, the assumption made in the model for conduction heat transfer in a substrate layer is that this layer was always saturated in early green roof models, and this is not practical in the real situation. However, updated models in recent years (Sailor and Hagos, 2011, Sun *et al*., 2013, Jim and Tsang, 2011) have tried to include this water effect in the substrate layer; but these models have some unexplainable variables in their equations that make their models true only in test conditions. This issue has caused some errors when a green roof's substrate depth is increased.

Furthermore, the effect of compaction in the substrate on thermal conduction seems to be ignored. This compaction may have a significant effect on the installed green roof because the compaction level may reach 800 kilopascal (kPa) in a high foot traffic area (Sailor and Hagos, 2011). This compaction effect, as a consequence, will influence the

absorption of water into the substrate layer. This effect also has a significant influence in a drying mechanism.

For this reason, in order to produce a realistic simulation of the thermal behaviour of a green roof, an improved model is needed. This research aims to produce a substrate moisture transfer model, by focusing on the absorption and desorption cycle. The sharp front theory (Hall and Hoff, 2009) will be used to clarify and improve the wetting model of the green roof substrate, whilst the model for evaporation of a porous medium (Platten, 1985) will explain the drying mechanism. In addition, this research will study the compaction effect on the moisture transfer and thermal conductivity.

This improvement requires laboratory work and computer models to justify appropriate variables for the green roof thermal simulation. The focus of the work is on applications in temperate climates where heating is needed, but it is anticipated that the principles could be applied to situations where a green roof is employed for cooling.

1.2 Aim and objective

The aim of this research is to improve the accuracy of green roof simulation by proposing an alternative model for the substrate layer. This work needs to be done extensively with laboratory tests and simulation results, which will address the objectives below.

1.2.1 Green roof substrate properties measurement

There are three relationships of fundamental green roof substrate properties required in this study:

- The relationship between moisture content and compaction level
- The relationship between porosity and compaction level
- The relationship between thermal conductivity, moisture content and compaction level

1.2.2 Thermal conduction in a substrate layer due to the absorption

There are four main steps involved in this objective.

- Measure sorptivity values of a typical green roof substrate when the moisture content is varied

- Measure sorptivity values of a typical green roof substrate when the compaction is varied

- Predict water transport phenomenon in a substrate layer by the sharp front model

- Linking sharp front theory and thermal conductivity together to develop the substrate layer conduction model

1.2.3 Thermal conduction in a substrate layer due to the evaporation

There are four main steps involved in this objective.

- Measure the moisture content of green roof substrate samples at different compaction levels in each layer from saturated until dry

- Determine the evaporation rate in stages I and II of green roof substrate at different compaction levels

- Predict moisture content in each layer with calculated evaporation rates and a moisture balance equation

- Link moisture content in each layer with thermal conductivity, then calculate the hourly heat conduction through substrate

After these objectives are accomplished, the wetting and drying heat conduction of the roof will be combined in order to estimate the green roof's performance.

1.3 Data collection

The data collection in this research mainly comes from the experiment of sharp front theory and evaporative drying in green roof substrate. The intensive green roof substrate was kindly supplied by Shire Green Roof Substrate Limited (West Sussex); the company's product being the main sample in this experiment. Furthermore, test equipment, such as an environmental chamber, thermostatically controlled oven, top pan balances, and another material that assemble into the test apparatus, are held in the concrete laboratory of Heriot-Watt University (Edwin Chadwick Building).

The sharp front theory will use the value called the sorptivity (S). The value of S is considered by two main effects, (i) the changing in moisture content, and (ii) the changing in compaction (hydrological and mechanical effects respectively). The experiments will vary these two parameters to investigate S, which affects the hydrological transfer, and leads to the thermodynamic modification. The variation of moisture contents and compaction degrees will be listed as following.

- Moisture contents from dry to near saturation.
- A range of compaction levels up to a penetration resistance of 450 kPa.
- Compaction degrees in definition of dry densities are observed in order to identify a relationship between the penetration resistance and dry density (Dry density of each sample will be controlled by the number of blows of a tamper applied to a sample).

The evaporative drying occurs in two stages (Platten, 1985). In order to define these stages, the green roof substrate apparatus will be dried within a constant environment (relative humidity, temperature, and wind speed are constant). For this reason, a controlled environmental chamber will be used to operate this experiment, as described later in this thesis.

1.4 Format of thesis

This thesis is divided into eight chapters, which can be described as follows.

Chapter 1 introduces the origin of this research. This chapter also points out the aim and objectives of this work. Furthermore, the data collection method is introduced in this chapter. Finally, the format and layout of this thesis are depicted in this introduction chapter.

Chapter 2 presents the literature review, exploring previous green roof studies. This chapter also presents the general background of the green roof concept and its benefits. Essentially, the literature review on the issue of green roof thermal simulation is presented, and the research gap is explained at the end of this chapter.

Chapter 3 deals with the experiment on the green roof. This chapter clarifies methods and procedures used to obtain information that is necessary for a green roof substrate

thermal simulation. There are four fundamental properties of green roof substrate required for the simulation: moisture content, compaction, porosity, and thermal conductivity. These properties are related and this chapter is aiming to obtain data to explain their relationship.

Chapter 4 deals with the green roof thermal simulation by substrate absorption. This chapter will introduce the sharp front theory that is used for the green roof absorption mechanism. In addition, the experimental procedure and results of sorptivity values from different green roof substrate conditions are presented in this chapter. Finally, sorptivity values and thermal conductivity of substrate are combined and computed into the green roof thermal simulation with absorption.

Chapter 5 introduces the drying mechanism of green roof substrate from evaporation. The porous medium evaporation theory is presented in this chapter together with data regarding the experiment on the substrate. By combining these results and thermal conductivities (see chapter 3), the thermal conduction of green roof substrate due to the evaporative drying can be simulated and the results shown in this chapter.

Chapter 6 involves the combination of the drying mechanism (chapter 5) and absorbing mechanism (chapter 4). This chapter also describe the simulation process of both mechanisms, supported by flow chart data.

Chapter 7 is the discussion and implication chapter. This chapter compares this work with other studies, points out the limitations of this research initiative, and discusses the findings of this thesis. In addition, the implications of this work are presented by using the case study of the sample building with different types of roofs.

Chapter 8 draws the work together, from theory build-up to the results. The recommendation for future work relating to green roofs is also presented in this chapter.

1.5 Conclusion of the chapter

This chapter introduces the work of green roof performance simulation by offering a general background and highlighting problems with current green roof thermal performance theories. Furthermore, the aim and objectives of the research are discussed in this chapter, together with the data collection procedure. Finally, the format of this

thesis is presented and explained concisely. The next chapter is the literature review, which explores published accounts relating to green roof research.

Chapter 2: Literature review

2.1 Introduction

This chapter outlines previous literatures on green roofs. It will introduce background information relating to the green roof topic in technical detail, by highlighting such issues as types and components of green roofs, as well as the benefits of green roof installation. Furthermore, the review of previous research on green roof thermal simulation is discussed, together with identification and exploration of the research gap. In the latter part of this chapter, the problems found in green roof simulation will be discussed.

2.2 General background of green roofs

The general background of green roofs and roofing includes the history of green roof use from early ages to the current green roof system. This section also points out different types of green roofs and their components according to the green roof standard.

2.2.1 History of the green roof concept / idea

A green or living roof is one of the oldest constructions employed by humankind, to shelter and protect those early people from the outside environment. In the earliest days green roofing was built from rods of plant or turf sods tightened together to make a roof cover; as a result such a roof provided a small amount of weather insulation by its shading. However, this roof type did not provide aesthetic features; due to the development of human civilisation, green roofs were developed to satisfy this function. According to the history of Herodotus (5^{th} century B.C.), Babylon's hanging gardens, the first documented green roof, appeared around 590 B.C.; the gardens were considered to be one of the 'Seven Wonders of the Ancient World' (Ascione *et al*., 2013) (Figure 2.1). Although to this day there is no archaeological evidence of this garden, it was the most famous green roof in ancient times.

Figure 2.1 Babylon's hanging garden (Retrieved from http://commons.wikimedia.org/wiki/File:Hanging_Gardens_of_Babylon.jpg)

During the 17th and 18th centuries, green roofs became popular in Northern Europe. These roofs were once used in constructions by Vikings to protect their buildings and envelope their dwellings against thermal dispersions caused by wind and rain. The Faroe Islands, situated between Norway and Iceland, for instance, still have such traditional dwellings equipped with old style green roofs (Ascione *et al*., 2013). However, this roofing style slowly became less popular during the 19th century, due to the development and availability of low cost materials, such as steel construction resulting from the industrial revolution. Nevertheless, green roofing became popular again in United State of America, due to the possibility of combining the roofs with structures made from material such as reinforced concrete. The first green roof in the United States was installed in the Rockefeller Centre, New York, in 1930 (Getter and Rowe, 2006).

For energy considerations, Germany, in 1960, was the first country to consider the energy benefits of green roofs, in addition to their aesthetic and living qualities. Previously, the green roof idea had been used by well-known architects such as Le Corbusier, Walter Gropius and Frank Lloyd Wright (Newton *et al*., 2007). Fallingwater, for instance, is the famous work by Frank Lloyd Wright, which was accredited by the American Institute of Architects to be the best American architecture of all-time; it uses a green roof as a component. Those are some examples of the early history and development of green roofs and roofing.

However, the relatively modern examples of green roofs mentioned above were built to satisfy architectural features without considering negative issues such as plant root ingress or water leakage. For these reasons, modern green roof technology was developed in Germany in early the 1970s, to overcome these problems by providing sufficient irrigation, root and water protection for roof top gardens. This kind of roof is also accessible for activities; a concept which is known as an 'intensive green roof'.

It is important to note that this 'intensive' type of green roof puts massive loads on a roof structure because of its depth, which is likely to be greater than 300 mm; a detail that has resulted in the need for more expensive structural support than was the case for the less sophisticated previous models. In the late 1980s Germany, having recognised this depth problem, introduced the shallow green roof concept, called an 'extensive green roof', with lower growing media depths of 20mm to 200mm. This roofing model is amenable for retrofitting, due to its smaller imposed loads, compared to the thick and heavy 'intensive' green roof (Köhler, 2006). Although the extensive green roof was firstly employed as fire protection, the use of this roof became widespread in Germany due to the roof's durability; combined with the fact that it requires less maintenance as compared to an intensive type. Both types of green roof will be discussed in more detail in the following section.

Germany leads the world's popularity of modern green roofing, with the construction of around 13.5 million square meters of such roofing per year (Oberndorfer *et al*., 2007). Green roofs are estimated to cover 14% of all flat roofs in the country.

In Great Britain, green roofs were used for camouflaging military bases and airfields hangars during the 1930s (Getter and Rowe, 2006). However, the idea of a roof garden was proposed by Sennett (1905) in the book "Garden cities in theory and practice". The idea of roof gardens in Great Britain was inspired by the roof gardens of Berlin that existed at the end of nineteenth century. Nevertheless, the number of dwellings installed with green roofs in the early 20th century in Britain was still very low.

For modern British building construction, however, green roofing was introduced by the architecture firm Architype, and others associated with the Walter Segal Trust, in the late 1980s and early 1990s (Grant, 2006). They had introduced the idea of "footprint replacement", in which green space lost during construction is recreated on the roof of

the new 'intruding' building. This is the first principle for green roof development in the United Kingdom.

For the green roof situation in United Kingdom, Grant *et al*. (2003) estimated that there are 24,000 hectares, or 16 percent of roof cover in Greater London, where 20,000 hectares of existing roofs could be installed, using the 'extensive' model, with little or no structural modification. However, the numbers of green roofs in London and other parts of the United Kingdom are still very low. There are some examples of well-known green roofed buildings listed by English Heritage, such as the Willis, Faber and Dumas building in Ipswich (built in 1971) and Gateway House, Basingstoke (built in 1976). More examples of green roofed buildings can be found in a report from English Nature (Grant et al., 2003).

Research into green roofs in the UK, was pioneered by the University of Sheffield and Groundwork Sheffield (Dunnett and Kingsbury, 2004). A 'green roof forum' was established to spread knowledge and understanding of green roof techniques throughout the country. Furthermore, there are many companies that have developed and now provide green roof services; such as the UK based company Bauder or the German based company, ZinCo.

The history of green roof construction has a very long relationship with humans. Due to the global warming crisis, green roofs seem to be one of the best solutions for climate change adaptation and mitigation. However, the performance of green roofs needs to be optimised by improved understanding of their mechanism in order to facilitate their use throughout the world. These suggestions will be examined and discussed in this chapter.

2.2.2 Types of green roof

There are two types of green roof construction, as mentioned earlier: the intensive and extensive green roof. Their construction and use will depend on a client's purpose and the building's function. However, there is a German research organisation, founded in 1977, called the FLL (Forschungsgesellschaft Landschaftsentwicklung Landschaftsbau: the Landscape Research, Development and Construction Society) which has divided green roofing into three categories: i) the intensive green roof, ii) the semi-extensive green roof and iii) the extensive green roof.

The intensive green roof

Firstly, the intensive green roof, which is also known as a rooftop garden or high-profile green roof. It can provide a variety of plants, and even large trees or ponds in some buildings, depending on the depth of growing medium used and the building's structural possibilities. According to its massive weight, this roof needs complicated structural support and careful design to withstand its required large depth of soil, which usually amounts to more than 300 millimetres (Wark and Wark, 2003). In addition, special service systems are required underneath the roof for the garden's maintenance and irrigation because accessibility is very difficult after an intensive green roof is installed. Figure 2.2 illustrates the intensive green roof component.

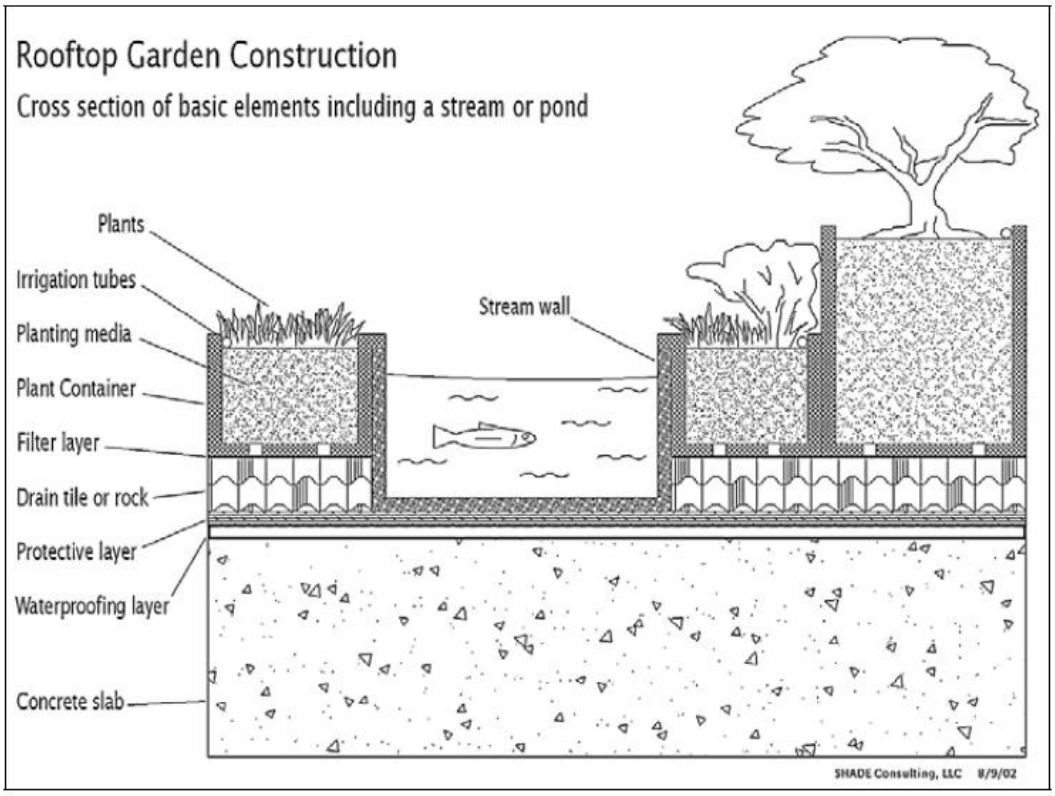

Figure 2.2 Intensive green roof components (Wark and Wark, 2003)

Tanner and Scholz-Barth (2004) stated that intensive green roofs are usually not considered as either environmentally and/or cost effective, if compared with extensive green roofs. Although, such a roof model can provide accessible features and some energy advantages, it requires high capital and operational costs. Many cost analysis models agree that an intensive green roof has a high return period, and sometimes has a negative return period due to the model's operational and maintenance costs (Bianchini and Hewage, 2012, Ascione *et al*., 2013).

Semi-extensive green roof

According to FLL, the semi-extensive green roof, or hybrid type, is not so clear-cut; it is a combination between the intensive and extensive green roof models. Dunnett and Kingsbury (2004) stated that the extensive green roof had been driven by its performance, but it lacked aesthetic consideration and was inaccessible. However, the semi-extensive roof, constructed with a lightweight substrate and modern green roof construction techniques, can create the desired aesthetic features. Equally, it is accessible in the same way as an intensive green roof, but more sustainable due to its thinner substrate (100-200 mm).

Extensive green roof

The other type of green roof that is used for environmental purposes and has been extensively tested and reported is *the extensive green roof*, sometimes called a low-profile or performance roof. In comparison with the previous mentioned roofs, this model has a thinner layer of substrate and is therefore lighter in weight. In general, it has 20 mm to 200 mm thickness of substrate and the weight is approximately 50 kg/m^2 and up to 100 kg/m^2 dependant on water content (Wark and Wark, 2003). Therefore, the structural support needed for this roofing model is simpler, and special service requirements (irrigation and maintenance) are easier, than those required for an intensive green roof.

Unlike an intensive green roof, an extensive green roof does not create public access or increase living spaces. The main consideration for this roof is to improve performance of the building and for this reason the plants used in this roof should be able to withstand harsh conditions and not require attention during the roof's operation (Oberndorfer *et al*., 2007). For this reason, large trees or non-native plants are not suitable for use with this roof model.

The main components of an extensive green roof are similar to those in an intensive green roof, which are mainly used for protecting a roof structure from water leakage and root ingression. The structure of the extensive green roof is presented in figure 2.3 and each component will be explained in the next section of this chapter.

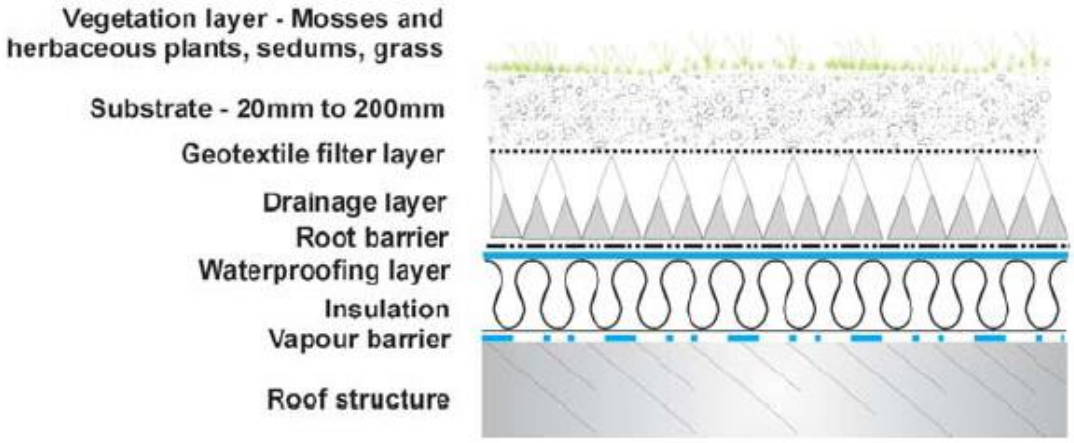

Figure 2.3 Components of an extensive green roof (Newton *et al.*, 2007)

Dunnett and Kingsbury (2004) summarised the characteristics of an extensive green roof, compared to an intensive green roof, as presented in table 2.1 below.

Table 2.1 A comparison of extensive and intensive green roofs (Dunnett and Kingsbury, 2004)

Characteristic	**Extensive green roof**	**Intensive green roof**
Purpose	Functional; storm-water management, thermal insulation, fireproofing	Functional and aesthetic; increase living space
Structure requirement	Typically within standard roof weight-bearing parameter; additional 70-170 kg/m^2	Planning required in design phase or structure improvements necessary; additional 290 – 970 kg/m^2
Substrate type	Lightweight; high porosity, low organic matter	Lightweight to heavy; high porosity, low organic matter
Average substrate depth	2 to 20 cm	More than 20 cm
Plant communities	Low-growing communities of plants and mosses selected for stress-tolerance quality	No restriction other than those imposed by substrate depth, climate, building height and exposure, and irrigation facilities
Irrigation	Most require little or no irrigation	Often require irrigation
Maintenance	Little or no maintenance required; some weeding or mowing as necessary	Same maintenance requirement as similar garden at ground level
Cost (above waterproofing membrane)	\$100 to \$300 per m^2	More than \$200 per m^2
Accessibility	Generally function rather than accessible; will need basic accessibility for maintenance	Typically accessible; addition live load required in design phase

The extensive green roof model can be divided into three subcategories: i) a complete system, ii) a modular system and iii) a pre-cultivated vegetation blanket (Oberndorfer *et al*., 2007) as shown in figure 2.4. The complete system is a traditional in-situ extensive green roof construction, built by installing each (new) component over an already finished layer. The modular system, or tray system, on the other hand is the model involving a green roof being cultivated ex-situ, before installation then placed over an existing roof structure. This roofing model comprises an interlocking container filled with a foliage layer, substrate and drainage system (Dunnett and Kingsbury, 2004). Similarly to the modular system, the pre-cultivated vegetation blanket, sometimes called a 'mat system', is also cultivated ex-situ prior to installation. However, the entire system is rolled, instead of boxed, to minimise space for transportation. As a result, this system will have the thinnest construction layer of any of the green roof models discussed above. Both mat and tray systems are very quick to install and can produce a greenery effect immediately after installation (Hui and Chan, 2008).

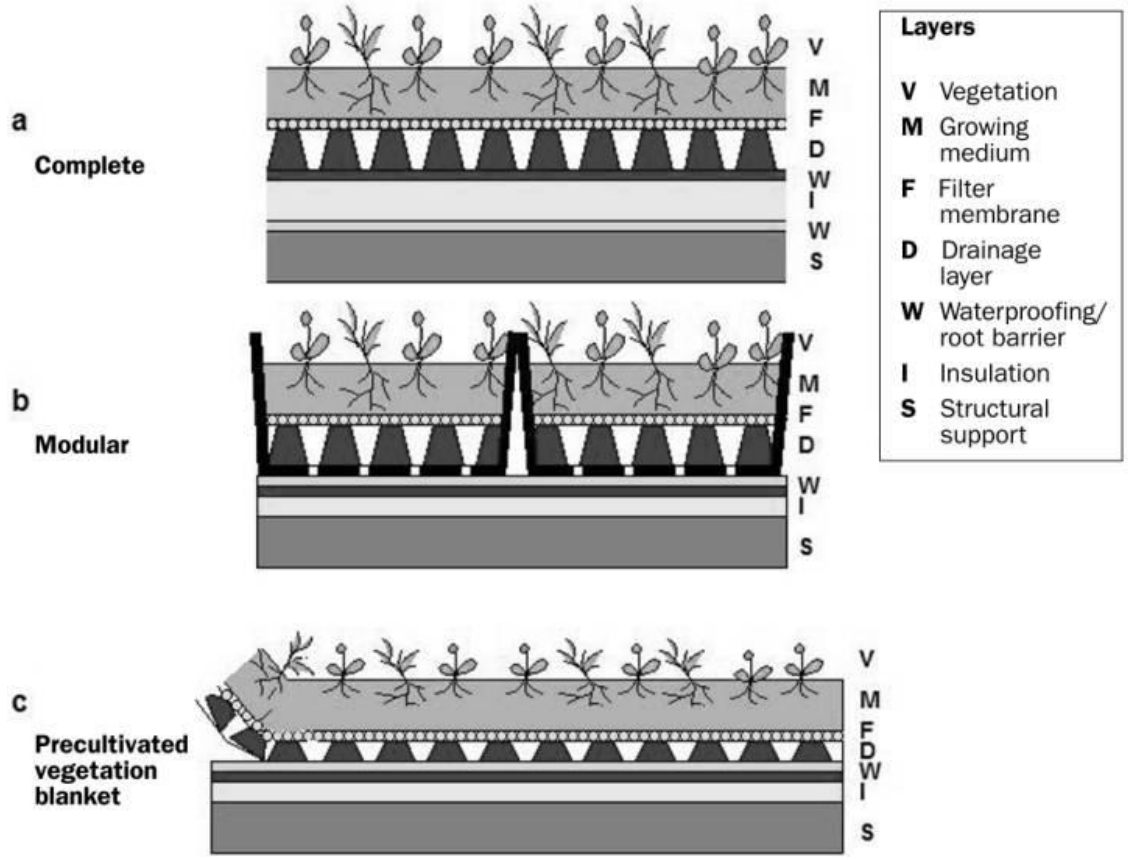

Figure 2.4 Types of extensive green roof system (Oberndorfer *et al*., 2007)

The technique of green roof construction continues to develop to satisfy building functions, such as sloping or curved roofs. Hui and Chan (2008) mentioned the Sack

green roof system that can conform to irregular and curved areas. The growing media and vegetation seeds are sealed in the fabric module and ready for planting after positioning them on the roof that is to be 'greened'.

There are many types of green roofs that appear in the market nowadays, and the usage and application of these roofs depend on functions, budgets, time constraints and accessibility for construction.

2.3 Green roof's components

Although there are many types of green roofs, their main components are similar. The definition of each component was given by Newton (2007) and the details are categorised below. The arrangement of each component is shown in figure 2.3.

- The roof structure
- The water proof membrane
- The thermal insulation
- The root barrier
- The drainage layer
- The filter layer
- The substrate (also referred to as "growing medium" and "soil layer")
- The foliage layer (also referred to as "vegetation layer" and "plant layer")

The roof structure

The most important component of a green roof structure is its support structure. It is the main and first thing to consider before establishing a green roof system. For a new building, a green roof will influence the capital cost of the building's construction. In the case of an existing building, the weight issue will affect the possibility of green roof installation, because structural strengthening of such a building will need to be considered, together with the costs involved.

According to Peck and Kuhn (2003), a typical lightweight extensive green roof with soil depths between 5-15 cm can impose a load on the roof of around 70-170 kg/m^2 ; for an intensive system the loading would range from 290 to 970 kg/m^2. As seen in the loading pattern, it is almost impossible (and certainly unwise) to put an intensive green roof system over an existing structure. In contrast, an extensive system is suitable for retrofit.

In some countries like Canada, the roof must support a load of at least 195 kg/m^2 for a roof system and snow load; however, a typical snow load is 107 kg/m^2, which means there is an additional capacity of 88 kg/m^2 required in order to install a simple extensive green roof. In the UK, on the other hand, the load bearing capacities for roofs are given in BS 6399, which specifies the requirements of self-weight of the roof, dead load for materials, snow, live load from people and the effect of wind shear (Dunnett and Kingsbury, 2004). These concerns must be addressed by a structural engineer before installation of a green roof.

The main component of all green roof systems is the substrate layer, the weight of which is varied by its compaction and water content. In general, the designer uses the saturated weight of the soil to calculate the building's structural requirements. Weights of each substrate materials are listed in table 2.2.

Table 2.2 Substrate weight of typical green roof system (Dunnett and Kingsbury, 2004)

Substrate Materials	**Weight of 10 mm layer (kg/m^2)**
Gravel	16-19
Pebbles	19
Pumice	6.5
Brick (solid with mortar)	18
Sand	18-22
Sand and gravel mixed	18
Topsoil	17-20
Water	10
Lava	8
Perlite	5
Vermiculite	1
Light expanded clay granules (LECA)	3.4

The waterproof membrane

This essential layer is used to protect the structure from water penetration; the membrane can be laid over the roof structure or applied by chemical fluid. According to Dunnett and Kingsbury (2004), there are three types of this layer on the market: i) the built-up roof, ii) the single-ply membrane and iii) the fluid-applied membrane.

The built-up roof is the traditional waterproof system in the UK, being composed of the bitumen/asphalt roofing felt or bituminized fabrics. These roofing materials have a lifespan around 15-20 years and are vulnerable to degradation from temperature fluctuation and ultraviolet radiation, which cause cracking and leakage. Although green

roofs can reduce these risks, with such roofs there is the hazard from root penetration. For this reason, a built-up roof system always requires a root protection layer.

The most common waterproof system for a green roof is a single-ply roof membrane. It is a rolled sheet of plastic, or synthetic rubbery material, that is overlapped at the joint and then heat-sealed (Osmundson, 1999). This membrane can perform as an effective water barrier if it is installed properly. However, the seams or bonds between the layer and tiles or joints can create weak points that may risk being vulnerable to root penetration. Ultraviolet radiation, likewise, can cause degradation of this membrane, but this is unlikely in service. The single-ply roof membrane can also integrate with root-deterring chemicals to perform the roles of both water and root barriers.

Finally, the fluid-applied membrane is a liquid system that is sprayed or painted over the roof surface. It can form a complete unbroken barrier and therefore eliminates the problem of joint sealing (Osmundson, 1999). This liquid system is appropriate for complex shaped roofs and vertical surfaces, and is therefore also suitable for living or greenery walls.

The root barrier

The layer next to the waterproof layer is the root barrier, which is a sheet mounted to protect roof structures from root damage because roots grow, strengthen and seek nutrition and water further from the substrate layer. As a result, the root barrier is presented to avoid this problem; normally being a biocide material combined with a waterproof material, or applied on top of a waterproof membrane.

According to Bianchini and Hewage (2012), there are two different types of root barriers in the market: the physical and the chemical models. The physical barrier is a thin layer (approximately 0.5 mm) of a low-density polyethylene or polypropylene placed over the roof. Chemical root barriers use toxins such as copper based products to inhibit root ingress. This kind of root barrier cannot provide water- proofing and therefore needs to be installed over an existing waterproof layer.

The drainage layer

The drainage layer is the layer that is used to retain water for vegetation survival during rain-free periods. Apart from water supply, it also provides sufficient drainage space to reduce waterlogging in the rainy season, which can cause plants to rot. In addition, the

drainage layer controls the amount of water run-off from the roof, which is a key feature of storm water management. This layer can be categorised into three types: i) granular materials (sand or gravel), ii) porous mats and iii) a modular system. The drainage layer system is shown in figure 2.5.

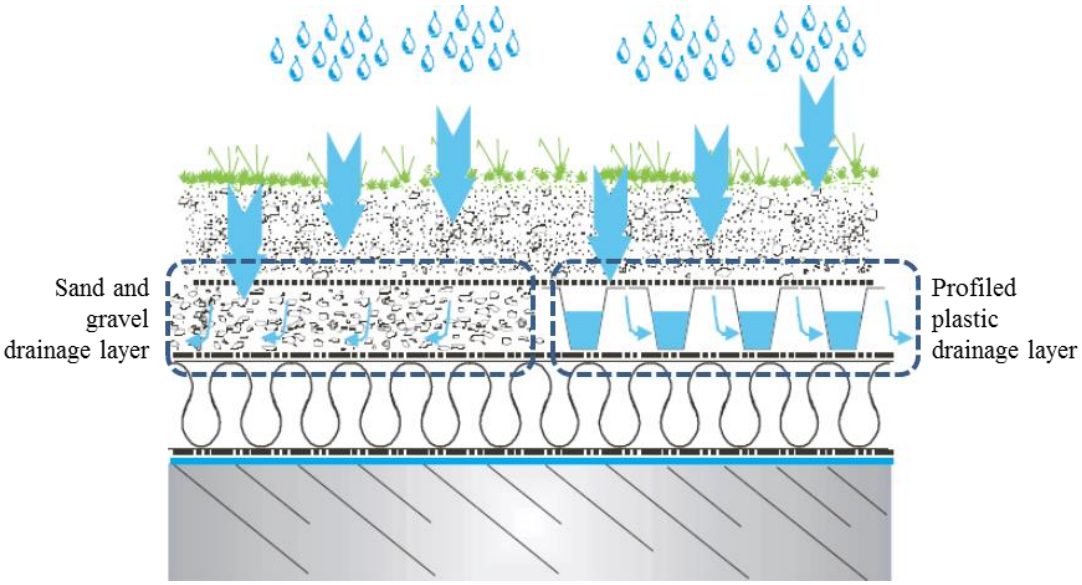

Figure 2.5 The drainage layer system, with granular system on the left and modular system on the right (Newton *et al*., 2007)

The granular system uses coarse granular materials such as gravel, stone chips, broken tiles, lava rock, pumice, expanded shale, or expanded clay. These materials contain large amounts of pore space to enable water to drain from vegetation and the substrate layers above (Dunnett and Kingsbury, 2004). This drainage method is derived from a traditional plant pot where the gardener lays coarse materials on the bottom to provide space for root penetration and water pockets for more stable moisture content.

Secondly, a porous mat can be constructed from many kinds of sponge-like materials, such as recycled cloth. This system can capture water into the structure and provide sufficient moisture for plant survival. On the other hand, this system could be a danger for the plant because it can be too absorbent, unintentionally removing moisture from the substrate layer above (Dunnett and Kingsbury, 2004). This drying effect may have a negative effect on the wellbeing of the plants.

The last type of drainage layer is the lightweight plastic drainage module. These modules have various designs according to their manufacturer, but most of them are thinner than 2.5 cm; with dimples or reservoirs to store water for the plants during dry

periods, as well as providing a permanent free-flowing lightweight drainage area beneath the substrate layer (Dunnett and Kingsbury, 2004). The structure of this layer is rigid enough to withstand the load of vegetation and soil above and, in addition, its strength can be increased by adding granular media.

The selection of a drainage layer depends on available materials and the budget. For instance, in some areas, a plastic drainage module may not be available, but there may be plenty of recycled materials, such as broken bricks and gravel. As a result, the granular type of drainage layer is suitable for this case, but its additional loading weight must be taken into consideration.

The filter layer

When a drainage layer is installed, a filter layer is also required; the latter being a semi-permeable polypropylene fabric laid on top of a drainage layer. It prevents fine substrate materials from being washed into the drainage layer's pore spaces, which would cause blockage of the drain outlet (Dunnett and Kingsbury, 2004).

This layer also provides substrate and vegetation integrity, which binds a substrate layer together with a drainage layer (Bianchini and Hewage, 2012). This bonding technique produces easy installation and mobility, and is used in a modular type green roof and a pre-cultivated vegetation blanket.

The substrate layer

This layer is the deepest layer of the system and has the highest weight compared to the roof's other layers; as a result its dimensions are used to differentiate between the extensive and intensive green roof models. The substrate layer is required for plant anchorage, as well as to supply nutrients and moisture for plants. However, it needs to have draining ability to prevent oversaturation that causes plants to rot and die. The substrate weight, furthermore, is an important property of both intensive and extensive roofing systems, since it is necessary to reduce the roof load by as much as is possible. Dunnett and Kingsbury (2004) summarised and commented upon the substrates that are usually used in green roofs (see table 2.3 below).

Table 2.3 Materials used as a basis of green roof substrates (Dunnett and Kingsbury, 2004)

Type	Materials	Comments
Natural minerals	Sand	Lack of pore space as a result of fine texture. In addition, it needs constant irrigation because of its free-draining property.
	Lava (scoria)	Lightweight but expensive.
	pumice Gravel	Relatively heavy.
Artificial minerals	Perlite	Particles have a risk to collapse over time.
	Vermiculite	Very lightweight, but lack of water and nutrients retention and has a possibility of particle disintegration.
	Light expanded clay granules (LECA)	Lightweight, produces large amounts of pore space because of granule size, and absorbs water because of their porous nature.
	Rockwool	Very lightweight, but needs lots of energy of production and has no nutrient-holding capacity
Recycled or waste materials	Crushed clay brick or tiles, brick rubble	Stable and uniform, some nutrient and moisture retention. Brick rubble may contain mortar and cement, which will raise the pH of substrate.
	Crushed concrete	Limited moisture retention and nutrient availability, alkaline. However, cheap and available in quantity as a demolition material.
	Subsoil	Heavy, low fertility, readily available as by-product of construction.

Some substrates used in gardening may not be suitable for green roofs, as noted by Dunnett and Kingsbury (2004). High fertility soils, for instance, such as garden soil and topsoil are not suitable for green roofs since such materials encourage vigorous lush growth that is susceptible to environmental stress. Additionally, clay has good water-holding capacity and surfaces that attracts nutrients inside, but also presents a high risk of blocking drainage layers and outlets. On the other hand, it can be used in small proportions with other substrates, which is preferable in the green roof substrate. In most green roofs, a mix of materials with low organic matter (to avoid rapid fire spread)

and with good moisture retention may be used; depending, of course, on local weather and plant selection.

The depth of substrate is varied according to the plant types that are supported by it. Green roofs can have shallow depths of 20-30 mm, but these are prone to rapid drying. In contrast, a substrate that is too deep may add a massive and potentially dangerous load to its host structure. The sedum growth in a substrate of depth 25 mm was less satisfactory than with 50 or 70 mm. For the depths of 50-80 mm, taller sedums and grasses are able to grow, as are low-growing, drought-tolerant herbaceous species and alpines. Depths of 100 mm, however, begin to cause structural problems for extensive green roofs since the load is greater than 120 kg/m^2 (Dunnett and Kingsbury, 2004).

Selections of substrate types and depths depend greatly on vegetation types and structural capacity; points stressed by green roof suppliers. Green roof standards in each country, in addition, are another requirement to be taken into account. For example, in the United Kingdom substrate depths of 70 mm are required as a minimum for extensive green roofs (Dunnett and Kingsbury, 2004).

The foliage layer

Vegetation used for green roofs is different from garden plants because they have to survive in different climatic conditions such as frost, snow, wind chill and drought, without regular maintenance. The selection of plant species for a certain location is difficult since some plants grow effectively in one location, but are unsuitable in another. Nevertheless, Dunnett and Kingsbury (2004) suggest important features to note for plants used on the rooftop:

- Ability to cover and anchor the substrate surface within a reasonable time after planting.
- Be able to form a self-repairing mat, so that new growth will be capable to fill any areas that become damaged.
- Capability to take up and transpire the water from the soil.
- Can survive the climatic conditions prevailing at the rooftop, with particular attention to cold hardiness and drought tolerance.

Dunnett and Kingsbury (2004) also suggested some suitable plant species informed by substrate depth, accessibility and visibility of the roof, as presented in table 2.4.

Table 2.4 Appropriate plants corresponded to substrate depth, the accessibility and the visibility of the roof (Dunnett and Kingsbury, 2004)

Depth	**Inaccessible/ Invisible**	**Inaccessible/ visible from a far distance**	**Inaccessible/ visible from a close distance**	**Accessible**
0-50 mm	Simple sedum/moss communities	Simple sedum/moss communities	Simple sedum/moss communities	Simple sedum/moss communities
50-100 mm		Dry meadow communities, low-growing drought-tolerant perennials, grasses and alpines, small bulbs	Dry meadow communities, low-growing drought-tolerant perennials, grasses and alpines, small bulbs	Dry meadow communities, low-growing drought-tolerant perennials, grasses and alpines, small bulbs
100-200 mm			Semi-intensive mixtures of low to medium dry habitat perennials, grasses and annuals; small shrubs; lawn, turf grass	Semi-intensive mixtures of low to medium dry habitat perennials, grasses and annuals; hardy sub shrubs
200-500 mm				Medium shrubs, edible plants, generalist perennials and grasses
More than 500 mm				Small deciduous trees and conifers

As seen in table 2.4, higher substrate depth can result in various types of plants, which provide aesthetic benefits, as well as accessibility.

In summary, the intensive and extensive roof models can be similar in their components, but they have different requirement due to issues of depth, weight,

irrigation and maintenance. The latter (extensive) model requires less structural support and services than the intensive roof. Because of these reasons compared to its performance, the extensive green roof is considered to be more environmentally and cost effective than is the intensive green roof.

2.4 Benefits of green roof installation

A green roof has many benefits to the micro (building) and macro (surrounding) environments. According to Newton (2007), a green roof provides potential benefits to its surrounding environment, such as increased biodiversity, storm water amelioration, climate change alleviation and adaptation. This is summarised in Figure 2.6.

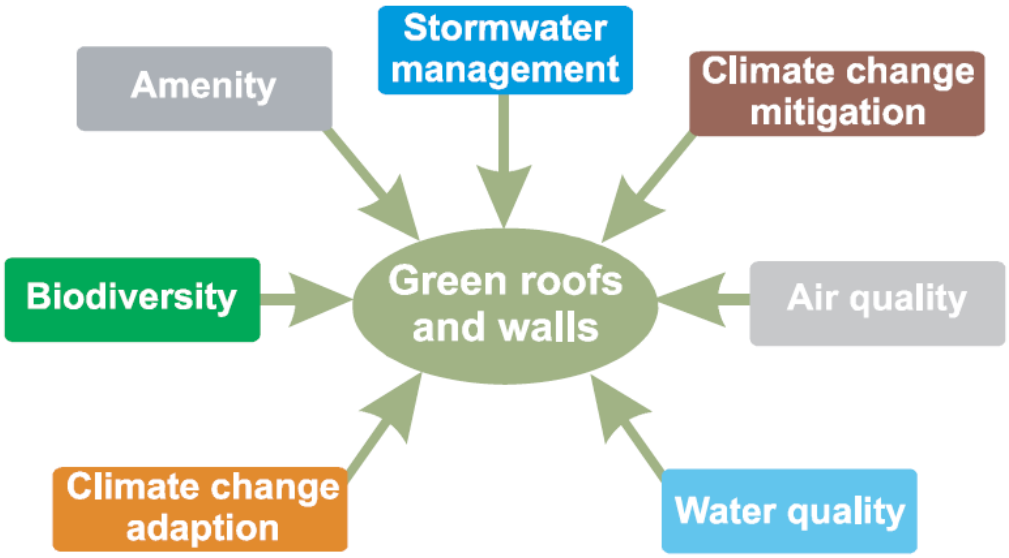

Figure 2.6 Benefits of a green roof (Newton *et al*., 2007)

In addition to macro environmental aspects, a green roof can also improve a building's performance when it has been installed. For example, it can reduce energy usage from heating and cooling because of its additional thermal mass. Acoustic property, furthermore, could be improved after installation because it comprises highly absorbent material. Some characteristics will be discussed further in the following section.

2.4.1 Water management

During the rainy season, water management is an important matter, which needs to be considered particularly in urban areas, because if there is no suitable surface water management strategy, cities will become flooded. Therefore, many cities build lots of infrastructures to remove water out of their cities as fast as possible. Bangkok, for

instance, built a large water tunnel to take away rain-water directly from the middle of the city when there is surface-flooding or in order to prevent excessive flooding. Although this method is effective and rapid, it does not solve the main cause of flooding and is not sustainable. A more effective flood management approach is by using sustainable construction, such as a green roof. For example, the installation of a green roof is a clever policy used to manage storm water in many cities, such as those in Germany; there are many studies reporting the success of using green roofs for this objective.

According to the roof's components and characteristics, it can retain water inside pores between soil particles and the holes of a drainage layer, before generating run-off from the roof, acting like a rainwater attenuator. Newton *et al*. (2007) stated that a green roof can reduce volume of runoff by between 30% and 85%, depending on its construction. The roof also slows the flow rate down even if it is filled with water. The deeper the substrate the greater amount of water it can hold. Nevertheless, the greater roof weight will increase the structure support requirement. Figure 2.7 shows the water retention capacity of a green roof in different soil depths.

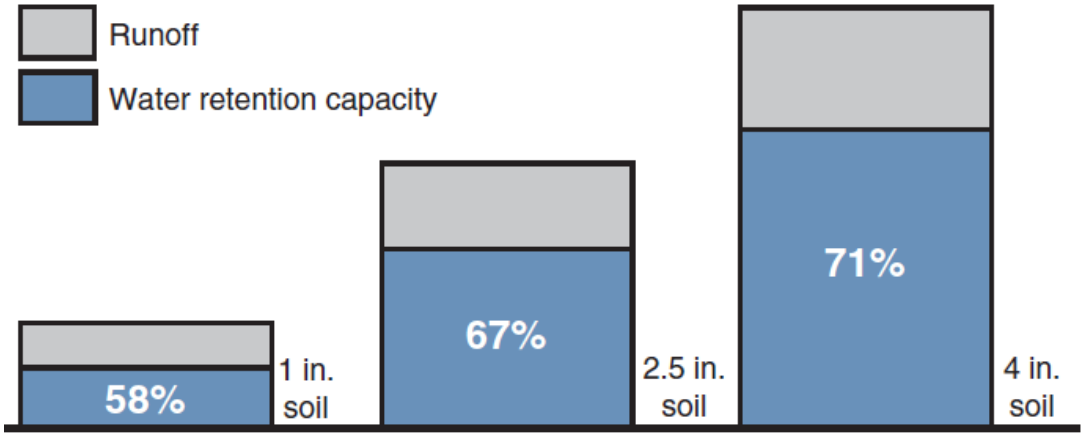

Figure 2.7 Water retention capacity of a green roof at different soil depths, 1 inch (25 mm), 2.5 inches (62.5 mm), and 4 inches (100 mm) (Scholz-Barth and Tanner, 2004)

In some situations, green roofs are used together with urban sewage systems to gain maximum efficiency in water management. Because of the roof's high absorption property, it can absorb much in the first inch of a rainfall event and release the water later by self-drainage and evaporation (Scholz-Barth and Tanner, 2004). Figure 2.8 shows the high number of rainfall events recorded in Washington D.C. with intensities

lower that one inch. Consequently, such a potential should reduce the pressure that impacts drainage infrastructure at the peak flow times.

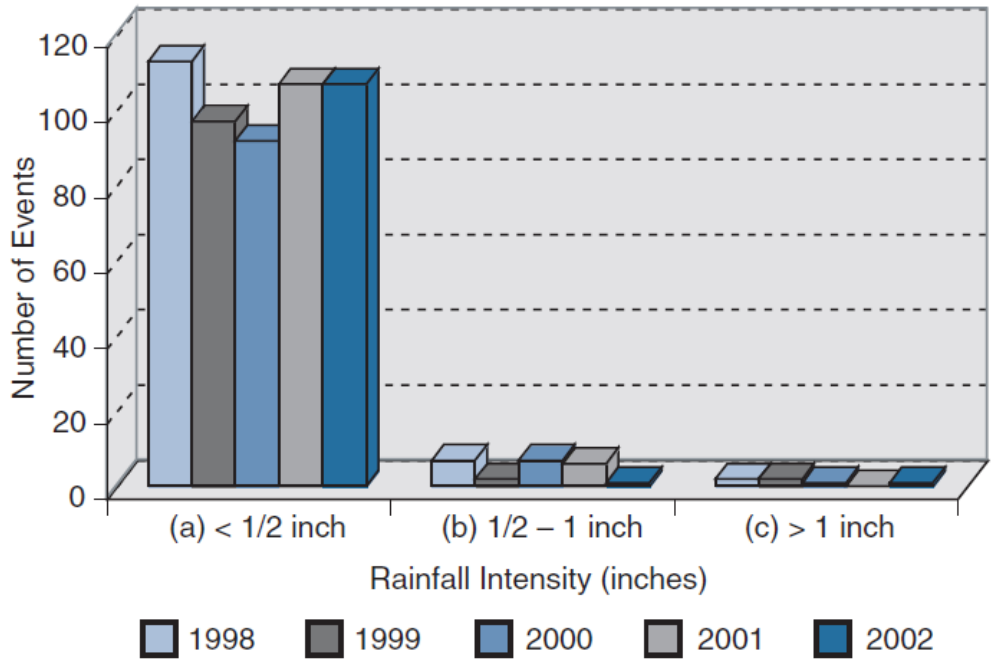

Figure 2.8 Rainfall intensity at 1 hour duration in Washington, D.C. (Scholz-Barth and Tanner, 2004)

In terms of water pollution, some studies suggest that green roofs can capture contamination came from atmospheric water, such as nitrogen and phosphorus and turn them into plant fertiliser. As a result, the water drained from a roof becomes cleaner and cooler (Scholz-Barth and Tanner, 2004). Furthermore, Johnston and Newton (2004) stated that 95 percent of heavy metals are captured by a roof before runoff. However, Newton et al. (2007) countered that green roofs may cause pollution, rather than reduce it, if an unsuitable design was used. They suggested that fertiliser should only be used sparingly on an established roof to avoid over-nutrition and pollution by run-off.

All things considered, a green roof can both effectively reduce storm water runoff and purify that water before it gets into the sewage system. Although, a greater thickness can retain more water, it also requires more structural support due to the weight of the roof itself, together with the additional weight from any retained water. Additionally, if using green roofs for water quality improvement, the study of roof plant nutrition may be a major concern regarding the incidence of pollutant leaching out of the roofs.

2.4.2 Acoustic control

Noise is an important consideration and can come from the environment such as road traffic, aircraft or people talking. Most of these sources are of considerable annoyance and therefore there is a need to reduce them as much as possible to maintain reasonable conditions of comfort. As a result, many products have been made to overcome this problem, such as sound insulation materials and sound absorbers. The green roof can offer good acoustic benefits, which can be used as acoustic insulation and absorption material. This section of the review will discuss the issue of the sound absorption and insulation properties of green roofs.

As pointed out above, roofs made from natural materials have had a long history, dating back to the time when buildings were shelters with roofs created from straws and reeds. Straw and reed are high sound absorption fibres that can produce significant absorption mechanisms when frequencies increase (Oldham *et al*., 2011). The spectrum of the straw and reed absorption coefficients is shown in figure 2.9.

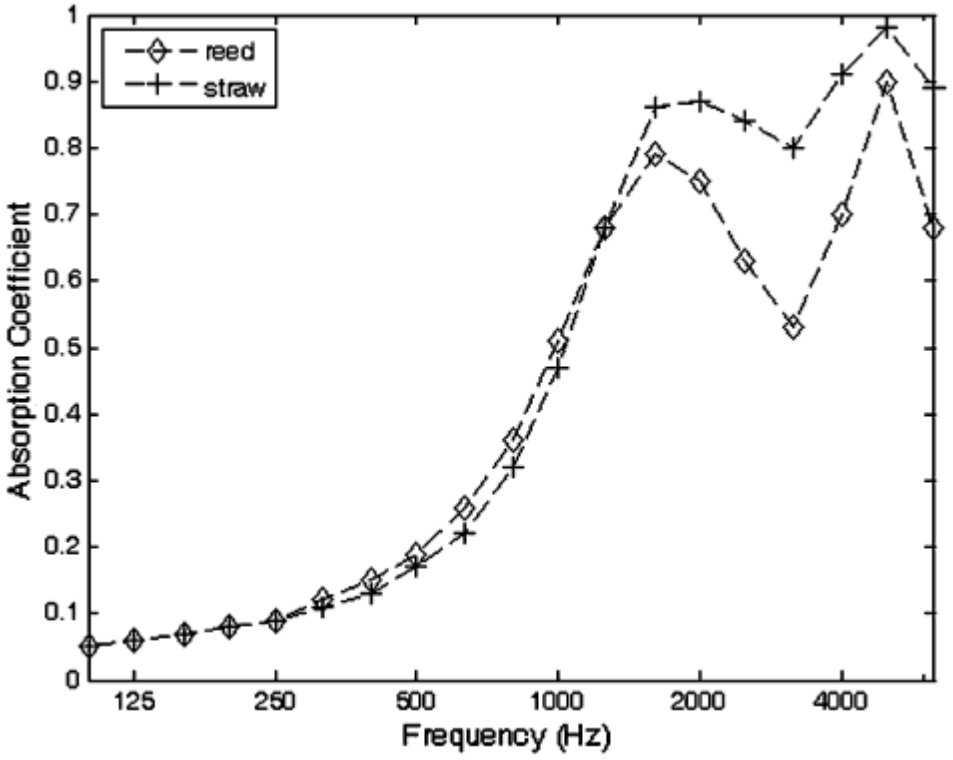

Figure 2.9 Acoustic absorption coefficients of straw and reed (Oldham *et al*., 2010)

Because of its terrific absorption property, many studies have investigated the acoustic absorption mechanism of vegetable matter. Wong *et al.* (2010), for instance, evaluated

the absorption property of eight diffent green walls in Singapore. They tested two different method. Firstly, they evaluated the insertion loss of sound passed through eight green walls (a vertical green system) installed in Hort Park, Singapore. The other test was held in a reverberation chamber to determine sound absoption coefficients. Results from the first test showed that 6 from 8 green walls had a noise reduction capacity of around 5-10 dB for low to middle frequency, which may be noticeble after installation. The results of these tests are shown in figures 2.10 and 2.11.

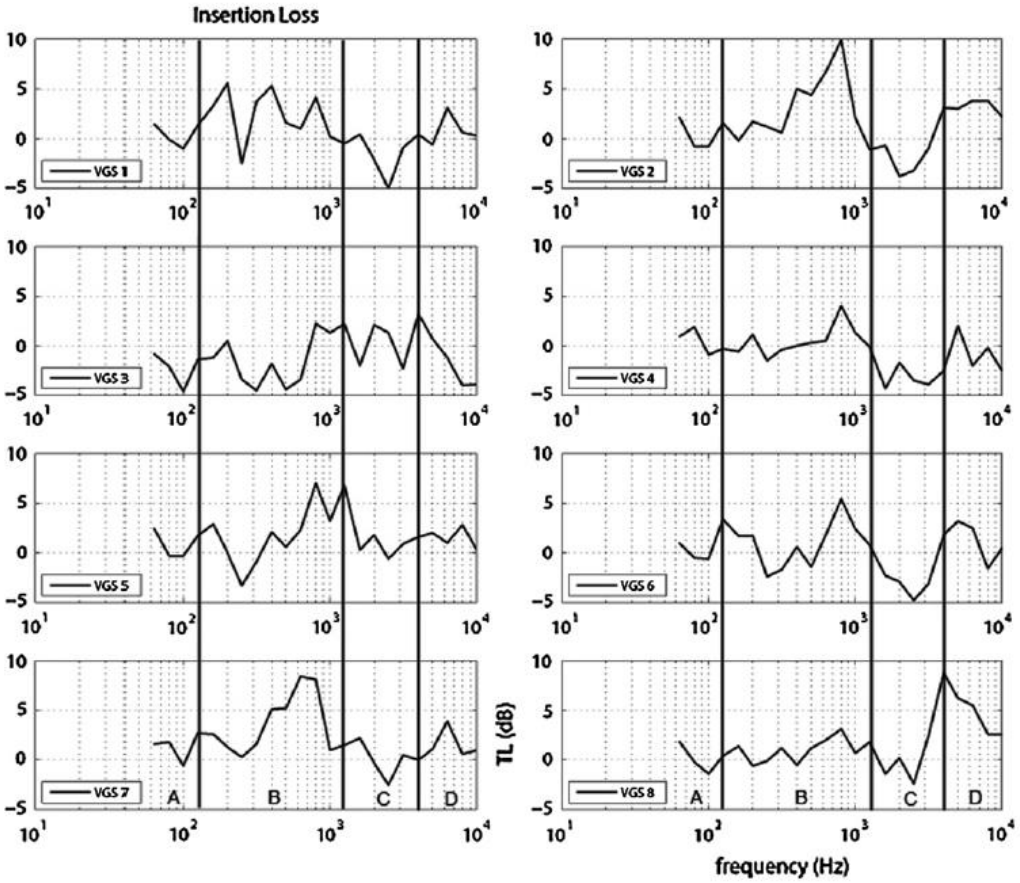

Figure 2.10 The sound insertion loss of eight vertical green systems, VGS1-VGS8 (Wong *et al.*, 2010).

Figure 2.11 Pictures of eight vertical green systems, VGS1-VGS8 (left to right and top to bottom) (Wong *et al*., 2010)

In the tests to establish the sound absorption coefficients, green walls produced high absorption properties when compared with other building materials. In addition, it was found that when the green cover was increased, the sound absorption coefficient also improved (Wong *et al*., 2010). Figure 2.12 shows sound absorption comparisons between green walls and conventional building materials.

As a consequence of the tests, results suggest a green wall could be effectively used to reduce urban traffic noise before that noise gets inside a building. Although, green walls are not cost effective, if compared with other noise control materials, such a wall can also give architectural benefits for landscape design, which is a popular option.

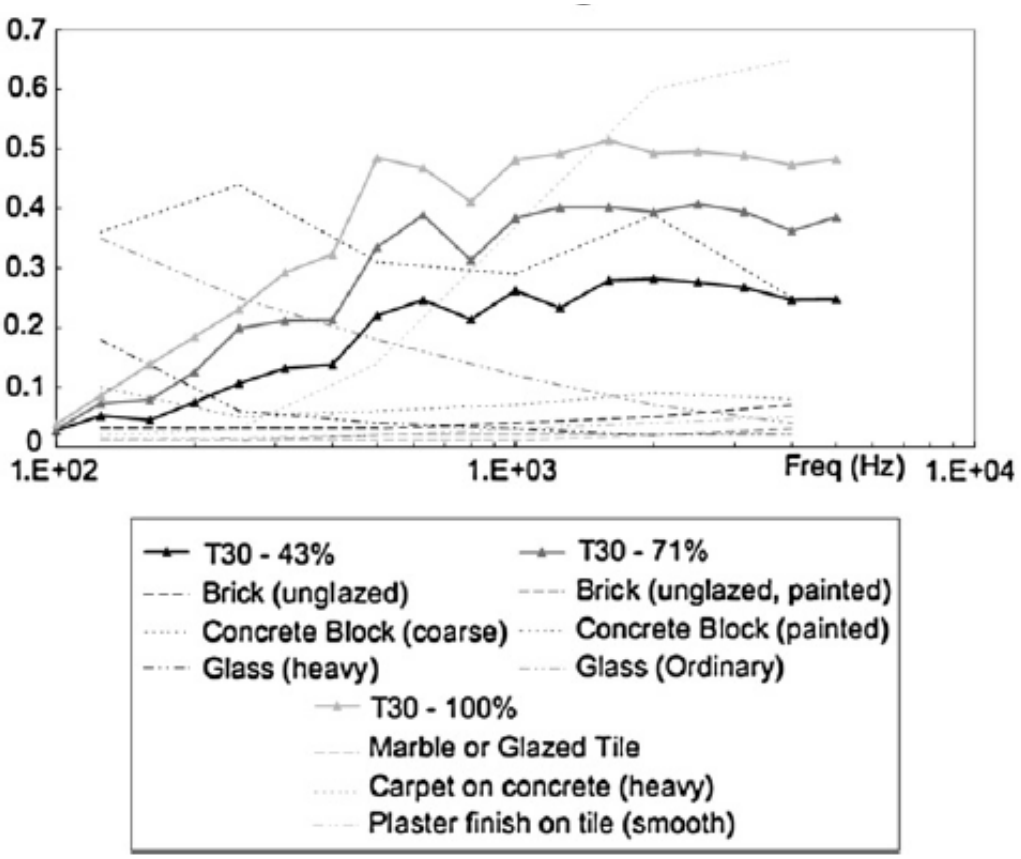

Figure 2.12 Sound absorption coefficients of vertical greenery walls and other building materials (Wong *et al*., 2010)

For the sound absorption of green roofs, many researchers have investigated the sound absorption characteristics of different green roof systems. For example, the measurement of sound absorption in common soil, extensive and semi-intensive green roof samples in impedance tubes (Pittaluga *et al*., 2012). After the experiment, the researchers found that the semi-intensive roof had the highest absorption property for both signals, followed by the extensive green roof and then common soil.

Yang *et al*. (2012) studied the sound propagation over a green roof. They found that sound was reduced via green roofs by around 20 dB maximum, at the high frequency range, and could be reduced further when the roof area was increased. However, the reduction of sound levels through leaf cover was not significantly improved; only 3-5 dB reduction, which is hardly noticeable.

Because of the high sound absorption property of a green roof, it could be used in practical ways to reduce airborne noise from traffic. The roof of an underground car park, for instance, can be covered with vegetation, which may reduce traffic noise

before it can get inside the building. This idea not only takes advantage of green noise control potential, but also improves architectural and other benefits mentioned above.

Another function of the green roof is sound insulation, as opposed to absorption. The best material for sound attenuation has high mass, low stiffness and high damping, such as sand (Connelly and Hodgson, 2008). However, using sand for insulation is not suitable because it is difficult to hold it in shape and the weight is too high for roof structure support. A green roof has the closest property to sand, but is easier to construct, lighter in weight, has better architectural purpose and can maintain building comfort. Therefore, using a green roof is better than using sand for noise insulation.

2.4.3 Building's energy saving

The other purpose of a green roof installation is to improve thermal comfort inside the building. It can be used as a passive cooling strategy in hot countries, and to increase thermal mass to reduce heat loss in many cold regions. Both advantages will be discussed and compared in this section.

For cooling efficiency, the green roof has the capability to reduce heat gain from solar radiation in summer and in hot climate regions. The roof covers the structure with leaves and soil. As a result, it will reduce room temperature, and therefore the energy used for cooling will also be reduced.

Liu and Minor (2005) presented the green roof performance by two different roofs. A reference roof was built from steel deck and thermal insulation, and compared with an extensive green roof. After measurement, it was found that a green roof can provide 70-90 percent better performance in reducing heat gain. According to researchers in Canada, they found that the extensive green roof can effectively decrease temperature in the membrane underneath. When compared with the reference roof, a green roof recorded only 18 out of 660 days, when the room temperature went above 30 degrees Celsius. On the other hand, the reference roof had 342 out of 660 days when the temperature went beyond 30 degree Celsius (Scholz-Barth and Tanner, 2004). The results are presented in table 2.5.

Table 2.5 Temperature in the waterproof membrane below a green roof over 660 days (Scholz-Barth and Tanner, 2004)

Temperature Greater Than	Reference Roof		Green Roof		Ambient	
	No. of Days	% of Days	No. of Days	% of Days	No. of Days	% of Days
86°F (30°C)	342	52	18	3	63	10
104°F (40°C)	291	44	0	0	0	0
122°F (50°C)	219	33	0	0	0	0
140°F (60°C)	89	13	0	0	0	0
158°F (70°C)	2	0.3	0	0	0	0

Source: National Research Council of Canada

Additionally, figure 2.13 shows the heat flow of a green roof compared with the reference roof in each month over two years. The most effective period is in spring and summer.

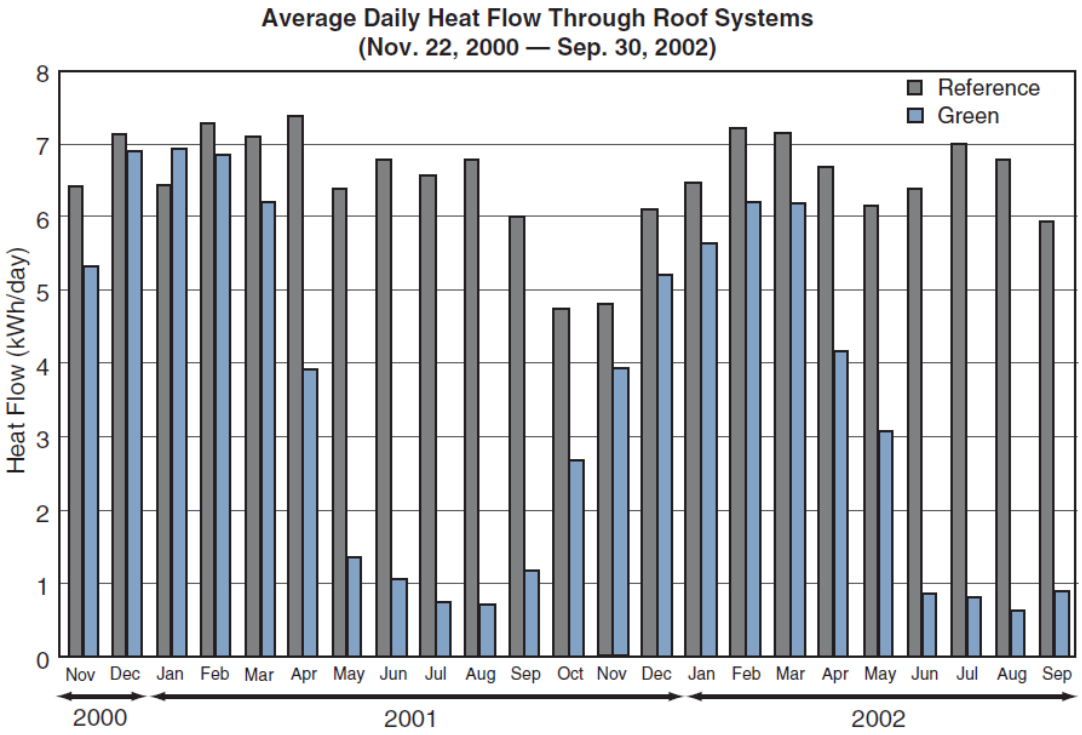

Measurements of heat flow show that average daily energy demand for the green roof was significantly less than that of the reference roof in spring and summer. (Source: National Research Council of Canada)

Figure 2.13 Heat flow over 24 months comparing the performance of a green and a reference roof (Scholz-Barth and Tanner, 2004)

Leaves have an important role to reduce solar radiation on the top of the roof, forming the structure known as a 'canopy'. The shading formed protects the soil from solar radiation absorption. The LAI (leaf area index) is an important parameter calculated

from total leaf surface per unit volume. Barrio (1998) suggested that selecting plants that have high LAI value and that grow in horizontal leaf distibution could limit solar radiation transmission between plant and soil by shading and reflecting from the leaf canopy. In addition, he found that canopy evapotranspiration, and air exchange between leaf and soil, have secondary effects in reducing heat flux on the roof. Consequently, heat that passes through the soil and the roof will decrease. Figure 2.14 describes this canopy structure and the heat transfer process.

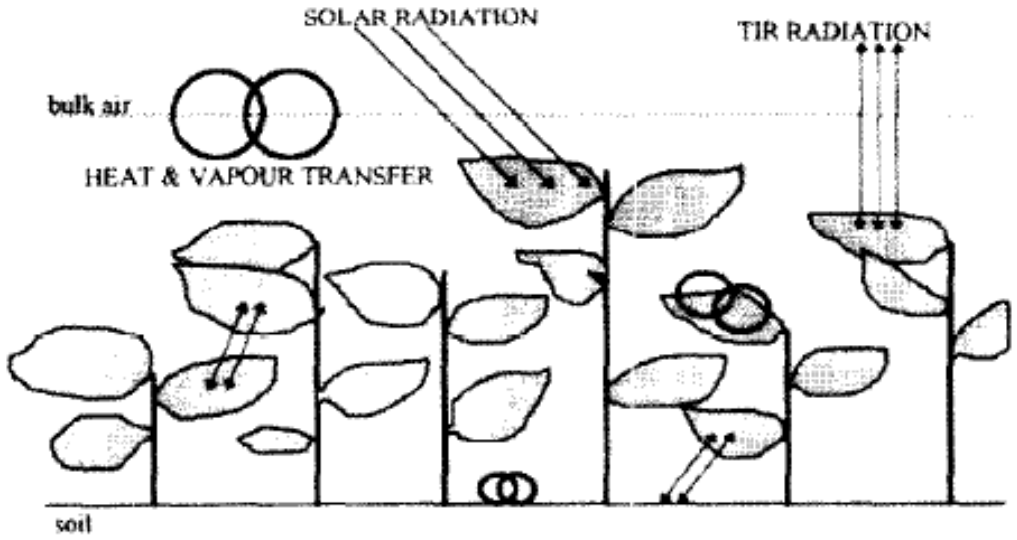

Figure 2.14 Canopy and heat transfer mechanism (Barrio, 1998). (TIR is a longwave radiative exchange)

Another part of a green roof that plays an important role in reducing heat gain is the substrate. It is not only a growing medium for vegetation, but also acts like insulation. The substrate can, in addition, improve the thermal mass for the roof. Different kinds of substrate give different values of thermal transmittance (a U-value). For example, in the real scale test under dynamic condition, the Rockwool substrate with 10 cm depth has a U-value equal to 0.38 W/m^2K whereas the same depth of perlite gave 0.651 W/m^2K (Kotsiris *et al*., 2012).

Furthermore, the other significant factor affecting the U-value is moisture content. Because the thermal conductivity of water is greater than air, it will increase the total U-value of the soil, due to water replacing the air voids between soil particles. Kotsiris *et al*. (2012) also found that the U-value of the 10 cm. deep perlite mixture substrate will increase when the moisture content increases, as shown in figure 2.15. As a consequence, if thermal conductivity increases the roof will gain more heat.

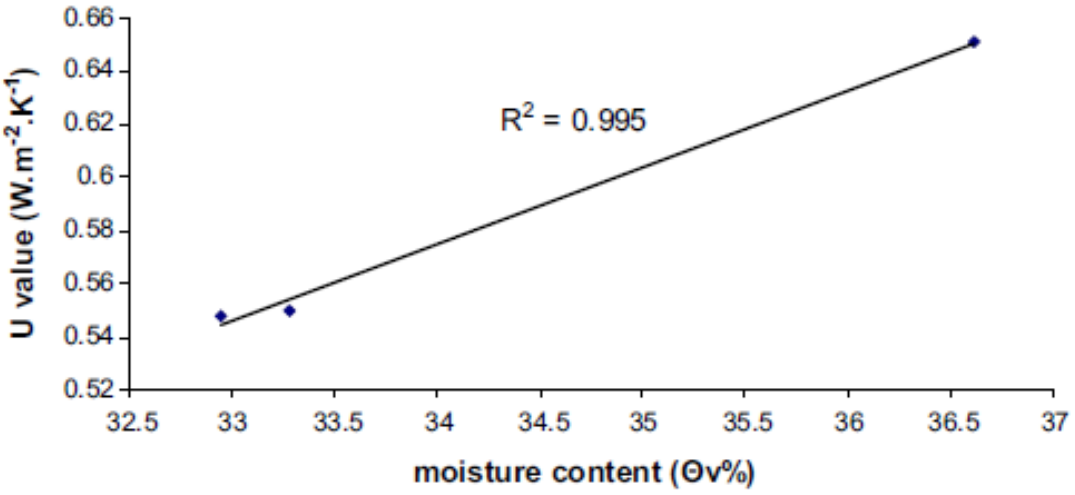

Figure 2.15 U-value of 10 cm. deep perlite mixture substrate in relation to moisture content (Kotsiris *et al*., 2012)

In winter, green roofs play an important role in thermal insulation, adding thermal mass. However, when compared with the cooling potential, a green roof's heating ability is considerably lower. Although the roof reduces an average of 75 percent of heat transfer in summer, it manages only 26 percent average on reducing heat transfer in winter (Scholz-Barth and Tanner, 2004).

From the aforementioned studies, it can see that green roofs have significant roles to play in reducing energy consumption. On the other hand, adding a green roof to a newly established building, which is already well insulated, will not bring about any significant changes in energy performance. According to building regulations in the UK, after 1965 insulation was required in every new building and the U-values of those buildings are equal to, or better than, green roofs. In other words, green roofs may have greater impact on old buildings rather than new ones. The use of green roofs in retrofitting old buildings would be a practical strategy for an energy saving option (Castleton *et al*., 2010).

2.4.4 Summary

So far, this chapter has reviewed the types of green roof construction and their performance as contributors to reducing the environmental impact of buildings, both newly constructed and retrofitted. It is now common for the energy performance of buildings to be simulated at the design stage, using an appropriate software package.

The remainder of this chapter therefore reviews the physics of thermal performance of green roofs, in order to set the context for the research described later in the thesis.

2.5 Green roof thermal simulation

Research investigations into the thermal performance of green roofs can be divided into three types: a) experimental measurements in the laboratory or field, b) theoretical analysis, and c) combination of the two.

At first, experimental thermal performance was measured by the heat flux reduction from the reference roof (normally a bare concrete roof), compared with the green roof in the same situation. As a result, the thermal resistance (R-value) was calculated by deducing the green roof's R-value from the layers in another roof assembly (Sonne, 2006, Wong *et al*., 2003). Wong et al. (2003) found that the green roof with a high Leaf Area Index (LAI) reduced the cooling energy required, and this factor became important for green roof simulation. The growing substrate is also important because the researchers found that a green roof with wet soil had a lower cooling efficiency than dry soil because it has a lower R-value (Wong *et al*., 2003). However, this model did not consider the effect of evaporation from wet soil, which could result in more heat loss from the roof. For this reason, researchers have been studying this important phenomenon and trying to explain it by numerical methods.

The plant respiration and soil evaporation are unique features of a green roof, both of which affect thermal transfer by latent heat removal on foliage and substrate surfaces. This issue was studied by Balick *et al*. (1981) and Deardorff (1978) to evaluate ground surface temperature when vegetation is present. These models were later developed by Frankenstein and Koenig (2004a) into the FASST soil and vegetation model, by using the energy balance method. After the development of building energy simulation software, those theories were applied in the EnergyPlus simulation software. The software included the effects of short and long-wave solar radiation, interlayer long-wave emission, sensible heat flux from wind, and finally latent heat flux from plant respiration in an unsteady state condition (Sailor, 2008).

The evapotranspiration calculations in the former green roof models were calculated by using the Bowen ratio or a convective mass transfer coefficient, ignoring stomata and substrate resistance (GRO, 2011, Poë *et al*., 2011, He and Jim, 2010). This ratio is very convenient to use in any green roof model, but it is useable only if evapotranspiration is not directly related to water content. To satisfy this requirement, it is assumed that the green roof is well irrigated (Tabares-Velasco, 2012).

On the other hand, most modern evapotranspiration models use the Vapour Pressure Deficit (VPD) method (Barrio, 1998, Lazzarin *et al*., 2005, Sailor, 2008, Alexandri and Jones, 2007). The VPD method takes the difference between the moisture present in the air and the amount that the air can hold when saturated. Nevertheless, each model uses a different function of the resistance in order to calculate evapotranspiration of a foliage layer, such as wind correlation and vapour resistance. This method was applied to the latent heat flux calculation.

The next section will review the energy budget method that is used in many green roof simulations.

2.5.1 Energy budget at foliage layer

According to its non-homogenous structure, this method requires a roof to be divided into two separate layers: the foliage layer and the substrate layer (The substrate layer will be discussed in the next section). The equations for each layer are then combined to get one final equation.

The idea of the energy budget method in the foliage layer is to balance between absorbed shortwave and longwave solar heat flux, the emitted longwave heat flux, the sensible heat flux, the latent heat flux and precipitation heat flux (Frankenstein and Koenig, 2004a). These heat fluxes need to be considering in each time step. The energy budget equation between foliage and atmosphere is given in equation 2.1.

$$F_f = 0 = \sigma_f\left[I_s^{\downarrow}\left(1-\alpha_f\right) + \varepsilon_f I_{ir}^{\downarrow} - \varepsilon_f \sigma T_f^4\right] + \frac{\sigma_f \varepsilon_f \varepsilon_g \sigma}{\varepsilon_1}\left(T_g^4 - T_f^4\right) + H_f + L_f \qquad (2.1)$$

Where; F_f is net heat flux to the foliage layer (W/m^2),

σ_f is fractional vegetation coverage,

$I_s^{\downarrow}$ is total incoming short-wave radiation (W/m^2),

$I_{ir}^{\downarrow}$ is total incoming long-wave radiation (W/m^2),

α_f is albedo of the plant canopy,

ε_f is emissivity of plant canopy,

ε_g is emissivity of ground surface,

$\varepsilon_1 = \varepsilon_f + \varepsilon_g - \varepsilon_f \varepsilon_g$,

σ is the Stefan-Boltzmann constant (5.67 x 10^{-8} W/m^{2}K^4),

T_f is foliage temperature (K),

T_g is ground temperature (K),

H_f is foliage sensible heat flux (W/m^2),

L_f is foliage latent heat flux (W/m^2).

Each term in equation 2.1 will be explained respectively in the following section.

Shortwave and longwave radiation

The first mechanism in this layer is absorbed and reflected solar radiation heat fluxes. The vegetation reflected shortwave solar radiation is given by $I_s^{\downarrow}\alpha_f$. However, this layer consists of a vegetation covering that diverges according to the types of plants. For this reason, the foliage fractional coverage σ_f and foliage Leaf Area Index (LAI) were presented to make the energy budget equation more accurate. The foliage fractional coverage is the ability of vegetation to shade the ground from sun light, whereas the Leaf Area Index is calculated from leaves overlapping each other. Ramirez and Senarath (2000) developed equations for σ_f and LAI, in which both variables can be estimated by equations and definitions below.

$$\sigma_f = 1 - \exp(-0.75LAI) \qquad \text{For grasses}$$

$$\sigma_f \begin{cases} \sigma_{f,max} & \text{For other vegetation } T_g > 298 \text{ K} \\ \sigma_{f,min} & T_g < 298 \text{ K} \\ \sigma_{f,max} - \left[1 - F(T_g)\right]\left[\sigma_{f,max} - \sigma_{f,min}\right] & 273.15 \leq T_g \leq 298 \text{ K} \end{cases}$$

And

$$LAI = LAI_{min} + F(T_g)[LAI_{max} - LAI_{min}] \tag{2.2}$$

$$F(T_g) = 1.0 - 0.0016\left[298.0 - T_g\right]^2 \tag{2.3}$$

Some properties of low vegetation were reported by (Yang *et al*., 1998) and that data is presented in table 2.6 below.

Table 2.6 Low vegetation properties (Yang *et al*., 1998)

Biome	high/medium /low	$\sigma_{f\,max}$ (%)	$\sigma_{f\,min}$ (%)	LAI_{max} (m^2/m^2)	LAI_{min} (m^2/m^2)	SAI_{min} (m^2/m^2)
crop	m	85	25	6.0	0.5	0.5
short grass	l	80	70	2.0	0.5	4.0
tall grass	m	80	50	6.0	0.5	2.0
desert	l	5	0	2.0	0.0	0.5
tundra	m	60	40	6.0	0.5	0.5
irrigated crops	m	80	20	6.0	0.5	0.5
semidesert	m	10	0	6.0	0.5	2.0
bog/marsh	l	80	40	6.0	0.5	2.0
evergreen shrub	h	80	60	6.0	5.0	2.0
deciduous shrub	h	80	50	6.0	1.0	2.0

Including the foliage fraction, the reflected shortwave radiation by vegetation will be $\sigma_f I_s^{\downarrow} \alpha_f$. In the energy budget theory, only the absorbed shortwave radiation is considered in this equation. Consequently, the absorbed shortwave radiation by the foliage layer is rearranged by $\sigma_f I_s^{\downarrow}(1 - \alpha_f)$.

The other absorbed solar radiation is longwave or infrared radiation absorption, calculated by the foliage longwave emissivity ε_f, assuming this emissivity is equal to the longwave absorptivity. Similar to shortwave radiation flux, the infrared radiation flux in this layer is given as $\varepsilon_f \sigma_f I_{ir}^{\downarrow}$ where $0.90 \leq \varepsilon_f \leq 0.96$ and ε_f varies linearly between these values according to $\varepsilon_f = 0.90 + F(T_g)[0.96 - 0.90]$ (Frankenstein and Koenig, 2004a).

While the object is absorbing solar radiation, some energy is released back into the atmosphere by longwave emission. The foliage layer shares similarities with a black body, so an infrared emission can be calculated by $-\varepsilon_f \sigma_f \sigma T_f^4$. The minus sign in this equation represents the loss of energy. For the first time step, in addition, Frankenstein and Koenig (2004a) suggested that T_f should be set equal to $0.9T_a$ in order to calculate this value, where $T_a$is the surrounding air temperature.

Shortwave absorption, infrared absorption and infrared emission are combined together to get the first term of the foliage-atmosphere energy balance equation 2.1. This is expression 2.4.

$$\sigma_f I_s^{\downarrow}(1 - \alpha_f) + \varepsilon_f \sigma_f I_{ir}^{\downarrow} - \varepsilon_f \sigma_f \sigma T_f^4 \tag{2.4}$$

Then the foliage fractional coverage is subtracted, so creating expression 2.5, which is the first term in equation 2.1.

$$\sigma_f\left[I_s^{\downarrow}(1-\alpha_f)+\varepsilon_f I_{ir}^{\downarrow}-\varepsilon_f\sigma T_f^4\right] \tag{2.5}$$

Interlayer radiation exchange

The interlayer radiation exchange is the emission between two layers, which in this case are the foliage layer and substrate surface layer obtained by the multi-reflection method. During the emission process, a foliage layer absorbs heat from a ground layer then reflects that heat back to a ground layer again. This process is called multiple reflection.

By assuming that longwave emissivity is equal to the longwave absorptivity, the reflectance can be defined as $R=(1-\varepsilon)$. As a result, the foliage reflectance is $R_f=(1-\varepsilon_f)$ and the ground reflectance is $R_g=(1-\varepsilon_g)$.

Considering the emission from the ground, the top of a low foliage layer absorbs a total emitted heat flux, as described in figure 2.16.

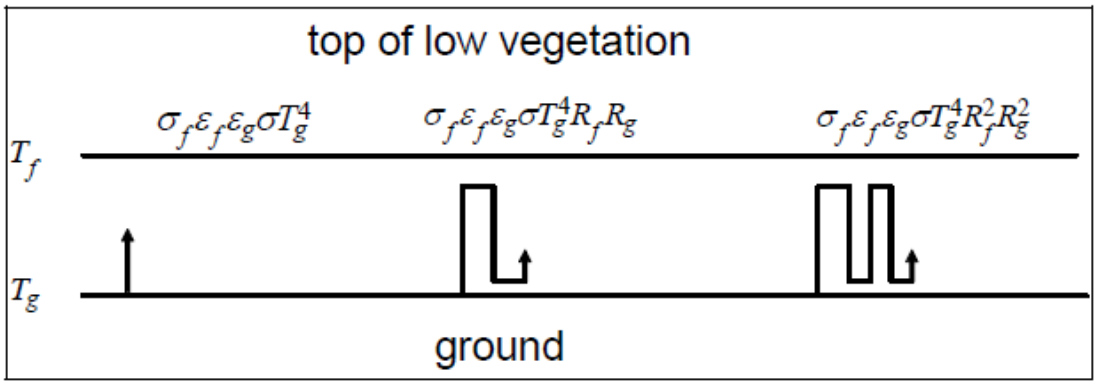

Figure 2.16 Heat flux from multiple reflection from ground surface (Frankenstein and Koenig, 2004a)

The summation of absorbed heat flux for the foliage layer is given by expression 2.6.

$$\sigma_f\varepsilon_f\varepsilon_g\sigma T_g^4(1+R_fR_g+R_f^2R_g^2+\cdots) \tag{2.6}$$

Because $R_g\leq 1$ and $R_f\leq 1$, the expression is transformed to

$$\sigma_f\varepsilon_f\varepsilon_g\sigma T_g^4\left(1-R_fR_g\right)^{-1} \tag{2.7}$$

On the other hand, if considering the emission from the foliage layer, the top of that layer also absorbs the total emitted heat flux from the ground, described in figure 2.17.

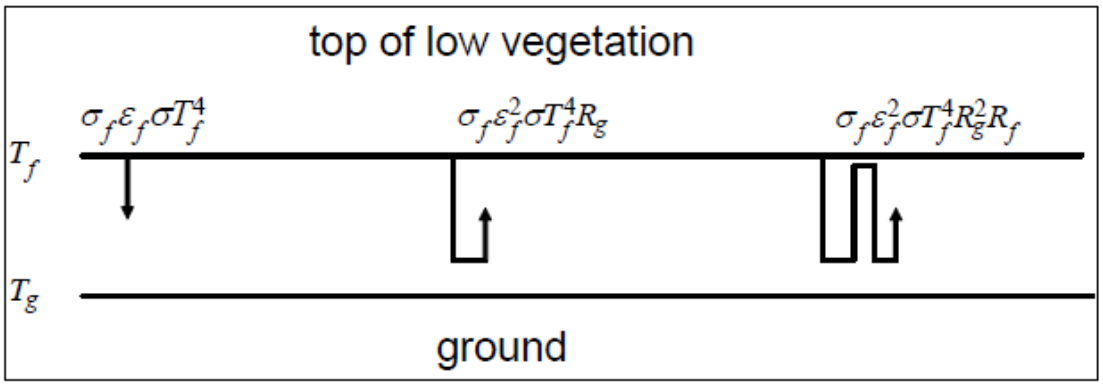

Figure 2.17 Heat flux from multiple reflection from vegetation surface (Frankenstein and Koenig, 2004a)

Similarly, summation of the absorbed heat flux for the foliage layer is given as

$$\sigma_f \varepsilon_f^2 \sigma T_f^4 R_g \left(1 + R_f R_g + R_f^2 R_g^2 + \cdots\right) - \sigma_f \varepsilon_f \sigma T_f^4 \tag{2.8}$$

Because of $R_g \leq 1$ and $R_f \leq 1$, the expression 2.8 is transformed to

$$\sigma_f \varepsilon_f^2 \sigma T_f^4 R_g \left(1 - R_f R_g\right)^{-1} - \sigma_f \varepsilon_f \sigma T_f^4 \tag{2.9}$$

With a mathematical manipulation, the expression 2.9 reduces to

$$-\frac{\sigma_f \varepsilon_f \varepsilon_g \sigma T_f^4}{1 - R_f R_g} \tag{2.10}$$

Combining absorbed heat flux from the ground with that from the foliage layer, to obtain total emission heat flux in the foliage layer, gives expression 2.11, which is the second term of equation 2.1.

$$\frac{\sigma_f \varepsilon_f \varepsilon_g \sigma}{\varepsilon_1} \left(T_g^4 - T_f^4\right) \tag{2.11}$$

Where, $\varepsilon_1 = \varepsilon_f + \varepsilon_g - \varepsilon_f \varepsilon_g$, as before

The ground emissivity (ε_g) depends on soil type and varies between 0.92 and 0.97.

Sensible heat flux

Sensible heat transfer in this layer is the energy exchange between the foliage and the surrounding air that results in changing temperature. Deardorff (1978) suggested the sensible heat flux in this layer by equation 2.12.

$$H_f = \left(e_0 + 1.1LAI\rho_{af}c_{p,a}C_fW_{af}\right)\left(T_{af} - T_f\right) \quad (2.12)$$

Where;

e_0 is the windless exchange coefficient for sensible heat (2.0 W/m^2),

C_f is the bulk transfer coefficient,

T_{af} is air temperature in a foliage (Kelvin),

W_{af} is wind speed at the air and foliage interface (m/s),

$c_{p,a}$ is specific heat of air at constant pressure (1005.6 J/kg.K).

The air density in the air/foliage interface ρ_{af} (kg/m^3) is the average of the air density (ρ_a) and air inside foliage density (ρ_f).

$$\rho_{af} = \frac{\rho_a + \rho_f}{2}$$

The density of air and foliage can be calculated by the ideal gas law ($\rho = \frac{P}{RT}$) where *P* is the measured atmospheric pressure *(P_a= 101.325 x 10^3 Pa)* and *R* is the gas constant of the air, equal to 287.058. For the air density, the air temperature is measured at the shelter height Z_a (m) (Kotsiris *et al*., 2012). For the air in the foliage, on the other hand, it cannot be measured in the first time step. For this reason, in order to calculate this value T_f is set to $0.9T_a$ in the initial time step (Deardorff, 1978).

Air temperature inside the foliage (T_{af}) is calculated by equation 2.13.

$$T_{af} = \left(1 - \sigma_f\right)T_a + \sigma_f\left(0.3T_a + 0.6T_f + 0.1T_g\right) \quad (2.13)$$

C_f is the bulk transfer coefficient calculated by equation 2.14.

$$C_f = 0.01\left(1 + \frac{0.3}{W_{af}}\right) \quad (2.14)$$

Where W_{af} is the wind speed in the foliage, as modelled by equation 2.15;

$$W_{af} = 0.83\sigma_f W' \sqrt{C_{hn}^f} + (1 - \sigma_f)W' \tag{2.15}$$

W' is the wind speed; if W is less than 2.0 m/s, W' will be set equivalent to 2.0 m/s for maintaining ambient wind speed. In addition, C_{hn}^f is the bulk transfer coefficient at the top of vegetation, which is used to indicate the transfer momentum between the atmosphere and the foliage. It can be calculated by equation 2.16.

$$C_{hn}^f = \left[k/ln\left(\frac{Z_a - Z_d}{z_0^f}\right)\right]^2 \tag{2.16}$$

The roughness length z_0^f (m) is the height where the average wind speed $\overline{u(z)}$ (m/s) goes to zero, for which some typical data are presented in table 2.7.

Table 2.7 Stomata resistance and roughness length of foliage (Frankenstein and Koenig, 2004a)

Biome	$r_{s,min}$ (s/m)	z_0^f (m)
crop	120	0.06
short grass	200	0.02
tall grass	200	0.1
desert	200	0.05
tundra	200	0.04
irrigated crops	200	0.06
semidesert	200	0.1
bog/marsh	200	0.03
evergreen shrub	200	0.1
deciduous shrub	200	0.1

The zero displacement height Z_d (m) is the height at which the logarithmic wind profile starts to displace upwards after reaching zero, when foliage is present. Balick *et al*. (1981) gave an equation for the zero displacement height and also recommended that if Z_0^f is greater than 0.02 m, the roughness length can be estimated by his equations (2.17 and 2.18).

$$Z_d = 0.701 Z_f^{0.975} \tag{2.17}$$

$$Z_0^f = 0.131 Z_f^{0.997} \tag{2.18}$$

Z_f is the vegetation height: typical values of low, medium and high vegetation are listed in table 2.8.

Table 2.8 Low vegetation model (Frankenstein and Koenig, 2004a)

Variable	low	medium	high
$(1-\sigma_f)_{min}$	0.7	0.7	0.7
$(1-\sigma_f)_{max}$	0.85	0.85	0.85
$Z_{f,min}$ (cm)	5	35	85
$Z_{f,max}$ (cm)	50	60	85
$r_{s,max}$ (s/m)	500	500	500

Because of the range between minimum and maximum values, exact values of these variables are calculated by function of ground temperature (T_g) in equation 2.19.

$$Variable = Variable_{max} - (1.0 - f)(Variable_{max} - Variable_{min}) \quad (2.19)$$

Where; $f = 1.0 - 0.016\left[298.0 - T_g\right]^2$.

H_f, as defined in this discussion (equation 2.12), is the sensible heat flux in the foliage layer and is the third term in equation 2.1.

Latent heat flux

The latent heat flux (the final term in equation 2.1) is the heat exchange between the vegetation and the nearby atmosphere for changing phase without altering the temperature, such as evaporation of water and sublimation of ice. This heat flux is calculated by equation 2.20 given by Deardorff (1978)

$$L_f = LAI\rho_{af}C_f l W_{af} r''\left(q_{af} - q_{f,sat}\right) \quad (2.20)$$

The l in this equation is either the latent heat of evaporation (l_{evap}) or sublimation (l_{sub}= 2.838x10^6 J/kg). The latent heat of evaporation depends on the air and ground surface temperature, which can be calculated by equation 2.21.

$$l_{evap} = 2{,}500{,}775.6 - 2369.723\left[\frac{T_a - T_g}{2} - 273.15\right] \quad (2.21)$$

The bulk transfer coefficient (C_f), the wind speed at the air/foliage interface (W_{af}) and the air density in foliage (ρ_{af}) are those used in the sensible heat flux calculation.

The foliage surface wetness factor (r'') represents a function of the air and stomata resistance to vapour diffusion.

$$r'' = \frac{r_a}{r_a + r_s} \tag{2.22}$$

r_a is the atmospheric resistance to water vapour diffusion given by equation 2.23.

$$r_a = \frac{1}{C_f W_{af}} \tag{2.23}$$

r_s is the stomata resistance to water vapour diffusion suggested by (Chen *et al*., 1996)

$$r_s = \frac{r_{s,min}}{LAI} f_1 f_2 f_3 \tag{2.23}$$

Where

$$\frac{1}{f_1} = min\left[1, \frac{0.004 I_s^{\downarrow} + 0.005}{0.81\left(0.004 I_s^{\downarrow} + 1\right)}\right]$$

$$\frac{1}{f_2} = \begin{cases} 0 & \theta_r > \bar{\theta} \; or \; \bar{\theta} > \theta_{max} \\ \dfrac{\bar{\theta} - \theta_r}{\theta_{max} - \theta_r} & \theta_r \leq \bar{\theta} \leq \theta_{max} \end{cases}$$

$$\frac{1}{f_3} = exp\left(-g_D\left[e_{f,sat} - e_a\right]\right)$$

θ_r and θ_{max} are residual and maximum soil moisture content (m^3/m^3) depending on different soil types.

In order to calculate thermal transfer in the unsteady state condition of green roofs, some assumptions are needed to reduce difficulties in modelling:

- A green roof foliage and substrate layer are horizontally homogeneous
- The horizontal length of a green roof is much greater than its vertical depth and the horizontal heat transfer is negligible, in order to simplify the models to handle one-dimensional heat transfer
- The air under the stomata (foliage layer) is always saturated
- Any heat flux during biochemical photosynthesis reactions is negligible

- Conduction heat transfer does not occur in the foliage layer
- A foliage layer is irrigated, fully grown and completely covers the substrate layer
- There is homogenous distribution of water in the canopy

With these assumptions, together with available information on the relevant parameters, the heat flux in the foliage layer can be calculated by using equation 2.1 mentioned earlier. The next section will consider the energy budget theory in the substrate surface.

2.5.2 Energy budget at substrate layer

The substrate energy budget is influenced by the substrate thermal property and the covering from the vegetation canopy. However, the model ignores the change of vertical moisture transport in the substrate layer (Sailor, 2008).

From (Frankenstein and Koenig, 2004a) the energy balance at the substrate surface is given by equation 2.24. This is analogous to equation 2.1.

$$F_g = (1-\sigma_f)\left[I_s^{\downarrow}(1-\alpha_g) + \varepsilon_g I_{ir}^{\downarrow} - \varepsilon_g \sigma T_g^4\right] - \frac{\sigma_f \varepsilon_g \varepsilon_f \sigma}{\varepsilon_1}\left(T_g^4 - T_f^4\right) + H_g + L_g + \left(K \times \frac{\partial T_g}{\partial z}\right) \quad (2.24)$$

Where:

F_g is net heat flux to the substrate surface (W/m^2),

α_g is albedo of the substrate surface,

H_g is the substrate sensible heat flux (W/m^2),

L_g is the substrate latent heat flux (W/m^2),

K is the thermal conductivity (W/m.K),

z is the depth of the substrate (m).

The other variables have been defined previously.

Shortwave and longwave radiation

The first term of equation 2.24 is the shortwave and longwave solar radiation. Despite the foliage layer, this solar radiation into the substrate surface is the remaining radiation from the foliage covering, as indicated by $(1-\sigma_f)$ in the front of the first term.

By subtracting the foliage fraction, the reflected shortwave radiation by the substrate surface will be $(1-\sigma_f)I_s^{\downarrow}\alpha_g$. In the energy budget, only the absorbed shortwave radiation is considered in this equation. Therefore, the absorbed shortwave radiation by foliage layer is rearranged by $(1-\sigma_f)I_s^{\downarrow}(1-\alpha_g)$, where $0.23 \leq \alpha_g \leq 0.40$ depending on substrate type.

The longwave solar radiation is calculated by the substrate longwave emissivity ε_g, assuming this emissivity is equal to the longwave absorptivity. Similarly to the shortwave radiation flux, the infrared radiation flux in this layer is given as $(1-\sigma_f)\varepsilon_g I_{ir}^{\downarrow}$ where $0.92 \leq \varepsilon_g \leq 0.97$ depending on substrate type (Frankenstein and Koenig, 2004a).

While the substrate surface is absorbing solar radiation, some energy is released back to the atmosphere by longwave emission. The substrate layer is like a black body, so an infrared emission can be calculated by $-(1-\sigma_f)\varepsilon_g\sigma T_g^4$. The minus sign in this equation represents the loss of energy.

Shortwave absorption, infrared absorption and infrared emission are combined together to get the first term of the substrate surface energy balance (equation 2.24).

$$(1-\sigma_f)\left[I_s^{\downarrow}(1-\alpha_g)+\varepsilon_g I_{ir}^{\downarrow}-\varepsilon_g\sigma T_g^4\right] \tag{2.25}$$

Interlayer radiation exchange

The energy loss due to the interlayer reflection, between the substrate surface and foliage layer in the substrate surface energy balance equation, is the same as the foliage energy balance equation mentioned earlier. This is the second term in equation 2.24.

Sensible heat flux

Sensible heat transfer in the substrate surface layer is the energy exchange between the substrate and the surrounding air that results in changing temperature. This heat flux

depends upon the temperature difference and the wind speed over the layer, which can be written as equation 2.26.

$$H_g = \rho_{ag} C_{p,a} C_{hg} W_{af} \left(T_{af} - T_g\right) \tag{2.26}$$

The ρ_{ag} is the density of the air near the substrate surface (kg/m^3), which is the average of the density of air at the substrate surface temperature (ρ_a) and the density at the surrounding air temperature (ρ_a).

$$\rho_{ag} = \frac{\rho_a + \rho_g}{2}$$

The C_{hg} is the bulk transfer coefficient, which is given by linear combination of the bulk transfer coefficient near the ground (C_{hng}) and near the foliage-atmosphere interface (C_{hnf}), multiplied by stability factor (Γ_h). The equation 2.27 represents the bulk transfer coefficient.

$$C_{hg} = \Gamma_h \left[\left(1 - \sigma_f\right) C_{hng} + \sigma_f C_{hnf}\right] \tag{2.27}$$

The bulk transfer coefficient near the ground and near the foliage-atmosphere interface can be calculated by equations 2.28 and 2.29.

$$C_{hng} = r_{ch}^{-1} \left[\frac{K_v}{\ln(Z_a / Z_{o,g})}\right]^2 \tag{2.28}$$

$$C_{hnf} = \left[\frac{K_v}{\ln(Z_a - Z_d / Z_{o,f})}\right]^2 \tag{2.29}$$

Where: $Z_{o,g}$ is the roughness length of the substrate,

$Z_{o,f}$ is the roughness length of the foliage,

K_v is the von Karman constant (0.4), and

r_{ch} is the turbulent Schmidt number (0.63).

The atmospheric stability factor is based on the sign of the bulk Richardson number (R_{ib}), as shown in equation 2.30.

$$\Gamma_h = \begin{cases} \dfrac{1.0}{(1.0 - 16.0R_{ib})^{0.5}} & \text{For } R_{ib} < 0 \\ \dfrac{1.0}{(1.0 - 5.0R_{ib})} & \text{For } R_{ib} > 0 \end{cases} \quad (2.30)$$

Where, R_{ib} is determined from equation 2.31.

$$R_{ib} = \frac{2gZ_a(T_{af} - T_g)}{(T_{af} + T_g)W_{af}^2} \quad (2.31)$$

H_g, defined in this way, it the third term in equation 2.24.

Latent heat flux

The latent heat flux in the substrate surface (the final term in equation 2.24) is the heat exchange between the substrate and the nearby atmosphere for changing phase without altering the temperature, such as removal of water vapour from the surface. This heat flux depends on the difference between the mixing ratio of the substrate and air, and the wind speed, which can be presented by equation 2.32.

$$L_g = C_{e,g} l_g W_{af} \rho_{ag} (q_{af} - q_g) \quad (2.32)$$

$C_{e,g}$ is the bulk transfer coefficient for latent heat transfer, which corresponds to the bulk transfer coefficient for sensible heat transfer. Equation 2.33 gives the bulk transfer coefficient for latent heat transfer.

$$C_{hg} = \Gamma_e \left[(1 - \sigma_f) C_{eng} + \sigma_f C_{hnf} \right] \quad (2.33)$$

Where Γ_e is the latent heat transfer stability correction factor, which is assumed to be equal to the sensible heat transfer stability correction factor (Γ_h),

C_{eng} is the near ground bulk transfer coefficient for latent heat flux,

l_g is latent heat of vaporisation at ground temperature (J/kg),

q_{af} is the mixing ratio between foliage and atmosphere, and

q_g is the mixing ratio at the substrate surface, which can be calculated by equation 2.34.

$$q_g = M_g q_{g,sat} + (1 - M_g) q_{af} \quad (2.34)$$

Where; M_g is the moisture saturation factor.

Conduction heat flux

The energy budget theory describes in detail the heat flux through the foliage layer by, the thermal conductivity (K) of the substrate layer is assumed to be homogeneous throughout the layer, and the changing of heat flux due to the vertical water transport is ignored (Frankenstein and Koenig, 2004a, Sailor, 2008). As a result, the term $K\frac{\partial T_g}{\partial z}$ changes with the temperature difference and the thermal conductivity of the whole substrate layer.

Furthermore, the function in the EnergyPlus simulation assumes a green roof to be well irrigated at times when there is no precipitation over the roof. As a result, the thermal conductivity of the substrate layer is taken to be that in the saturated condition.

2.5.3 Reviewing the agreement between theory and experiment

The comparison between calculated and measured results of the green roof thermal simulation is presented in this section in order to demonstrate the accuracy of current simulation tools.

For the energy budget theory used in the EnergyPlus simulation, many studies develop their models based on this theory (Sailor, 2008, Djedjig *et al.*, 2012, Chan and Chow, 2013, Ouldboukhitine *et al.*, 2012). Their measurements considered the temperature at the foliage layer and the substrate surface, which are demonstrated by Sailor (2008) in figure 2.18.

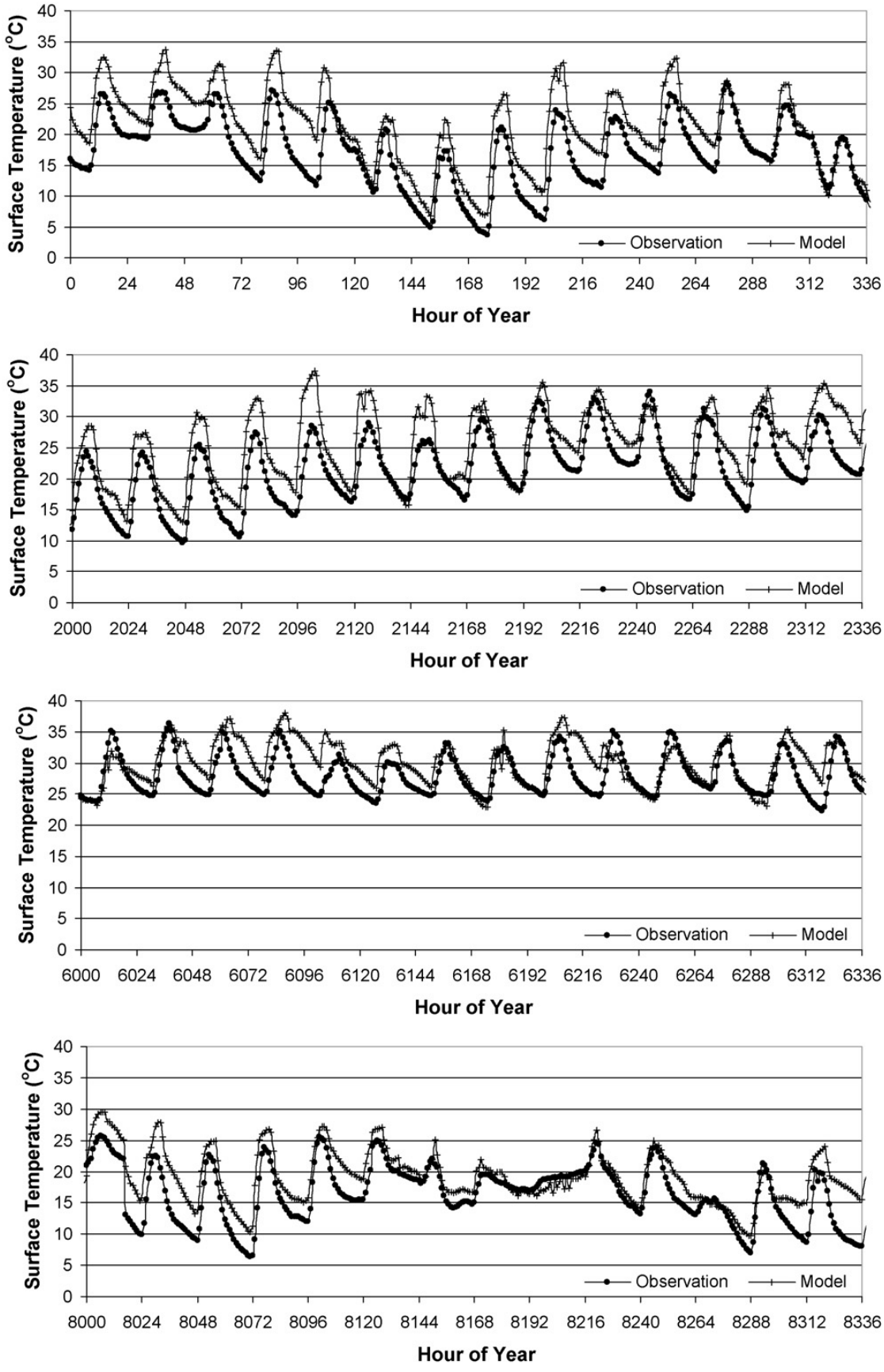

Figure 2.18 Green roof module predictions as compared to measured substrate surface temperatures for green roofs at the University of Central Florida test site. The figure panels represent 2 weeks of hourly data within each of 4 seasons. (Sailor, 2008)

Figure 2.18 compares the substrate surface temperature between the measured result and the result obtained from the green roof module. Sailor (2008) demonstrated that the average bias of this simulation is 2.9^{o}C with the root mean square error equal to 4.1^{o}C. He believed that this bias came from inadequate information such as the Leaf area index and stomata resistance.

Later on, Chan and Chow (2013) investigated the green roof performance in Hong Kong with the intention to create the overall thermal transfer value (OTTV) for the green roof energy consumption. The physical properties of plants used in their green roof were well defined (plant species, plant height, leaf area index, leaf reflexivity, and fractional coverage). The comparison between the measured and simulated surface temperature on this green roof is presented in the figure 2.19.

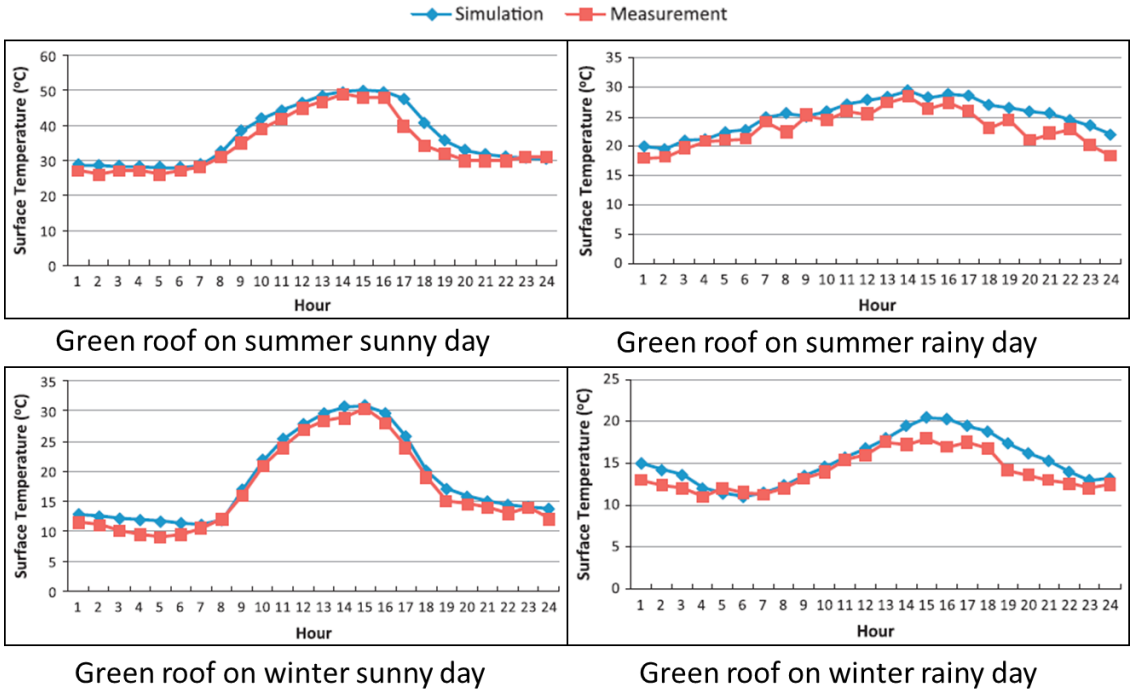

Figure 2.19 Validation of measurement data and simulation data of green roof surface temperature on different season and condition (Chan and Chow, 2013)

From figure 2.19, the comparison between measured and simulated data of green roof surface temperature shows better accuracy than Sailor (2008)'s study. The comparison in the summer day shows the mean bias error of 2.3-2.7^{o}C (2.4-3.0^{o}C for the root mean square error) on the sunny day, and 1.9-2.4^{o}C (2.3-2.7^{o}C for the root mean square error) on the rainy day. For the winter measurement, the surface temperature comparison shows the mean bias error of 1.6-1.9^{o}C (1.5-2.1^{o}C for the root mean square error) for the winter sunny day and 2.2-2.5^{o}C (2.4-2.7^{o}C for the root mean square error) for the

winter rainy day. In addition, the figure 2.20 presents the comparison of heat flux through the green roof.

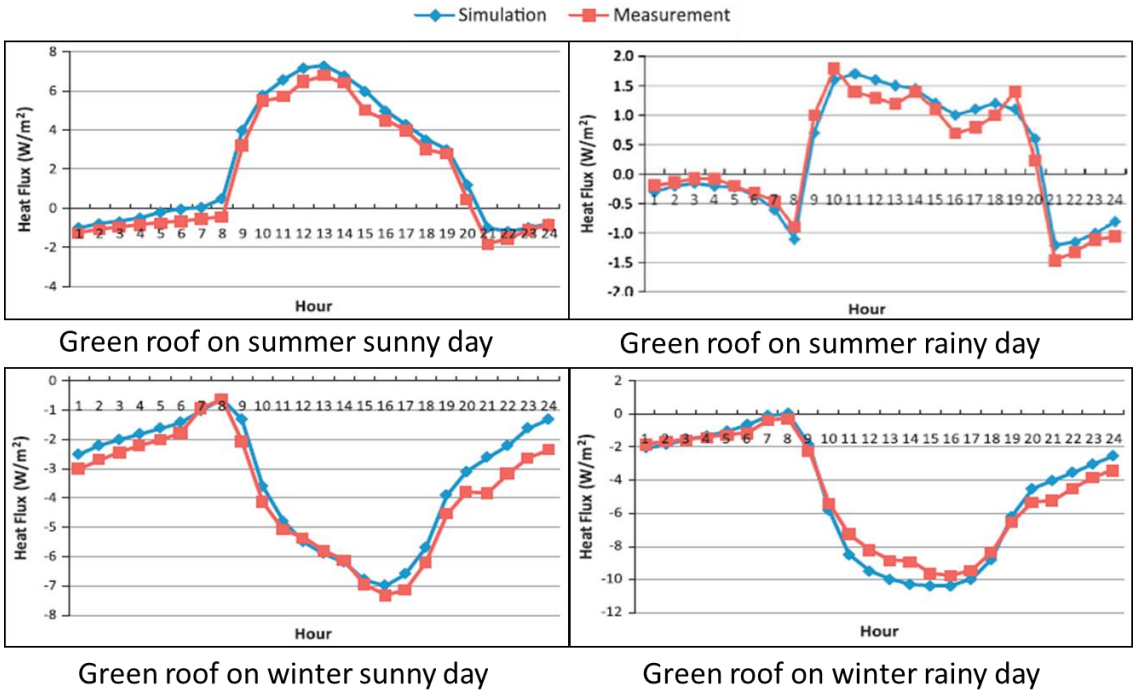

Figure 2.20 Validation of measurement data and simulation data of heat flux through green roof on different season and condition (Chan and Chow, 2013)

The hourly heat flux through the green roof was measured and simulated in figure 2.20. The mean bias error between measurement and simulation is 0.23-0.57 W/m^2 (with 0.34-0.62 W/m^2 root mean square error) for the summer sunny day, and the mean bias error is 0.18-0.49 W/m^2 (with 0.21-0.65 W/m^2 root mean square error) for the summer rainy day. The mean bias error between measurement and simulation is 0.29-0.58 W/m^2 (with 0.36-0.62 W/m^2 root mean square error) for the winter sunny day, and the mean bias error is 0.15-0.27 W/m^2 (with 0.47-0.72 W/m^2 root mean square error) for the winter rainy day.

Although this study (Chan and Chow, 2013) shows the better accuracy than the previous work from Sailor (2008), the condition of green roof in this study was the partial set-up condition, which irrigation scheduled at 10:00 am and 3:00 pm every day. With this setting, the moisture content in the substrate varies from 22-23.3% in the winter sunny day, to 24-26.8% in the winter rainy day, and from 20.1-21.7% in the summer sunny day, to 23-25.1% in the summer rainy day. For this reason, this study may not be accurate for the green roof under normal operating conditions.

The other study developed from the energy budget theory is from Djedjig *et al*. (2012). They simulated and monitored the green roof substrate temperature at a depth of 2 cm below the surface at the University of La Rochelle, which is presented in figure 2.21.

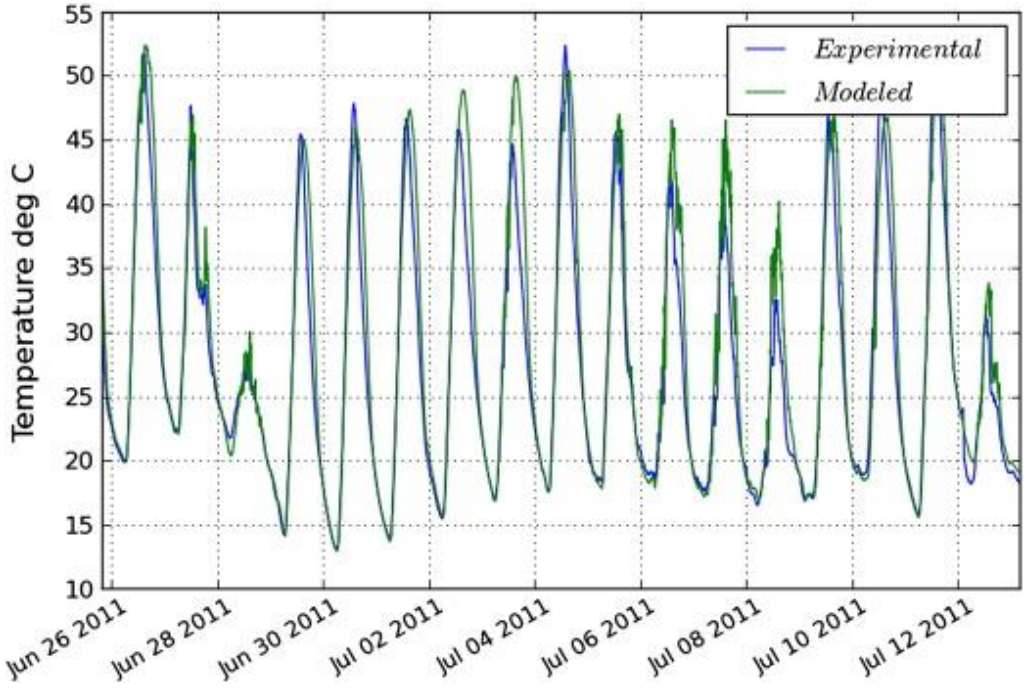

Figure 2.21 Comparison between the numerical and the experimental temperature results at a depth of 2 cm below the substrate surface (Djedjig *et al*., 2012)

According to figure 2.21, Djedjig *et al*. (2012) estimated that their model had 0.8^{o}C for the mean difference between simulated and measured result, and 80% of the computed temperatures were close to the measurement temperature with a ±10% relative precision. In addition, the moisture content of the substrate at 2 cm depth below the surface was monitored and simulated by a numerical method as shown in figure 2.22.

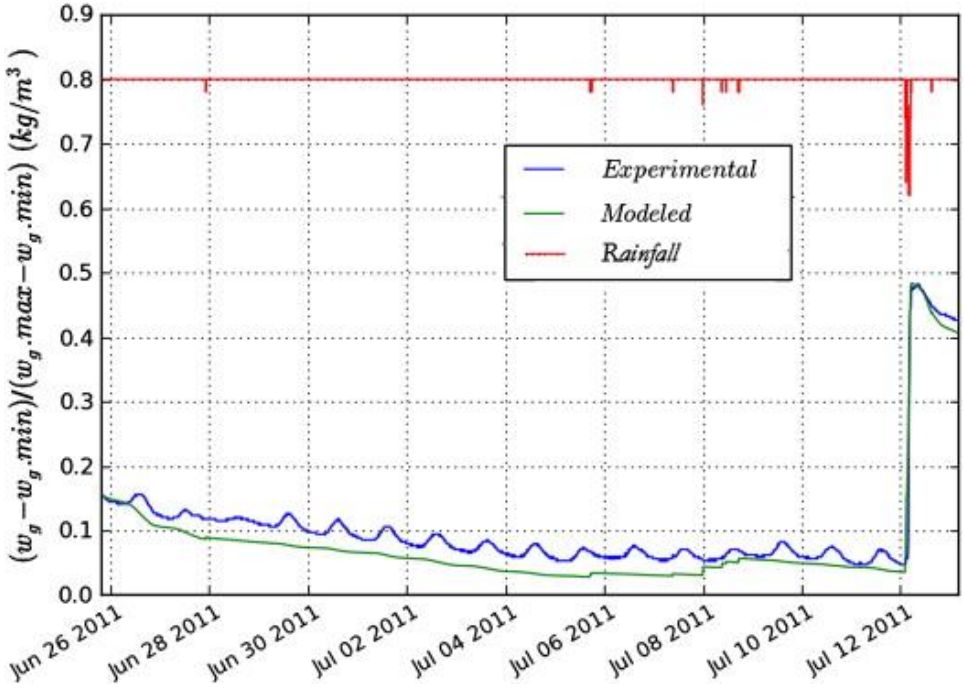

Figure 2.22 Comparison between the numerical and the experimental results for the degree of saturation in the substrate (Djedjig *et al.*, 2012)

From the comparison of the degree of saturation (figure 2.22), the simulated result showed a good relation when compare to the measurement with the sudden peak during the storm event at 12th July 2011. However, most of the simulated data were below the measured data.

In addition, Djedjig *et al*. (2012) extended the work on the energy budget theory by studying the effect of substrate moisture content on the temperature of substrate, which they called the "soil inertia". From their study, the substrate surface temperature will increase when the saturation ratio is low. In contrast, the substrate surface temperature will be closer to the ambient temperature when the saturation ratio is increased. This effect is demonstrated in figure 2.23.

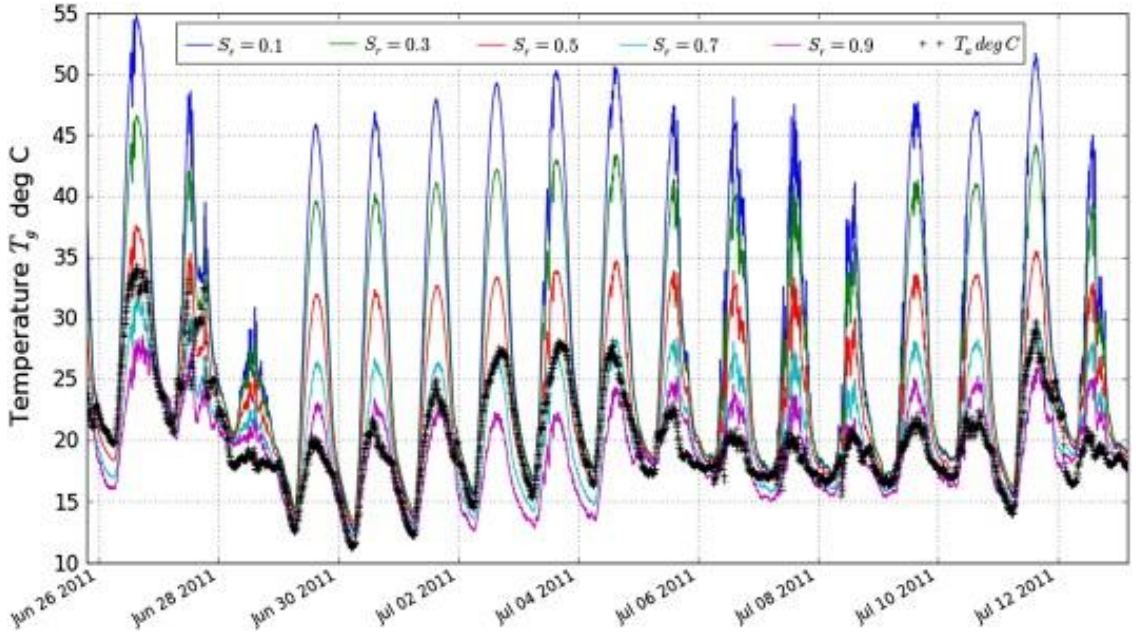

Figure 2.23 Comparison of the substrate surface temperature T_g to the air temperature T_a (Black line) for different degrees of substrate saturation (Djedjig *et al*., 2012)

With the soil inertia, they compared the surface temperature to the temperature inside the substrate layer and the conduction heat flux through the green roof predicted by the numerical model in figure 2.24 and 2.25 respectively.

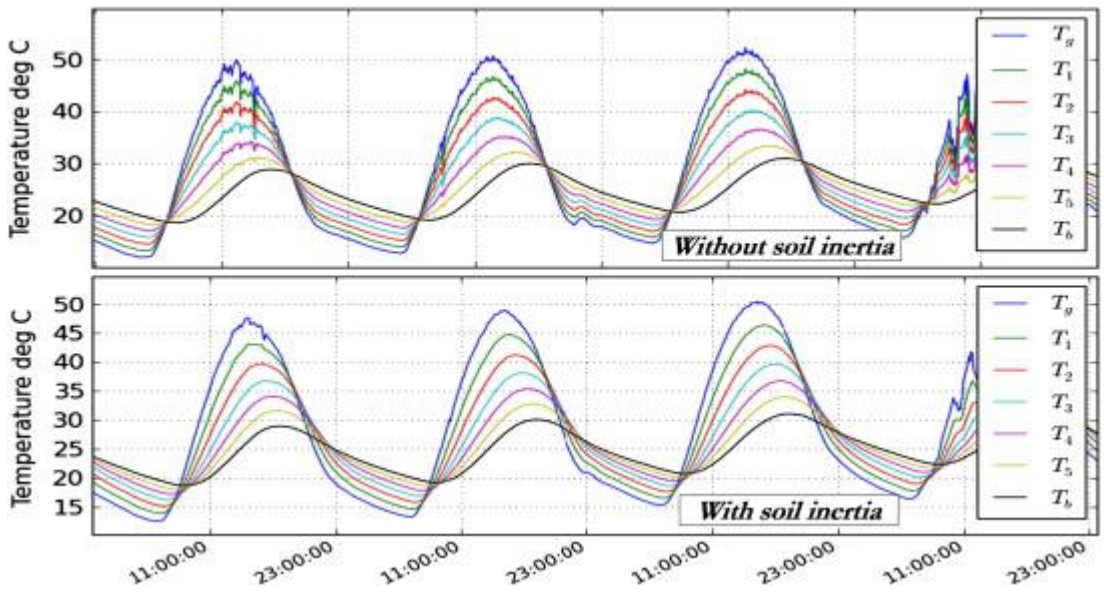

Figure 2.24 Comparison between the numerical results for temperatures at different depths of the substrate that were obtained with or without accounting for green roof component inertia (Djedjig *et al*., 2012)

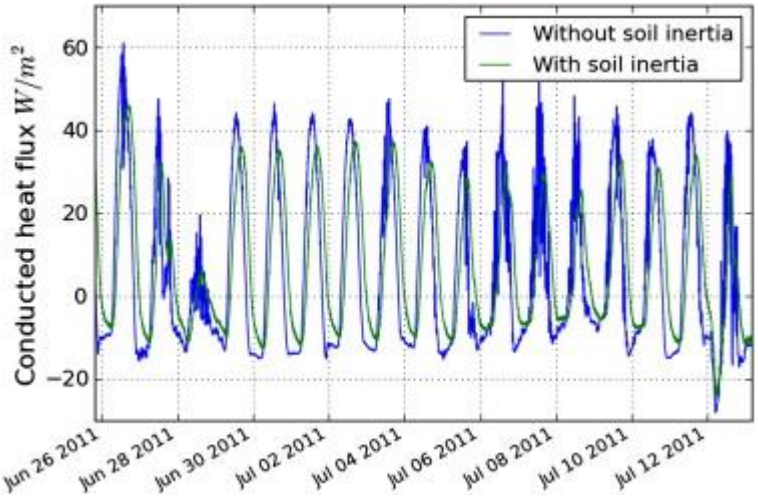

Figure 2.25 Comparison between the numerical results for conducted heat flux through the substrate that were obtained with or without accounting for green roof component inertia (Djedjig *et al*., 2012)

From figure 2.24, Djedjig *et al*. (2012) suggested that there is approximately 1^{o}C overestimation in temperature if the soil inertia effect is neglected. In addition, from the heat flux comparison in figure 2.25, they observed that there is 10 W/m^2 overestimation in heat flux at the peaks when the soil inertia is neglected.

Although this study shows a good correlation between heat flux and surface temperature between the computation data and the measurement, the heat conduction through the substrate calculation was still based on the difference between the surface temperature and the temperature at the bottom of substrate. The substrate thermal conductivity in this study was considered as one layer, of which moisture content affected the thermal conductivity and the surface temperature.

2.5.4 Summary

This section has discussed details of the energy budget theory that can be applied to many current green roof simulations. The theory effectively explains heat transfer at the surface of the foliage layer and substrate layer. On the other hand, the below surface heat transfer, such as occurs in the substrate and drainage layer, was not considered, and this layer dominates most of the green roof thickness. For this reason, the next section will discuss this aspect of green roof thermal simulation.

2.6 Sources of error in green roof thermal simulation

Despite the fact that the green roof simulations discussed above produce reasonable results compared with the test results, the studies were conducted with impractical and controlled green roof conditions. For a green roof in the normal operating situation, the estimates of thermal transfer might be in error and this section explores possible sources of error.

The features of the various green roof thermal simulation models are summarised in table 2.9.

Table 2.9 Summary of green roof thermal simulation (based on Tabares-Velasco (2009) with additions)

	Decruz *et al*. (2012)	**Djedjig *et al*. (2012)**	**Tabares-Velasco and Srebric (2012)**	**Sailor (2008)**	**Alexandri and Jones (2007)**	**Lazzarin *et al*. (2005)**	**Barrio (1998)**
Short-wave Radiation	Beer's law	Beer's law	Beer's law	Beer's law	Beer's law	Beer's law	Beer's law
Long-wave Radiation	Plant-Sky Substrate-Sky Substrate-Plants (Plants surrounding substrate)	Plant-Sky Substrate-Sky Substrate-Plants (infinite plates)	Plant-Sky Substrate-Sky Substrate-Plants (infinite plates)	Plant-Sky Substrate-Sky Substrate-Plants (infinite plates)	Plant-Sky Substrate-Sky Substrate-Plants (Plants surrounding substrate)	Adduction coefficient	Plant-Sky Substrate-Sky Substrate-Plants (Plants surrounding substrate)
Convection	2 Factor + empirical equation for aerodynamic resistance based on plant characteristics +LAI	1.1 factor + logarithmic profile + instability factors + LAI (equation 2.12)	Horizontal flat plate, convective coefficient based on roughness (plant) and Nusselt No (substrate)	1.1 factor + logarithmic profile + instability factors + LAI (equation 2.12)	Logarithmic profile	Adduction coefficient	2 Factor + empirical equation for aerodynamic resistance based on plant characteristics +LAI
Evapotranspiration	VPD for plants and substrate covered/uncovered	VPD for plants and substrate covered/uncovered	Modified VPD for plant and substrate covered/uncovered	VPD for plants and substrate covered/uncovered	VPD for plants and substrate covered	Penman's equation	VPD for plants and substrate covered
Stomata Resistance to Atmosphere	Adopted from other model	A function of moisture content, sun (multiplicative)	A function of moisture content, VPD, temperature, and sun (multiplicative)	A function of moisture content, sun (multiplicative)	A function of moisture content, sun (additive)	Empirical wind equation	A function of moisture content, sun, temperature and CO_2 (additive)
Substrate Resistance to Atmosphere	Function of vapour pressure at surface and the air	Alpha method (equation 2.32)	A function of moisture content to the saturated moisture content	Alpha method (equation 2.32)	A function of moisture content, moisture content at saturation	Not considered	Not considered
Substrate Thermal Conductivity	Divide into three layers (upper, middle, and lower layer). Each layer has distinct thermal properties	Single layers and depending on moisture content, consider substrate inertia (surface temperature effect)	Single layer and use quasi-state conduction, conductivity depend on moisture content	Single layer, conductivity is varied by moisture content	Exponential function depending on moisture content, but consider as one layer	Energy balance in each node, which include thermal accumulation and evaporation	Power + exponential function depending on moisture content and density

*Abbreviations: LAI – Leaf area index, VPD – Vapour pressure deficit

By using the EnergyPlus simulation developed from the energy balance equation, many studies, such as those by Sailor (2008) and Frankenstein and Koenig (2004a); the simplified version by Feng et al. (2010); and the overall thermal transfer value (OTTV) derived from this theory by Chan and Chow (2013), had focused on heat transfer at the surface of the vegetation and substrate layer(s). The test measured the temperature at the surface of the vegetation and substrate, where the test and simulated results are sufficiently close. This theory is sufficiently accurate when studying the surface heat transfer and the urban heat island effect (Getter and Rowe, 2006, Gaffin *et al*., 2005, Santamouris, 2014), in which the surface temperature of the building plays an important role.

However, regarding heat conduction through the building, the role of the substrate layer is of no concern to the model. In the energy budget theory, the thermal conductivity in the substrate layer was assumed to be consistent for the whole layer. This assumption is only reasonable when the substrate is thin.

Furthermore, those researchers assumed that the substrate was in the saturated condition, because green roofs are regularly irrigated. For example, Chan and Chow (2013) used daily irrigation scheduled for 10:00am and 3:00pm; thereby ensuring the substrate was always saturated. Regular irrigation is ideal for green roofs, because the water maintains the top layer of vegetation in a healthy condition. Scheduled irrigation is common in the early stage of a green roof (pre-installation), but uncommon after the roof has been installed for a while, and therefore unrealistic when considering the normal operation of a building.

Resulting from the aforementioned problems (constant and saturated thermal conductivity in the substrate layer), the overall green roof thermal simulation can produce some errors in the deeper substrate layer. In the deep growing-medium section, thermal conduction in the substrate layer will play a more important role, when compared with thermal transfer at the surface of the substrate and foliage. A calculation (presented in Appendix A) estimates the error if the distribution of moisture content in substrate layer is ignored.

2.6.1 The effect of substrate on the error in green roof thermal simulation

The calculation presented in Appendix A show that a green roof with a substrate thicker than 200 mm will show signs of error if the substrate layer is considered to be thermally homogeneous, and this error will increase with the substrate thickness. As a result, intensive study in this layer is justified.

The only study to consider in detail the moisture content of the substrate layer is that by Djedjig *et al*. (2012) which also used the energy budget theory. In contrast to previous studies, this research expanded the substrate layer into several nodes and then measured these nodes' temperature, which were related to the moisture content. However, the relation of moisture content and temperature was used as a thermal inertia, which only affected the surface temperature modelling. The change of thermal conductivity due to the moisture content in each layer was not made clear. In addition, the impact of compaction on thermal conductivity was not considered.

Nevertheless, there is a theoretical framework of a green roof model that is proposed to apply with the ESP-r building simulation by Decruz *et al*. (2012). In their framework, the foliage layer heat exchange theory was adopted from previous works on green roof foliage simulation (Barrio, 1998, Sailor, 2008). However, there were some changes in the substrate layer, which their model did not assume to be thermally homogeneous. The substrate layer was discretised into three parts. The substrate in the upper layer involves the heat flux from the solar radiation, the convection heat flux, the evaporation heat flux, and conduction heat flux to the middle layer. Thereafter, the middle layer will conduct the heat from the top layer, which involves the latent heat of vaporisation and thermal conductivity. The substrate in the bottom layer is similar to the middle layer but includes the effect of the support structure thermal conductivity.

However, Djedjig *et al* (2012)'s framework is not yet verified and the substrate thickness in each discretised layer is not clearly suggested. In addition, the thermal conduction through the substrate layer in this framework seems to consider only the middle and bottom layer, which may not be enough to overcome the problem mentioned earlier (section 2.6.1).

2.6.2 Drainage layer

There is one more problem in the thermal modelling of an extensive green roof – the presence of an abiotic layer such as a drainage layer. The drainage layer is ignored by most models, despite it being an important service layer integrated with current green roof systems. Only a small number of studies have included this layer in their models, using a constant R-value for the materials in the drainage layer, plus an R-value of the air gap in order to calculate heat conduction (Ascione *et al*., 2013, Lazzarin *et al*., 2005). However, this assumption cannot be true for a porous material. The thermal conductivity of a green roof's drainage layer depends on its porosity, which is changed by the inflow and drainage of water.

In addition, the drainage layer facilitates the flow of excess water, which removes some heat by convection from the roof's surface. In a flat green roof, convection does not have a significant effect on heat transfer, since the flow velocity is low. In contrast, on a sloping green roof, the higher water velocity increases convection heat transfer and removes the heat from the roof surface faster than from a flat roof. This mechanism is not mentioned in any previous models.

2.6.3 Summary

In summary, the problems found in the existing green roof thermal simulations are as follows:

- The conduction heat transfer in the substrate is not considered in detial.
- The effect of water absorption on the moisture content and thermal conductivity in the substrate layer (from dry to saturated) is ignored.
- The effect of water evaporation from the substrate on the moisture content and thermal conductivity is considered as a single layer, which may be inappropriate for heat conduction in a green roof with a thick substrate (more than 200 mm or an intensive green roof).
- The impact of compaction on moisture transfer and thermal conductivity is not considered.
- Heat conduction through the drainage layer is considered as a single membrane with a constant value of thermal conductivity, which is not true in practice.

- The convection heat transfer underneath the drainage layer is ignored.

Informed by these problems and their implications, the research in this thesis aims to reduce the knowledge gap in our understanding of the thermal simulation of green roofs.

2.7 Proposed improvements to green roof simulations

This research aims to improve the simulation of conduction heat transfer through the green roof substrate layer. The work will focus intensively on water movement through the growing-medium layer, and will be divided into two phases: the absorption phase and the evaporation phase.

For the absorption phase, the study will track the change in water movement in the dry green roof until it is saturated. The improved simulation will calculate the heat conduction, based on the simulated dry and saturated layers of the substrate, and their thermal conductivity. The Sharp Front theory will be used together with the steady state heat conduction method, to enable an effective thermal resistance to be calculated.

For the evaporation cycle, the substrate will be divided into several layers and the study will observe the moisture content of each layer as evaporation occurs. As a result, the evaporation rate of substrate at different compaction levels will be determined; this rate will be used again in the moisture content prediction simulation of substrate layers. Finally, the moisture content will be translated into the thermal conductivity and then the conduction heat flux can be calculated, based on given information.

Whilst acknowledging the significance of the drainage layer, the heat transfer in the drainage layer will not be considered in this study, because of time constraints and availability of resources. However, the suitable theories that can be applied with the drainage layer conduction will be discussed in the final chapter, in which suggestions for future research are considered.

2.8 Conclusion

This chapter has reviewed published studies of green roofs undertaken by other researchers. The literature review began with a brief history of green roof development from early human development until the present day, with its modern green roof systems. In addition, the review presented basic information about this roofing model, such as the types of green roofs and their components. The components of a green roof, including the foliage layer, the substrate layer, the filter layer, the drainage layer, the root barrier, the waterproof membrane, and the supporting structure, were all individually explained. Furthermore, benefits of green roof installation were discussed, with particular reference to the issues of: water management, acoustic control and building energy saving.

For the green roof thermal simulation, this chapter reviewed the energy budget theory used in most green roof simulation exercises. The theory encompasses shortwave and longwave radiation, the reflection between layers, the sensible heat flux, and the latent heat flux of both foliage and substrate layers. Finally, the proposed plan for improvement of green roof thermal simulation was presented. The next chapter will discuss details of the experimental procedure employed to obtain some thermal and other green roof properties, which are necessary for improved simulation.

Chapter 3: Experiments for green roof substrate properties

3.1 Introduction

In order to complete and improve green roof substrate thermal simulation, some experimental measurements of substrate properties need to be carried out. This chapter will present details of experimental procedures and results, alongside their relationship to other green roof substrate properties. The literature review on methods will be introduced in order to show the significant contribution of each property to the overall heat performance. The substrate properties considered in this chapter are moisture content, compaction, porosity, and thermal conductivity of green roof substrate.

3.2 Moisture content (drying and wetting)

3.2.1 Literature review on method

The moisture content is a crucial property for all porous materials, such as substrate. For a green roof substrate, this property plays an important role in the water absorption and drying mechanism. Furthermore, moisture content has important consequences for the thermal conductivity, as investigated by Sailor and Hagos (2011) and Kotsiris *et al.* (2012), who agree that increasing the moisture content increases the thermal conductivity and thermal transmittance (U-value). Figures 3.1 and 3.2 present the effect of moisture content on both values.

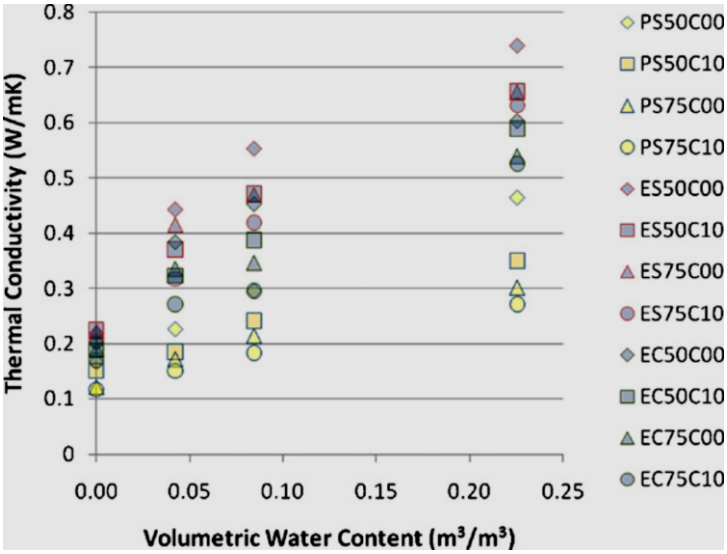

Figure 3.1 Thermal conductivities of green roof substrate samples as a function of volumetric water content (Sailor and Hagos, 2011)

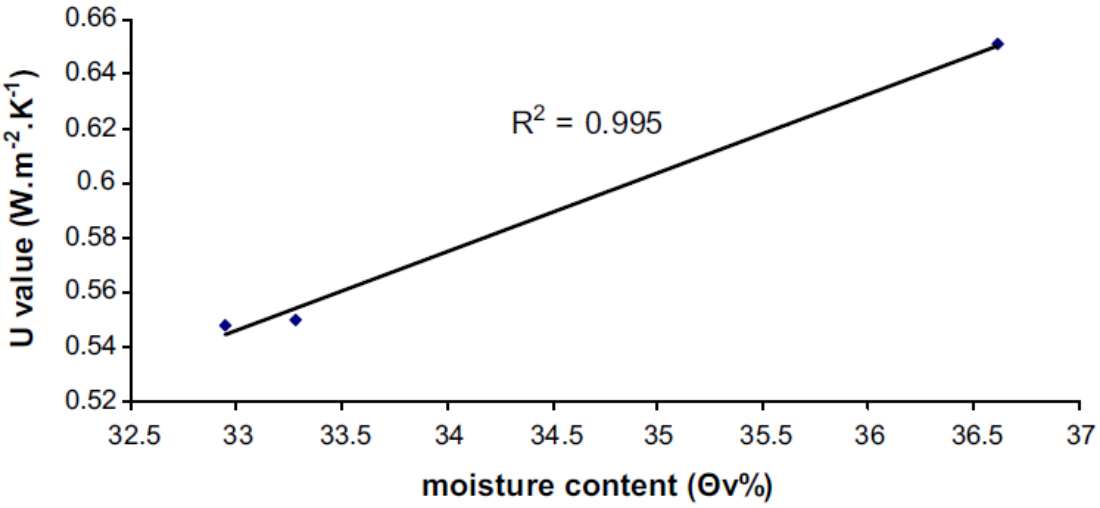

Figure 3.2 Linear relation between the estimated thermal transmittances and the moisture content fluctuation for a green roof (Kotsiris *et al*., 2012)

However, the moisture content does not only influence the thermal property; it also significantly influences the water absorption rate, which can be described by the sharp front theory (Hall and Hoff, 2009). This theory applies to porous material such as substrates, concrete and green roof substrate. It explains how the water movement into the deeper layer according to time is defined by use of the property called "sorptivity".

The sorptivity value measurement is ideally tested when the material is in a dry condition. However, in green roof substrate, it is almost impossible for substrate to stay completely dry, with 0% moisture content, when established. For this reason, the variation of moisture content will be included in a measurement to record the realistic sorptivity value of each moisture content.

It is important to establish the standard of sample mixing in order to reach a certain value of moisture content. Values of moisture content used for this measurement are 0%, 4.2%, 8.4%, 22.5%, and 24.4%, according to the measurements from Sailor and Hagos (2011). In order to control moisture content, the substrate dry mass must be known, and then the mass of water needed to reach each specific moisture content value can be calculated from the relationship, as outlined in the next section.

3.2.2 Procedure and calculation

In this measurement, the mass of water needs to be known by using information for the mass of a dry substrate, together with a moisture content value. From the gravimetric

water content in equation 3.1, the mass of water required for certain moisture content can be calculated.

$$u = \frac{M_{wet} - M_{dry}}{M_{wet}} \tag{3.1}$$

$$uM_{wet} = M_{wet} - M_{dry} \tag{3.2}$$

Where, $M_{wet} = M_{dry} + M_{water}$, thus

$$u\left(M_{dry} + M_{water}\right) = M_{dry} + M_{water} - M_{dry} \tag{3.3}$$

$$\therefore\ M_{water} = \frac{u}{(1-u)} M_{dry} \tag{3.4}$$

Note:

$u = \frac{mc}{100}$, where mc is moisture content

M_{wet} = mass of substrate before drying process

M_{dry} = mass of substrate after drying process

M_{water} = mass of water

By using equation 3.4 and known information, the sample re-hydration followed this procedure

1. Begin with the dried and cooled sample from air-tight container, pour substrate into the mixing container and weigh this sample (include container) in grams to get total mass (M_{total}). The container weight (M_{cont}) is measured prior to this stage.
2. Calculate the amount of water required for each moisture content from equation 3.4, where M_{dry} is the mass of dry sample in a container only ($M_{total} - M_{cont}$)
3. Mix dry substrate and water together by employing a mixing machine, until the water is uniformly distributed through the substrate

4. Spread the substrate in a tray, then divide it into 16 sections as shown in figure 3.3; then pick two sections randomly and place them in ceramic cups. These samples will be used to validate a moisture content of the whole substrate (this process is to ensure the moisture content of mixed substrate is uniformly distributed).

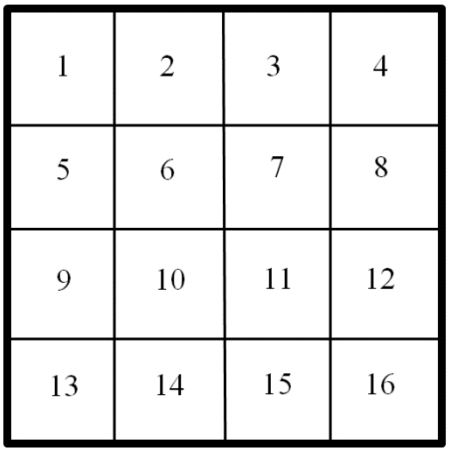

Figure 3.3 Divided sections of sample

5. Now, the substrate is ready to use.

This procedure outlines the green roof sample preparation for another experiment, described in later sections.

3.3 Compaction

3.3.1 Literature review on method

Compaction increases substrate density by packing the particles closer together, resulting in a reduction of the volume of air (Knappett J and Craig R.F, 2012). For green roofs, the compaction is varied according to their construction method and foot traffic on those roofs. Sailor and Hagos (2011) state that the compaction value (assessed by the resistance to penetration experienced by a standard needle penetrometer) of an established green roof substrate varies between 500-800 kPa, with the highest compaction level area corresponding to the area with the highest foot traffic.

The compaction can influence many green roof behaviours. Connelly and Hodgson (2015) found that increasing compaction decreases the sound absorption of the roof (sound absorption coefficient). Furthermore, Sailor and Hagos (2011) indicate that the

higher compaction level can result in higher thermal conductivity, as presented in figure 3.4.

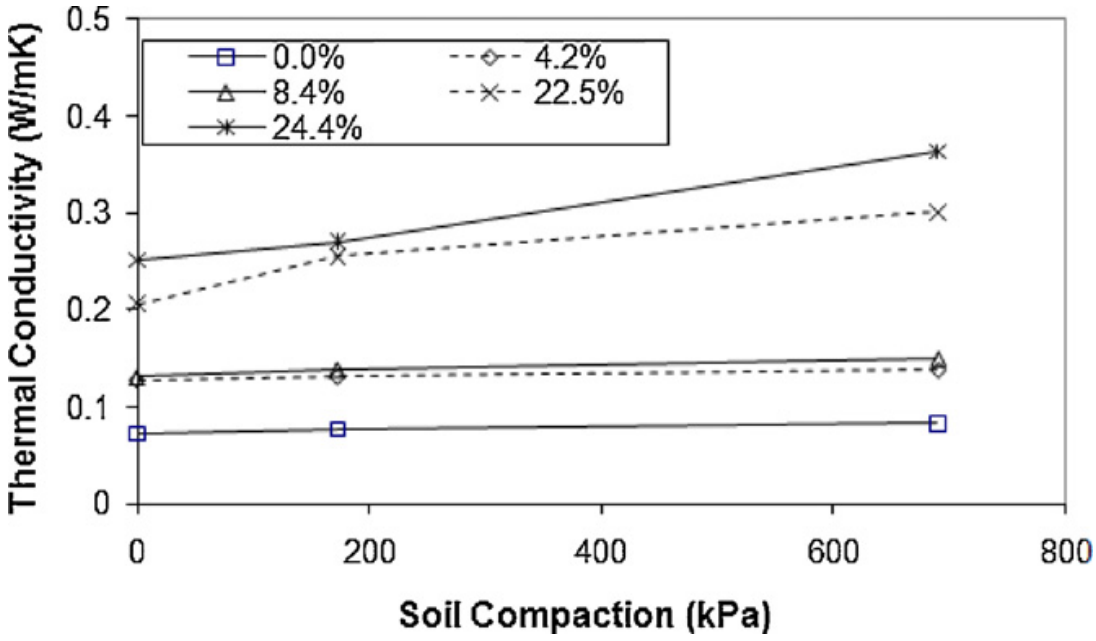

Figure 3.4 Investigated values of thermal conductivity of green roof substrate as a function of compaction for moisture levels ranging from 0.0 to 24.4% by volume. (Sailor and Hagos, 2011)

However, compaction does not only influence the thermal conductivity and sound absorption of a green roof medium. Because compaction reduces the spaces between particles, this can result in difficulty with moisture transfer into the inner layer of the substrate during the absorption process. Similarly, in the drying process, the compaction might reduce the evaporation rate because the liquid's outlet may be packed together, making it difficult for moisture to exit.

For this reason, the compaction experiment and preparation are designed to investigate compaction's effects on the absorption and evaporation mechanisms. In addition, the standard of compaction method needs to be clarified to maintain uniformity of measurements.

3.3.2 Compaction procedure

In this measurement, the range of compaction levels will be varied according to the number of impact blows applied by a Proctor hammer. The compaction level will be defined by a penetrometer, which is a needle probe used to penetrate in to a green roof

sample (Sailor and Hagos, 2011). Furthermore, the density of the substrate sample is measured by a known mass and volume, as it will be used in the porosity calculation.

The procedure is based on the standard Proctor test ASTM D698 (Standard Test Methods for Laboratory Compaction Characteristics of Soil Using Standard Effort (12 400 ft-lbf/ft^3 (600 kN-m/m^3))). However, the method of sample compaction needs to be refined in order to create the same standard for this experiment. Two scenarios were tested, in order to compare the behaviour of two substrate samples after compaction, as follows:

- First scenario is to prepare a substrate sample by placing three layers and then compact only the top layer with 75 blows from a Proctor hammer.
- Second scenario is to prepare a substrate sample by placing three layers (same as in the first scenario), but compact each layer by 25 blows from a Proctor hammer.

In order to define the degree of compaction (as distinct from the penetration resistance), the dry density is normally used in soil mechanic studies (Knappett J and Craig R.F, 2012). Equations used for this calculation are presented below.

$$\rho = \frac{M_t}{V_t} \tag{3.5}$$

$$\rho_{dry} = \frac{\rho_{m.c}}{1 + m.c} \tag{3.6}$$

ρ = density

ρ_{dry} = dry density

$\rho_{m.c}$ = density at certain moisture content

M_t = total mass

V_t = total volume

$m.c$ = moisture content

Procedure for first scenario

1. Obtain 1500g of substrate sample with known moisture content, and then divide this sample into three equal parts (500g each).
2. Pour the first part of the sample into a prepared container then distribute a layer of a substrate in order to create as flat a surface as possible, without disturbing the sample, and measure the height of this layer in the container.
3. Place a circular cut filter layer on the top of this layer. This filter layer will separate each layer, and make a clear visible line after compaction takes place.
4. Repeat steps 2 and 3 until the container is filled with three substrate layers.
5. Compact the top surface of the third layer with 75 impacts by a standard Proctor hammer (5.5 lb hammer falling from 12 inches through a steel tube).
6. Measure the height of each layer after compaction.

Procedure for second scenario

1. Obtain 1500g of substrate sample with certain moisture content, and then divide this sample into three parts equally (500g each).
2. Pour the first part of the sample into a prepared container, then distribute the sample's layer to makes it as flat as possible, without disturbing the sample, and measures the height of the sample in this container.
3. Compact the top surface of this layer with 25 blows from a standard proctor hammer.
4. Measure the height of this layer after compaction.
5. Place a circular cut filter layer on the top of this layer.
6. Repeat steps 2 and 5 until the container is filled with three compacted substrate layers.

By putting the same total amount of compaction energy (75 times with the same dropping height) in both scenarios, results can be compared.

3.3.3 Compaction method result and discussion

Comparison of the results of both scenarios will look at the distribution of layer height after compaction took place. The figure 3.5 illustrates the arrangement of the three layers.

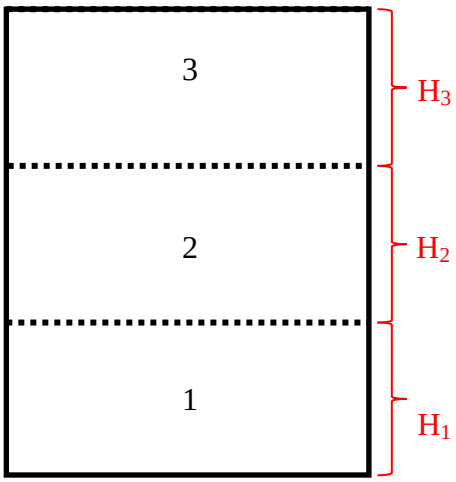

Figure 3.5 Layer arrangement illustration of compacted sample

The table 3.1 presents results from two scenarios of two different moisture content samples (0% and 8.4% m.c.).

Table 3.1 The height comparison between two scenarios of 0% and 8.4% m.c. samples

Layer	**0% m.c.**		**8.4% m.c.**	
	1st Scenario	**2nd Scenario**	**1st Scenario**	**2nd Scenario**
H_3	45 mm	45 mm	40 mm	40 mm
H_2	45 mm	45 mm	40 mm	40 mm
H_1	55 mm	45 mm	45 mm	40 mm

Figure 3.5 and table 3.1 (second column) present the height of 0% moisture content substrate sample layer after compaction with both methods. The initial height of each layer before compaction is 55 mm per layer.

Similarly, figure 3.5 and table 3.1 (third column) presents the height of 8.4% moisture content substrate sample layer after compaction with both methods. The initial height of each layer before compaction is 50 mm per layer.

For 0% moisture content samples, it clearly summarises that the second scenario can produce better distributed compaction results than the first scenario, with the same compaction energy. In the first scenario, the compaction effort put into the sample only affects layers 3 and 2. The compact energy cannot transfer into the deepest layer (layer 1) because the substrate does not have enough plasticity. On the other hand, the second scenario yields better result in distributing the compaction effort. Three distributed layers are presented as a consequence of an equal compaction energy on each layer (25 blows/layer).

Similary, 8.4% moisture content samples share similar results of both scenarios. Table 3.1 clearly presents a better compaction result in the second scenario, similar to the 0% moisture content sample. However, the height, before compact, of the 8.4% moisture content sample is lower than a dry sample. The 0% moisture content sample has 55 mm for each layer at the beginning, but the 8.4% moisture content sample has 50 mm for each layer. This difference is a result of capillary attraction that has drawn particles closer together.

The first scenario of a wet sample produces a good compaction result in layers 2 and 3, while some energy is transferred into the bottom layer because this sample has more plasticity than the dry one. As a result, the layer 1, 2, and 3 became 45, 40, and 40 mm in height respectively after being compacted. Nevertheless, the second scenario still yields better compaction results than the first scenario with distributed heights of 40 mm for each layer.

For this reason, the second scenario will be used as a method of sample compaction preparation. The next section will set out the procedure to determine penetration resistance and the dry density.

3.3.4 Compaction and penetration resistance procedure

The other challenge of sample compaction is how to achieve the required level of compaction by using penetration resistance as an indicator. Thus, the following experiment was performed to investigate the relationship between number of blows from the proctor hammer, dry density, and penetration resistance of a substrate for each moisture content.

1. Obtain 500 gram sample of substrate and pour it into the prepared container (only one layer is tested).
2. Measure the height of the uncompacted sample (0 blows) to calculate a dry density.

$$\rho_{dry} = \frac{\rho_{m.c}}{1 + m.c}$$

3. Measure the penetration resistance from the penetrometer for 5 positions and take an average of penetration resistance reading. However, there is a possibility that a penetrometer hits a rock and cannot go further, which results in very high reading. If this effect occurs, this position must be removed from the average (use only 4 positions). The unit in a penetrometer is in ton/ft^2, but is converted into kilo Pascal (kPa) by multiplying by 96.
4. Compact this sample 10 times with a Proctor hammer, and then measure the height and the penetration resistance after compaction.
5. Remove a compacted sample from the container, and then repeat steps 2-4 with 25 and 75 hammer blows.

Results of dry density and penetration resistance against the amount of compaction blows are presented in the next section.

3.3.5 Compaction and penetration resistance results

From the results in the previous section, the volumetric density of the substrate can be calculated from the mass and volume of that substrate, which can be turned into dry density data by use of equation 3.6. As a result, dry density and penetration resistance can be presented in a linear relationship, with a fitted equation of $y = 1654.9x - 1732.3$ as shown in figure 3.6.

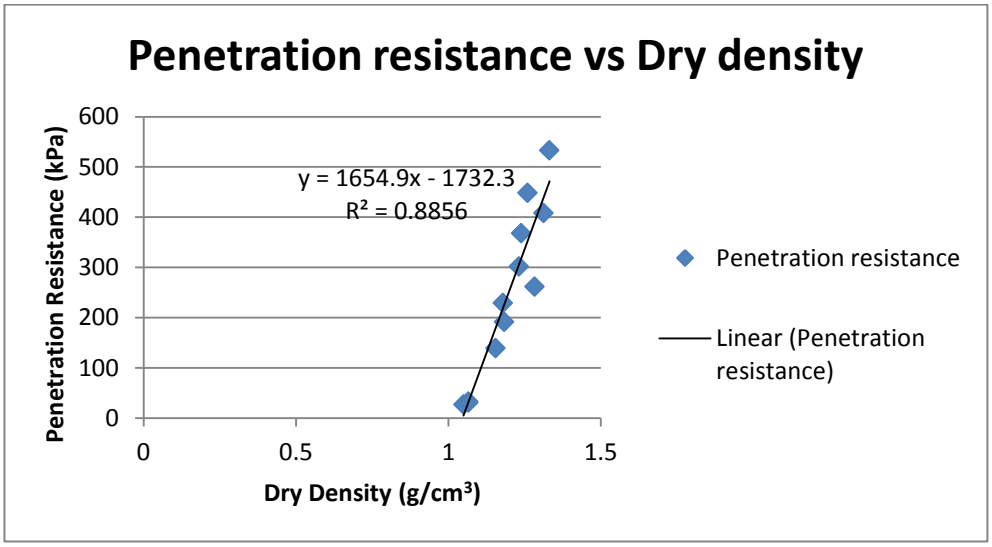

Figure 3.6 Linear relation between dry density and penetration resistance

Although this experiment observed behaviours from 0%, 4.2%, 8.4%, 13.6%, and 22.4% moisture content samples, figure 3.6 presents results from only the first three (0%, 4.2%, and 8.4%) specimens. The reason to ignore the last two samples (13.6%, 22.4%) is because the 13.6% moisture content produces a highly cohesive layer when compaction is increased. This effect is to harden the top layer and prevents use of a penetrometer, as it cannot break through the hardened surface, and therefore the penetration resistance value cannot be read. On the other hand, the 22.4% sample is near saturated moisture content resulting in very loose particle and therefore no penetration resistance reading can be performed. As a result, this graph can only display data from 0%, 4.2%, and 8.4% moisture content samples.

Even though the figure 3.6 shows a clear relationship, where increasing dry density results in higher penetration resistance, the dry density and numbers of blows have a distinct relationship in each moisture content. Figures 3.7 to 3.9 show the relationship between dry density, number of blows and penetration resistance.

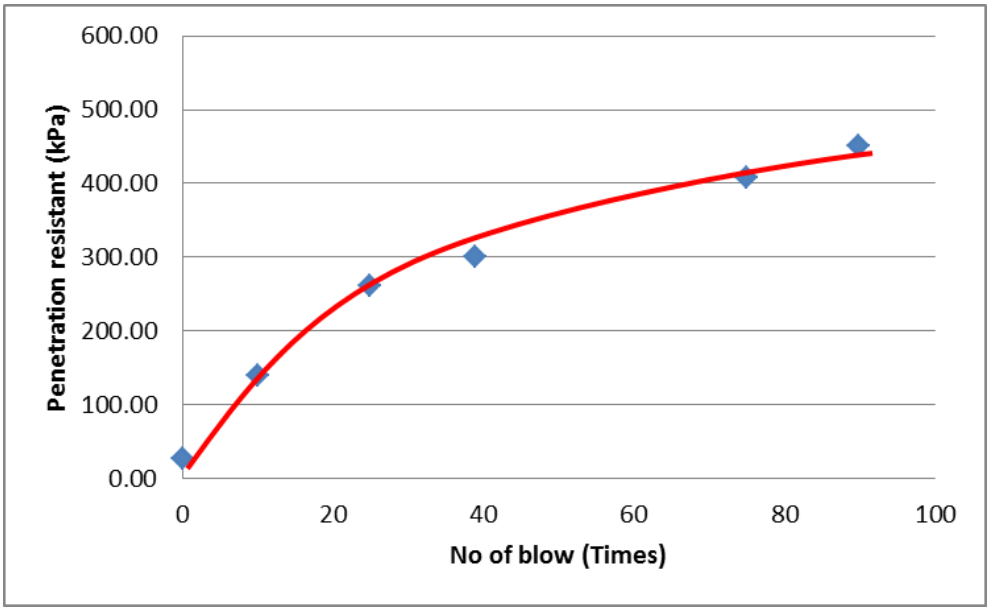

Figure 3.7 Number of blows against penetration resistance for 0% moisture content

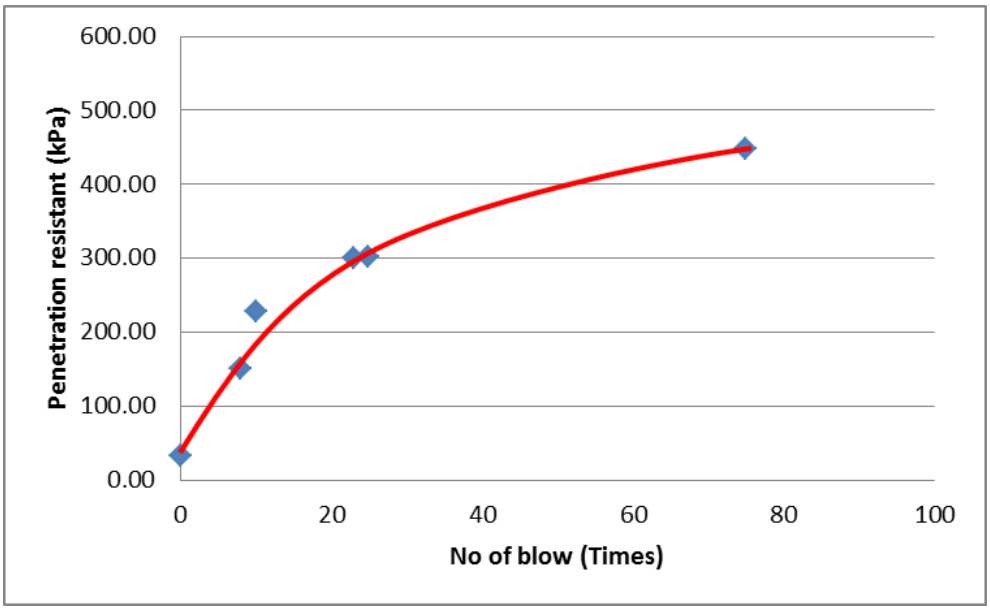

Figure 3.8 Number of blows against penetration resistance for 4.2% moisture content

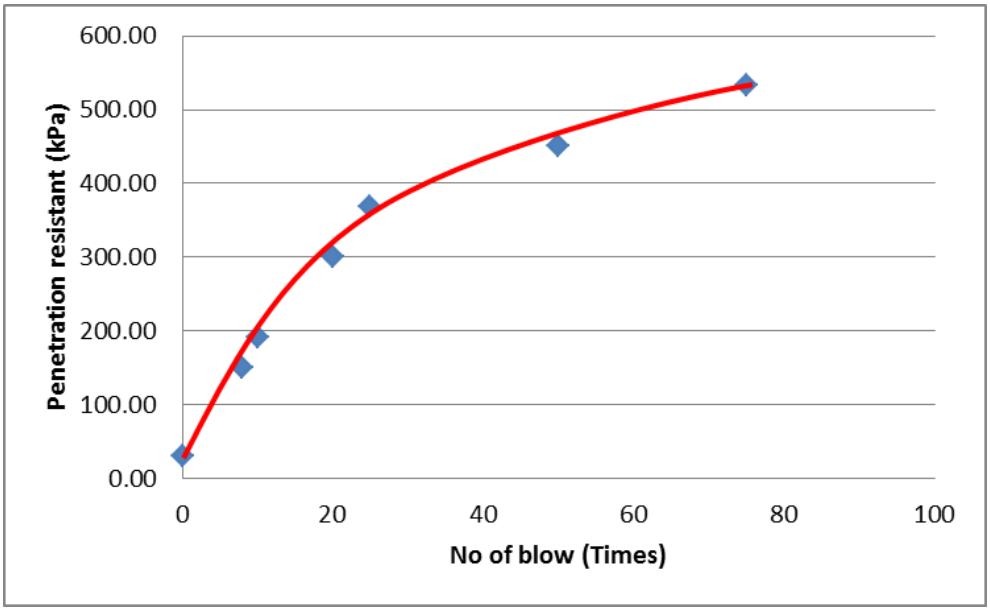

Figure 3.9 Number of blows against penetration resistance for 8.4% moisture content

From the results shown in figure 3.7 to 3.9, a smooth curve shows the trend, from which table 3.2 shows the required number of hammer blows for each sample, in order to reach a certain penetration resistance.

Table 3.2 Number of blows required for each moisture content

Moisture content (%)		Penetration resistance (kPa)		
		150	300	450
No of blow (times)	0	13	39	90
	4.2	8	23	76
	8.4	8	20	50

This number of blows will be used in every sample preparation for thermal conductivity, sorptivity and evaporation measurement. The next section considers porosity measurement, where compaction can reduce the porosity of a green roof substrate.

3.4 Porosity

3.4.1 Literature review of method

Porosity is a fundamental property of porous materials, which may be defined as the ratio of the volume of voids (air spaces) and the total volume of material (Knappett J and Craig R.F, 2012). Porosity has a significant effect in the sharp front theory. In the sharp front theory, the porosity is applied together with the sorptivity value in order to calculate the depth of a saturated layer when water or other liquids are absorbed by a porous medium (Hall and Hoff, 2009). Although, the sorptivity value can predict a distance (by volume) of water absorbed by a material ($n_{water} = St^{1/2}$), the distance of saturated layer is different because it consists of solid particles and pores (that later fill with water). For this reason, the saturated distance of porous material (n_{sat}) has to include the effect of material porosity as shown in figure 3.10 and 3.11.

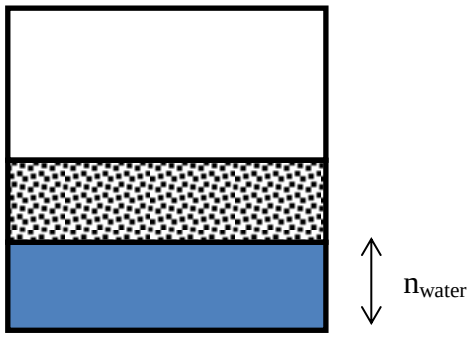

Figure 3.10 Distance of water (n_{water}) calculated from sorptivity value

Figure 3.10 shows the distance of water absorbed by a substrate (n_{water}), which is directly calculated from the sorptivity equation. This n_{water} is not a distance of saturated layer because it does not include the effect that water replaces pore spaces.

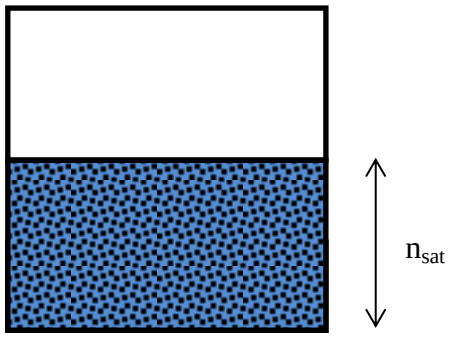

Figure 3.11 Distance of saturated layer (n_{sat}) where water replace pores inside the substrate

As a result, figure 3.11 presents a true saturated layer (n_{sat}) in which the effect of porosity is included, as shown in equation 3.7.

$$n_{sat} = \frac{n_{water}}{\epsilon} = \frac{St^{1/2}}{\epsilon} \tag{3.7}$$

Where: ϵ is a porosity of material.

However, the porosity depends on many properties, such as dry bulk density and compaction. In order to calculate the porosity when compaction is changed, the relationship between dry bulk density (ρ_{bulk}) and solid density (ρ_{solid}) will be clarified.

$$\rho_{bulk} = \frac{Mass_{total}}{Volume_{total}} \tag{3.8}$$

And the solid density is a density of the solid particles only (volume of pores must be removed)

$$\rho_{solid} = \frac{Mass_{total}}{Volume_{total} - Volume_{pores}} \tag{3.9}$$

$$Volume_{total} - Volume_{pores} = \frac{Mass_{total}}{\rho_{solid}} \tag{3.10}$$

Divide this equation with $volume_{total}$

$$1 - \frac{Volume_{pores}}{Volume_{total}} = \frac{\rho_{bulk}}{\rho_{solid}} \tag{3.11}$$

The volume of pores divided by the total volume of material is porosity. Therefore, equation 3.11 changes into:

$$\epsilon = 1 - \frac{\rho_{bulk}}{\rho_{solid}} \tag{3.12}$$

From the aforementioned relationships, the most important property for porosity calculation is the solid density, and this experiment will use the water displacement method to measure this value. The next section is the procedure to obtain the porosity value.

3.4.2 Procedure

Equipment required to do this experiment is:

1. An electronic balance
2. A graduated glass container and lid
3. Intensive green roof substrate
4. A water container

Procedures of porosity measurement are:

1. Measure the mass of an empty graduated glass container and its lid (M_{cont})
2. Slowly fill a container with water until water rises above the top of a container (meniscus curve is created). Remove excess water and bubbles by slowly moving a glass lid over the top of container, and then clean this container with absorbent paper (remove excess water from the side). Measure the mass of container plus water ($M_{cont,water}$).
3. Remove water and clean the container until dry. Pour an intensive green roof substrate into the container until it fills half of the container; then weigh the mass of container plus substrate ($M_{cont,sub}$)
4. Fill the container, with substrate inside, with water. The water will stay on the top of the substrate to be absorbed later by capillary effect (figure 3.12). Leave this container open for between 8-10 hours to ensure that water fully replaces the voids in the substrate, ensuring full saturation (figure 3.13).

Figure 3.12 Substrates in container when first filled with water (stage 4)

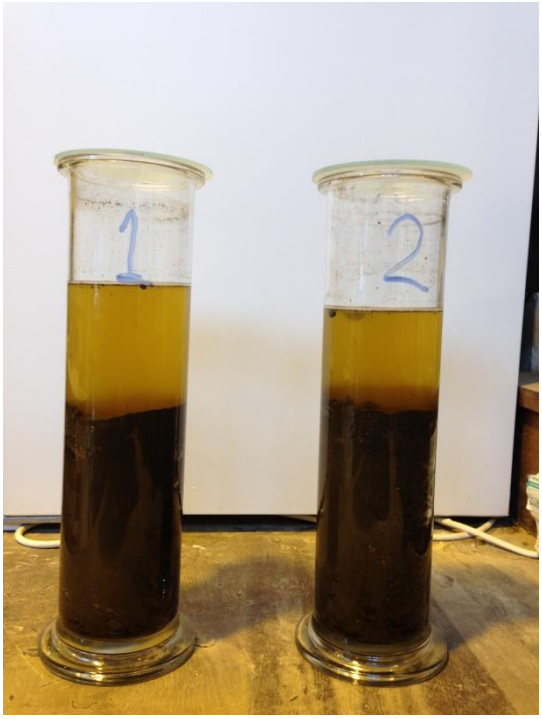

Figure 3.13 Substrates in container after being in water for 8-10 hours

5. After voids in substrate are replaced with water, pour more water to the top of the container until the meniscus curve is visible (figure 3.14). Remove excess water and bubbles by slowly moving a glass lid over the top of the container, and then clean this full container with absorbent paper (removing any excess

water from the side). Measure the mass of container, substrate, and water ($M_{cont,sub,water}$).

Figure 3.14 Meniscus of water is created after the container is filled (stage 5)

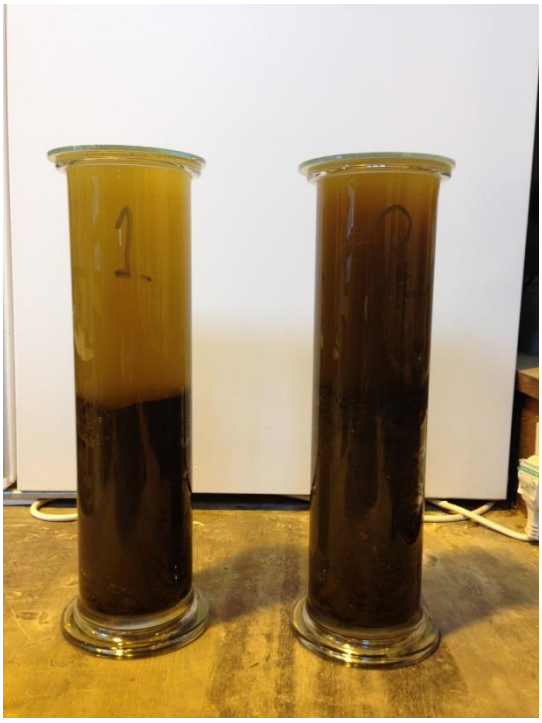

Figure 3.15 Containers filled with green roof substrates and water (no residual air bubbles)

The calculation of porosity value will be presented in the next section.

3.4.3 Calculation and result

Calculating the porosity of green roof substrate begins by calculating the volume of space inside the container (V_{cont}), mass of container when it is full with water ($M_{cont,water}$), mass of empty container (M_{cont}), and density of water (ρ_{water}) as shown in the equations below.

$$V_{cont} = \frac{M_{cont,water} - M_{cont}}{\rho_{water}} \tag{3.13}$$

To calculate the volume of water that fills a container (after putting in the substrate)

$$V_{water} = \frac{M_{water}}{\rho_{water}} = \frac{M_{cont,sub,water} - M_{cont,sub}}{\rho_{water}} \tag{3.14}$$

Determine the volume of substrate and mass of substrate, and then calculate the solid density

$$V_{sub} = V_{cont} - V_{water}$$

$$M_{sub} = M_{cont,sub} - M_{cont}$$

Therefore, the solid density can be calculated.

$$\rho_{solid} = \frac{M_{sub}}{V_{sub}} \tag{3.15}$$

Finally, the porosity is determined by using equation 3.12. This result, of two porosity measurements, is shown in terms of averaged solid density in table 3.3 below:

Table 3.3 Averaged solid density (calculation and result)

Container	**1**	**2**
Mass of container (g)	863.3	865.5
Mass of container and water (g)	2123.9	2113.4
Mass of container and substrate (g)	1558.6	1584.9
Mass of container, substrate, and water (g)	2509.5	2510.6
Mass of water in empty container (g)	1260.6	1247.9
Mass of substrate (g)	695.3	719.4
Mass of water (g)	950.9	925.7
Density of water (g/mm^3)	0.001	0.001
Volume of empty container (mm^3)	1260600	1247900
Volume of water (mm^3)	950900	925700
Volume of substrate (mm^3)	309700	322200
Density of substrate (g/mm^3)	0.002245	0.0022328
Density of substrate (kg/m^3)	2245.076	2232.7747
Density of substrate (g/cm^3)	2.24	2.23
Average density of substrate (g/cm^3)	**2.24**	

The average solid density of green roof substrate is approximately 2.24 g/cm^3 and this value will be used with a dry bulk density of each green roof substrate in different compaction and moisture content levels. The relationship of dry bulk density and solid density is demonstrated in equation 3.12.

Thereafter, this solid density will be calculated together with the dry bulk density from the previous section: compactions and densities. The next section will draw together the relationship between compaction and porosity of a green roof substrate.

3.5 Relationship between porosity, moisture content, and compaction

Tables 3.4 to 3.6 present results of the porosity of green roof substrate samples in each moisture content and compaction level. By using the solid density data (ρ_{solid}) from the previous section (2.24 kg/cm^3), the porosity is calculated from equation 3.12.

Table 3.4 Porosity of 0% moisture content samples in each compaction level

No of blows (times)	Height of layer (cm)	Density (g/cm^2)	Dry density (g/cm^2)	Porosity	Penetration resistance (kPa)
0	5.5	1.05	1.05	0.53	27.05
10	5	1.15	1.15	0.48	139.10
25	4.5	1.28	1.28	0.43	261.21
75	4.4	1.31	1.31	0.41	408.04

Table 3.5 Porosity of 4.2% moisture content samples in each compaction level

No of blows (times)	Height of layer (cm)	Density (g/cm^2)	Dry density (g/cm^2)	Porosity	Penetration resistance (kPa)
0	5.2	1.11	1.07	0.52	32.46
10	4.7	1.23	1.18	0.47	228.75
25	4.5	1.28	1.23	0.45	301.39
75	4.4	1.31	1.26	0.44	448.22

Table 3.6 Porosity of 8.4% moisture content samples in each compaction level

No of blows (times)	Height of layer (cm)	Density (g/cm^2)	Dry density (g/cm^2)	Porosity	Penetration resistance (kPa)
0	5	1.15	1.07	0.52	30.91
10	4.5	1.28	1.18	0.47	191.65
25	4.3	1.34	1.24	0.45	367.85
75	4	1.44	1.33	0.41	533.23

From the porosity results, it can be concluded that porosity is reduced when compaction level increases since it packs particles together. Likewise, the moisture content can reduce the porosity since it replaces voids with water and increases the workability of compaction. As a result, the porosity tends to reduce, while penetration resistance increased. This effect is shown in the penetration resistance and porosity of each sample when moisture content is changed (figures 3.16 to 3.18).

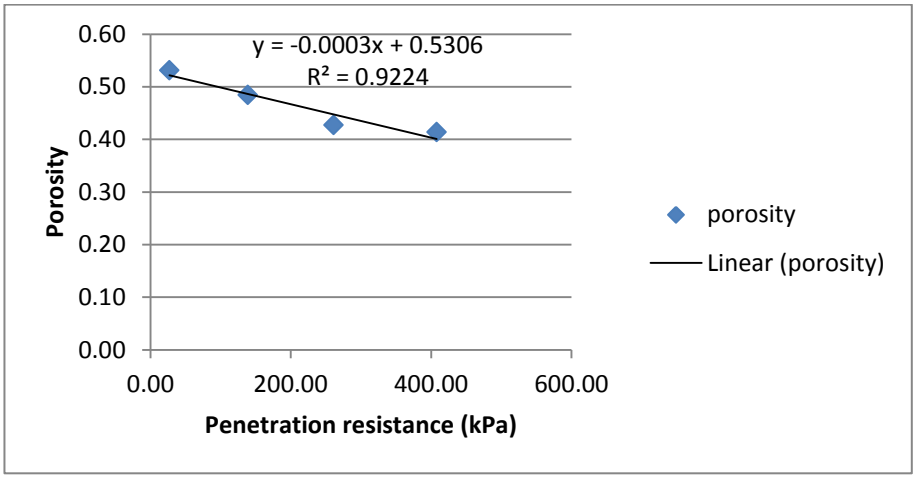

Figure 3.16 Porosity against penetration resistance of 0% moisture content sample

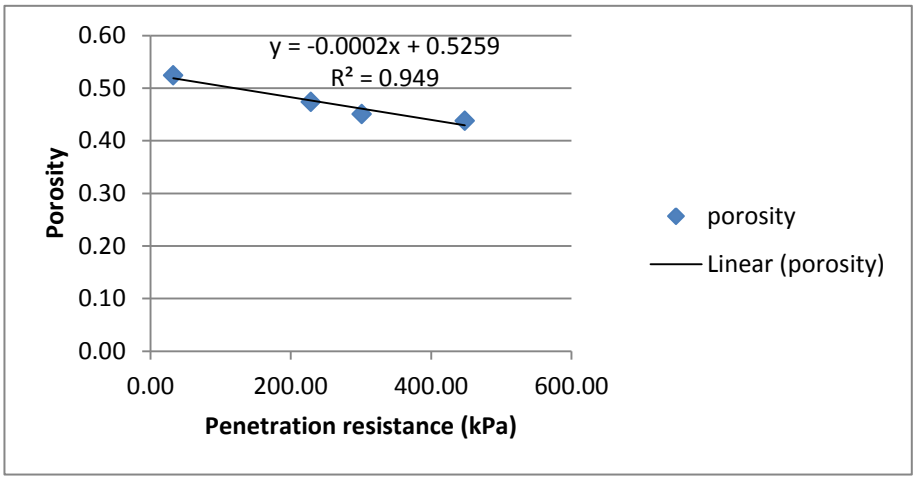

Figure 3.17 Porosity against penetration resistance of 4.2% moisture content sample

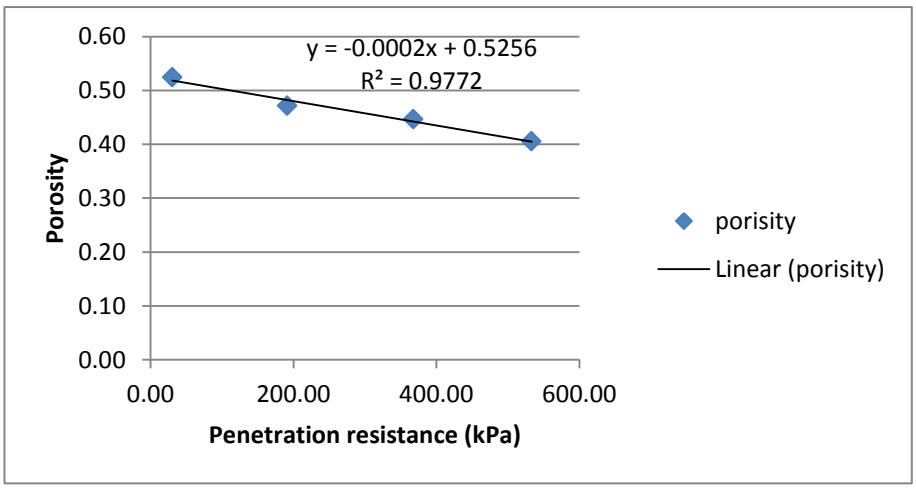

Figure 3.18 Porosity against penetration resistance of 8.4% moisture content sample

These linear equations can be converted into porosity values for each penetration resistance value. Furthermore, each moisture content and compaction level can be indicated by number and abbreviation, in which the first two letters represent the type of green roof substrate, the first three digits indicate the moisture content, and the last three digits indicate the degree of penetration resistance.

As a result, table 3.7 shows sample identifications, where moisture content, penetration resistance, and porosity are described.

Table 3.7 Porosity values of each sample

Sample	moisture content (percentage)	Penetration resistance (kPa)	Porosity
IN000000	0	0	0.53
IN000150	0	150	0.49
IN000300	0	300	0.44
IN000450	0	450	0.40
IN042000	4.2	0	0.53
IN042150	4.2	150	0.50
IN042300	4.2	300	0.47
IN042450	4.2	450	0.44
IN084000	8.4	0	0.53
IN084150	8.4	150	0.50
IN084300	8.4	300	0.47
IN084450	8.4	450	0.44

This identification will be used throughout this study. The next section deals with the thermal conductivity measurement of a green roof substrate.

3.6 Thermal conductivity

The other crucial parameter for green roof thermal modelling is thermal conductivity. This property is affected by the substrate's solid structure (e.g. organic and inorganic content), amount of water, and compaction level. However, the solid structure is considered to be the same, by using a same type of green roof substrate. For this reason, only moisture contents and compaction levels will be varied, with the same configuration as for previous measurements.

- 0%, 4.2%, 8.4% and saturated moisture content
- 0, 150, 300, and 450 kPa for penetration resistance

The procedure will follow the ASTM D5334-14 standard test method for determination of thermal conductivity of soil and soft rock by a thermal needle probe procedure. This method uses a small needle probe to simulate the infinitely thin and long heat source; the probe contains a heating element and thermal sensor. A known electric current is applied to the probe that results in a temperature rise over time, which is recorded. Finally, the thermal conductivity is obtained from temperature data during heating and cooling cycles.

The Thermtest TLS-100 portable soil thermal conductivity meter is used for this measurement. It measures thermal conductivity and resistance according to standard ASTM D5334-14, which covers a conductivity range from 0.1 to 5 W/mK.

Figure 3.19 TLS-100 thermal conductivity meter (https://www.thermtest.com/index.php?page=tls-100)

The simplified method from ASTM D5334-14 is being used in this thermal conductivity test unit. If a constant amount of heating energy is applied to the probe, the temperature response of a sample, due to the heat input, follows the equation 3.16.

$$\Delta T = -\frac{Q}{4\pi K} E_i\left(\frac{-r^2}{4Dt}\right) \qquad 0 < t \leq t_1 \qquad (3.16)$$

The temperature response after the heat is removed (and sample cools down) follows equation 3.17.

$$\Delta T = -\frac{Q}{4\pi K}\left[E_i\left(\frac{-r^2}{4Dt}\right) + E_i\left(\frac{-r^2}{4D(t-t_1)}\right)\right] \qquad t > t_1 \qquad (3.17)$$

Where:

t = time from the beginning of heating (s),

ΔT = temperature changed from initial (K),

Q = heat input per unit length of the heating probe (W/m),

r = radius of heating probe (m),

D = thermal diffusivity (m^2/s),

K = thermal conductivity (W/m.K),

E_i = exponential integral, and

t_1 = heating time (s).

However, those equations cannot solve the thermal diffusivity and conductivity at the same time. Therefore, a non-linear least-squares inversion technique must be used. A simplified analysis of exponential integral, by the most significant terms of equations 3.16 and 3.17, is represented in equations 3.18 and 3.19.

$$\Delta T \cong -\frac{Q}{4\pi K}\ln(t) \qquad 0 < t \leq t_1 \qquad (3.18)$$

$$\Delta T \cong -\frac{Q}{4\pi K}\ln(\frac{t}{t-t_1}) \qquad t > t_1 \qquad (3.19)$$

Thermal conductivity can be determined by converting these equations into equations 3.20 and 3.21.

$$K \cong -\frac{Q}{4\pi \Delta T}\ln(t) \qquad 0 < t \leq t_1 \qquad (3.20)$$

$$K \cong -\frac{Q}{4\pi \Delta T}\ln(\frac{t}{t-t_1}) \qquad t > t_1 \qquad (3.21)$$

The term $\ln(t)/K$ and $\ln\left(\frac{t}{t-t_1}\right)/K$ can be determined by plotting the temperature changes against the natural logarithm of time. The slope of these data, therefore, can be resolved by fitting the linear regression. Nevertheless, the initial time of the heating phase has to be ignored from the slope fitting, because it is a transient phase, which the conductivity cannot be determined by a linear relationship. Figure 3.20 presents a slope fitting of heating and cooling data.

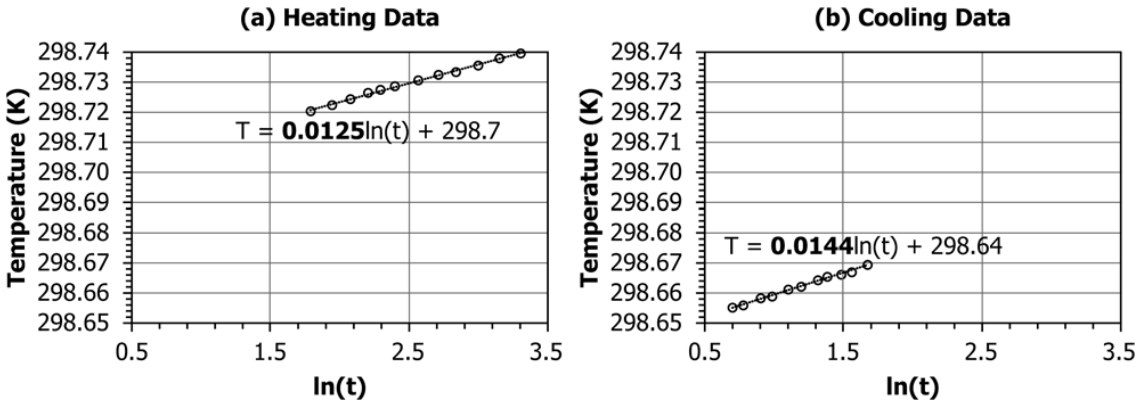

Figure 3.20 The slope fitting of (a) heating data and (b) cooling data (standard ASTM D5334-14)

Slopes of both heating (S_h) and cooling data (S_c) will be averaged and put back into equations 3.20 and 3.21; finally, the thermal conductivity can be determined by equation 3.22.

$$K = -\frac{Q}{4\pi S} \tag{3.22}$$

The Thermtest TLS-100 has built-in software which uses the theory and equations cited above to calculate thermal conductivity. The next section considers the procedure of the thermal conductivity measurement of green roof substrates for different moisture contents and compaction levels.

3.6.1 Procedure

1. The substrate sample is prepared according to the compaction and hydration measurement preparation (see section 3.2.2 and 3.3.2) in order to obtain the required moisture content (0, 4.2%, and 8.4%) and penetration resistance level (0, 150, 300, and 450 kPa).
2. Wait for a sample to cool down (heat may be produced during mixing and compaction processes) for 20-30 minutes or until it reaches thermal equilibrium.
3. Insert the TLS-100 needle probe into the substrate (some compacted sample might require a pre-drilled hole) and wait for 10 minute to reduce any temperature drift.
4. Push the start button and wait for the thermal conductivity meter to operate for 20 minutes.
5. After finishing the test, remove the needle probe from the sample and wait for that sample to cool down for another 20 minutes. Repeat steps 3 to 5 for five positions.

Results of this experiment are presented in the next section.

3.6.2 Results

The results in this section are presented for different compaction levels, in which thermal conductivities vary according to moisture content changes.

First of all, results of each sample are the average of measurements in five positions, and will be presented in table and graphical formation. However, the relationship that fits this measurement is the exponential curve, which is difficult to predict a confidence and prediction interval. Therefore, another set of results will be converted into a linear relationship by taking a natural logarithm (ln) to the tested thermal conductivity. Linear

regression theory will be used to find the 'best fit' equation in a certain prediction interval.

Thermal conductivity of 0 kPa penetration resistance

Thermal conductivity variations from dry to saturated of 0 kPa penetration resistance samples are shown in table 3.8.

Table 3.8 Thermal conductivity of substrate in each moisture content for 0 kPa

Moisture content (%)	Conductivity (W/m.K)
0	0.169
4.2	0.180
8.4	0.209
13.6	0.259
22.4	0.833
26.3	1.199
30.2	1.257

From these data, the graph can be plotted and fitted with exponential relationship, as shown in figure 3.21.

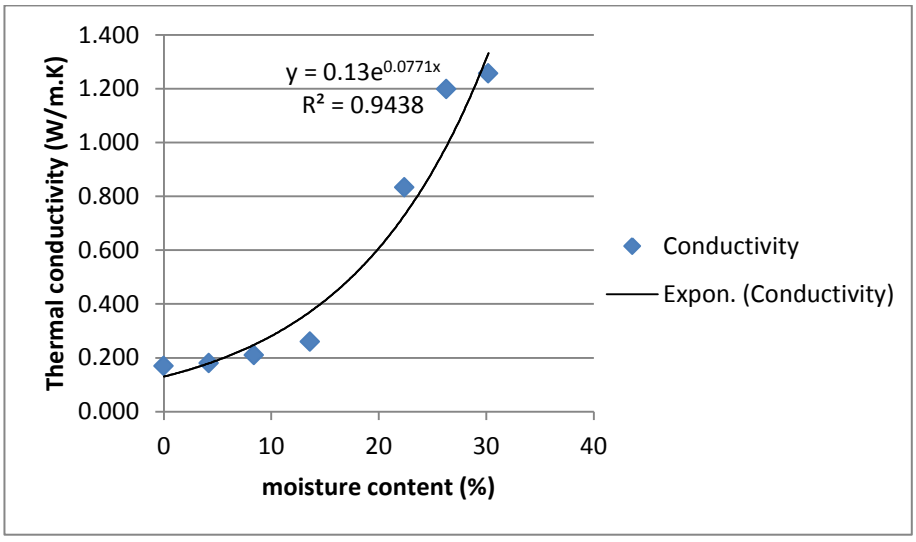

Figure 3.21 Relationship of thermal conductivity with different moisture content for 0 kPa

This exponential relationship can be recalculated by taking a natural logarithm (ln) to the thermal conductivity, against the moisture content. The result is presented in figure 3.22.

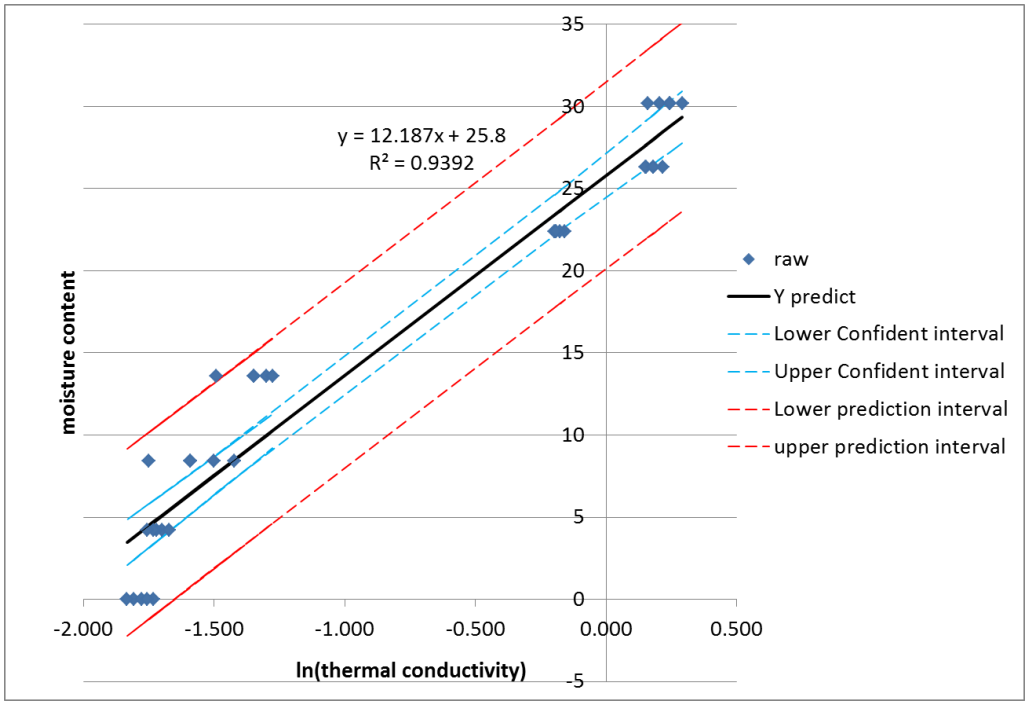

Figure 3.22 Linear relationships between thermal conductivity and moisture content of 0 kPa green roof sample

The linear equation associated with this relationship is:

$$mc = 12.187 \ln(thermal\ conductivity) + 25.8 \qquad (3.23)$$

Tested results are positioned between 95% prediction interval limits.

Thermal conductivity of 150 kPa penetration resistance

Thermal conductivity variations from dry to saturated of 150 kPa penetration resistance samples are shown in table 3.9.

Table 3.9 Thermal conductivity of green roof substrate with different moisture content for 150 kPa

Moisture content (%)	Conductivity (W/m.K)
0	0.243
4.2	0.279
8.4	0.382
27.4	1.358

From these data, the graph can be plotted and fitted with an exponential relationship, as shown in figure 3.23.

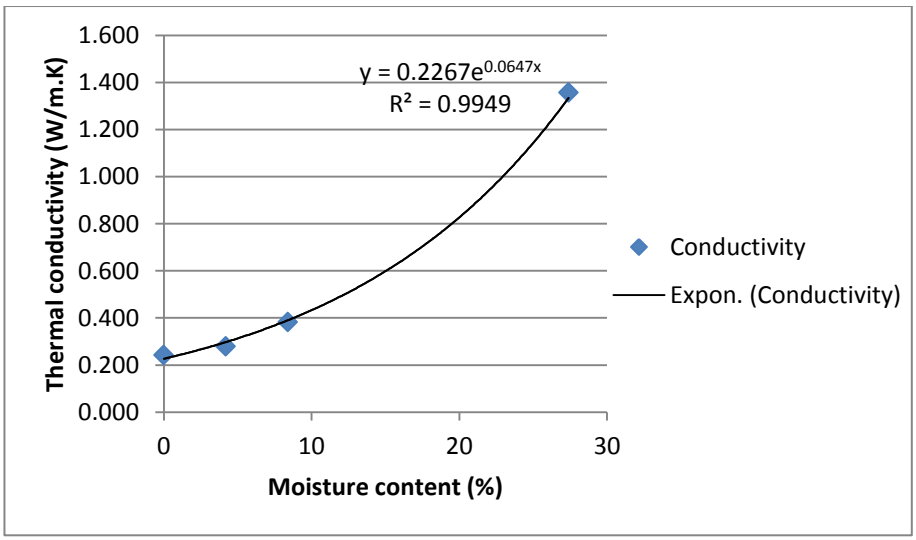

Figure 3.23 Relationship of thermal conductivity with different moisture content for 150 kPa

This exponential relationship can be recalculated by taking a natural logarithm (ln) to the thermal conductivity, against the moisture content. The result is presented in figure 3.24.

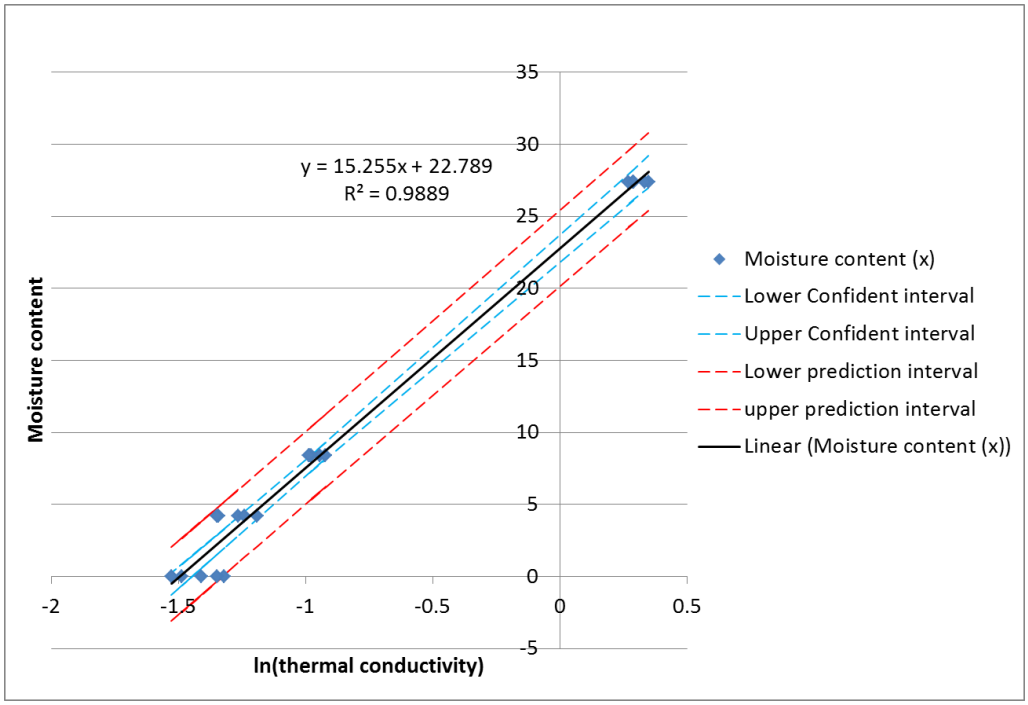

Figure 3.24 Linear relationship between thermal conductivity and moisture content of a 150 kPa green roof sample

The linear equation that associates with this relationship is:

$$mc = 15.255 \ln(thermal\ conductivity) + 22.8 \quad (3.24)$$

Tested results are positioned between 95% prediction interval limits.

Thermal conductivity of 300 kPa penetration resistance

Thermal conductivity variations from dry to saturated of 300 kPa penetration resistance samples are shown in table 3.10.

Table 3.10 Thermal conductivity of green roof substrate with different moisture content for 300 kPa

Moisture content (%)	Conductivity (W/m.K)
0	0.245
4.2	0.363
8.4	0.501
24.7	1.378

From these data, the graph can be plotted and fitted with an exponential relationship as shown in figure 3.25.

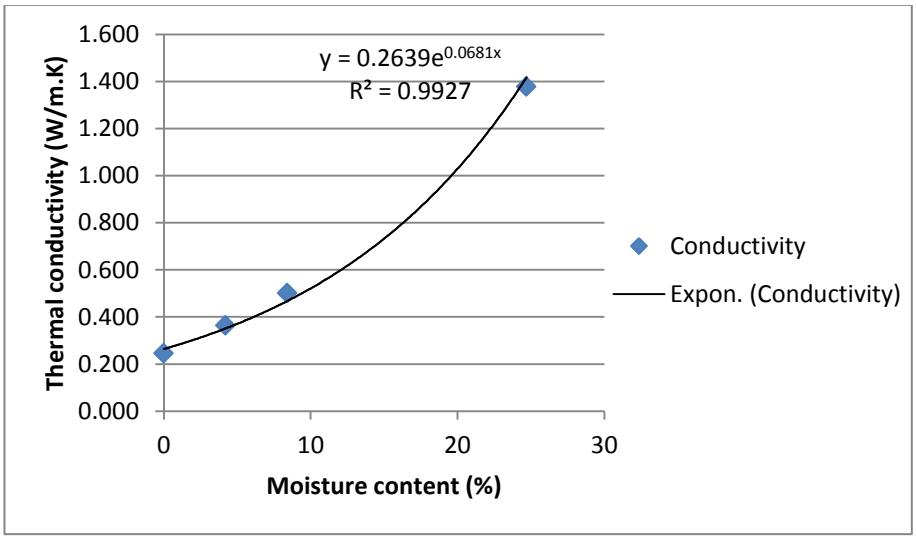

Figure 3.25 Relationship of thermal conductivity with different moisture content for 300 kPa

This exponential relationship can be recalculated by take a natural logarithm (ln) to the thermal conductivity, against the moisture content. The result is presented in figure 3.26.

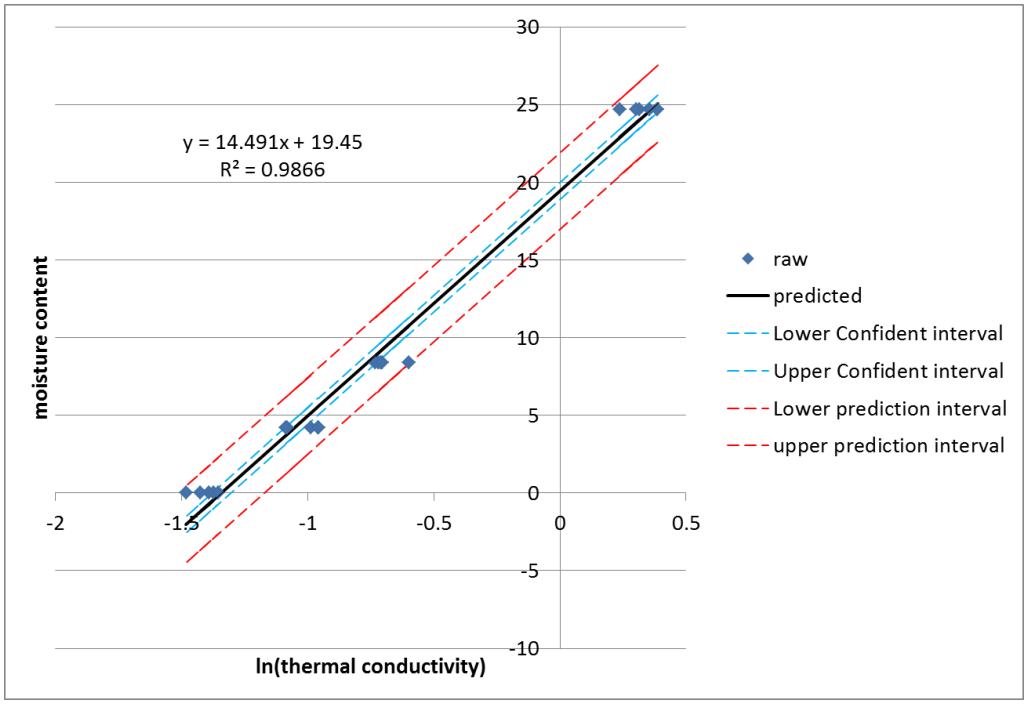

Figure 3.26 Linear relationship between thermal conductivity and moisture content of 300 kPa green roof sample

The linear equation associated with this relationship is:

$$mc = 14.491 \ln(Thermal\ conductivity) + 19.5 \qquad (3.25)$$

Tested results are positioned between 95% prediction interval limits.

Thermal conductivity of 450 kPa penetration resistance

Thermal conductivity variations from dry to saturated of 450 kPa penetration resistance samples are shown in table 3.11.

Table 3.11 Thermal conductivity of green roof substrate with different moisture content for 450 kPa

Moisture content (%)	Conductivity (W/m.K)
0	0.259
4.2	0.380
8.4	0.603
22.7	1.405

From these data, the graph can be plotted and fitted with an exponential relationship, as shown in figure 3.27.

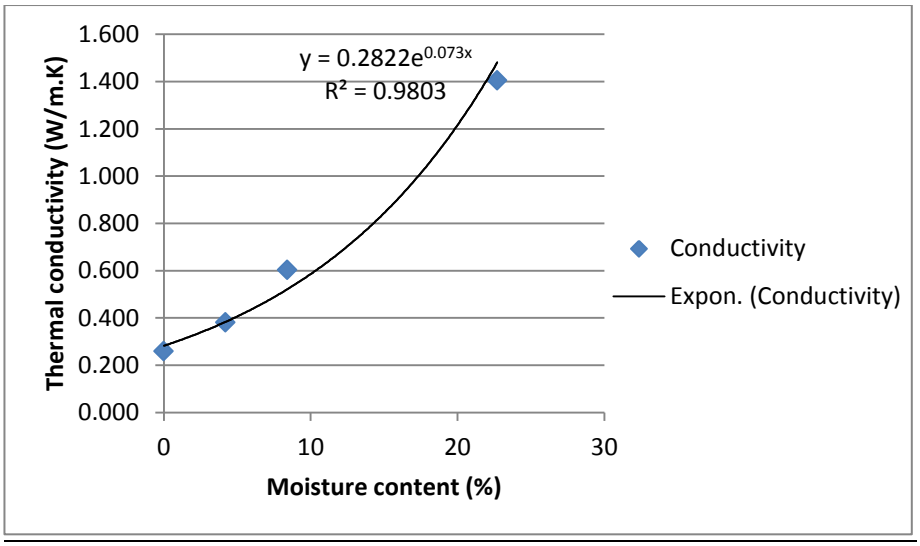

Figure 3.27 Relationship of thermal conductivity with different moisture content for 450 kPa

This exponential relationship can be recalculated by take a natural logarithm (ln) to the thermal conductivity,), against the moisture content. The result is presented in figure 3.28.

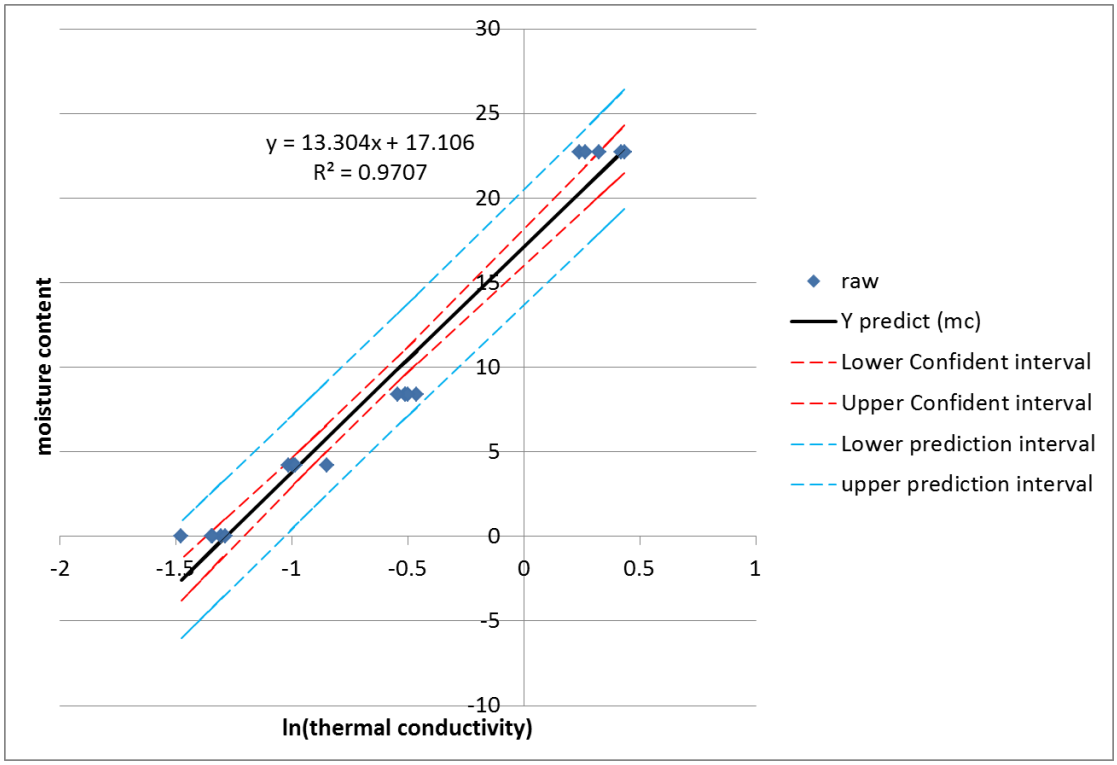

Figure 3.28 Linear relationship between thermal conductivity and moisture content of 300 kPa green roof sample

The linear equation associated with this relationship is:

$$mc = 13.304 \ln(Thermal\ conductivity) + 17.1 \qquad (3.26)$$

Tested results are positioned between 95% prediction interval limits.

Result combination

The data for each penetration resistance level shows the same configuration of exponential rise. The data are combined in figure 3.29 to determine the effect of moisture content and compaction, as in the spectrum graph.

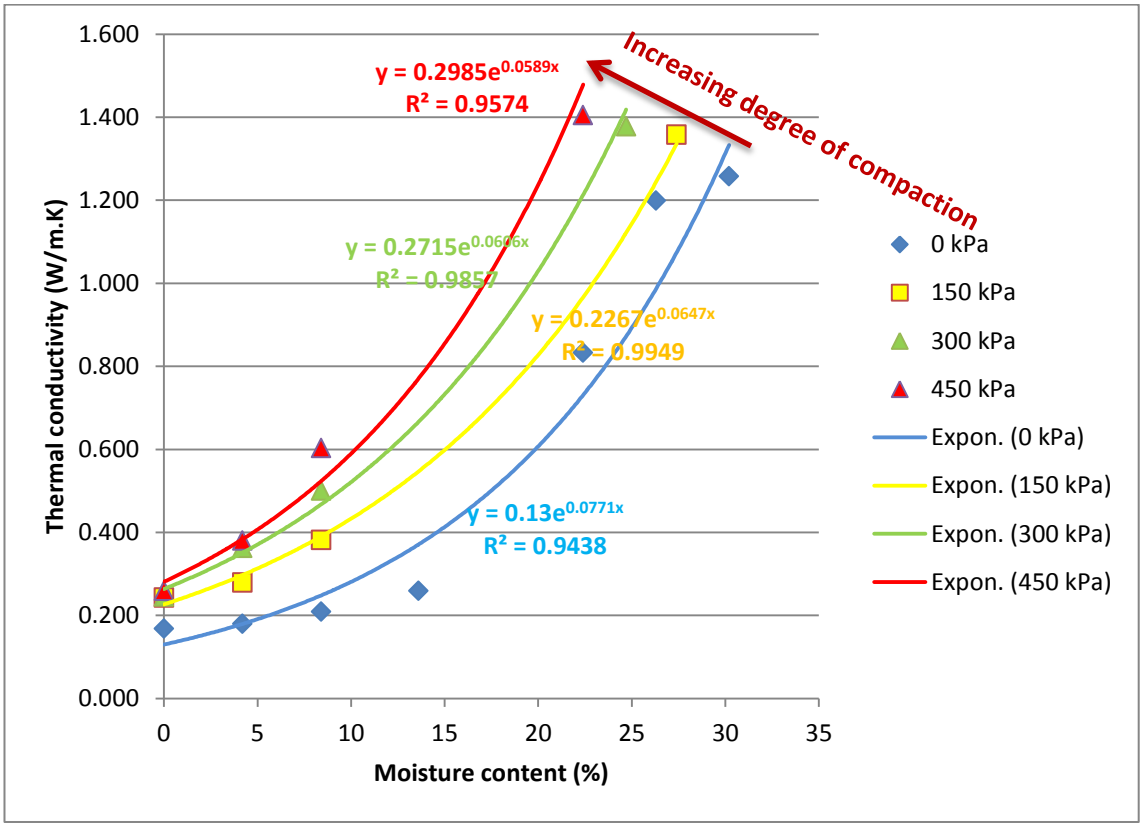

Figure 3.29 Thermal conductivity spectrum of green roof substrate from dry to saturated for each compaction level (exponential relationship)

Relationships between thermal conductivity, moisture content, and compaction are increased with an exponential function. The increase in compaction level resulted in a thermal conductivity increment when moisture content is raised, which is in accordance with the work of Sailor and Hagos (2011). The non-compacted sample yields the lowest thermal conductivity spectrum because there are lots of air spaces (low conductivity) inside that particular sample. In contrast, the 450 kPa specimen shows the highest thermal conductivity from all samples, because pore spaces were diminished during the compaction process and the low conductivity part (air) was removed from the sample.

This moisture content, compaction, and thermal conductivity relationship will be used again as a moisture content indicator in the measurement of evaporation from green roof substrates (chapter 5). For this reason, figure 3.29 needs to be presented in a linear relationship. The x-axis indicates the natural logarithm (ln) of thermal conductivity and y-axis indicates moisture contents, as shown in figure 3.30.

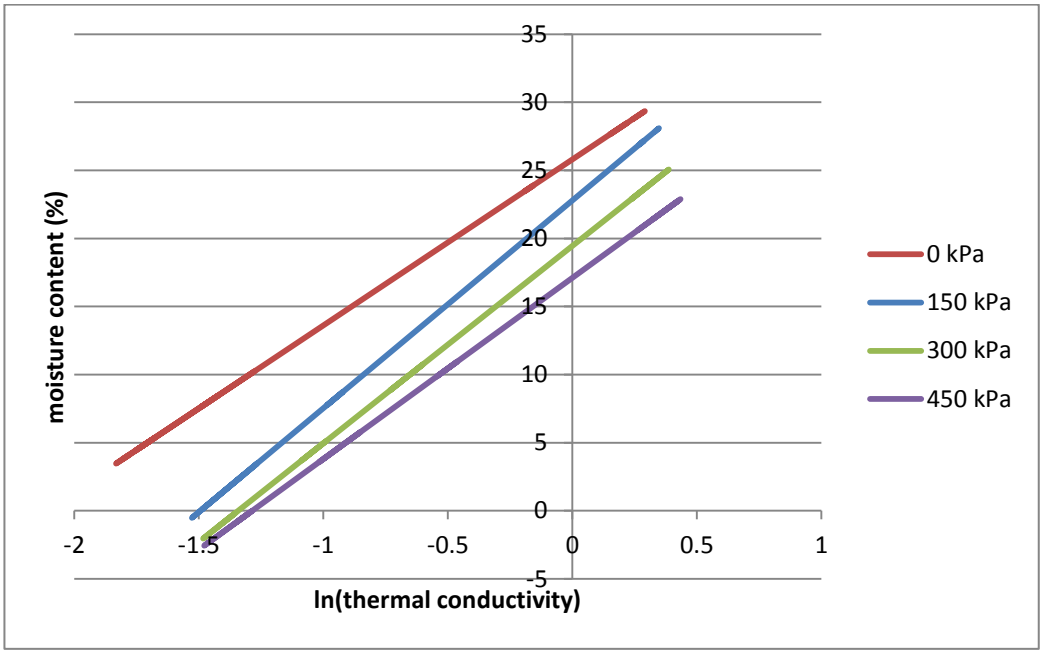

Figure 3.30 Moisture content spectrum of green roof substrate against natural logarithm of thermal conductivity in each compaction level (linear relationship)

Likewise, figure 3.30 displays the same increment of thermal conductivity and moisture content as figure 3.29. The moisture content is increased as the conduction increases. Fitted equations of each sample are already presented in equations 3.23 to 3.26, with 0 to 450 kPa compaction levels respectively.

3.7 Conclusion and discussion

This chapter has presented experimental procedures and results of the moisture content, compaction, porosity, and thermal conductivity measurements of green roof substrate samples. In addition, the importance of each parameter was pointed out in the literature review. Finally, the relationship between moisture content, compaction level, porosity, and thermal conductivity has been established.

Porosity is related directly to moisture content and compaction levels. Porosity is highest when the liquid content is zero and no compaction has been applied. However, the porosity will be reduced when moisture content and compaction levels are increased. This reduction happens because voids, or air spaces between substrate particles, are packed together.

Thermal conductivity of a green roof substrate increases as the porosity decreases. When air, which has a low thermal conductivity, is replaced by water, the overall thermal conductivity is increased. As a result, the medium has the lowest thermal conductivity in dry conditions when no compaction has been applied; in other words the medium is in a state of maximum porosity. Conversely, the medium has the highest conductivity when it is in a saturated condition, with a maximum compaction level and therefore minimum porosity.

The next chapter will introduce the absorption cycle of a green roof substrate, informed by the sharp front theory. The results presented in this chapter will be used for absorption prediction and thermal conductivity calculations.

Chapter 4: Green Roof Simulation with Absorption

4.1 Introduction

A porous medium, for example a green roof substrate, exhibits distinct moisture transfer behaviour as a result of its porous structure. The moisture, or other liquid, will transfer into the medium by capillary attraction. For this reason, this chapter will explain this absorption behaviour by using the Sharp Front theory, and then connect this theory with the steady state conduction heat transfer. Finally, the simulation process and results will be clarified by the end of the chapter.

4.2 Literature review

The Sharp Front theory will be applied together with heat conduction calculations. This theory has been confirmed by many experiments for inorganic construction materials, such as gypsum plaster, Portland limestone, and cement mortar (Hall and Hoff, 2009). However, there is a material variable which needs to be verified in order to calculate water transport by using this theory; a process which is called "sorptivity". Sorptivity is the property which expresses the tendency of a material to absorb and transmit water or other liquids by capillarity. The sorptivity can be used to estimate the time taken for the substrate to achieve saturation.

This following section will present a literature review of the Sharp Front theory.

4.2.1 Capillary force and substrate

The water transportation in porous materials is mainly driven by capillary force. Because of this force, a porous material is able to absorb the liquid which is in contact with that material’s surface or the entrance to the pore system. It would be better to understand how a porous medium, such as substrate, reacts with an entering liquid. According to Hall and Hoff (2009), the capillary rise in a vertical capillary tube in contact with a liquid reservoir is caused by surface tension (σ) which creates a pressure deficit arising from meniscus curvature. This pressure is balanced by the hydrostatic pressure of the liquid column.

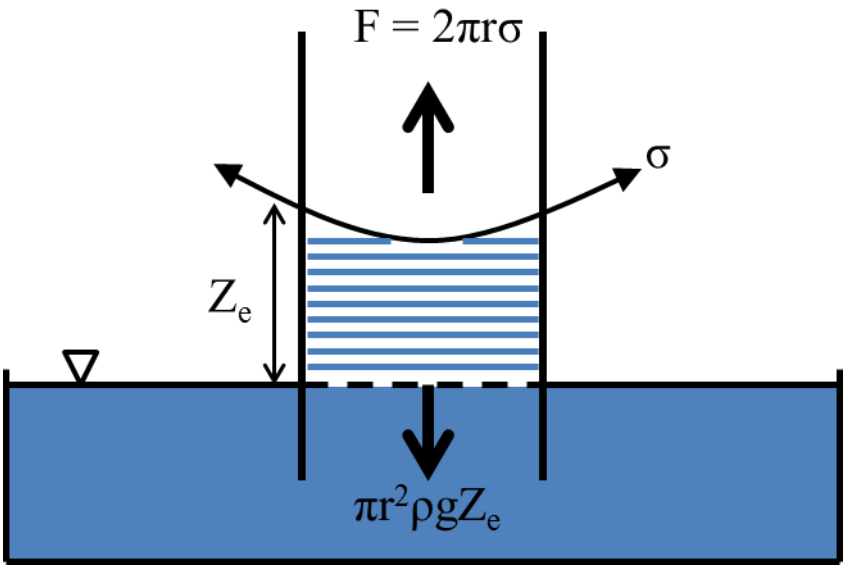

Figure 4.1 Balance in capillary tube

From figure 4.1, the water balance can be written in equation 4.1.

$$2\pi r\sigma = \pi r^2 \rho g Z_e \tag{4.1}$$

Then:

$$Z_e = \frac{2\sigma}{r\rho g} \tag{4.2}$$

From this relationship, it can be noticed that the capillary tube radius has a significant effect on the capillary rise, as a result of $Z_e \propto \frac{1}{r}$. This can be applied to porous media, since the smaller pore size can raise the liquid higher than with larger pores. In a packed bed of particles, pores size (i.e. the spaces between particles) is proportional to particle size.

The study by Buckingham (1907) depicted the relationship between soil types and their moisture content relative to the height of capillary rise. As shown in figure 4.2, the smaller particle sizes, such as clay and loam, gave higher capillary rises than the larger particles, like sand.

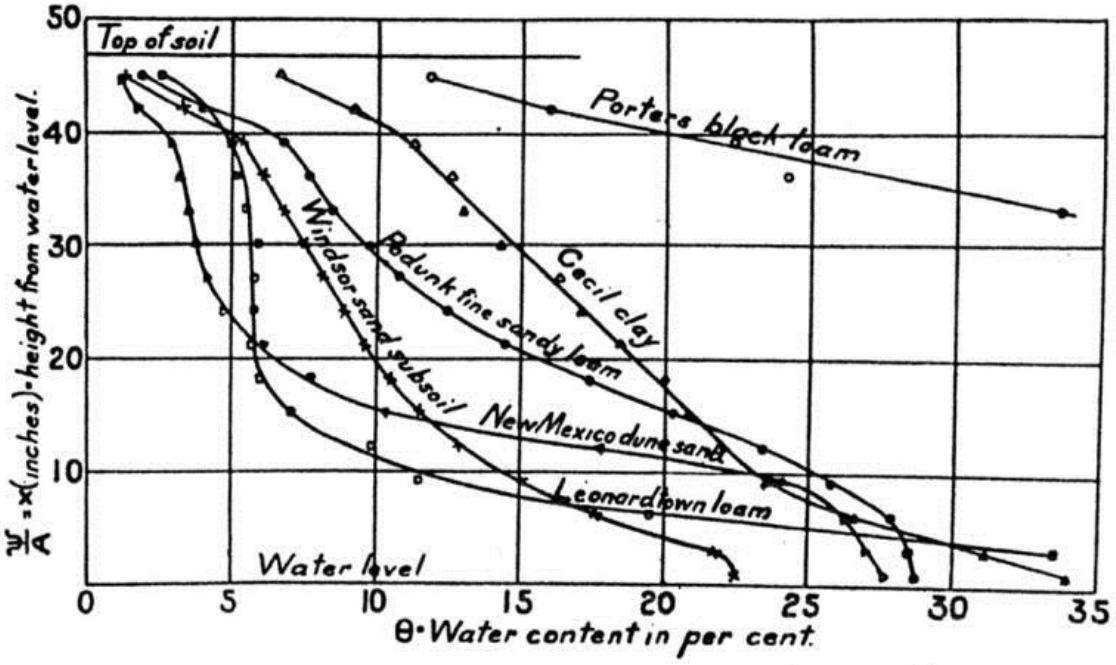

Figure 4.2 Capillary rise in unsaturated soil (Buckingham, 1907)

However, this capillarity effect and particle size relationship cannot explain the rate that porous media can absorb liquid. The suitable theory that can explain this behaviour is the Sharp Front theory and sorptivity, but it is necessary to first clarify the unsaturated flow behaviour.

4.2.2 Unsaturated flow: extended Darcy law

Porous material is dried in the initial state, after which it is exposed to liquid; then liquid is absorbed into the material's surface by capillary forces. Thus, this flow can be described by the extended Darcy equation (Hall and Hoff, 2009).

$$\mathbf{u} = K(\theta)\mathbf{F} \tag{4.3}$$

Where **u** is a vector flow velocity, θ is a ratio of liquid volume to bulk volume (volume fraction saturation), $K(\theta)$ is an unsaturated permeability at given liquid content (θ), and **F** is the capillary force that can be identified with the negative gradient of capillary potential Ψ. Thus, the extended Darcy equation is transformed to

$$\mathbf{u} = -K(\theta)\nabla\Psi \tag{4.4}$$

Ψ is the capillary potential per unit weight of liquid with dimension (L), which is the energy required to transfer a unit weight of liquid from the porous material to a

reservoir of the same liquid, at the same temperature and elevation (Hall and Hoff, 2009). This unsaturated flow mechanism is depicted in figure 4.3.

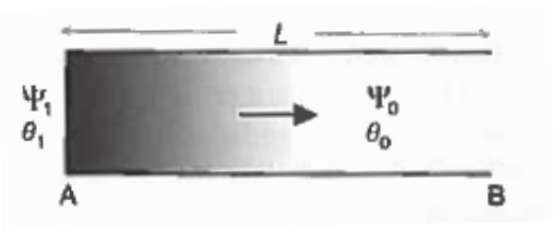

Figure 4.3 Unsaturated flow in porous material (Hall and Hoff, 2009)

However, the vector flow velocity (**u**) is difficult to measure in a material, and as a result, the previous equation is changed by combining it with a continuity equation.

$$\frac{\partial \theta}{\partial t} = \nabla K(\theta) \nabla \Psi \tag{4.5}$$

This is the fundamental equation of unsaturated flow called the Richards equation. To use this equation at least two properties of material need to be known ($K(\theta)$ and $\Psi(\theta)$), but it is more convenient to express this equation in terms of liquid content (θ). The hydraulic diffusivity (D) is defined in order to calculate the Richards equation, in which $D = K(\frac{d\Psi}{d\theta})$ and has the dimension (L^2T^{-1}). As a result, the Richards equation becomes

$$\frac{\partial \theta}{\partial t} = \nabla D \nabla \theta \tag{4.6}$$

The hydraulic diffusivity depends on the material and fluid, and signifies the tendency of the material to transport fluid by capillarity (Hall and Hoff, 2009). For one dimensional horizontal flow, this equation changes to

$$\frac{\partial \theta}{\partial t} = \frac{\partial}{\partial x}(D \frac{\partial \theta}{\partial x}) \tag{4.7}$$

If considering the initial state of liquid absorption under the action of a potential gradient, the boundary condition of this equation is $\theta = \theta_s$ (liquid content at saturation) for $x = 0$, $t \geq 0$ and $\theta = \theta_d$ (liquid content at dry stage) for $x > 0$, $t = 0$. However, this equation is not in an appropriate differential equation form. In order to offer an ordinary differential equation, θ is given by $\theta = f(\emptyset)$ where $\emptyset$ is a function of x and t given

by $\emptyset = xt^{-1/2}$, which is a Boltzmann transformation. The one dimensional horizontal flow equation, consequently, could be written

$$-\frac{\emptyset}{2}\frac{d\theta}{d\emptyset} = \frac{d}{d\emptyset}D\frac{d\theta}{d\emptyset} \tag{4.8}$$

With $\theta = \theta_s$ at $\emptyset = 0$ and $\theta = \theta_d$ as $\emptyset \to \infty$. Again, the one dimensional horizontal flow equation is then

$$x(\theta, t) = \emptyset(\theta)t^{1/2} \tag{4.9}$$

This equation shows a central point of unsaturated flow theory. It presents that as liquid is absorbed into a porous material, the liquid content against distance profile advances as $t^{1/2}$ holding constant shape $\emptyset(\theta)$. In other words, at $t > 0$, the liquid content at a distance x from the liquid entrance is θ_x, whereas beyond this point the liquid content remains zero θ_d. This represents a sharp front, and will be discussed in the following section.

4.2.3 The sorptivity

According to the unsaturated flow equation $x(\theta, t) = \emptyset(\theta)t^{1/2}$, liquid is absorbed horizontally into an initially dry porous material at all points with the wetting profile advancing as $t^{1/2}$. This has been confirmed by many experiments for inorganic construction materials, such as gypsum plaster, Portland limestone, and cement mortar (Hall and Hoff, 2009). The typical water content profiles of these materials are shown in figure 4.4.

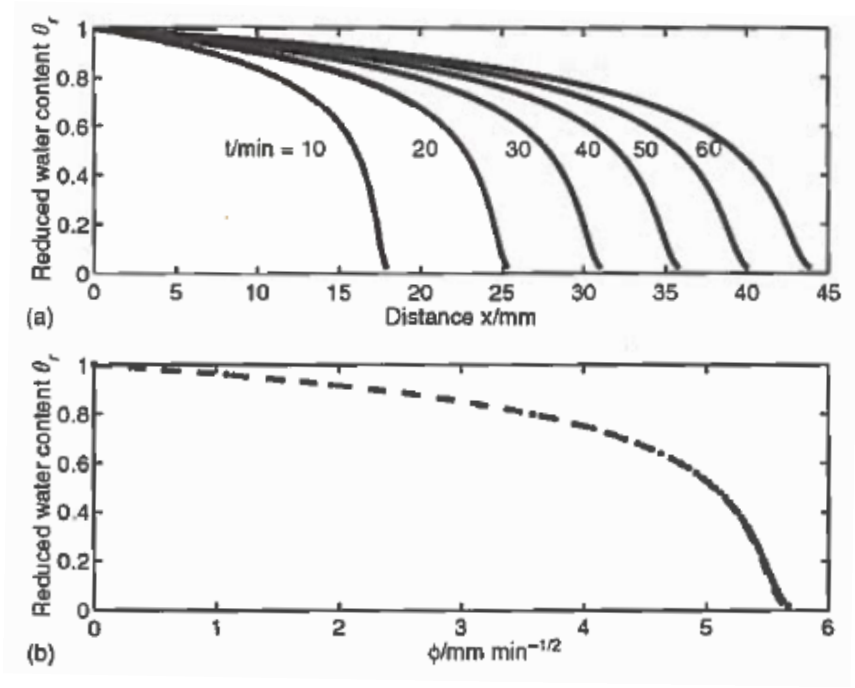

Figure 4.4 (a) Water content profiles according to time and distances (b) Master curve $\emptyset(\boldsymbol{\theta})_{\boldsymbol{r}}$ for the same material (Hall and Hoff, 2009)

In an integrated unsaturated flow equation, the total amount of liquid absorbed in time *t* is given by

$$\int_{\theta_d}^{\theta_s} x d\theta = t^{1/2} \int_{\theta_d}^{\theta_s} \emptyset(\theta) d\theta = S t^{1/2} \tag{4.10}$$

In this equation, sorptivity (*S*), which is the most important property of unsaturated flow in porous material, is defined. Sorptivity was first introduced by Philip in the field of soil physics and hydrology (Philip, 1957).

Sorptivity is the property which expresses the tendency of a material to absorb and transmit water and other liquids by capillarity. In contrast to the saturated permeability (K_s), it is sensitive to both the hydraulic conductivity (*K*) and the suction characteristics of a material (Hall and Hoff, 2009).

4.2.4 The Sharp Front model

The capillary diffusivity (*D*) of porous solids varies strongly with liquid content (θ), resulting in a very steep fronted capillary absorption profile. It is reasonable and convenient to represent this wetted front by a rectangular profile; thus, this approximation is called a 'sharp front'. Because of the simple rectangular profile, this

theory can be used with many mathematical and computational methods; for example, the finite difference model.

The advantage of using the Sharp Front model is to treat the wetted region as having uniform or constant water content, which is the saturation water content or some value close to it. Because of this assumption, the unsaturated flow problem can be reduced to an unconfined, free surface, saturated flow problem. However, the capillary potential (Ψ_f) has to remain constant, which means the total potential (Φ) of the liquid phase at the front differs from the pressure potential (P_0) just ahead of the front by an amount Ψ_f and remains constant throughout the absorption process. In other words Ψ_f could be called the capillary force acting at the front. This absorption mechanism is depicted in figure 4.5.

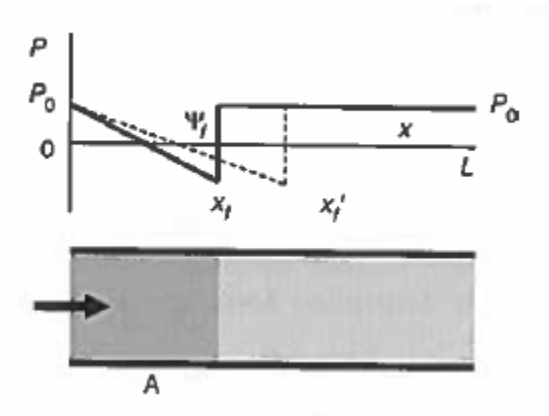

Figure 4.5 One-dimension water absorption: sharp front model (Hall and Hoff, 2009)

As shown in figure 4.5, the porous solid length L is placed in contact with liquid and it absorbs liquid simultaneously. After some time, the wet front locates at $x_f = l(t)$ and the water content in the wetted front is θ_e with the permeability of the material K_e (e represents effective quantities). In addition, it is useful to define an effective porosity (f_e) which relates the total water content of the wetted region.

$$f_e = \frac{I}{V} = i/l \tag{4.11}$$

Where:

I is the cumulative absorbed volume,

V is the material volume,

i is the cumulative absorption per unit area of inflow surface, and

l is the wetted zone length.

These quantities remain constant throughout the absorption process.

Applying the simple Darcy's law, then:

$$u = -K_e \frac{d\Phi}{dx} \tag{4.12}$$

Because $\Phi = P_0$ at $x = 0$ and $\Phi = P_0 + \Psi_f$ at $x = x_f$, then $\frac{d\Phi}{dx} = \frac{\Psi_f}{l}$ and we can write a second equation.

$$u = -K_e \frac{\Psi_f}{l} \tag{4.13}$$

Since the water content θ_e of the wetted region is dependent on position

$$\frac{du}{dx} = -K_e \frac{d^2\Phi}{dx^2} = 0 \tag{4.14}$$

This means that $\frac{d^2\Phi}{dx^2} = 0$, which is a one-dimensional form of Laplace's equation that is used in many mathematical and computational calculations. This is a reason why the Sharp Front model is very useful.

As a relation of $u = di/dt$ and $i = f_e l$, the simple differential equation can be obtained

$$\frac{di}{dt} = -K_e f_e \frac{\Psi_f}{i} \tag{4.15}$$

Then integrate this equation to obtain

$$i^2 = -2K_e f_e \Psi_f t + constant \tag{4.16}$$

At $i=0$ and $t=0$, so the constant is 0, then

$$i = (2K_e f_e |\Psi_f|)^{1/2} t^{1/2} \tag{4.17}$$

K_e and Ψ_f are model parameters, these values can be identified by the sorptivity measurement; the sorptivity is given by $S = (2K_e f_e |\Psi_f|)^{1/2}$. This is a relationship

between sorptivity and the Sharp Front model. The measurement of sorptivity will be described in the following section.

4.2.5 The measurement of sorptivity

The sorptivity can be measured in many ways, such as penetration distance method, measurement of moisture distribution method, and direct gravimetric method (Hall and Hoff, 2009). These methods share the same sorptivity and time relation with $i = St^{1/2}$.

The method based on penetration distance was initially proposed by Ho and Lewis (1984); the method measures a distance of the wetted front according to time. The sorptivity in the absorbed direction, called S_x in this case, is calculated by equation

$$S_x = x_{wf} t^{-1/2} \tag{4.18}$$

The value of x_{wf} is the distance advanced by the wet front in time *t*, which was defined in the Sharp Front model by $x_{wf} = l = i/f$, where f is a material porosity. Therefore, the sorptivity by the standard definition is now $S_x = S/f$, and porosity values of normal construction materials lie between 0.1 - 0.3.

However, to determine the actual wet front position is difficult since appreciable liquid contents may exist beyond the visible wet front. This phenomenon may result in an inaccurate sorptivity value, but accuracy can be improved by using thermal imaging.

The second method is based on the measurement of moisture distribution. It uses nuclear magnetic resonance imaging, positron emission tomography, neutron radiography, X-ray absorption or gamma ray absorption to measure the water content versus distance profile. Normally, the purpose of measuring this profile is to determine diffusivity, but the total volume of liquid absorbed can be estimated from the area under a profile, at a given time, in a one-dimensional absorption process. As a result, the sorptivity can be calculated by this direct method (Hall and Hoff, 2009). Although this is a direct and accurate method, it requires access to expensive and sophisticated equipment.

The final method for measuring sorptivity is by direct gravitational measurement. This is the most straightforward laboratory method to determine the sorptivity of porous materials, by monitoring the increase in weight of a tested material during capillary

absorption over time $\Delta W(t)$. The analysis in based on the Buckingham-Richards description of one-dimension unsaturated flow with initial condition $\theta_r = 0$ throughout material at $t = 0$ and $\theta_r = 1$ at $x = 0$ and $t > 0$. The arrangement of this test is shown in figure 4.6.

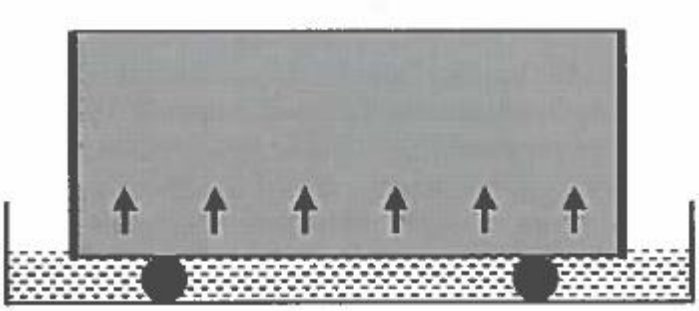

Figure 4.6 Gravimetric test for sorptivity (Hall and Hoff, 2009)

The analysis presents the cumulative absorption per unit of inflow surface area (A) as $i = \frac{\Delta W}{\rho A} = St^{1/2}$ with condition that the material is homogenous and gravitational effects are negligible. Furthermore, the cross-sectional area of an inflow surface must be parallel to a liquid reservoir; it is therefore more convenient to arrange this test in a vertical, rather than horizontal, orientation. Hall and Hoff (2009) note that there is no effect on orientation of the test due to gravity. Rectangular and cylindrical containers are suitable for this test.

During the measurement, the specimen is weighed at intervals (for instance at 1, 4, 9, 16 minutes) to determine the quantity of liquid absorbed. The weighing operation should be done as quickly as possible, lasting no longer than 30 seconds, and the clock should not be stopped while the weighing is carried out. In addition, it is necessary to mop excess liquid from the weighing apparatus with a damp cloth before each weighing takes place. A top pan balance, accurate to 0.1 gram, is suitable.

The sorptivity is determined from the gradient of the plot of volume of liquid absorbed (per unit area of inflow surface) against the square root of time. A minimum of 5 points or more is necessary to estimate a good sorptivity plot. Data obtained must show good linearity, but the $i(t^{\frac{1}{2}})$ plot should be checked for systematic curvature. If the data cannot be shown reasonably by a straight line, then no sorptivity can be determined.

For example, the following figure shows an experimental dataset obtained in a sorptivity test on a whole clay brick, which has an area of 2.264 x 10^4 mm^2, a dry weight of 2716 g., and absorbed water at a temperature of 24.8 ^oC.

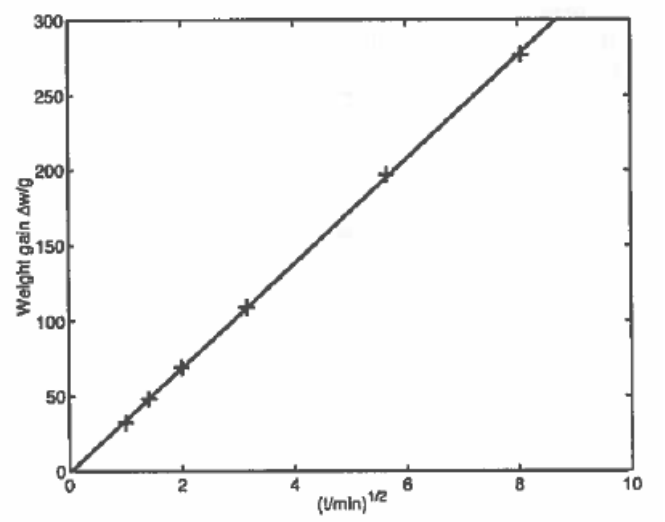

Figure 4.7 Experimental dataset of clay brick sorptivity test (Hall and Hoff, 2009)

According to the dataset of the test, the solid line is a least square fit to the data points, $\frac{\Delta w}{h} = 34.68\ (t/\text{min})^{1/2} - 1.08$, which corresponds to sorptivity S = 1.536 mm $min^{-1/2}$.

The sorptivity measurement could be done within one hour. However, a longer duration experiment could be made for a lower capillary suction material, which can result in higher test accuracy as shown in figure 4.8.

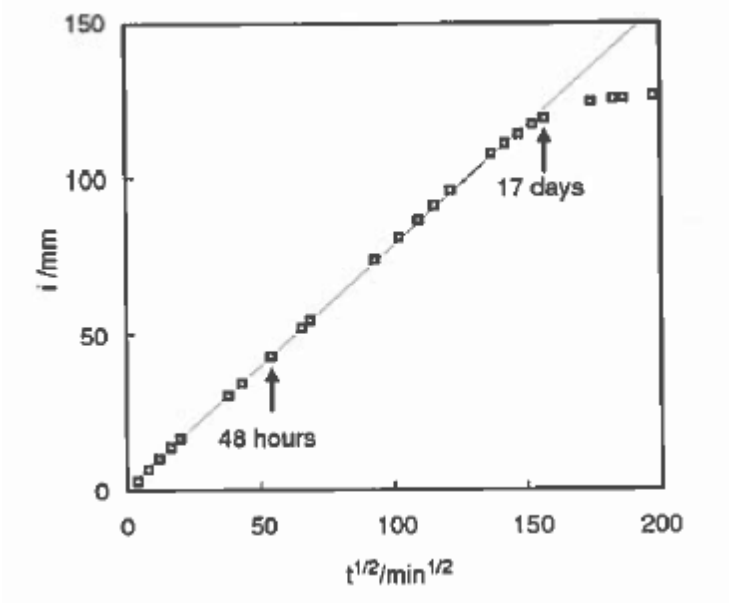

Figure 4.8 Long-term cumulative capillary absorption for water into a Lepine limestone specimen 630 mm high (Hall and Hoff, 2009)

As a result, the Sharp Front theory is suitable to estimate the thickness of the saturated layer according to the time $t^{1/2}$. The time dependent variation in the thicknesses of the saturated and dry layers can be linked with their respective thermal conductivities in order to calculate the overall thermal conductivity and hence estimate the heat conduction at every time step in the thermal simulation of a partly saturated green roof (section 4.5).

4.3 Experimental procedure

The direct gravitational method (Hall and Hoff, 2009) was used, as follows:

1. Prepare a tray of water and 6-12 mm diameter rounded steel bars, which will be used as the samples' supports.

2. Measure the cross-sectional area of an inflow surface and the initial weight of the substrate container before it contacts water.

3. Start the stop watch at the same time as a container is contacted with water (t = 0 min). The measurement set up is shown in the figure 4.6 and 4.9.

Figure 4.9 Experimental set up for direct gravitational sorptivity measurement (200 mm high specimen)

4. At a time equal to 1 minute (t = 1 min), remove a container from the water tray, and then place that container on a scale. This weight must be recorded in grams and the precision must be accurate to 0.1 gram. In addition, this weighing process has to finish as quickly as possible (maximum 30 seconds) and the experiment's timing clock must not be stopped.

5. The excess water on the scale must be removed with a damp cloth before next weighing process, since it might affect the next weighing, due to the left over liquid.

6. Repeat processes 4 and 5 with these time intervals, from the start of the experiment: 1, 2, 5, 10, 20, 30, and 60 minutes. Any circumstances or errors happening during the test must be recorded.

7. After receiving all time interval results, calculate the changes in weight and convert into the distance of water absorbed by the substrate from an initial state (t = 0). The equation used in this calculation is equation 4.19.

$$D_t = \frac{(M_t - M_0)}{A\rho_{water}} \tag{4.19}$$

Where:

M_0 is mass of a sample at initial (t = 0 minute),

M_t is mass of a sample at time interval (t = 1, 2, 5, 10, 20, 30, and 60 minutes),

A is the cross-sectional area of an inflow surface (mm^2),

P_{water} is the density of water (9.98×10^{-4} g/mm^3 at water temperature is 20 °C),

D_t is the distance of absorbed water at time t (mm).

Plot all absorbed distance of water against the square root of each time interval ($t^{1/2}$) in the graph, and then determine the slope of this graph. The fitted slope value shall be considered as the sorptivity value of this substrate. If the data cannot be shown reasonably by a straight line, then no sorptivity can be determined.

The next section will present the result for green roof substrate samples.

4.4 Experimental result

The experimental result will be present in two different comparisons. The first is sorptivity at different moisture content when there is no compaction applied (0, 4.2, 8.4, 13.6, and 22.4 percent moisture content). The second comparison shows the effect of compaction, which is started from 0, 150, 300, and 450 kPa. AT 450 kPa, however, only 0%, 4.2%, and 8.4% moisture content could be tested, because 13.6% and 22.4% samples cannot be compacted.

4.4.1 Sorptivity results without compaction

The first data set will be sorptivity values from an intensive green roof substrate sample, when moisture contents are varied. The moisture content will start from 0% then increase to 4.2%, 8.4%, 13.6%, and 22.4% consecutively.

The experimental data from measurements are shown in table 4.1. The identification of each material can be described as:

IN000000 = Intensive substrate, 0% moisture content, 0 compaction

IN042000 = Intensive substrate, 4.2% moisture content, 0 compaction

IN084000 = Intensive substrate, 8.4% moisture content, 0 compaction

IN136000 = Intensive substrate, 13.6% moisture content, 0 compaction

IN224000 = Intensive substrate, 22.4% moisture content, 0 compaction

Table 4.1 Increment of substrate mass of non-compacted samples in time interval

Time (min)	0 (dry)	1	2	5	10	20	30	60
Specimen	weight (grams)							
IN000000	1501.3	1607.5	1623.5	1653.3	1676.2	1713.2	1743.9	1803.4
IN042000	1395.6	1455.7	1467.9	1491.0	1516.8	1553.3	1577.9	1625.1
IN084000	1525.4	1564.6	1579.5	1610.2	1641.7	1675.1	1695.0	1725.5
IN136000	1523.3	1537.1	1545.9	1559.6	1572.7	1586.2	1594.4	1626.5
IN224000	1470.0	1499.0	1500.4	1508.3	1515.1	1522.8	1526.9	1543.3

Containers used in this experiment are the same size. Therefore, the diameter and the cross-sectional area of these containers are similar; a diameter of 105 mm. and a cross-sectional area = 8,659 mm^2. The density of water at 20^oC is 998.2 kg/m^2, the distance of water absorbed by a substrate can be calculated by use of equation 4.19. The results are presented in table 4.2.

Table 4.2 Distances of absorbed water by substrates in time interval

Time$^{1/2}$ (min$^{1/2}$)	0	1	1.41	2.24	3.16	4.47	5.48	7.75
Specimen	water distance (mm)							
IN000000	0.0	12.3	14.1	17.6	20.2	24.5	28.1	35.0
IN042000	0.0	7.0	8.4	11.0	14.0	18.2	21.1	26.6
IN084000	0.0	4.5	6.3	9.8	13.5	17.3	19.6	23.2
IN136000	0.0	1.6	2.6	4.2	5.7	7.3	8.2	11.9
IN224000	0.0	3.4	3.5	4.4	5.2	6.1	6.6	8.5

For the sorptivity determination, the first minute of the absorption process (0 to 1 minute) needs to be ignored because the amount of water absorbed in this time includes any water that is absorbed by the container as well. The evidence is the steep rise from 0 minute to 1 minute in a water distance chart (figure 4.10).

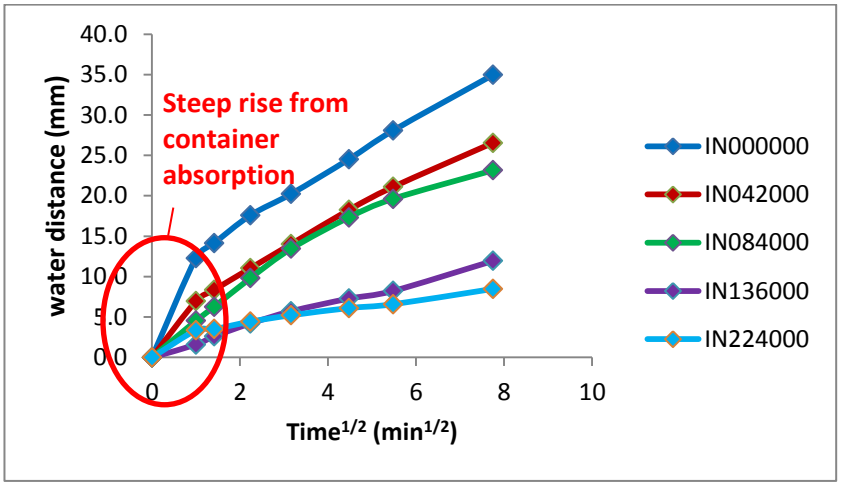

Figure 4.10 The steep rise in the early stage of absorption experiment

As a consequence, the sorptivity determination will use the data from 1 minute to 60 minutes, and the value will use the slope from the fitted linear regression equation. Figure 4.11 presents graphical results of 0% moisture content as an example.

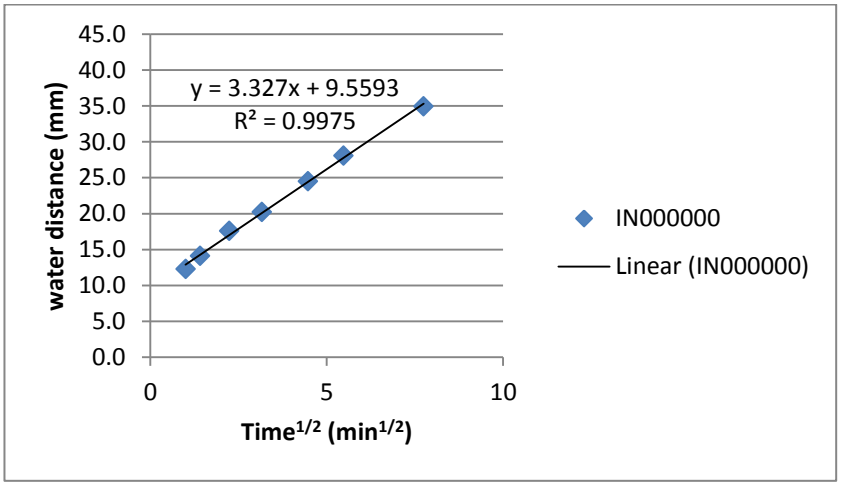

Figure 4.11 The water distance and sorptivity data of intensive substrate, 0% moisture content, 0 compaction

In every case, the graph of water distance against square root of time of different moisture content samples show a linear relationship with a good coefficient of determination (R^2 typically greater than 0.99). This behaviour means the absorption mechanism of green roof growing media in different moisture contents is according to the Sharp Front theory.

The slope represents the sorptivity value and according to the theory, the dry porous material has the highest hydraulic (capillary) potential (Ψ_f), which yields the highest

sorptivity value. In contrast, the saturated substrate has no capillary potential, so a sorptivity value cannot be justified. Figure 4.12 show the spectrum of sorptivity values at different moisture content.

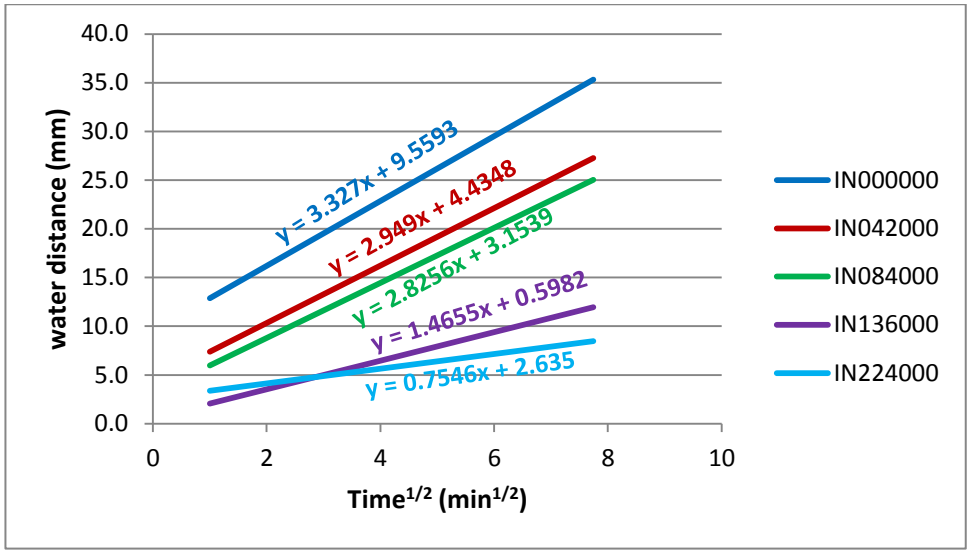

Figure 4.12 The sorptivity spectrum of green roof substrate in five different moisture contents

From figure 4.12, it can be seen that slope decrease as moisture content increases. The dry sample has a sorptivity value equivalent to 3.33 mm/min$^{1/2}$, which is the highest value of the green roof sample. The 4.2%, 8.4% and 13.6% wet samples have sorptivity values equal to 2.95, 2.83, and 1.47 mm/min$^{1/2}$ respectively. Finally, the near saturated specimen (22.4% moisture content) produced the least sorptivity, of 0.75 mm/min$^{1/2}$.

The aforementioned results are for non-compacted specimens, and are in accordance with the capillary absorption force. The next section will presents the results from compacted specimens.

4.4.2 Sorptivity results of samples with compaction

This section will present the results from sorptivity measurement, when green roof substrates are compacted to the desired compaction level. The procedure will follow that described in section 4.3 for un-compacted samples, but the sample preparation will follow the compaction procedure in section 3.3.2. Numbers of blows applied to achieve a satisfactory compaction level are related to table 3.1.

The dry, 4.2%, and 8.4% moisture content green roof substrates were investigated with 0, 150, 300, and 450 kPa compaction levels. The result will be shown for each moisture content with varied compaction.

The sample identifications are as follows:

IN000150 = Intensive substrate, 0% moisture content, 150 kPa compaction

IN000300 = Intensive substrate, 0% moisture content, 300 kPa compaction

IN000450 = Intensive substrate, 0% moisture content, 450 kPa compaction

IN042150 = Intensive substrate, 4.2% moisture content, 150 kPa compaction

IN042300 = Intensive substrate, 4.2% moisture content, 300 kPa compaction

IN042450 = Intensive substrate, 4.2% moisture content, 450 kPa compaction

IN084150 = Intensive substrate, 8.4% moisture content, 150 kPa compaction

IN084300 = Intensive substrate, 8.4% moisture content, 300 kPa compaction

IN084450 = Intensive substrate, 8.4% moisture content, 450 kPa compaction

Dry green roof substrate result

Table 4.3 shows the increment of specimen's weight of dry samples after water was absorbed in one hour.

Table 4.3 Increment of substrate mass of dry green roof specimens with variation of compaction levels in time interval

Time (min)	0 (dry)	1	2	5	10	20	30	60
Specimen	weight (grams)							
IN000000	1501.3	1607.5	1623.5	1653.3	1676.2	1713.2	1743.9	1803.4
IN000150	2025.6	2075.0	2085.7	2106.5	2129.0	2161.6	2184.2	2224.2
IN000300	2021.9	2059.6	2068.8	2088.5	2108.3	2135.2	2154.7	2192.9
IN000450	2026.5	2067.2	2074.9	2090.9	2108.2	2133.1	2150.8	2187.9

Increments in weight can be converted into absorbed water distance by equation 4.19; the size of the specimen container is still the same. Therefore, table 4.4 presents water distances of 0% moisture content with different compaction levels.

Table 4.4 The absorbed water distance of dry samples in each compaction level

Time$^{1/2}$ (min$^{1/2}$)	0	1	1.41	2.24	3.16	4.47	5.48	7.75
Specimen	water distance (mm)							
IN000000	0.0	12.3	14.1	17.6	20.2	24.5	28.1	35.0
IN000150	0.0	5.7	7.0	9.4	12.0	15.7	18.3	23.0
IN000300	0.0	4.4	5.4	7.7	10.0	13.1	15.4	19.8
IN000450	0.0	4.7	5.6	7.5	9.5	12.3	14.4	18.7

These water distance data are plotted into linear graphs to determine sorptivity values of each specimen, as shown in figure 4.13.

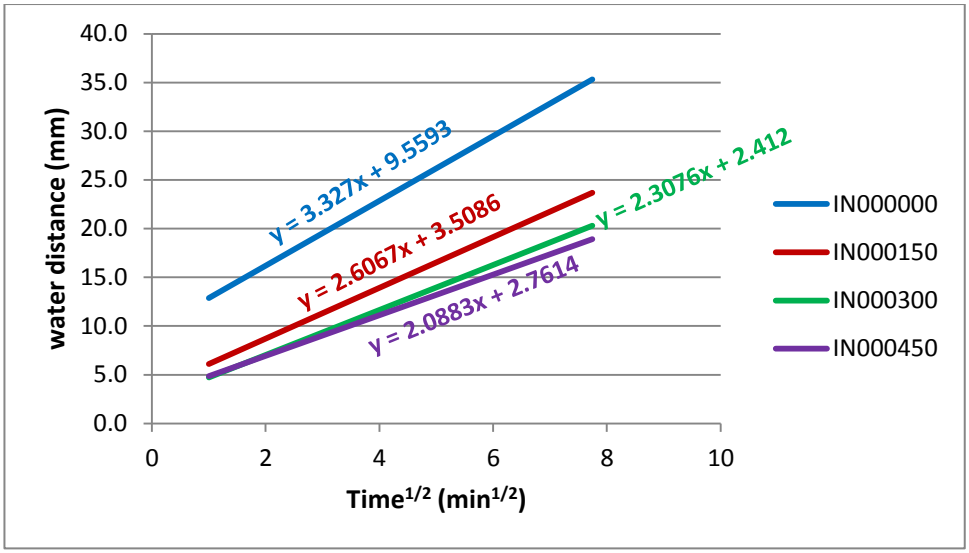

Figure 4.13 Absorbed water distances and fitted linear equation of 0% moisture content samples with variation of compaction level

From figure 4.13, the data suggests that the higher compaction level reduces the sorptivity value of dry samples. The un-compacted specimen produced the highest sorptivity of approximately 3.33 mm/min$^{1/2}$. The 150 kPa and 300 kPa samples have sorptivity values equivalent to 2.61 and 2.31 mm/min$^{1/2}$ respectively, while the lowest sorptivity is 2.1 mm/min$^{1/2}$ from a 450 kPa compacted sample. Coefficients of determination (R-values) are 0.997, 0.994, 0.995, and 0.998 for 0, 150, 300, and 450 kPa samples respectively.

4.2% mc green roof substrate result

The experimental results of substrate mass increments in one hour are presented in table 4.5.

Table 4.5 Increment of substrate mass of 4.2% moisture content green roof specimens with variation of compaction level in time interval

Time (min)	0 (dry)	1	2	5	10	20	30	60
Specimen	weight (grams)							
IN042000	1395.6	1455.7	1467.9	1491.0	1516.8	1553.3	1577.9	1625.1
IN042150	2024.5	2055.5	2064.9	2082.6	2102.0	2127.2	2144.7	2182.4
IN042300	2020.9	2048.4	2056.1	2070.0	2085.2	2106.6	2122.7	2156.2
IN042450	2025.5	2067.0	2072.2	2082.9	2094.3	2111.1	2124.3	2153.0

Increments in weight can be converted into absorbed water distance by using equation 4.19; the size of the specimen container is still the same. Therefore, table 4.6 presents water distances of 4.2% moisture content with different compaction levels against square root of times.

Table 4.6 The absorbed water distance of 4.2% moisture content samples in each compaction level

$Time^{1/2}$ ($min^{1/2}$)	0	1	1.41	2.24	3.16	4.47	5.48	7.75
Specimen	water distance (mm)							
IN042000	0.0	7.0	8.4	11.0	14.0	18.2	21.1	26.6
IN042150	0.0	3.6	4.7	6.7	9.0	11.9	13.9	18.3
IN042300	0.0	3.2	4.1	5.7	7.4	9.9	11.8	15.7
IN042450	0.0	4.8	5.4	6.6	8.0	9.9	11.4	14.8

These water distance data are plotted into linear graphs to determine sorptivity values of each specimen, as shown in figure 4.14.

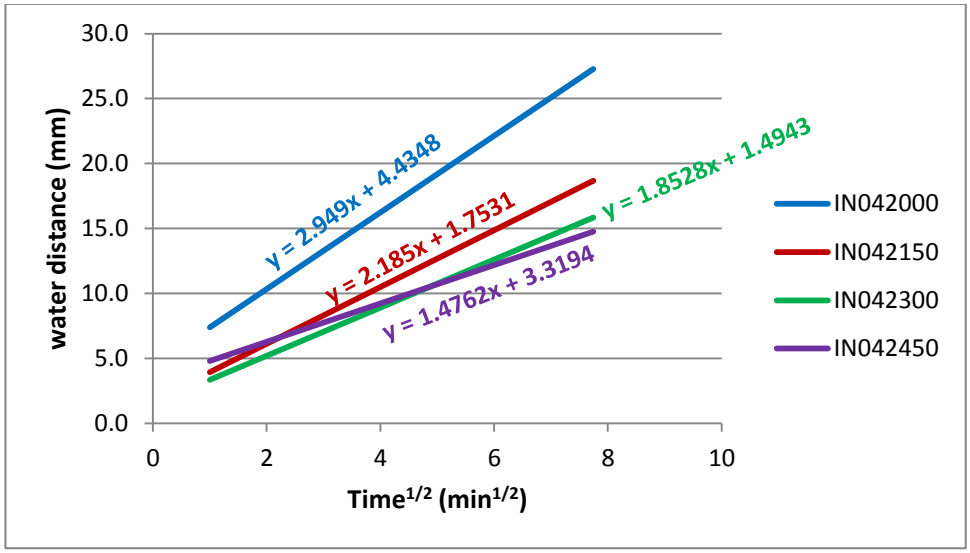

Figure 4.14 Absorbed water distances and fitted linear equation of 4.2% moisture content samples with variation of compaction level

Figure 4.14 shows the 4.2% sample has a similar sorptivity tendency to the dry sample data presented in the previous section. The un-compacted specimen produces the highest sorptivity which is approximately 2.95 mm/min$^{1/2}$. The 150 kPa and 300 kPa samples have sorptivity values equivalent to 2.19 and 1.85 mm/min$^{1/2}$ respectively. The lowest sorptivity is 1.48 mm/min$^{1/2}$ from the highest compacted sample. Coefficients of determination (R-values) are 0.995, 0.996, 0.999, and 0.999 for 0, 150, 300, and 450 kPa samples respectively.

8.4% mc green roof substrate result

The table 4.7 shows the increments of the 8.4% moisture content samples' weights after water was absorbed in one hour.

Table 4.7 Increment of substrate mass of 8.4% moisture content green roof specimens with variation of compaction level in time interval

Time (min)	0 (dry)	1	2	5	10	20	30	60
Specimen	weight (grams)							
IN084000	1525.4	1564.6	1579.5	1610.2	1641.7	1675.1	1695.0	1725.5
IN084150	2024.8	2045.2	2055.4	2074.5	2093.5	2118.7	2136.2	2168.7
IN084300	2028.0	2062.4	2069.3	2084.0	2096.8	2117.4	2135.1	2165.2
IN084450	2025.5	2062.0	2070.2	2082.2	2094.5	2108.7	2120.7	2137.8

Increments in weight can be converted into absorbed water distance in the same way as in the previous calculations. Therefore, table 4.8 presents water distances of the 8.4% moisture content samples with different compaction levels against square root of times.

Table 4.8 The absorbed water distance of 8.4% moisture content samples in each compaction level

Time$^{1/2}$ (min$^{1/2}$)	0	1	1.41	2.24	3.16	4.47	5.48	7.75
Specimen	water distance (mm)							
IN084000	0.0	4.5	6.3	9.8	13.5	17.3	19.6	23.2
IN084150	0.0	2.4	3.5	5.8	7.9	10.9	12.9	16.6
IN084300	0.0	4.0	4.8	6.5	8.0	10.3	12.4	15.9
IN084450	0.0	4.2	5.2	6.6	8.0	9.6	11.0	13.0

These water distance data are plotted into linear graphs to determine the sorptivity values of each specimen, as shown in figure 4.15.

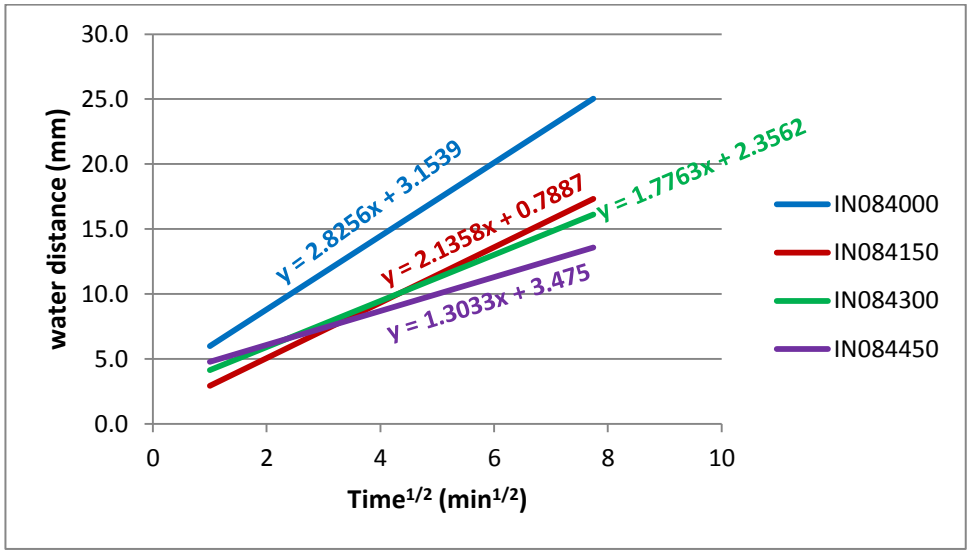

Figure 4.15 Absorbed water distances and fitted linear equation of 8.4% moisture content samples with variation of compaction level

From figure 4.15, sorptivity values of 8.4% mc samples exhibit a similar tendency as the dry and 4.2% mc samples presented in the previous sections. The un-compacted specimen produced the highest sorptivity, which is approximately 2.83 mm/min$^{1/2}$. The 150 kPa and 300 kPa samples have sorptivity values equivalent to 2.14 and 1.78 mm/min$^{1/2}$ respectively; the lowest sorptivity is 1.30 mm/min$^{1/2}$ from the highest compacted sample. Coefficients of determination (R-values) are 0.96, 0.991, 0.998, and 0.982 for 0, 150, 300, and 450 kPa samples respectively.

4.4.3 Conclusion of results

The results from previous section can be drawn together in order to compare the effect of moisture content and compaction level on sorptivity. Table 4.9 presents sorptivity and porosity values of green roof substrate specimens with different moisture contents and penetration resistances.

Table 4.9 Values of sorptivity and porosity of green roof substrates

Sample id	Sorptivity (mm/min$^{1/2}$)	Porosity
IN000000	3.33	0.53
IN000150	2.61	0.49
IN000300	2.31	0.44
IN000450	2.09	0.4
IN042000	2.95	0.53
IN042150	2.19	0.5
IN042300	1.85	0.47
IN042450	1.48	0.44
IN084000	2.83	0.53
IN084150	2.14	0.5
IN084300	1.78	0.47
IN084450	1.3	0.44

Furthermore, figure 4.16 illustrates trend lines of absorbed water distance together, in order to see the spectrum of sorptivity.

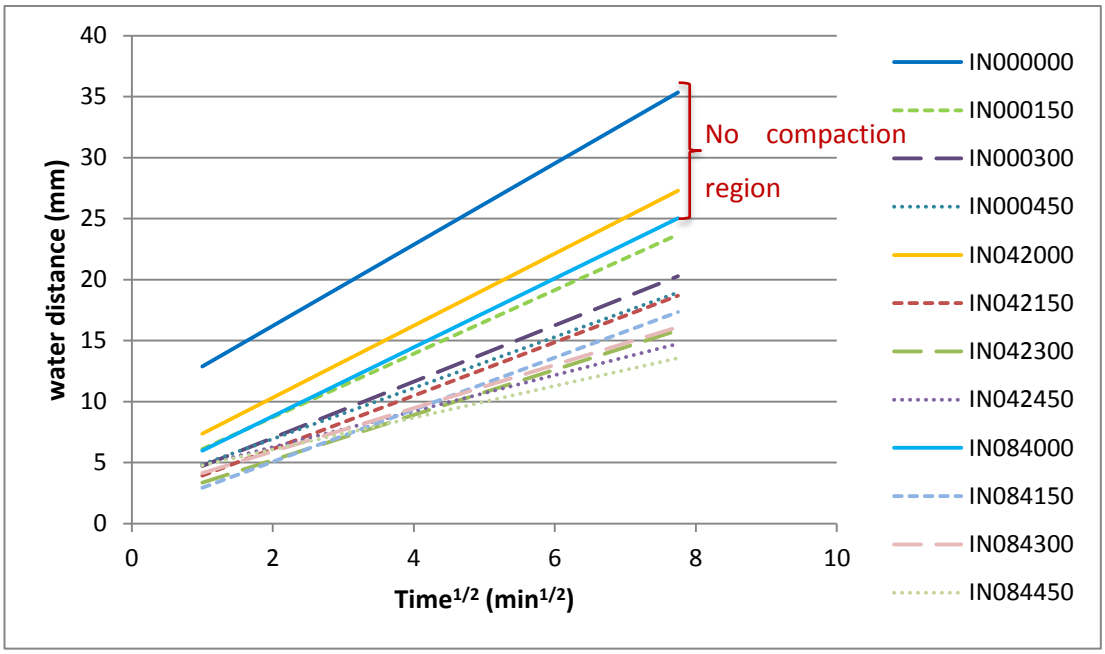

Figure 4.16 Spectrum of absorbed water distances

Table 4.9 and figure 4.16 clearly depict that moisture content has the most significant effect on sorptivity values. From the non-compaction region in figure 4.16, it can be seen that non-compacted samples have the highest absorbed water distance, with a dry sample (IN000000) having a standout linear line from the rest of samples, due to its rapid absorption rate at the beginning of the experimental process, because it has the highest hydraulic potential. The non-compacted 4.2% and 8.4% moisture content samples (IN042000 and IN084000) have lower absorbed water distances than the dry sample, due to their lower hydraulic potential. However, the sorptivity data (or slope of the graph) are very close to the dry sample, at 2.61 and 2.31 $mm/min^{1/2}$.

For compacted samples, the graphs in figure 4.16 shows that initial absorbed water distances start in a narrow range of between 2.5 and 6 mm. This behaviour might result from a difficulty of water in entering a substrate entrance surface, due to the compaction energy forcing substrate particles closer together, which consequently prevents water from entering the substrate. However, the hydraulic potential is continuing to absorb water, after it has passed through the substrate surface. This mechanism follows the Sharp Front theory; the sorptivity can be determined as reducing, as compaction is correspondingly increased.

The next section will explain the integration of sorptivity and thermal conduction, for which computer simulation will be used as a calculation tool.

4.5 Integration with thermal conductivity

In order to calculate the variation of heat flux with time, two features must be connected – the movement of the sharp front boundary between dry and saturated substrate, and the thermal conductivity of the both dry and saturated substrate. The computation is presented in this section and the heat flux calculated at each time step. From this, the simulation is developed.

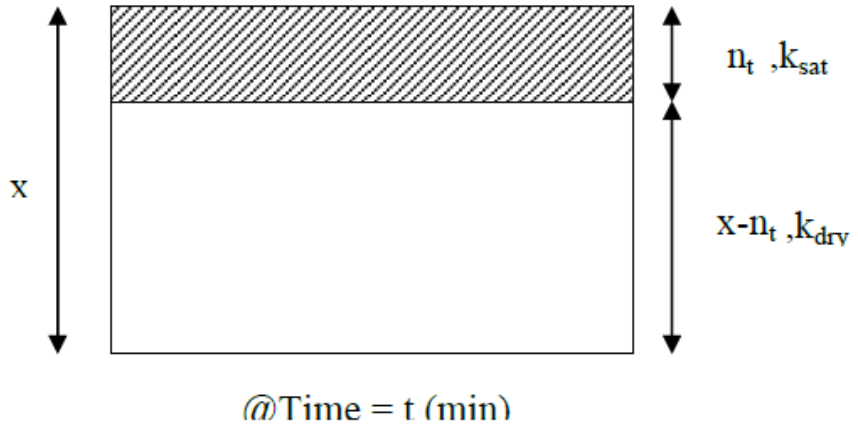

Figure 4.17 Formation of liquid transfer in a substrate layer

Figure 4.17 presents the boundary between the saturated and dry layers at a certain time step according to the Sharp Front theory; where:

x = the thickness of substrate layer (m),

t = time (min),

n_t = the thickness of saturated layer at time t (m),

x-n_t = the thickness of remaining dry layer (m),

k_{sat} = the thermal conductivity of saturated substrate layer (W/m.K), and

k_{dry} = the thermal conductivity of dry substrate layer (W/m.K).

Linking those variables by the thermal resistance equation

$$R_t = \frac{n_t}{K_{sat}} + \frac{x - n_t}{K_{dry}} \tag{4.20}$$

Where: R_t is the thermal resistance at time t (m^2K/W). In addition, the thickness of the saturated layer (n_t) can be calculated by using the sorptivity value (S), as shown in this equation.

$$n_t = \frac{S(t)^{\frac{1}{2}}}{\epsilon 1000} \tag{4.21}$$

S = sorptivity value ($mm/min^{1/2}$)

ϵ = porosity of substrate

The sorptivity value can be used to determine the amount of water absorbed by the material. The distance of the saturated layer (n_t), in contrast, includes solid particles and water that has replaced pore spaces. Therefore, the thickness of a saturated layer needs to consider the porosity, as shown in equation 4.21.

Putting these relationships into a thermal resistance equation gives:

$$R_t = \frac{x}{K_{dry}} + \frac{S(t)^{\frac{1}{2}}}{1000\epsilon}\left(\frac{1}{K_{sat}} - \frac{1}{K_{dry}}\right) \tag{4.22}$$

However, there is a limitation of equation 4.22 because the saturated front term ($\frac{S(t)^{\frac{1}{2}}}{1000\epsilon}$) cannot exceed the thickness of the layer (x). Boundary conditions used in this equation are:

- $\frac{S(t)^{\frac{1}{2}}}{1000\epsilon} < x$, the thermal resistance is $R_t = \frac{x}{K_{dry}} + \frac{S(t)^{\frac{1}{2}}}{1000\epsilon}\left(\frac{1}{K_{sat}} - \frac{1}{K_{dry}}\right)$
- $\frac{S(t)^{\frac{1}{2}}}{1000\epsilon} \geq x$, the thermal resistance is $R_t = \frac{x}{K_{dry}} + x\left(\frac{1}{K_{sat}} - \frac{1}{K_{dry}}\right)$

This thermal resistance value will be used to calculate the heat conduction in each time steps by the steady state heat conduction equation:

$$q_t = \frac{-(T_{out} - T_{in})}{R_t} \tag{4.23}$$

Where:

q_t is heat flux through a substrate layer at time t (W/m^2),

T_{out} is the outdoor temperature (^{o}C), and

T_{in} is the indoor temperature (^{o}C).

These equations are simulated in the MATLAB programme; the simulation codes being presented in the appendix. The following section presents the results of simulation from different green roof substrate conditions.

4.6 Simulation results

This section compares the simulation results of green roof substrate in different moisture content and compaction levels. The input data are as follows:

Thickness of the layer (x) = 0.1 m or 100 mm

Outdoor temperature (T_{out}) = 18^{o}C

Indoor temperature (T_{in}) = 25^{o}C

Initial condition: substrate is dry, wetting commences from above at start time.

Simulation time = 1440 minutes (24 hours), wetting continuously applied.

As noted in section 4.2.5, there is no effect of orientation on the sorptivity-related water flow. The sorptivity and porosity of substrates will follow table 4.9, and the thermal conductivity data will follow tables 3.8 to 3.11 in the previous chapter. The simulated results will be presented for 0%, 4.2%, and 8.4% moisture contents, with a variation of penetration resistance (0, 150, 300, and 450 kPa).

4.6.1 Simulation results of 0% mc green roof substrate

Information needed to simulate every one minute. Thermal resistance (R) and conduction heat flux due to an absorption cycle of 0% mc green roof substrate can be calculated from initial and saturated thermal conductivities, which is presented in different compaction levels in table 4.10.

Table 4.10 Thermal conductivities of 0% moisture content samples

Sample ID	Thermal conductivity (W/m.K)
IN000000 (initial)	0.169
IN000150 (initial)	0.243
IN000300 (initial)	0.245
IN000450 (initial)	0.259
IN000000 (saturated at 30.2% mc)*	1.257
IN000150 (saturated at 27.4% mc)*	1.358
IN000300 (saturated at 24.7% mc)*	1.378
IN000450 (saturated at 22.7% mc)*	1.405

Note **Saturated moisture content of compacted samples is different due to the available pore spaces.*

From the given information, the minute-by minute_thermal resistance can be calculated through MATLAB and presented in figure 4.18.

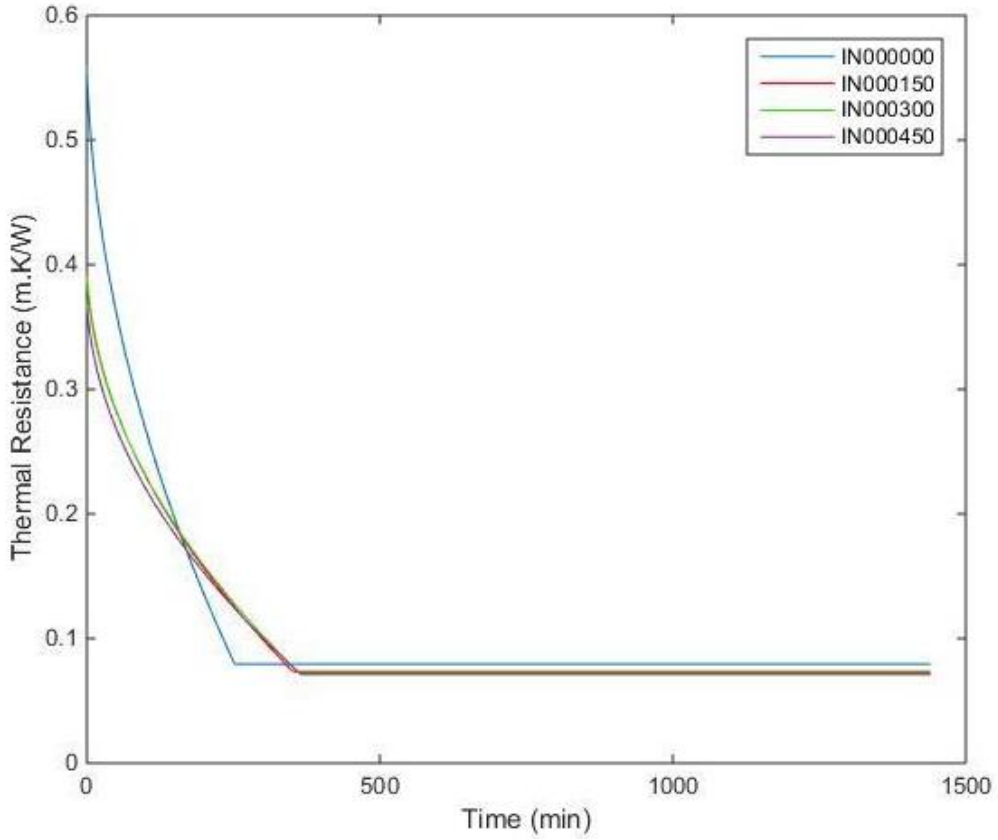

Figure 4.18 Thermal resistance of 0% mc samples in different compaction level

Figure 4.18 presents data showing the variation in thermal resistances of dry green roof growing media at four different compaction levels, simulated during 24 hours. The graphs clearly indicate that the non-compacted green roof (IN000000) has the highest resistance, but the decay rate of resistance is faster than the rest because the sorptivity and porosity of the non-compacted substrate are higher. For compacted substrates, thermal resistance and decay rates are very close, because initial and saturated thermal conductivity is very close, as well as sorptivity values.

This thermal resistance data can be converted into the minute-by-minute heat conduction during 24 hours at the outdoor and indoor temperatures defined earlier. The variation of the steady state conduction heat flux of the green roof substrate, due to absorption, is presented in figure 4.19.

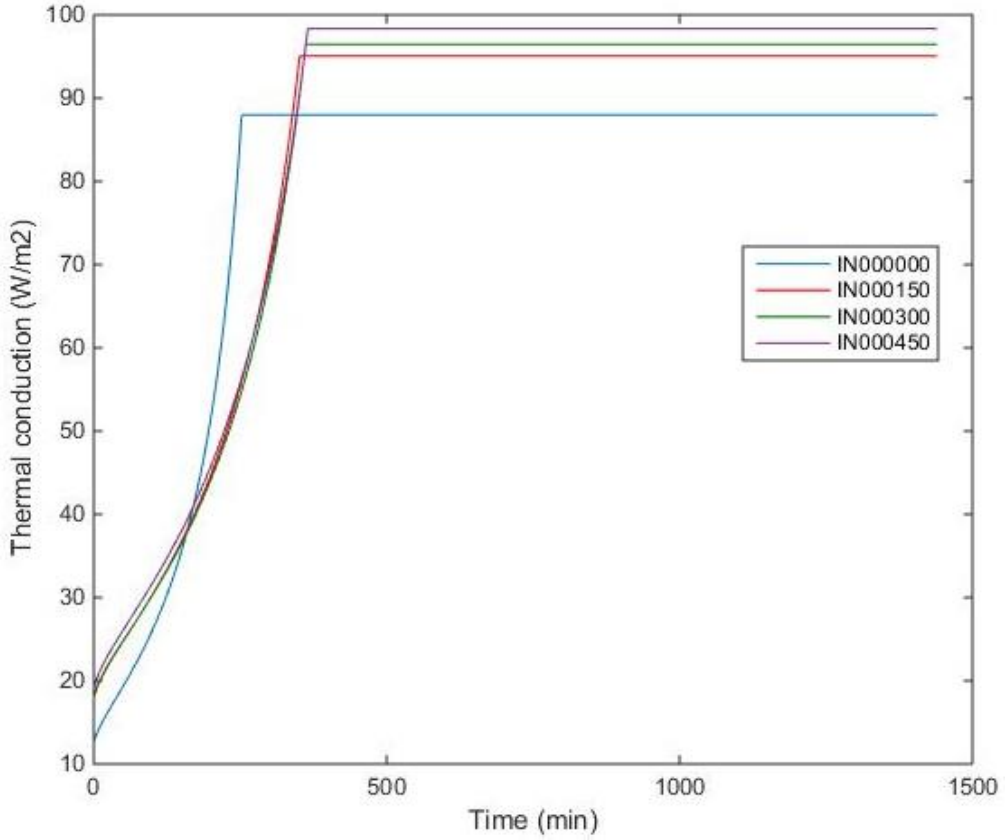

Figure 4.19 Conduction heat flux of 0% mc samples in different compaction level

Conduction heat fluxes of 0% mc samples are related directly to the previous thermal resistance data. The uncompacted sample has the lowest initial heat flux, but the progression rate of heat flux is greater than in a compacted sample. However, the final heat flux of this substrate is the lowest, which bring the total heat flux over 24 hours to be lower than the rest of the samples at 113,760 W/m^2. Total heat flux levels of 150, 300, and 450 kPa 0% mc green roof substrate samples are 119,520, 120,700, and 123,210 W/m^2 respectively.

4.6.2 Simulation results of 4.2% mc green roof substrate

Information needed to simulate minutely thermal resistance (R) and heat conduction due to the absorption cycle of a 4.2% mc green roof substrate are the initial and saturated thermal conductivities, which are presented for different compaction levels in table 4.11.

Table 4.11 Thermal conductivities of 4.2% moisture content samples

Sample ID	Thermal conductivity (W/m.K)
IN042000 (initial)	0.180
IN042150 (initial)	0.279
IN042300 (initial)	0.363
IN042450 (initial)	0.380
IN042000 (saturated at 30.2% mc)*	1.257
IN042150 (saturated at 27.4% mc)*	1.358
IN042300 (saturated at 24.7% mc)*	1.378
IN042450 (saturated at 22.7% mc)*	1.405

Note **Saturated moisture content of compacted samples are different due to the available pore spaces, but have same values in each compaction level.*

From the given information, the minute-by-minute thermal resistance can be calculated through MATLAB and is presented in figure 4.20.

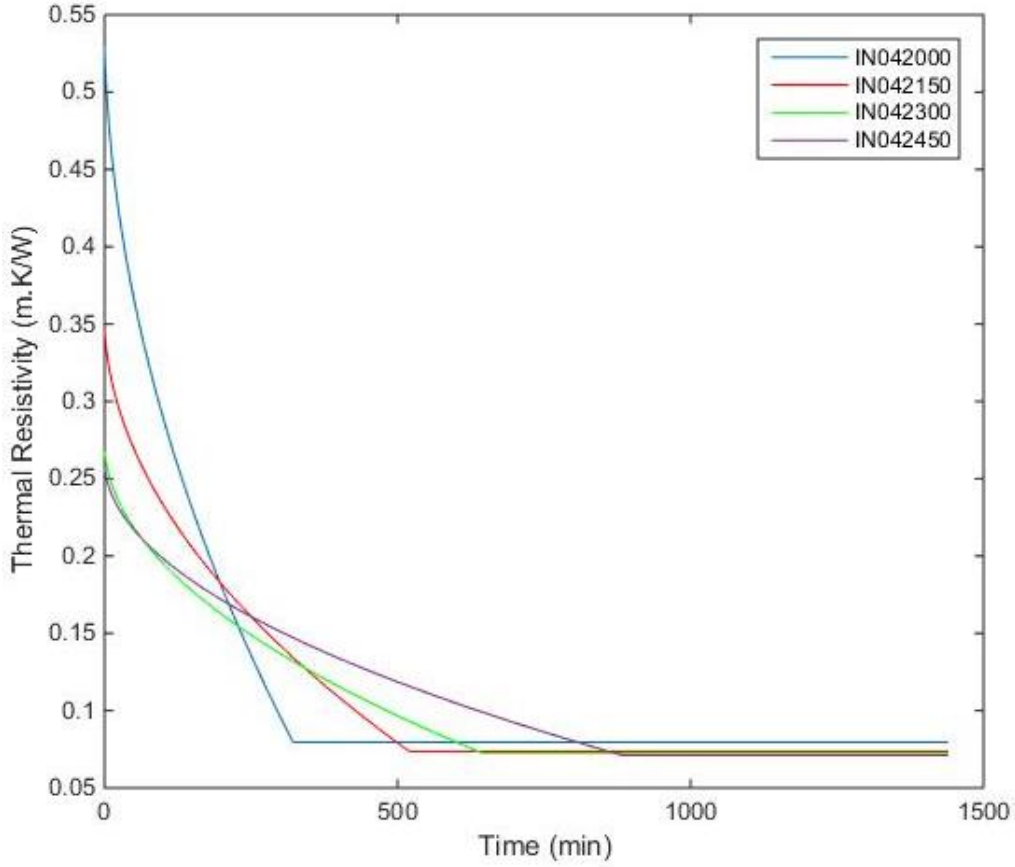

Figure 4.20 Thermal resistance of 4.2% mc samples in different compaction level

In figure 4.20, the 4.2% mc sample, with no compaction sample, shows the highest thermal resistance at the start of simulation, but the decay rate is greater than the other samples because of its high sorptivity. For the other samples, the more highly compacted sample will start with the higher heat resistance, but the decay rate of resistance is greater too. For this reason, sample IN042450 has the lowest thermal resistance and lowest decay rate.

This thermal resistance data can be converted into the minute-by-minute heat conduction during 24 hours at the outdoor and indoor temperatures defined earlier. The variation of the steady state conduction heat flux of the green roof substrate due to absorption is presented in figure 4.21.

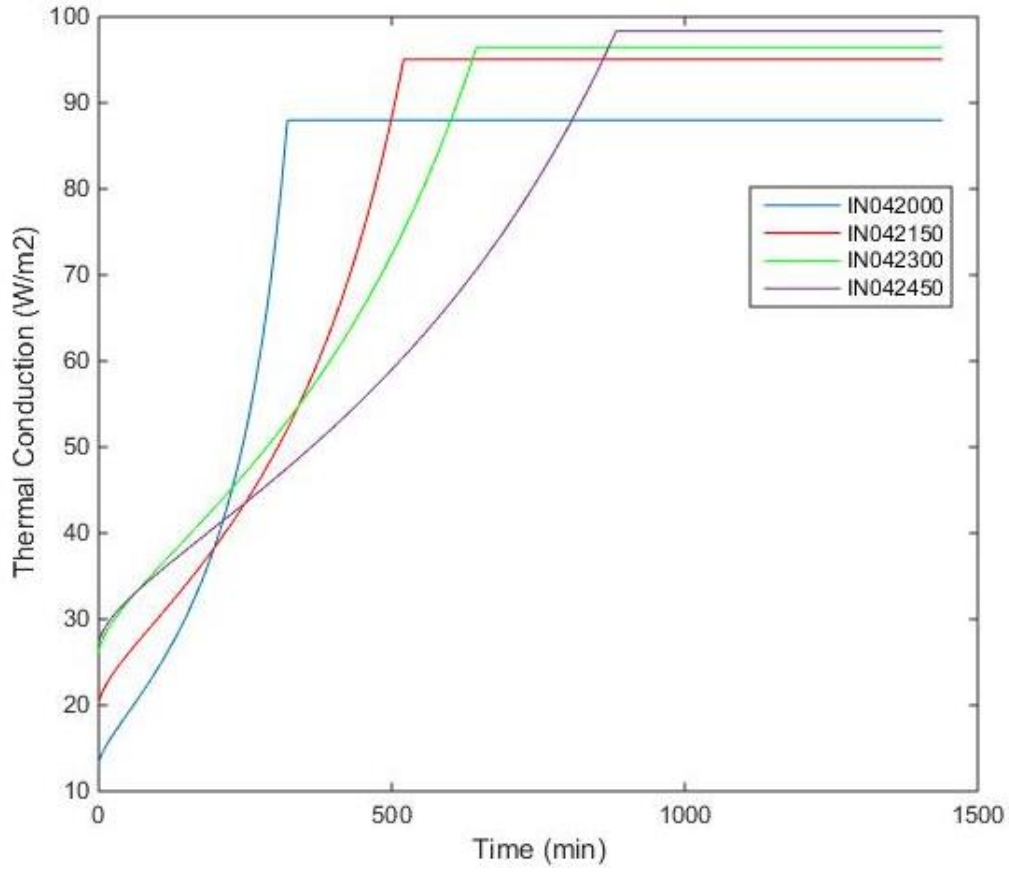

Figure 4.21 Conduction heat flux of 4.2% mc samples in different compaction level

Conduction heat fluxes of 4.2% mc samples are related directly to the previous thermal resistance data. The uncompact sample has the lowest initial heat flux, but the progression rate of heat flux is greater than for a compacted sample. However, the final heat flux of this substrate is the lowest, and the total heat flux over 24 hours is lower than the 150 and 300 kPa samples at 110,470 W/m^2. Total heat fluxes of the 150 and

300 kPa 4.2% mc green roof substrate samples are 112,880 and 112,890 W/m^2 respectively. The 450 kPa sample (IN042450) has the highest initial heat flux, but its decay rate is very low due to its low sorptivity. The total heat flux of this sample is the lowest at 105,900 W/m^2.

4.6.3 Simulation results of 8.4% mc green roof substrate

Information needed to simulate the thermal resistance (R) and heat conduction at one minute interval, due to an absorption cycle of 8.4% mc green roof substrate, are the initial and saturated thermal conductivities, which are presented for different compaction levels in table 4.12.

Table 4.12 Thermal conductivities of 8.4% moisture content samples

Sample ID	Thermal conductivity (W/m.K)
IN084000 (initial)	0.209
IN084150 (initial)	0.382
IN084300 (initial)	0.501
IN084450 (initial)	0.603
IN084000 (saturated at 30.2% mc)*	1.257
IN084150 (saturated at 27.4% mc)*	1.358
IN084300 (saturated at 24.7% mc)*	1.378
IN084450 (saturated at 22.7% mc)*	1.405

Note **Saturated moisture content of compacted samples are different due to the available pore spaces, but have same values in each compaction level.*

From the given information, the thermal resistance can be calculated at one minute interval through MATLAB and is presented in figure 4.22.

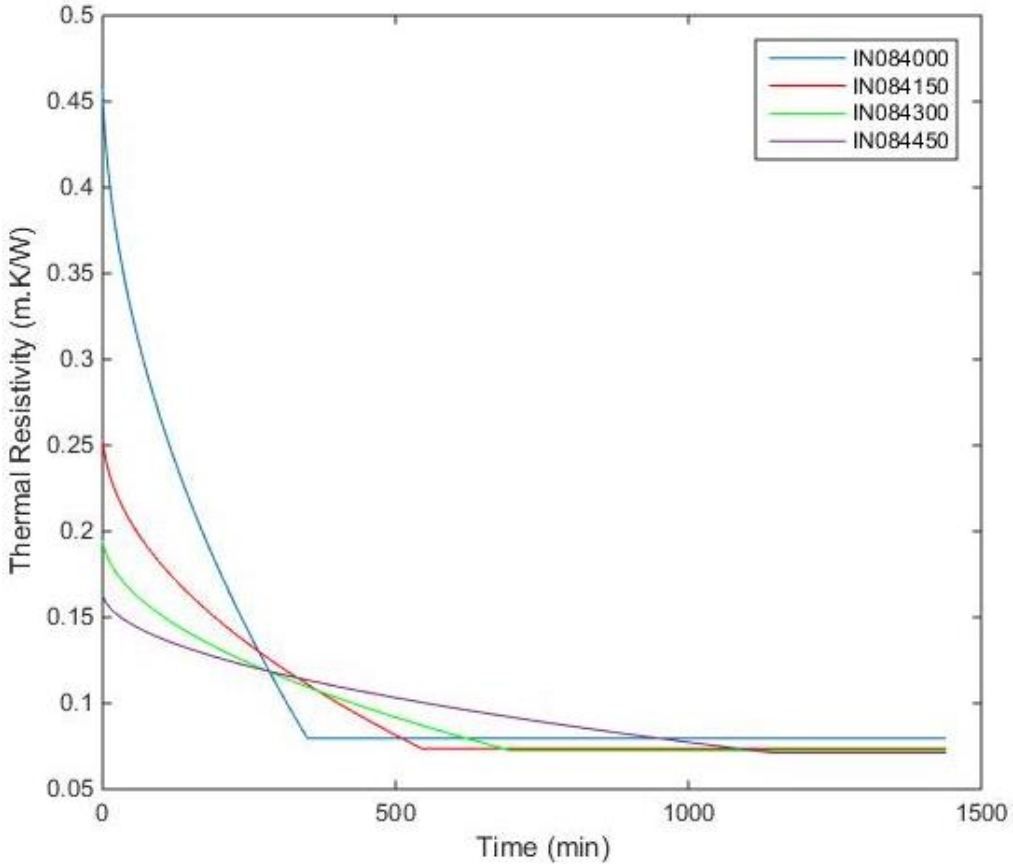

Figure 4.22 Thermal resistance of 8.4% mc samples in different compaction level

From figure 4.22, the 8.4% mc sample with no compaction shows the highest thermal resistance at the start of simulation, but the decay rate is greater than the others because of its high sorptivity. For the other samples, the more highly compacted ones will start with the higher resistance, but the decay rate of resistance is greater too. For this reason, the sample IN042450 has the lowest thermal resistance and lowest decay rate.

This thermal resistance data can be converted into the minute-by-minute heat conduction during 24 hours by at the outdoor and indoor temperatures defined earlier. The variation of the steady state conduction heat flux of the green roof substrate due to absorption is presented in figure 4.23.

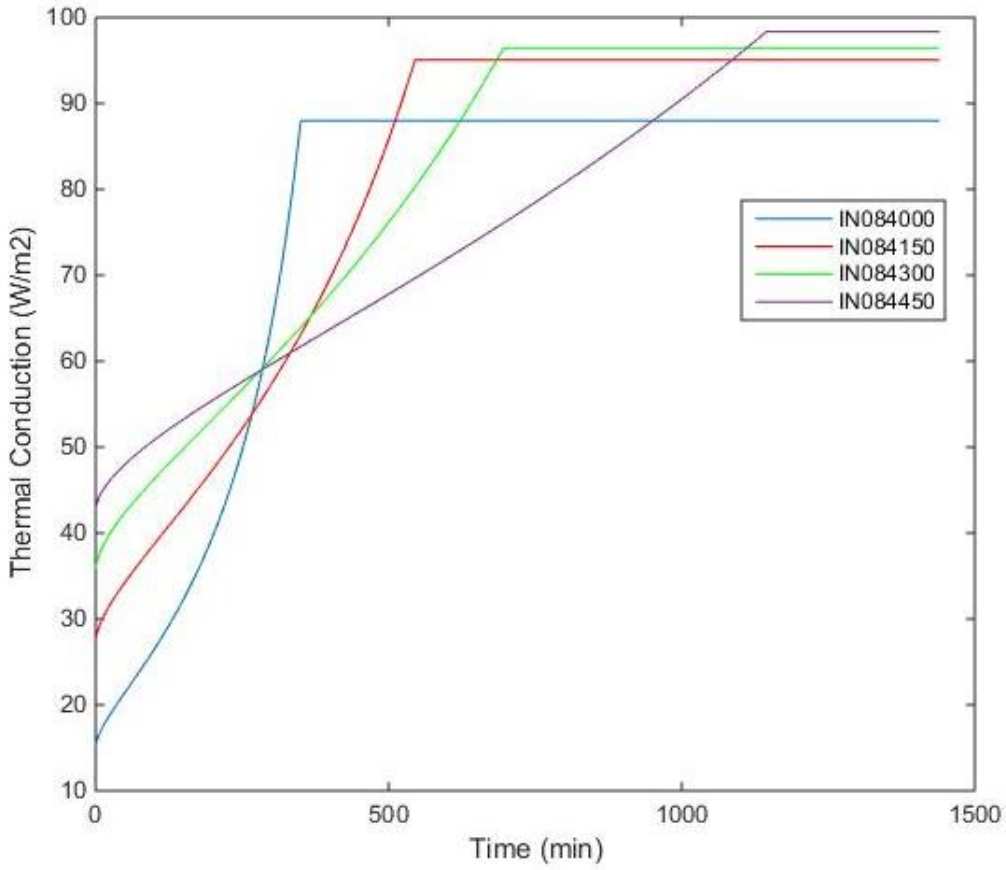

Figure 4.23 Conduction heat flux of 8.4% mc samples in different compaction level

Conduction heat fluxes of 8.4% mc samples are related directly to the previous thermal resistance data. The uncompact sample has the lowest initial heat flux, but the progression rate of heat flux is greater than in a compacted sample. However, the final heat flux of this substrate is the lowest, which indicates its total heat flux over 24 hours to be lower than 150 and 300 kPa samples at 110,150 W/m^2. Total heat fluxes of 150 and 300 kPa 8.4% mc green roof substrate samples are 116,190 and 117,090 W/m^2 respectively. The 450 kPa sample (IN042450) has the highest initial heat flux, but the decay rate is very low due to its low sorptivity. The total heat flux of this sample is 110,720 W/m^2, which is lower than 150 and 300 kPa substrates.

4.6.4 Conclusion of results

The thermal conduction fluxes can be drawn together in a single graph in order to see the behaviour of each substrate condition. Figure 4.24 represents the heat fluxes of all simulated green roof substrate over 24 hours.

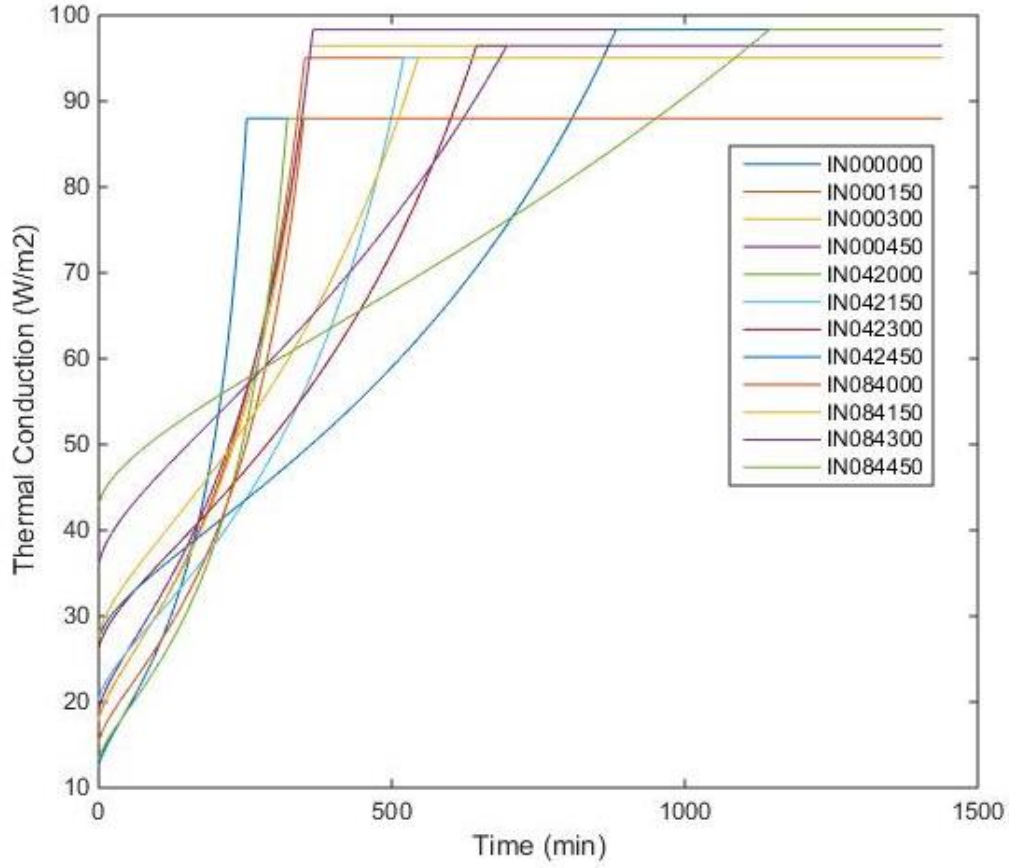

Figure 4.24 Heat flux of all simulated green roof substrates over 24 hours

The graph might look complicated but it can be seen that samples with the same compaction levels show similar heat flux when saturated. Otherwise, the heat flux growth rate and initial heat flux are different, due to the samples' sorptivity and moisture content respectively. As a result, total heat flux is different as summarised in table 4.13.

Table 4.13 Summary of total heat flux of each green roof substrate sample

Moisture content	Sample ID	Total heat flux (W/m^2)
0%	IN000000 IN000150 IN000300 IN000450	113,670 119,520 120,700 123,210
4.2%	IN042000 IN042150 IN042300 IN042450	110,470 112,880 112,890 105,900
8.4%	IN084000 IN084150 IN084300 IN084450	110,150 116,190 117,090 110,720

4.7 Conclusion

This chapter presents data relating to the development of a thermal conduction simulation for a green roof substrate, which is influenced by the moisture change through absorption. Due to the porous structure of the substrate, the Sharp Front theory was used to predict the penetration distance of the saturated substrate layer over time. Experiments were required to estimate the sorptivity value (S) of substrates with different moisture content and compaction levels. Sorptivity can be determined by absorbed water distances (mm) against square-root of time in minutes, where S is a slope of this graph.

The results from the experiment show that the lower moisture content yields the higher sorptivity. In addition, increased compaction of the sample reduces the sorptivity. The compaction also affects the initial absorbed water distance, because it is difficult for water to enter the substrate due to the packing of the surface. After water enters the compacted sample, the capillary force will draw water in and, as a result, the sorptivity value can be determined. Using sorptivity, porosity and thermal conductivity information (see chapter 3), the steady state heat conduction due to absorption can be simulated by computer.

From the simulation results, it can be concluded that a green roof substrate with less compaction will tend to have an initial higher thermal resistance, but the decay rate of thermal resistance is faster than with a more compacted sample. This effect is due to the higher sorptivity of a low compacted sample. As a consequence, the heat flux growth rate is higher, but the saturated heat flux is lower, in a less compacted sample.

A substrate with low moisture content has a higher thermal resistance at the start of simulation, but with a resistance decay rate which is higher than a substrate with higher moisture content. Therefore, the heat flux grows faster in the low moisture content substrate. However, if the moisture and compaction effects for the total heat flux are combined, the results are very close together, as shown in table 4.13.

Finally, this chapter presented data relating to the effects of moisture content and compaction on conduction heat transfer, due to absorption. The next chapter will investigate the evaporation effect on steady state heat conduction.

Chapter 5: Green Roof Simulation with Evaporation

5.1 Introduction

In the previous chapter, details of the green roof substrate thermal simulation with absorption, determined by combining the Sharp Front theory and steady state conduction, were presented. However, a real green roof cannot securely maintain water levels inside its porous structure. Water will leave the roof by a draining process and evaporation from wind flow or solar radiation. For this reason, this chapter will investigate the effect of evaporation on the green roof moisture content distribution in each layer, and then combine this effect with steady state heat conduction in order to simulate an hourly effective thermal resistance.

5.2 Literature review

After water is absorbed into the green roof, the next process is the drying, which also has a significant effect on thermal property changes. Water will leave a green roof system by evaporation at the substrate surface level, respiration of the plant, and run-off from the gravitational effect. However, this study will focus on drying due to the evaporation loss at the surface, which has been studied by many researchers in the area of construction materials (Platten, 1985, Hall *et al*., 1984, Hall and Hoff, 2009). Furthermore, the drainage from the bottom of substrate is ignored in this case because the model will assume that during any evaporation taking place, water at the bottom layer of the roof will be held by capillary force.

Platten (1985) suggested there are three stages of evaporative drying in porous materials. In the first stage (stage 1), the evaporation rate depends on the surrounding environmental factors such as vapour pressure, relative humidity, temperature and airflow over the evaporative surface. This rate is constant throughout the stage. In the second stage (stage 2) evaporation is controlled by the water movement from inside the material (by capillary) to the evaporative surface. The evaporation rate in stage 2 depends on the moisture content inside the material. Finally, the third stage (stage 3) involves the evaporation as a result of water vapour movement inside a material. Nevertheless, the third stage plays only a small part in moisture change, compared to the first and second stages. As a consequence of these three issues, Hall and Hoff (2009) considered only stages 1 and 2 in their work. This study also only considers these two stages because they comprise the most significant role in thermal property change.

The following section will explain stage 1 and stage 2 evaporation in more detail.

5.2.1 Stage 1 evaporation

According to Platten (1985), the stage 1 drying depends on the environmental condition at the surface, where drying will continue for as long as there is a supply of freely available water at the drying surface. The drying rate is constant in this stage; a rate which is influenced by any variation of the surface vapour pressure (p_s) and the vapour pressure potential (dp/dx). The transfer rate of water in the vapour phase can be explained by Fick's first law of mass transfer in equation 5.1.

$$r_1 = \frac{M.D_v}{RT}\left(\frac{dp}{dx}\right) = \frac{M.D_v}{RT}\left(\frac{p_s - p^*}{\delta}\right) \tag{5.1}$$

This equation can be demonstrated by figure 5.1.

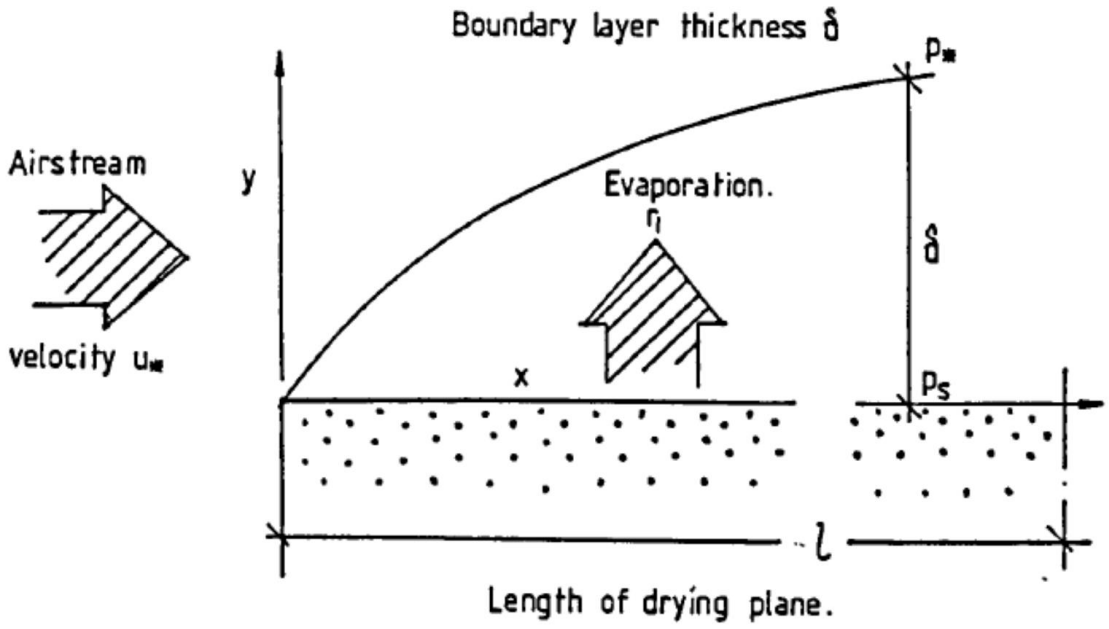

Figure 5.1 Boundary layer existing above the drying surface of the material when airstream is presented (Platten, 1985)

Where; r_1 is stage 1 drying (evaporation) rate (kg/m^2.s),

D_v is vapour diffusion coefficient of water (m^2/s),

M is molecular weight of water (mole),

R is universal gas constant (J/mole.^{o}K),

T is temperature (^{o}K),

p_s is surface vapour pressure (kg/m^3),

δ is boundary layer thickness (m),

p* is vapour pressure existing outside the boundary layer (kg/m^3), which is given by $p^* = p_0 * \frac{Rh}{100}$, and

p_0 is saturated vapour pressure of water.

Substituting for p* in equation (5.1) gives:

$$r_1 = \frac{M.D_v}{R.T}\left(\frac{p_s - (p_0 \times RH/100)}{\delta}\right) \tag{5.2}$$

The surface vapour pressure (p_s) could be redefined as the hydraulic suction or potential (Ψ_s) that depends on the saturation level in the material.

$$\frac{p_s}{p_0} = \exp\left(\frac{-\Psi_s.Mg}{R.T}\right) \tag{5.3}$$

Normally, the hydraulic potential varies with moisture content. However, Ψ_s can be assumed to be zero because the surface is saturated in the first stage of evaporation, which causes equation (5.3) to become $\frac{p_s}{p_0} = \exp(0)$, and as a result, $p_s = p_0$ in this stage. Equation (5.2) becomes.

$$r_1 = \frac{M.D_v}{R.T}\left(\frac{p_0(1 - RH/100)}{\delta}\right) \tag{5.4}$$

By assuming H = (1-RH/100), this equation turns into:

$$r_1 = \frac{M.D_v}{R.T}\left(\frac{p_0 H}{\delta}\right) \tag{5.5}$$

This equation is mainly used in stage 1 evaporative drying, but does not consider effects of the air flow over an evaporative surface and any temperature factors. These effects will be discussed next.

Effect of airflow and temperature

The first effect is the airflow over the surface, which directly affects the thickness of the evaporative boundary layer (δ). This effect changes the vapour pressure potential (dp/dx). The effect of airflow can be defined by the Sherwood number (N_{SH}), according to standard mass transfer theory (Skelland, 1974).

For laminar airflow, the Sherwood number is given by

$$N_{SH} = 0.646 N_{RE}^{1/2} N_{SC}^{1/3} \tag{5.6}$$

Where; N_{RE} is the Reynolds number, and

N_{SC} is the Schmidt number.

The Sherwood number modifies equation (5.5) to give the evaporation rate under laminar airflow conditions.

$$\overline{r_1} = \frac{M.D_v}{R.T}\left(\frac{p_0 H}{\delta}\right) N_{SH} \tag{5.7}$$

$$\overline{r_1} = \frac{M.D_v}{R.T}\left(\frac{p_0 H}{\delta}\right) 0.646 N_{RE}^{1/2} N_{SC}^{1/3} \tag{5.8}$$

In laminar flow, the boundary thickness (δ) is defined as the square root of the length of the drying plane (L) ($\delta = L^{1/2}$). The Reynolds and Schmidt numbers can be calculated by.

$$N_{RE} = \frac{\rho_a U_* L}{\mu_a}$$

$$N_{SC} = \frac{\mu_a}{D_v}$$

Where; ρ_a is the density of air (kg/m^3),

U_* is the laminar airflow velocity (m/s), and

μ_a is the viscosity of air (Ns/m^2).

Substituting those variables in the equation (5.8) gives:

$$\overline{r_1} = \mathrm{A}.\, U_*^{1/2} (p_0 H) \tag{5.9}$$

Where, $A = \frac{M.D_v^{\frac{2}{3}}}{R.T} 0.646 \frac{\rho_a^{\frac{1}{2}}}{\mu_a^{\frac{1}{6}}}$

For turbulent airflow, the Sherwood number and the boundary thickness are changed (Skelland, 1974):

$$N_{SH} = 0.0365 N_{RE}^{0.8}$$

$$\delta = 0.376.L.N_{RE}^{-0.2}$$

Substituting the effects of turbulent airflow into equation (5.7) gives:

$$\overline{r_1} = \frac{M.D_v}{RT}\left(\frac{p_0 H}{0.376.L}\right) 0.0365 N_{RE} \tag{5.10}$$

$$\overline{r_1} = \frac{M.D_v}{RT}(p_0 H).0.097 \frac{\rho_a U_*}{\mu_a} \tag{5.11}$$

However, some of the parameters are affected by temperature, such as the diffusion coefficient (D_v), vapour pressure (p_o), air density (ρ_a), and air viscosity (μ_a). The mathematical operation of those variables is shown by Platten (1985). The resulting stage 1 evaporation rate, including airflow and temperature effects, is presented in equation (5.12):

$$\overline{r_1} = \exp\left(\frac{-C}{T}\right) U_*^{1/2} \left(\frac{K}{L^{1/2}}\right)(1 - RH/100) \tag{5.12}$$

Where; C is a constant equal to 5320 (K), and K is a constant which is approximately $7x10^6$ (kgs^2/m^2).

Equation 5.12 includes the effects of airflow and temperature from the surrounding environment, but not the effect of the material. The next section will present the effect of a material surface on the stage 1 evaporation.

Effect of surface potential

In equation (5.4), the main assumption is that the surface is always saturated, which causes hydraulic potential at the surface (Ψ_s) to become zero and makes surface vapour pressure (p_s) equal to the saturated vapour pressure of water in the environment. In contrast, when there is no free supply of water to the surface, the surface moisture

content will be reduced during evaporation and a new assumption needs to be made in equation (5.3) which becomes:

$$p_s = p_0 \exp\left(\frac{-\Psi_s . Mg}{R.T}\right) \tag{5.13}$$

Substituting p_s in equation (5.2) gives:

$$r_1 = \frac{M.D_v}{R.T}\left(\frac{p_0 \exp\left(\frac{-\Psi_s . Mg}{R.T}\right) - (p_0 \times RH/100)}{\delta}\right)$$

$$r_1 = \frac{M.D_v}{R.T} P_0 \left(\frac{\exp\left(\frac{-\Psi_s . Mg}{R.T}\right) - (RH/100)}{\delta}\right) \tag{5.14}$$

Comparing equations (5.4), (5.12) and (5.14), the term (1-RH/100) is humidity without the surface potential effect. If the surface potential effect is considered, the humidity term in equation (5.12) can be replaced by the humidity term with surface potential ($\exp\left(\frac{-\Psi_s . Mg}{R.T}\right) - (RH/100)$) term. As a result, the equation (5.12) will become:

$$\overline{r_1} = \exp\left(\frac{-C}{T}\right) U_*^{1/2} \left(\frac{K}{L^{1/2}}\right)\left(\exp\left(\frac{-\Psi_s . Mg}{R.T}\right) - (RH/100)\right) \tag{5.15}$$

This is the final form of the stage 1 evaporation rate equation, and will be used in the simulation. The next section will discuss stage 2 evaporation.

5.2.2 Stage 2 evaporation

The second stage of drying happens just after the first stage of drying and is dominated by the internal flow within an unsaturated material toward the evaporative surface. Platten (1985) developed the simple unsaturated flow model, with the effect of evaporation, from the extended Darcy equation.

Finite difference flow model

Considering two adjacent elements in a porous material, as shown in figure 5.2, each element possesses distinct hydraulic properties (moisture content, hydraulic conductivity, and hydraulic potential) with the same thickness (Δx) and cross-sectional area (A).

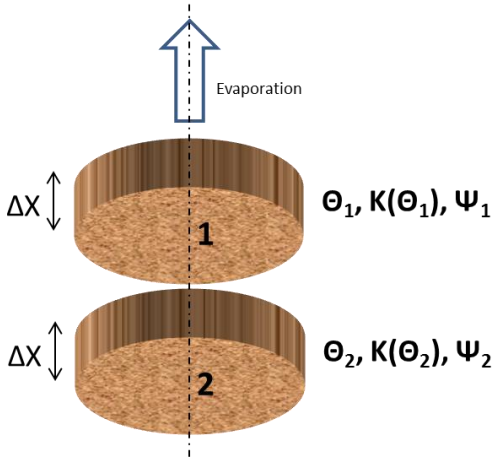

Figure 5.2 Schematic representation of liquid flow between two elements

At saturation, both elements have the same hydraulic properties ($\theta_1 = \theta_2$, $K(\theta_1) = K(\theta_2)$, and $\Psi_1 = \Psi_2$). This brings the hydraulic gradient equal to zero ($\frac{\Psi_1 - \Psi_2}{\Delta x} = o$) with no capillary suction from the upper element. Therefore, there is no water movement during this period.

When evaporation takes place, the moisture content of element 1 (the exposed surface) gradually drops until it is lower than element 2. This situation impacts the hydraulic gradient between these two layers, whereby hydraulic potential in this first element is greater than the second. Consequently, the hydraulic gradient in this condition is $\frac{\Psi_1 - \Psi_2}{\Delta x} > o$ and that creates the flow in element 2 towards element 1. The flow rate of moisture transfer is given by the extended Darcy equation.

$$Q_{1-2} = K(\theta_m)\frac{\Delta\Psi_{1-2}}{\Delta x} \tag{5.16}$$

where: $Q_{1\text{-}2}$ is the flow rate between element 1 and 2,

$K(\theta_m)$ is the mean effective hydraulic conductivity of element 1 and 2, and

$\frac{\Delta\Psi_{1-2}}{\Delta x}$ is the hydraulic potential gradient over element 1 and 2.

From Platten (1985), the duration of transfer period (t) can be determined by the equilibrium in equation 5.17, when the system is saturated and the resultant flow rate ($Q_{1\text{-}2}$) is zero. By assuming $\Psi_1 = \Psi_2$ to be in a state of equilibrium, which is always true in homogeneous materials, then by adding the moisture flow from element 2 into element 1 the moisture transfer balance can be stated by equation (5.17):

$$\theta_1 + inflow\ volume = \theta_2 - outflow\ volume$$

$$\theta_1 + \frac{Q_{1-2}\rho At}{M} = \theta_2 - \frac{Q_{1-2}\rho At}{M} \tag{5.17}$$

where: ρ is the density of water (g/m^3),

A = cross sectional area (m^2),

t = transfer period (sec), and

M = mass of water within saturated body (g).

The transfer period can be calculated be rearranging equation (5.17).

$$\mathrm{t} = \frac{(\theta_2 - \theta_1)M}{2Q_{1-2}\rho A} \tag{5.18}$$

As this transfer finishes at time t, the system will reach equilibrium when the moisture content and another hydraulic property (hydraulic potential and hydraulic conductivity) are equal. This moisture transfer mechanism between two elements ignores evaporation, but the next section will include the effect of evaporation from the first element.

Dynamic flow model

The additional evaporation outflow ($\bar{r}$) from the top surface (element 1) is required. Considering equation (5.17), the moisture balance will never exist when there is a continuity effect from evaporation on the exposed surface. By setting up the new continuity condition $\theta_1<\theta_2$, the equation (5.17) becomes:

$$\theta_1 - evaporation\ loss + inflow\ volume = \theta_2 - outflow\ volume$$

$$\theta_1 - \frac{r\rho At}{M} + \frac{Q_{1-2}\rho At}{M} = \theta_2 - \frac{Q_{1-2}\rho At}{M} \tag{5.19}$$

Where, r is evaporation rate (m/s).

After the transfer period t is finished, the new moisture content in each element can be redefined as:

$$\theta_{1,t} = \theta_1 - \frac{r\rho At}{M} + \frac{Q_{1-2}\rho At}{M}$$

$$\theta_{2,t} = \theta_2 - \frac{Q_{1-2}\rho A t}{M}$$

where: $\theta_{1,t}$ and $\theta_{2,t}$ are the moisture contents of elements 1 and 2 at t period.

These moisture contents will then be reassessed with the new flow rate until the material has dried. This continuity will be explained in the extended finite difference model.

Extended finite difference model

The moisture transfer model presented in the previous section considers only the relationship between two elements. However, for a deeper section, such as a 200 mm thick green roof, this model must be extended into many elements.

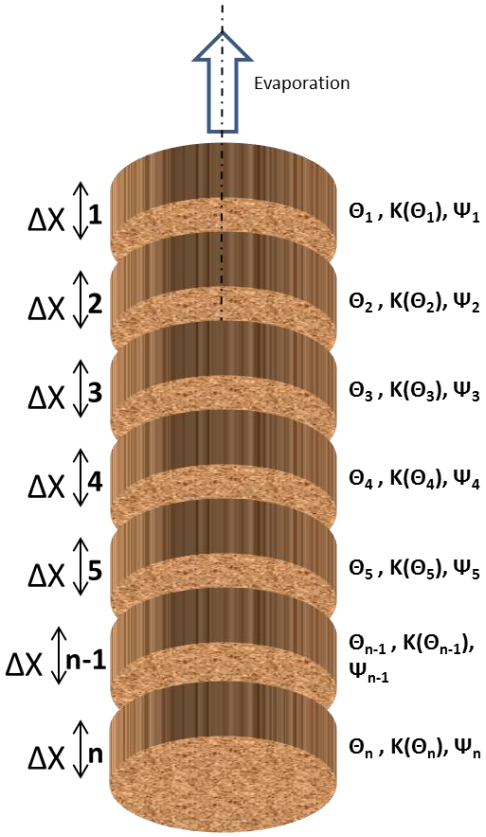

Figure 5.3 Schematic representation of a porous material with a number of individual elements

Considering figure 5.3, the porous material with finite length is divided into individual elements from 1 to n. Each element has the same thickness (Δx), and exhibits distinct saturation levels or moisture content from element 1 to element n (θ_1 to θ_n). Therefore,

the corresponding hydraulic potentials and hydraulic conductivities are Ψ_1 to Ψ_n and $K(\theta_1)$ to $K(\theta_n)$.

Initially, the material is saturated and elements are assumed to have the same moisture content. Thereafter, element 1 is allowed to be exposed to the environment and the bottom element (n) is sealed (no moisture loss is assumed). Evaporation takes place at the surface of element 1, whereupon $\theta_1 < \theta_2$ shown in equation (5.19). However, for every element beyond element 2, the moisture also flows from the higher to the lower moisture element. The continuity flow condition for finite porous material is given by $\theta_1 < \theta_2 < \theta_3 \ldots < \theta_{n-1} < \theta_n$, which creates the flow direction from element n to element 1. This is a one directional flow since the element n is sealed, the element 1 is the only opening, and no flow can occur sideways.

This continuity equation from element 1 to element n is shown below:

$$\theta_1 - \frac{r\rho At}{M} + \frac{Q_{1\leftarrow 2}\rho At}{M} < \theta_2 - \frac{Q_{1\leftarrow 2}\rho At}{M} + \frac{Q_{2\leftarrow 3}\rho At}{M} < \theta_3 - \frac{Q_{2\leftarrow 3}\rho At}{M} + \frac{Q_{3\leftarrow 4}\rho At}{M} < \cdots < \theta_{n-1} - \frac{Q_{(n-2)\leftarrow(n-1)}\rho At}{M} + \frac{Q_{(n-1)\leftarrow n}\rho At}{M} < \theta_n - \frac{Q_{(n-1)\leftarrow n}\rho At}{M} \quad (5.20)$$

This flow mechanism will continue until the entire multi-layer material reaches dryness.

The aforementioned theory builds an understanding of the moisture flow from a porous element to the environment by the process of evaporation. The continuity flow model can predict the moisture content of each layer in certain time. However, in order to simulate the moisture content of each element in every time-step, a moisture content of each layer at a certain time-step needs to be considered and a computational method has to be used. The concept of this method will be presented in the next section.

5.3 Methodology

5.3.1 Adapted finite difference flow model with time step

The previous section presents and explains the evaporation in both stages. However, the finite different flow model for stage 2 evaporation is not a time continuity equation. This section will combine stages 1 and 2, and will also present a new method of evaporative moisture content prediction in different time-steps with a continuity equation.

However, in order to predict moisture contents in the next time-step, some assumptions and mathematical processes need to be applied to the continuity equation (5.20). Assumptions and requirements that apply in this model are:

- The porous material is homogenous in every element.
- There are no evaporation losses and no drainage to the side and bottom (only one-directional flow in the top layer).
- The time steps are equal.
- The surface area is constant throughout simulation.

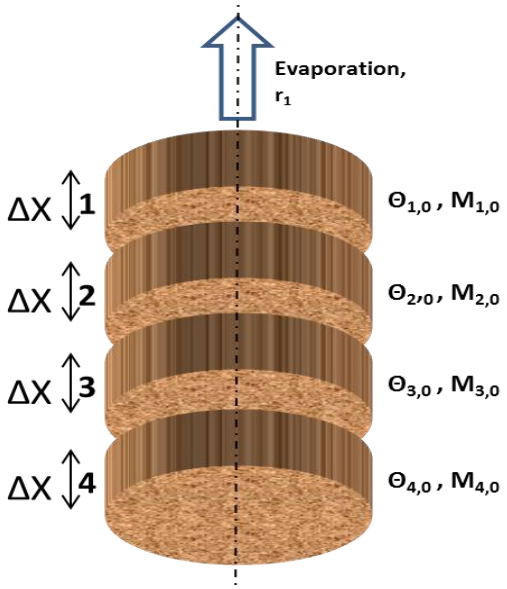

Figure 5.4 Schematic representation of a porous material in the first time step

From figure 5.4, the continuity equation at the start (t = 0) is in equation 5.21.

$$\theta_{1,0} - \frac{r\rho At}{M} + Q_{(1,t)\leftarrow(2,0)}\frac{\rho At}{M} < \theta_{2,0} - Q_{(1,t)\leftarrow(2,0)}\frac{\rho At}{M} + Q_{(2,t)\leftarrow(3,0)}\frac{\rho At}{M} < \theta_{3,0} - Q_{(2,t)\leftarrow(3,0)}\frac{\rho At}{M} + Q_{(3,t)\leftarrow(4,0)}\frac{\rho At}{M} < \theta_{4,0} - \quad (5.21)$$

$$Q_{(3,t)\leftarrow(4,0)}\frac{\rho At}{M}$$

Equation 5.21 presents the continuity equation for a single time step. In order to calculate the moisture content in the next time step, some mechanisms have to be carefully clarified, as illustrated in figure 5.4, which shows the flow behaviour of the material from initial time step into the next time step.

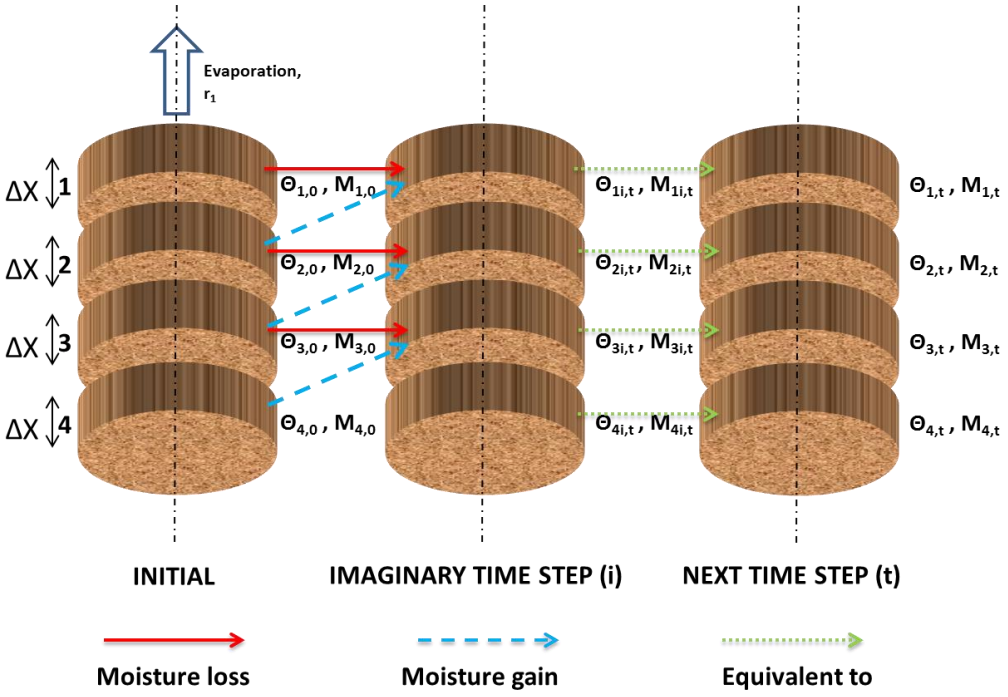

Figure 5.5 Schematic of moisture flow between considered time step to the next time step

Initially, each element has the same moisture content (θ) and mass of water (M). After allowing evaporation from the top surface, the moisture content in element 1 suddenly drops. The flow is started due to the hydraulic difference between elements 1 and 2. However, before element 1 reaches the next time step, it will stay in the stage that is just before the moisture from element 2 enters. This stage will be called an imaginary time step (i).

At the imaginary time step, the moisture content of element 1 is decreased from the evaporation and the moisture content in the imaginary time step ($\theta_{1i,t}$) is presented as equation 5.22.

$$\theta_{1i,t} = \theta_{1,0} - \frac{r\rho At}{M_{1,0}} \tag{5.22}$$

After that, the moisture will transfer from element 2, which brings the moisture content in element 1 to the next time step, as shown below in equation 5.23.

$$\theta_{1,t} = \theta_{1i,t} + Q_{(1i,t)\leftarrow(2,0)} \frac{\rho A t}{M_{Ave\ 1,2}} \tag{5.23}$$

As a result, $\theta_{1i,t}$ as in 5.22 is placed into equation 5.23 in order to get a moisture content of layer 1 in the next time step, as shown in equation 5.24.

$$\theta_{1,t} = \theta_{1,0} - \frac{r\rho A t}{M_{1,0}} + Q_{(1i,t)\leftarrow(2,0)} \frac{\rho A t}{M_{Ave\ 1,2}} \tag{5.24}$$

For the 'below' (or lower) element, the moisture content in the imaginary time step is calculated from the moisture loss to the top element. The imaginary time step for the moisture content of element 2, for instance, can be calculated as equation 5.25.

$$\theta_{2i,t} = \theta_{2,0} - Q_{(1i,t)\leftarrow(2,0)} \frac{\rho A t}{M_{Ave\ 1,2}} \tag{5.25}$$

The flow from the lower element will be included thereafter as shown in the equation 5.26.

$$\theta_{2,t} = \theta_{2i,t} + Q_{(2i,t)\leftarrow(3,0)} \frac{\rho A t}{M_{Ave\ 2,3}} \tag{5.26}$$

Again, place the imaginary moisture content of layer 2 ($\theta_{2i,t}$) from equation 5.25 into equation 5.26. The second layer's moisture content, in the next time step, is shown in equation 5.27.

$$\theta_{2,t} = \theta_{2,0} - Q_{(1i,t)\leftarrow(2,0)} \frac{\rho A t}{M_{Ave\ 1,2}} + Q_{(2i,t)\leftarrow(3,0)} \frac{\rho A t}{M_{Ave\ 2,3}} \tag{5.27}$$

This concept will be applied in every element in every time step. Therefore, there will be an imaginary time step in every connected time step until this porous material reaches dryness. Referring to figure 5.5, the moisture balance equation of these four layers is presented in the equation (5.28).

$$\theta_{1,0} - \frac{r\rho A t}{M_{1,0}} + Q_{(1i,t)\leftarrow(2,0)} \frac{\rho A t}{M_{Ave\ 1,2}} < \theta_{2,0} - Q_{(1i,t)\leftarrow(2,0)} \frac{\rho A t}{M_{Ave\ 1,2}} + Q_{(2i,t)\leftarrow(3,0)} \frac{\rho A t}{M_{Ave\ 2,3}} < \tag{5.28}$$

$$\theta_{3,0} - Q_{(2i,t)\leftarrow(3,0)} \frac{\rho A t}{M_{Ave\ 2,3}} + Q_{(3i,t)\leftarrow(4,0)} \frac{\rho A t}{M_{Ave\ 3,4}} < \theta_{4,0} - Q_{(3i,t)\leftarrow(4,0)} \frac{\rho A t}{M_{Ave\ 3,4}}$$

This continuity equation will be applied with a computation simulation. If there are more layers, this equation can be extended in this manner. However, there are some variables that can be eliminated by mathematical processing, such as a flow rate (Q), density (ρ), area, duration of time step, and mass of water in some layers.

5.3.2 Mathematical process

This process is introduced in order to eliminate variables and reduce the complexity of equation 5.28 in order to obtain better simulation times for the computation. In this section, the substrate is redefined in three parts as follows:

- The top layer, where evaporation occurs (layer 1).
- The middle layer (layer 2), which includes every other layer except the top and bottom layers.
- The bottom layer, which is the sealed layer at the bottom of the substrate (layer 3).

The flow rate from the higher moisture content layer to the lower will play a crucial role in this equation modification. This component, from equation 5.17, can be redefined into equation 5.29.

$$\theta_{low} + \frac{Q_{high-low}\rho A t}{M_{average}} = \theta_{high} - \frac{Q_{high-low}\rho A t}{M_{average}} \tag{5.29}$$

where: θ_{low} is a lower moisture content layer,

θ_{high} is a higher moisture content layer,

$Q_{high\text{-}low}$ is the flow rate from a higher moisture content layer to the lower, and

$M_{average}$ is an average mass of water between these two elements.

As a result, the flow rate can be calculated as shown in equation 5.30.

$$Q_{high-low} = \frac{(\theta_{high} - \theta_{low})(M_{average})}{2\rho A t}$$

$$Q_{high-low} = \frac{(\theta_{high} - \theta_{low})[(M_{high} + M_{low})/2]}{2\rho At}$$

$$Q_{high-low} = \frac{(\theta_{high} - \theta_{low})(M_{high} + M_{low})}{4\rho At} \quad (5.30)$$

This flow rate arrangement simplifies the flow rate in equation 5.28.

The top layer

The first term of equation 5.28 represents the moisture content in the next time step of the top layer. The future moisture content is based on the moisture contents of layers 1 and 2 in a current time step, and the evaporation rate. Consequently, the prediction of the moisture content in the top layer can be rewritten as equation 5.31.

$$\theta_{1,t+\Delta t} = \theta_{1,t} - \frac{r_t \rho At}{M_{1,t}} + Q_{(1i,t+\Delta t)\leftarrow(2,t)} \frac{\rho At}{M_{Ave\ 1i,2}} \quad (5.31)$$

where: imaginary part of the layer is $\theta_{1i,t+\Delta t} = \theta_{1,t} - \frac{r_t \rho At}{M_{1,t}}$

By using flow rate relationships in equation 5.30, the term $Q_{(1i,t+\Delta t)\leftarrow(2,t)}$ is changed and equation 5.31 transforms into:

$$\theta_{1,t+\Delta t} = \theta_{1,t} - \frac{r_t \rho At}{M_{1,t}} + \left[\frac{(\theta_{2,t} - \theta_{1i,t+\Delta t})(M_{2,t} + M_{1i,t+\Delta t})}{4\rho At}\right]\left[\frac{2\rho At}{M_{2,t} + M_{1i,t+\Delta t}}\right]$$

$$= \theta_{1,t} - \frac{r_t \rho At}{M_{1,t}} + \left[\frac{(\theta_{2,t} - \theta_{1i,t+\Delta t})}{2}\right]$$

$$= \theta_{1,t} - \frac{r_t \rho At}{M_{1,t}} + \left[\frac{\theta_{2,t} - \left(\theta_{1,t} - \frac{r_t \rho At}{M_{1,t}}\right)}{2}\right]$$

$$\therefore \theta_{1,t+\Delta t} = \frac{\theta_{1,t}}{2} + \frac{\theta_{2,t}}{2} - \frac{r_t \rho At}{2M_{1,t}} \quad (5.32)$$

The equation 5.32 is the operating equation for the top layer.

The middle layer

The second and third terms in equation 5.28 will share the similarity as a middle layer, which represents the moisture content in the future time step. This moisture is calculated from the moisture content of nearby layers, which are the moisture content of

a top layer at the next time step and a bottom layer at the current time step. Therefore, the predicting moisture content in the middle layer can be rewritten as equation 5.33.

$$\theta_{2,t+\Delta t} = \theta_{2,t} - Q_{(1i,t+\Delta t)\leftarrow(2,t)} \frac{\rho A t}{M_{Ave\ 1i,2}} + Q_{(2i,t+\Delta t)\leftarrow(3,t)} \frac{\rho A t}{M_{Ave\ 2i,3}} \quad (5.33)$$

By using the flow rate relationship in equation 5.30, flow rates in equation 5.33 can be calculated and transformed into an easier equation with this procedure.

$$\theta_{2,t+\Delta t} = \theta_{2,t} - \left[\frac{(\theta_{2,t}-\theta_{1i,t+\Delta t})(M_{2,t}+M_{1i,t+\Delta t})}{4\rho A t}\right]\left[\frac{2\rho A t}{M_{2,t}+M_{1i,t+\Delta t}}\right] + Q_{(2i,t+\Delta t)\leftarrow(3,t)} \frac{\rho A t}{M_{Ave\ 2i,3}}$$

$$= \theta_{2,t} - \left[\frac{(\theta_{2,t}-\theta_{1i,t+\Delta t})}{2}\right] + Q_{(2i,t+\Delta t)\leftarrow(3,t)} \frac{\rho A t}{M_{Ave\ 2i,3}}$$

$$= \theta_{2,t} - \left[\frac{\theta_{2,t}-\left(\theta_{1,t}-\frac{r_t \rho A t}{M_{1,t}}\right)}{2}\right] + Q_{(2i,t+\Delta t)\leftarrow(3,t)} \frac{\rho A t}{M_{Ave\ 2i,3}}$$

$$\theta_{2,t+\Delta t} = \left(\frac{\theta_{1,t}}{2} + \frac{\theta_{2,t}}{2} - \frac{r_t \rho A t}{2M_{1,t}}\right) + Q_{(2i,t+\Delta t)\leftarrow(3,t)} \frac{\rho A t}{M_{Ave\ 2i,3}}$$

It can be noticed that the first two terms in this equation are an imaginary part of the moisture content of layer 2 ($\theta_{2i,t+\Delta t}$), which is now transformed into $\frac{\theta_{1,t}}{2} + \frac{\theta_{2,t}}{2} - \frac{r_t \rho A t}{2M_{1,t}}$. These terms are also equal to the moisture content of layer 1 in the next time step ($\theta_{1,t+\Delta t}$). This procedure will continue as follows:

$$\theta_{2,t+\Delta t} = \left(\frac{\theta_{1,t}}{2} + \frac{\theta_{2,t}}{2} - \frac{r_t \rho A t}{2M_{1,t}}\right) + Q_{(2i,t+\Delta t)\leftarrow(3,t)} \frac{\rho A t}{M_{Ave\ 2i,3}}$$

$$= \left(\frac{\theta_{1,t}}{2} + \frac{\theta_{2,t}}{2} - \frac{r_t \rho A t}{2M_{1,t}}\right) + \left[\frac{(\theta_{3,t}-\theta_{2i,t+\Delta t})(M_{3,t}+M_{2i,t+\Delta t})}{4\rho A t}\right]\left[\frac{2\rho A t}{M_{3,t}+M_{2i,t+\Delta t}}\right]$$

$$= \left(\frac{\theta_{1,t}}{2} + \frac{\theta_{2,t}}{2} - \frac{r_t \rho A t}{2M_{1,t}}\right) + \left[\frac{(\theta_{3,t}-\theta_{2i,t+\Delta t})}{2}\right]$$

$$= \left(\frac{\theta_{1,t}}{2} + \frac{\theta_{2,t}}{2} - \frac{r_t \rho A t}{2M_{1,t}}\right) + \left[\frac{\left(\theta_{3,t}-\left(\frac{\theta_{1,t}}{2}+\frac{\theta_{2,t}}{2}-\frac{r_t \rho A t}{2M_{1,t}}\right)\right)}{2}\right]$$

$$\therefore \theta_{2,t+\Delta t} = \frac{\theta_{1,t}}{4} + \frac{\theta_{2,t}}{4} + \frac{\theta_{3,t}}{2} - \frac{r_t \rho A t}{4M_{1,t}} \quad (5.34)$$

On the other hand, equation 5.34 can be written with the relationship of a top layer at the next time step moisture content ($\theta_{1,t+\Delta t}$) and a bottom layer in the current time step ($\theta_{3,t}$) by equation 5.35.

$$\theta_{2,t+\Delta t} = \frac{\theta_{1,t+\Delta t}}{2} + \frac{\theta_{3,t}}{2} \tag{5.35}$$

The equation 5.35 is the operating equation for the middle layer.

The bottom layer

Finally, the bottom layer, which is the last term in equation 5.28, will only lose the moisture to the next top layer; there is no inflow to this layer. In addition, the moisture is assumed to transfer in an upward direction only (no loss from drainage). The future time step of the bottom layer can be determined by equation 5.36.

$$\theta_{4,t+\Delta t} = \theta_{4,t} - Q_{(3i,t+\Delta t)\leftarrow(4,t)} \frac{\rho A t}{M_{Ave\ 3i,4}} \tag{5.36}$$

By using the flow rate relation in equation 5.30, flow rates in equation 5.36 can be calculated and transformed into an easier equation with this procedure.

$$\begin{aligned}
\theta_{4,t+\Delta t} &= \theta_{4,t} - Q_{(3i,t+\Delta t)\leftarrow(4,t)} \frac{\rho A t}{M_{Ave\ 3i,4}} \\
&= \theta_{4,t} - \left[\frac{(\theta_{4,t}-\theta_{3i,t+\Delta t})(M_{4,t}+M_{3i,t+\Delta t})}{4\rho A t}\right]\left[\frac{2\rho A t}{M_{4,t}+M_{3i,t+\Delta t}}\right] \\
&= \theta_{4,t} - \left[\frac{\theta_{4,t}-\theta_{3i,t+\Delta t}}{2}\right] \\
&= \frac{\theta_{4,t}}{2} + \frac{\theta_{3i,t+\Delta t}}{2} \\
\therefore \theta_{4,t+\Delta t} &= \frac{1}{2}(\theta_{4,t} + \theta_{3i,t+\Delta t})
\end{aligned} \tag{5.37}$$

The equation 5.37 is the operating equation for the bottom layer.

5.3.3 Determination of evaporation rate

The important factor for this evaporation simulation is the evaporation rate, which has been discussed in section 5.2.1. However, the discussed evaporation rate is only applied for stage 1 evaporation; after the substrate turns into stage 2, this rate cannot be used because there is no free water on the top layer that could sustain the stage 1 rate.

Platten (1985) indicated that stage 1 evaporation will exist in the very first hours; thereafter the porous material will move into stage 2 evaporation. The rate in stage 2 will be reduced from that of stage 1 following an exponential decay function. The figure 5.6 shows the hourly evaporation rate of a lepine limestone.

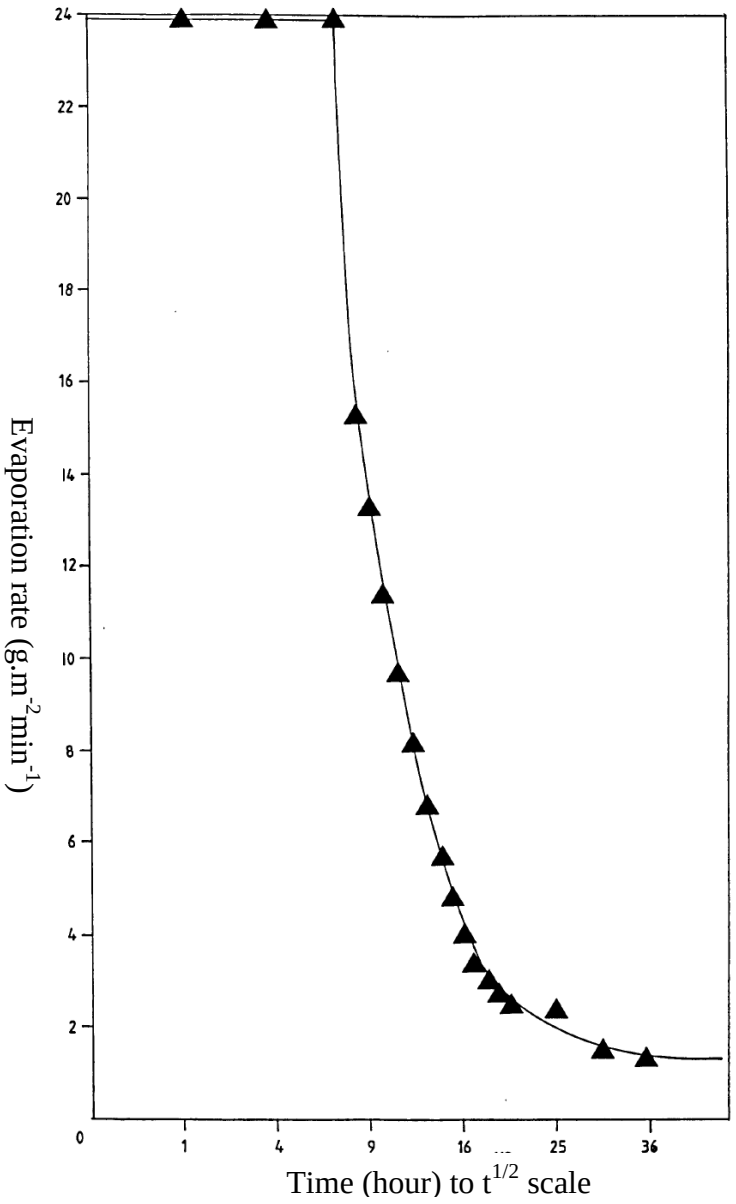

Figure 5.6 The evaporation rate over time of lepine limestone (Platten, 1985)

This limestone has a constant stage 1 evaporation rate at 24 $g.m^{-2}min^{-1}$ from the start of drying for 6 hours. However, at the seventh hour, the evaporation rate suddenly drops and follows an exponential decay function. This seventh hour indicates the beginning of the stage 2 evaporation rate.

In order to verify this rate, an experiment needs to be performed and the evaporation rate can then be calculated by the loss of moisture content from the top layer. However, the moisture content must be known. The fundamental equation used to calculate an evaporation rate is a moisture prediction equation for the top layer, taken from equation 5.32

By knowing a current and a next time step moisture content for layers 1 and 2, the equation 5.32 can be converted backwards and the evaporation rate of the current time step can be determined.

$$r_t = \left(\frac{\theta_{1,t} + \theta_{2,t} - 2\theta_{1,t+\Delta t}}{\rho A t}\right) M_{1,t} \tag{5.38}$$

The equation 5.38 will be used to determine the evaporation rate in the simulation. The next section describes an experiment to verify green roof substrate evaporation.

5.4 Experiment on Evaporation

This experiment to investigate the evaporation from a green roof substrate is performed to validate the theory presented in section 5.3, as well as the stage 1 evaporation rate and the decay rate in stage 2.

The experiment on evaporation needs to be performed in a controlled and stable environment in order to maintain a constant evaporation rate. From the equation 5.12, the temperature, relative humidity, and wind speed must be constant throughout the test. For this reason, the environmental chamber is used in this experiment.

This section describes about sample preparation and the operation of the evaporation test, which had been adapted according to the available resources.

5.4.1 Sample preparation

Sample preparation for the evaporation test is very important because it needs to simulate the real substrate condition after precipitation, in which a green roof substrate is saturated throughout its depth. This saturation effect needs to be verified, especially at the top layer, since the stage 1 evaporation must be verified when the top layer is saturated.

In order to saturate a substrate specimen, the constant head water supply is attached to the substrate's container, and then water drains out at the bottom layer. The set-up is shown in figure 5.7.

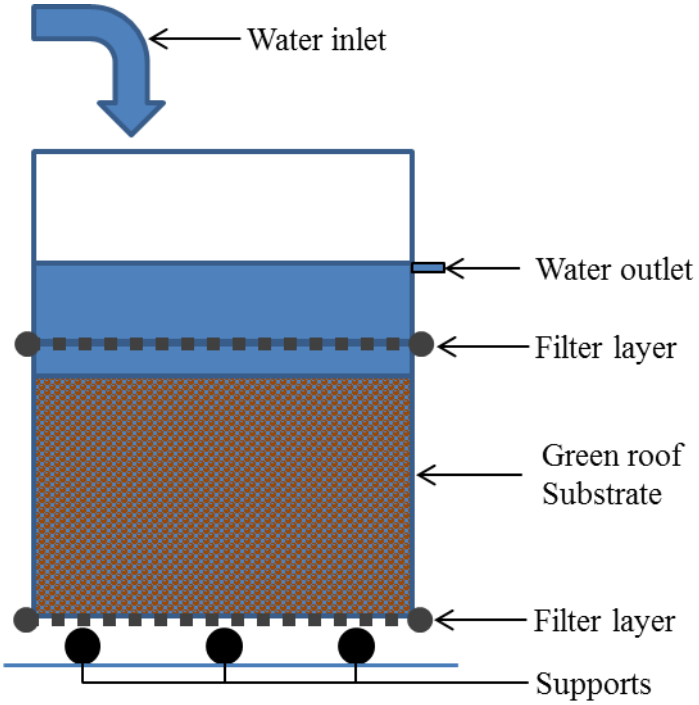

Figure 5.7 The saturation of green roof substrate preparation set-up

The height of the water supply is approximately 20 mm above the top surface, because this height does not spoil the sample by adding more compaction to it. This sample is left for more than 24 hour to ensure that water has reached the bottom layer and drained out. As a result, the green roof substrate specimen becomes saturated.

After the substrate is saturated, the container is drilled with six holes, through which later a conductivity needle probe (TSL-100) for thermal conductivity measurement (as a non-destructive determination of moisture content) will be inserted. The final specimen is shown in figure 5.8.

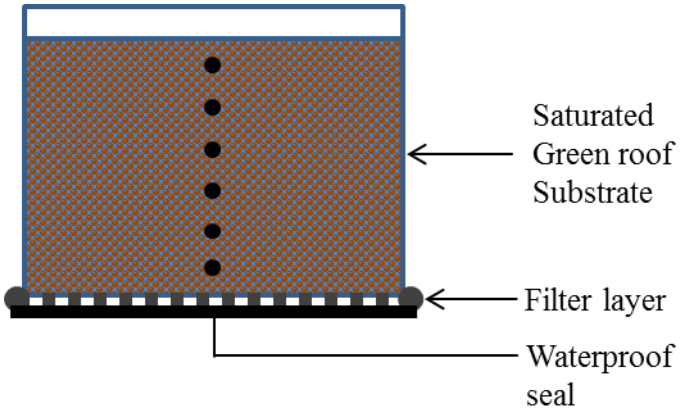

Figure 5.8 The saturated substrate sample before being placed in an environmental chamber

These six holes must be sealed in order to prevent further moisture loss from each layer. The next section will describe how to measure the moisture content of each layer during the evaporation test.

5.4.2 Evaporation measurement

The prepared specimen is placed in the environmental chamber, controlled at 25^{o}C and 50% relative humidity, which are near the laboratory condition. However, the laboratory condition fluctuates due to people traffic and variations in outdoor temperature and humidity. Furthermore, the environmental chamber can provide a constant wind speed over the specimen, which cannot occur in an open room. The test arrangement is illustrated in figure 5.9.

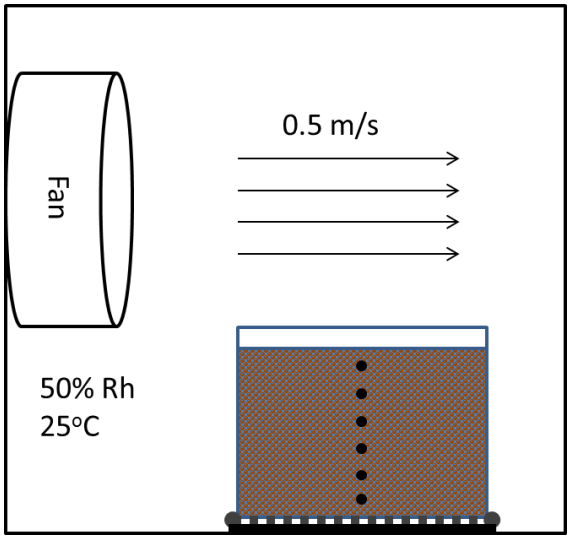

Figure 5.9 The green roof substrate specimen in the environmental chamber

The wind speed reading of 0.5 m/s over the specimen's surface is measured by a handheld anemometer.

Procedure

The test aims to observe the moisture content changes in each substrate layer after evaporation occurs. However, the moisture content in each layer cannot be observed by the direct method (oven dry method) because such an approach needs the removal of substrate from the container, which spoils the substrate and terminates the test. For this reason, the relationship between thermal conductivity and moisture content in section 3.6.2 is used to consider the moisture content in each layer.

The arrangement and thickness of substrate layers is presented in figure 5.10.

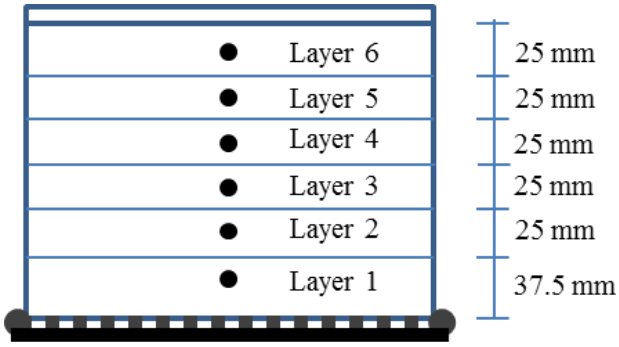

Figure 5.10 The arrangement of the substrate layers

Because of the thermal conductivity meter's requirement, the adjacent layers, such as layer 6 and layer 5, cannot be tested consecutively. This is a result of the heating energy that is conducted from the probe, which affects the adjacent layer by increasing the temperature around it, which in turn can cause an error in thermal conductivity reading.

The measurement at each point takes around 10 minutes, involving 2 minutes for bringing the needle probe's temperature equal to a layer's temperature, 5 minutes for the probe to read the conductivity value, and 3 minutes for cooling the probe down. After completing a layer, the measurement will continue to the next-but-one layer; the sequence of this test is therefore layer 6, 4, 2, 5, 3, and 1 in order.

Test durations are divided into two parts, which according to two stages of evaporation rate are as follows:

- Stage 1 evaporation is tested at one hour intervals for the first five hours.
- Stage 2 evaporation is tested at 24 hour intervals for three weeks.

The total time for both measurements is 504 hours or 3 weeks.

The results from the measurement are shown in the thermal conductivity values, which will be converted into the moisture content by the relationship between moisture content and thermal conductivity in different compaction levels. Relations between moisture content and thermal conductivity are summarised in table 5.1 derived from results in chapter 3.

Table 5.1 Summary of moisture content and thermal conductivity relations in different moisture content

Compaction level	**Linear Relation**
0 kPa	$mc = 12.187 \ln(thermal\ conductivity) + 25.8$
150 kPa	$mc = 15.255 \ln(thermal\ conductivity) + 22.8$
300 kPa	$mc = 14.491 \ln(Thermal\ conductivity) + 19.45$
450 kPa	$mc = 13.304 \ln(Thermal\ conductivity) + 17.1$

The next section will present results from evaporation experiments of specimens at different compaction levels.

5.5 Experimental Results

The results of the green roof substrate evaporation tests will be presented in the context of different compaction levels, with the saturated moisture content at the beginning of the experiment. Two sets of results will be shown as: i) moisture content of each layer over the 504 hours experimental duration, and ii) the calculated evaporation rate obtained from the test.

5.5.1 Evaporation of the 0 kPa green roof sample

The 0 kPa green roof substrate was divided into 5 layers, because after the specimen was saturated, the substrate in the container shrank (downwards). This is a result of liquid that drives the loose substrate particles in the less-compacted substrate closer together, as they are easier to move than in a more highly compacted substrate. As a result, the initial 6 layered substrate became 5 layers. The layers are numbered as in figure 5.10.

Figure 5.11 presents moisture content in 5 layers during the 504 hours of evaporation in the environmental chamber of the 0 kPa green roof substrate specimen.

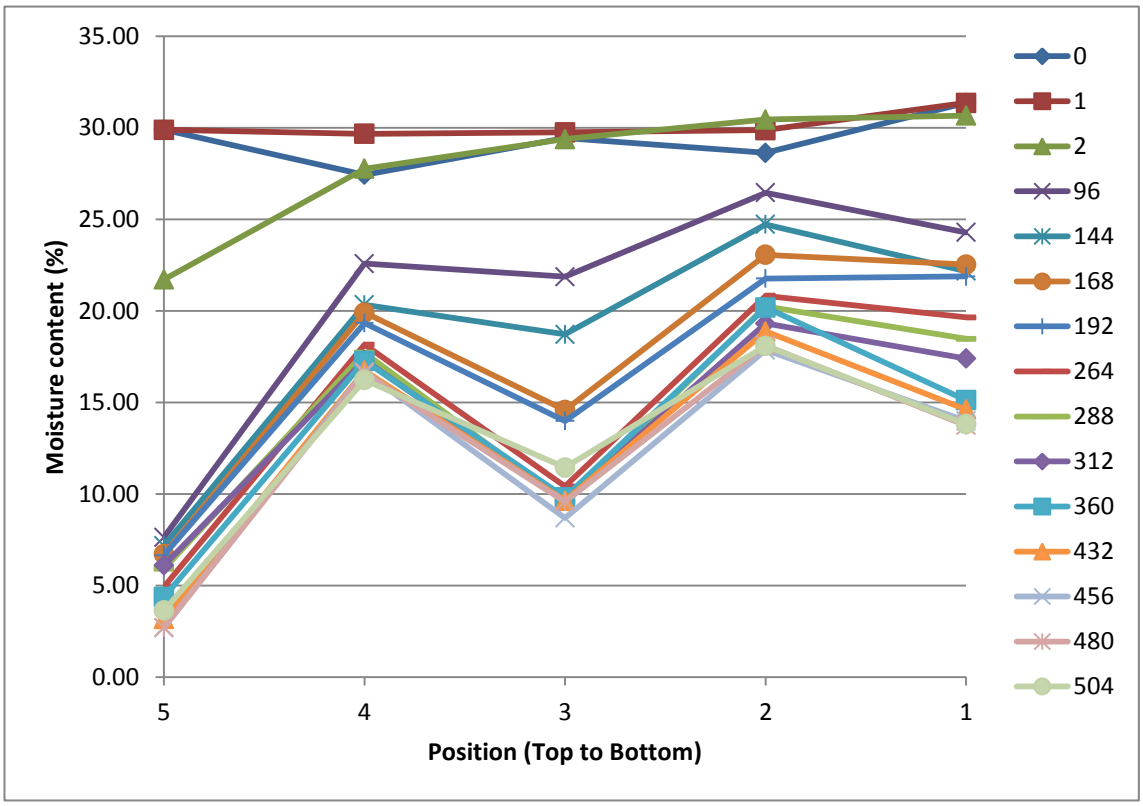

Figure 5.11 Moisture contents of 0 kPa compaction in 5 layers during 504 hours

From figure 5.11, it can be seen that the moisture contents in every layer are gradually reduced over 3 weeks. From the start to 2 hours, the first stage evaporation can be observed since there is a huge reduction in moisture content from 30% to 22% on the top layer (layer 5), while the lower layers' moisture contents are slightly reduced. From 96 to 504 hours, in contrast, the moisture content in the top layer is very close together between 2% and 8% which is a result from stage 2 evaporation or internal moisture flow. Moisture content profiles can be clearly seen after 96 hours, where moisture content on the top layer is very low but moisture content on the bottom layer (layer 1) is still high, in that the material sample is still wet.

However, there is an apparently significant dip in the moisture content in the middle layer (layer 3), which might come from the increasing compaction level in an initially low compaction substrate. When liquid leaves the sample, substrate particles are packed closer together and therefore the compaction level increases. To verify this, the moisture content with conventional oven drying of layers 5 and 4 were checked.

From the direct (oven dry) method, the top layer's (5) moisture content was measured as 2% at 504 hours drying period. This moisture content is very close to the moisture content measured by the indirect thermal conductivity method, which is 1.85% mc. However, the moisture content of layer 4 is over-estimated by the indirect method at 15.8% compared to 10% by the direct oven dry method. This error may have resulted from an increment of compaction in some layers during evaporation, thereby causing the over-estimation in moisture content calculation. Therefore, the measured moisture content of layer 4 was recalculated by using different thermal conductivity-moisture content relationships (table 5.1). The recalculation showed that the 150 kPa compaction equation yields the closest result to the direct oven dry result.

Likewise, layer 2 appeared to show over-estimated moisture content, which was recalculated using the 150 kPa compaction level equation. The moisture contents of layers 4 and 2 in figure 5.11 were recalculated and presented again in figure 5.12.

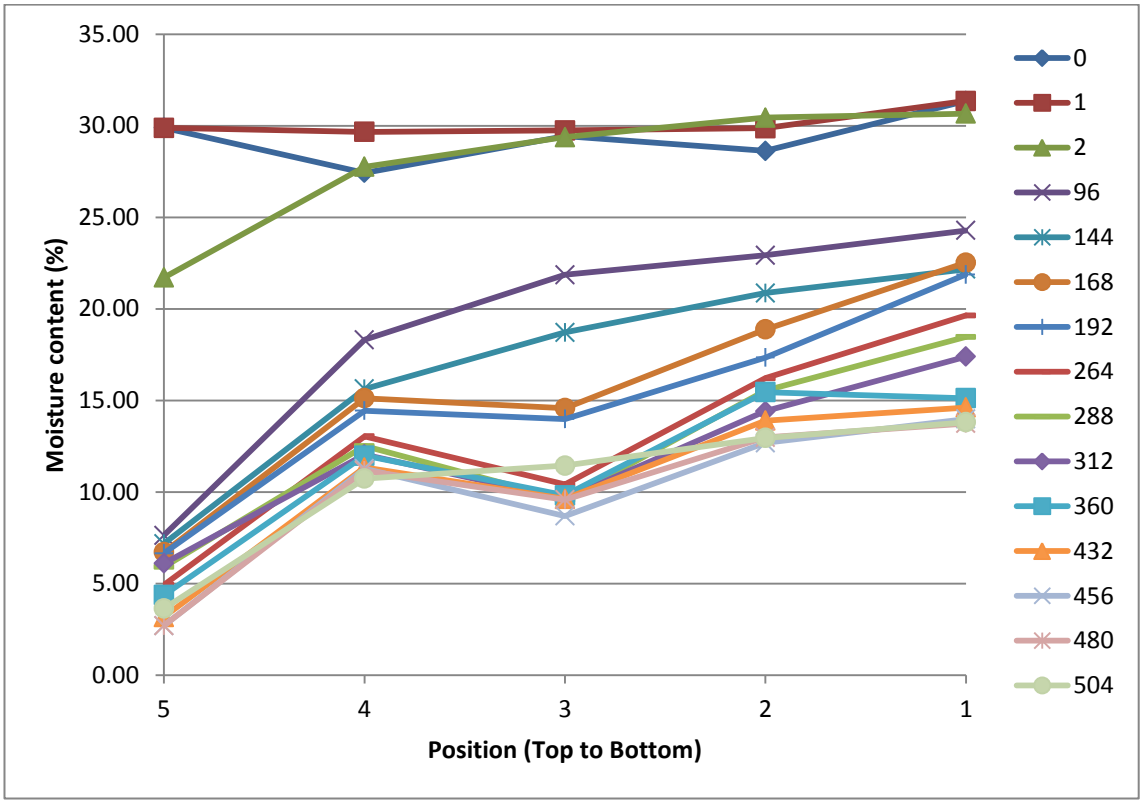

Figure 5.12 Recalculated moisture contents of 0 kPa compaction in 5 layers during 504 hours

The moisture content profile of the recalculated graph shows reasonable behaviour, where the top layer has the highest moisture loss, while that in the lower layers is gradually reduced. Although the moisture content of layer 3, after 168 hours, still shows a dip in the profile, this is within the 95% prediction interval range (±2.5% mc.) of the measurement.

From this information, the evaporation rate from the top layer of the 0 kPa green roof specimen can be calculated and presented in figure 5.13.

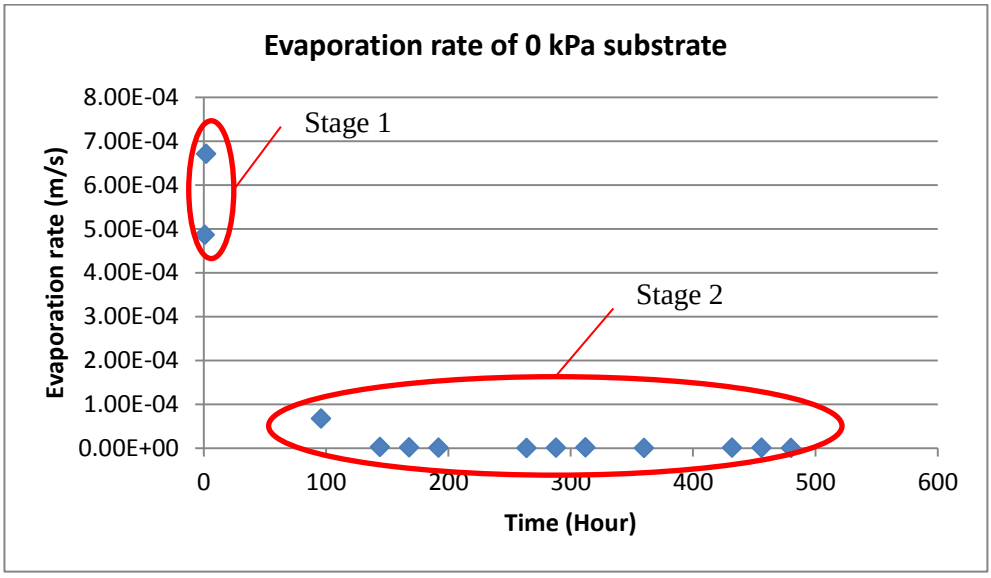

Figure 5.13 Calculated evaporation rate of the 0 kPa substrate

Figure 5.13 shows the evaporation rates of stage 1 and stage 2, which are defined in the figure. The theoretical stage 1 evaporation rate from wind speed, temperature, and humidity in the environmental chamber is 1.40 x 10^{-4} m/s. However, calculated stage 1 evaporation rates are higher than expected, which may have resulted from loose particles that allow liquid to leave the surface easily. The stage 2 evaporation rate is significantly lower than the stage 1 and cannot be seen clearly in the figure 5.13. The figure 5.14 expands the scale to show the stage 2 evaporation rate of the 0 kPa substrate.

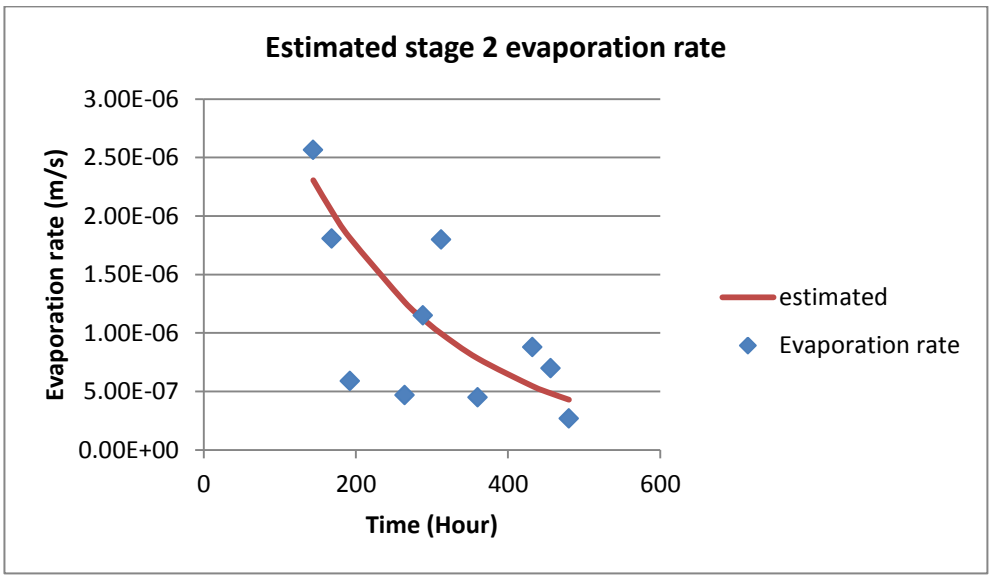

Figure 5.14 Stage II evaporation rate of 0 kPa substrate

Although the stage 2 evaporation rate of the 0 kPa green roof substrate seems to fluctuate, this rate decreases with time and an exponential decay function is shown.

The exponential decay function in figure 5.14 is shown by the equation

$$r_2 = \left(\frac{r_1}{30}\right) e^{-0.005(t-3)} \tag{5.39}$$

where: r_1 is the stage 1 evaporation rate 1.40 x 10^{-4} m/s,

r_2 is the stage 2 evaporation rate, and

The (t-3) term means the duration which, for the first stage evaporation rate, has been ignored (first 3 hours).

The equation will be used in the evaporation simulation.

5.5.2 Evaporation of 150 kPa green roof sample

The 150 kPa green roof substrate specimen was divided into 6 layers and then placed inside the environmental chamber with the conditions mentioned earlier in section 5.4.2. The moisture contents in each layer over a 504 hour evaporation period of a 150 kPa green roof specimen are presented in figure 5.15.

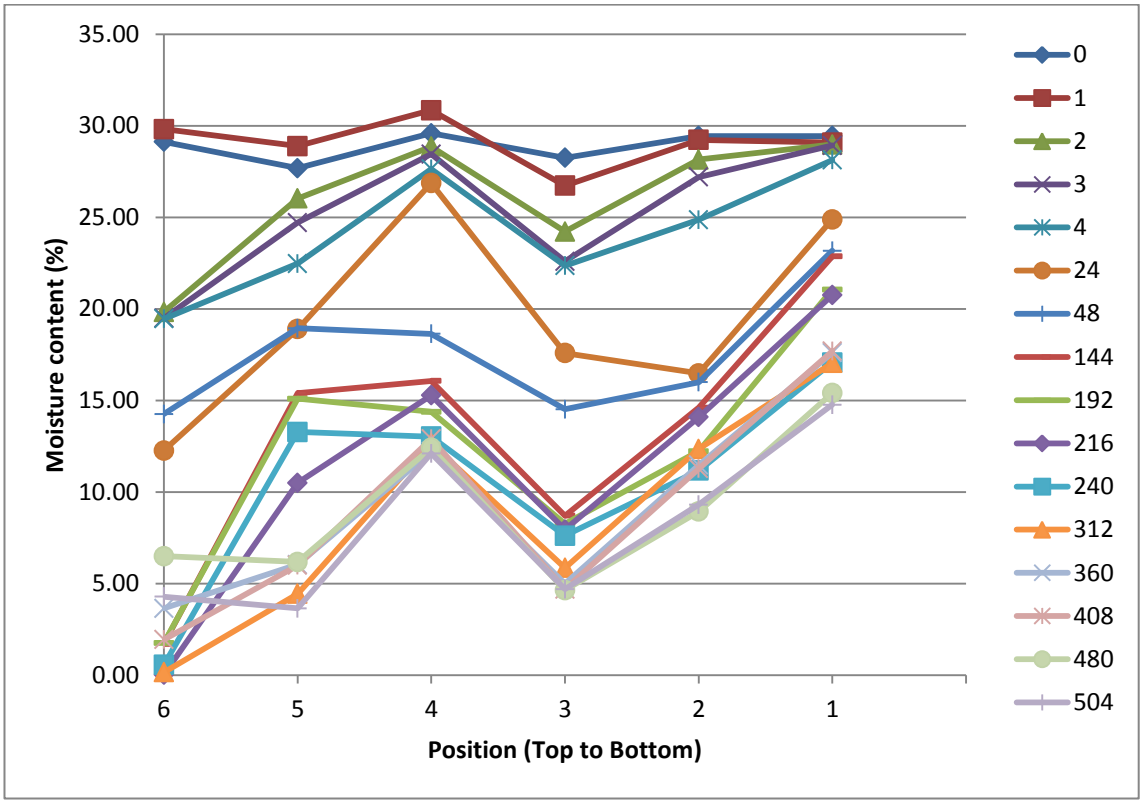

Figure 5.15 Moisture contents of 150 kPa compaction in 5 layers during 504 hours

The moisture content profiles of the 150 kPa green roof substrate fluctuated greatly over 3 weeks, especially layer 3 and layer 4. In addition, the moisture content of the top layer varied randomly. This may be caused by changes in compaction levels due to the shrinkage of layers that cause error in thermal conductivity readings. As a result, the evaporation rate of this specimen cannot be determined.

5.5.3 Evaporation of 300 kPa green roof sample

The 300 kPa green roof substrate specimen was divided into 6 layers and then placed inside the environmental chamber, with conditions as mentioned earlier in section 5.4.2. The moisture contents in each layer over a 504 hour evaporation period of a 300 kPa green roof specimen are presented in figure 5.16.

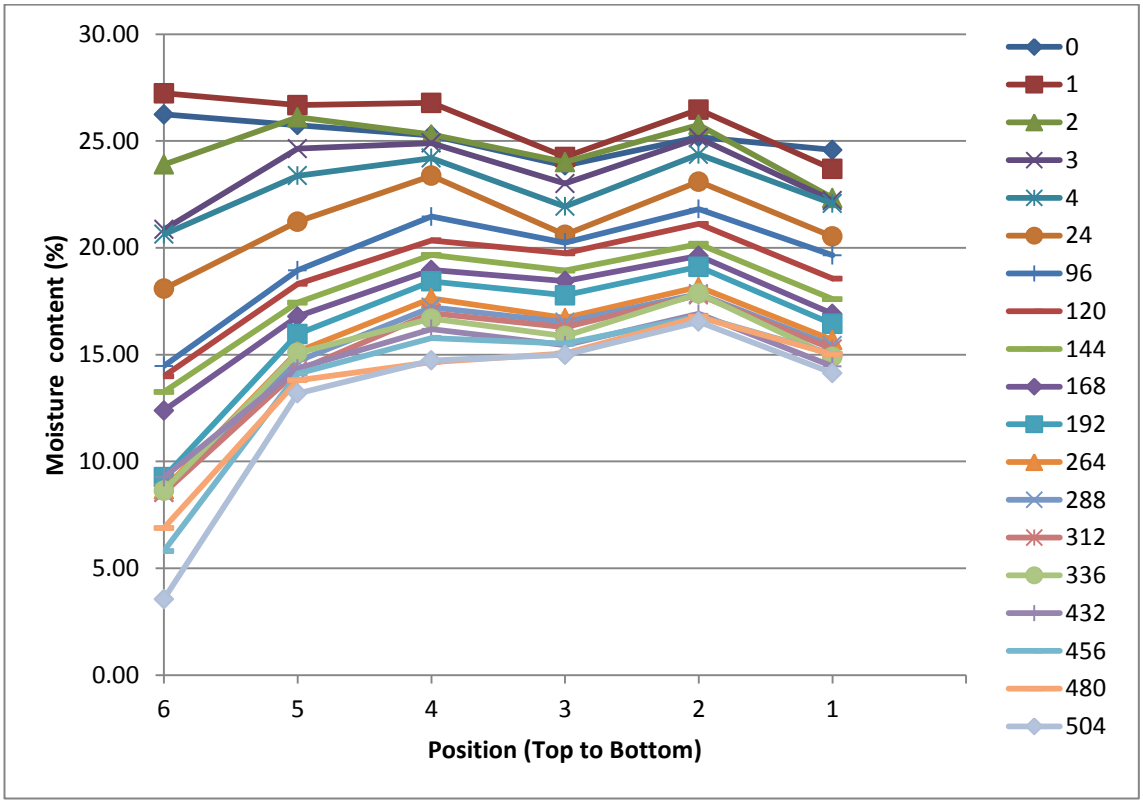

Figure 5.16 Moisture contents of 300 kPa compaction in 5 layers during 504 hours

The moisture content results of a green roof substrate with 300 kPa penetration resistance show the ideal moisture content profile. For the first 4 hours, the profile is in stage 1 evaporation range, where the top layers (layer 6 and 5) register a major reduction in moisture content, whereas the lower layers remain almost constant. After that, this specimen will reach the second stage evaporation, during which moisture content profiles start to form a curve. The top layer has the lowest moisture content and the bottom layer (layer 1) has the highest moisture content. From this information, the evaporation rate can be calculated and is presented in figure 5.17.

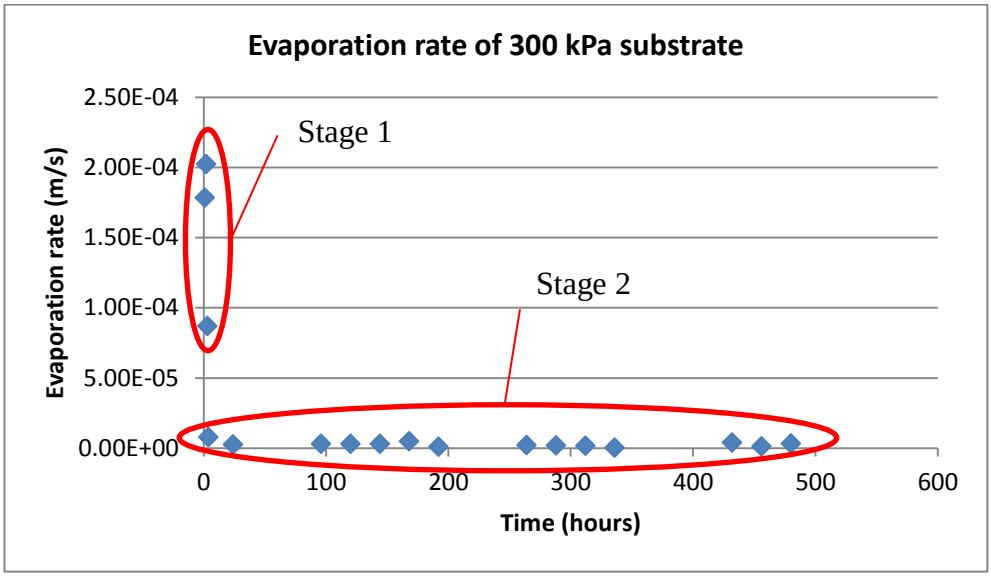

Figure 5.17 Calculated evaporation rate of the 300 kPa substrate

From figure 5.17, two stages of evaporation can be seen; stage 1 evaporation is within the first three hours, while stage 2 starts at the 4th hour. The theoretical stage 1 evaporation rate is 1.40 x 10^{-4} m/s according to environmental chamber conditions, but calculated rates from the experiment are between 9 x 10^{-5} to 2 x 10^{-4} m/s. This error may be caused from the measurement error and fluctuations in the environmental chamber (there are ±1.0^{o}C and ±20% RH in the chamber). For stage 2, figure 5.18 expands the results.

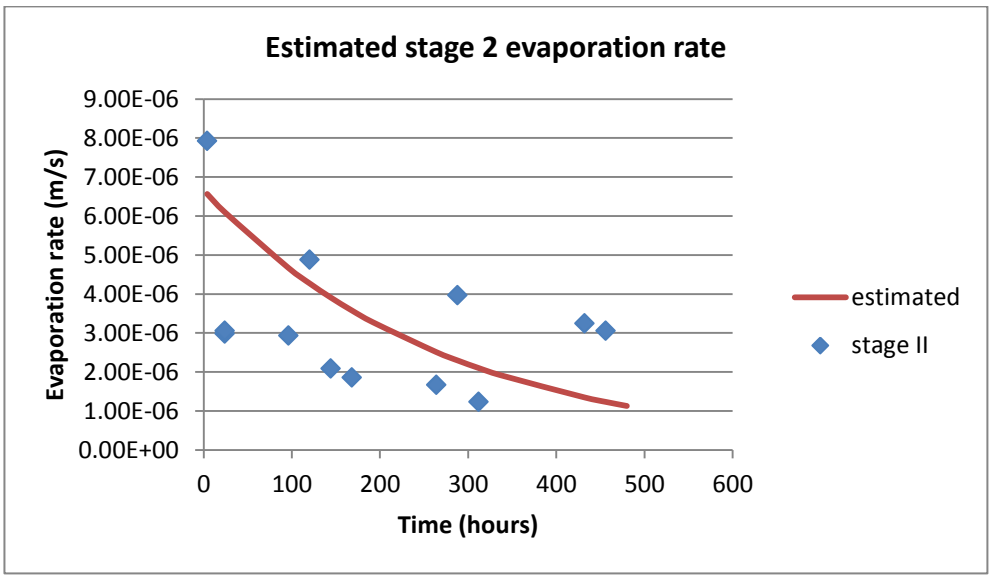

Figure 5.18 Stage 2 evaporation rate of the 300 kPa substrate

Although the stage 2 evaporation rate of the 300 kPa green roof substrate seems to fluctuate, this rate decreases with time and an exponential decay function is shown.

The exponential decay function in figure 5.18 is shown by equation.

$$r_2 = \left(\frac{r_1}{20}\right) e^{-0.0037(t-3)} \tag{5.40}$$

The equation will be used in the evaporation simulation.

5.5.4 Evaporation of the 450 kPa green roof sample

The 450 kPa green roof substrate specimen was divided into 6 layers and then placed inside the environmental chamber with the same conditions as described above. The moisture contents in each layer over the 504 hour evaporation period of a 450 kPa green roof specimen are presented in figure 5.19.

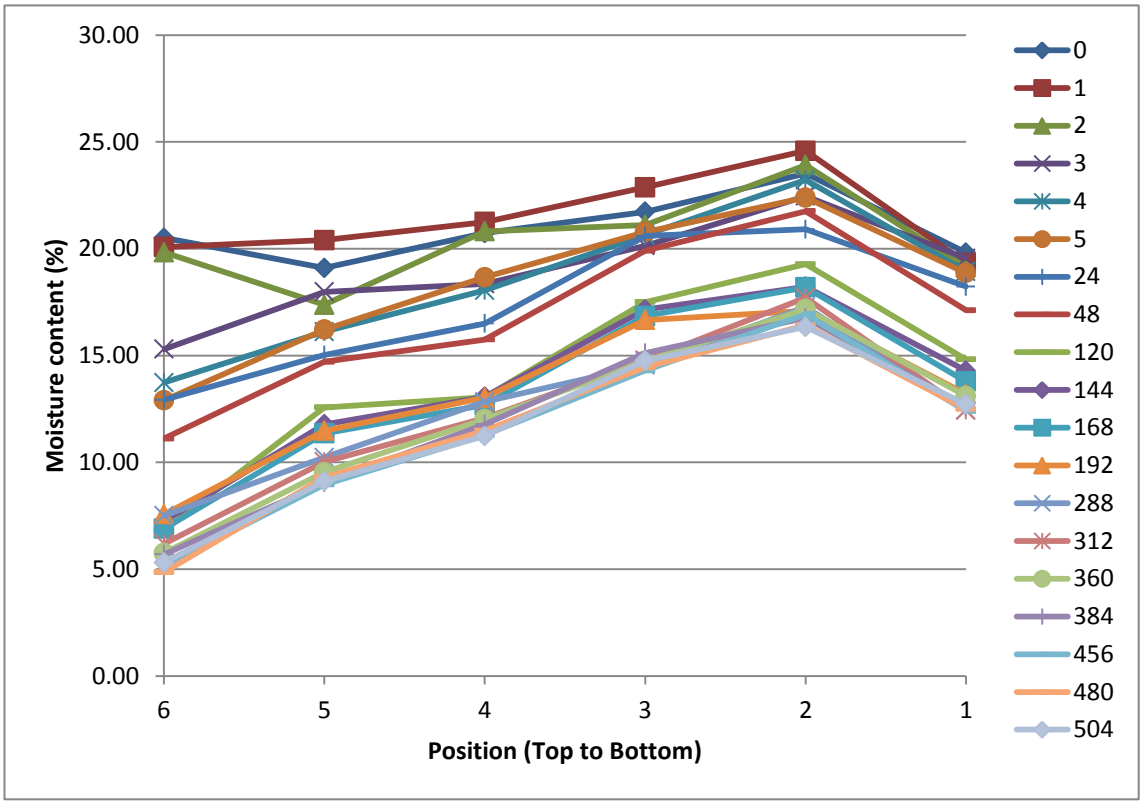

Figure 5.19 Moisture contents of a 450 kPa compaction in 5 layers during 504 hours

The moisture content results of a green roof substrate with a 450 kPa penetration resistance show a reasonable moisture content profile. From the start of evaporation to

the 3rd hour, the profile is in the stage 1 evaporation range, where the top layers 6 and 5 experience a major reduction in moisture content, whereas the moisture in the lower layers stays almost constant. However, there are some fluctuations in moisture content in the first and second hours. After that, this specimen reaches the stage 2 evaporation, during which moisture content profiles start to form a curve with the top layer, which has the lowest moisture content, and when layer 2 has the highest moisture content. Layer 1 shows lower moisture content than expected from the start, which may be caused by a highly compact surface layer that creates an error in the thermal conductivity reading. From this information, the evaporation rate can be calculated and presented in figure 5.20.

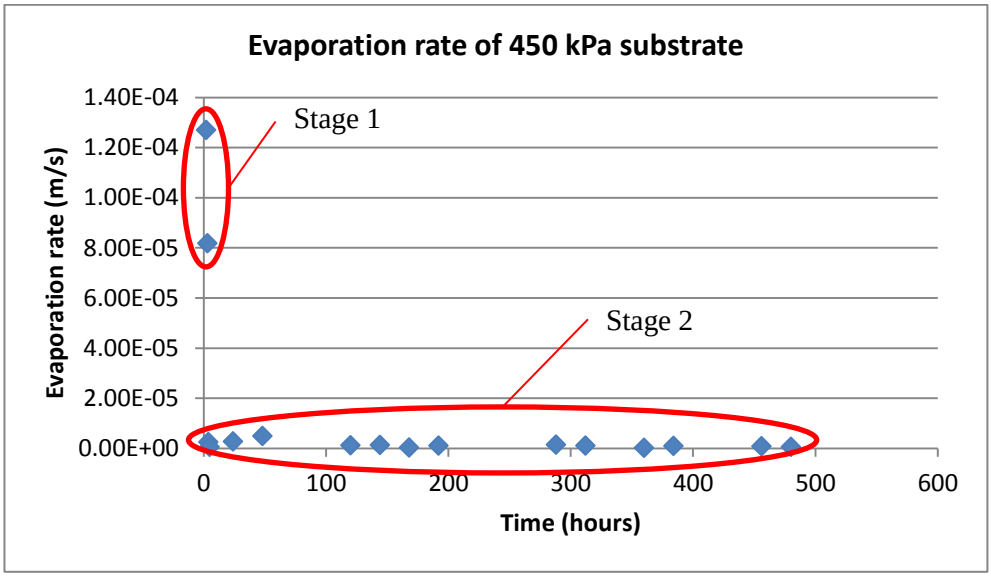

Figure 5.20 Calculated evaporation rate of a 450 kPa substrate

From figure 5.20, two stages of evaporation can be seen; stage 1 evaporation is within the first three hours, while stage 2 starts at the 4th hour. The theoretical stage 1 evaporation rate is 1.40 x 10^{-4} m/s according to environmental chamber conditions, but calculated rates from the experiment are between 8 x 10^{-5} to 1.2 x 10^{-4} m/s (ignoring the evaporation rate between 1st and 2nd hour). This error may be caused by the measurement error and fluctuations in the environmental chamber (there are ±1.0°C and ±20% Rh in the chamber). For stage 2, figure 5.21 expands the results.

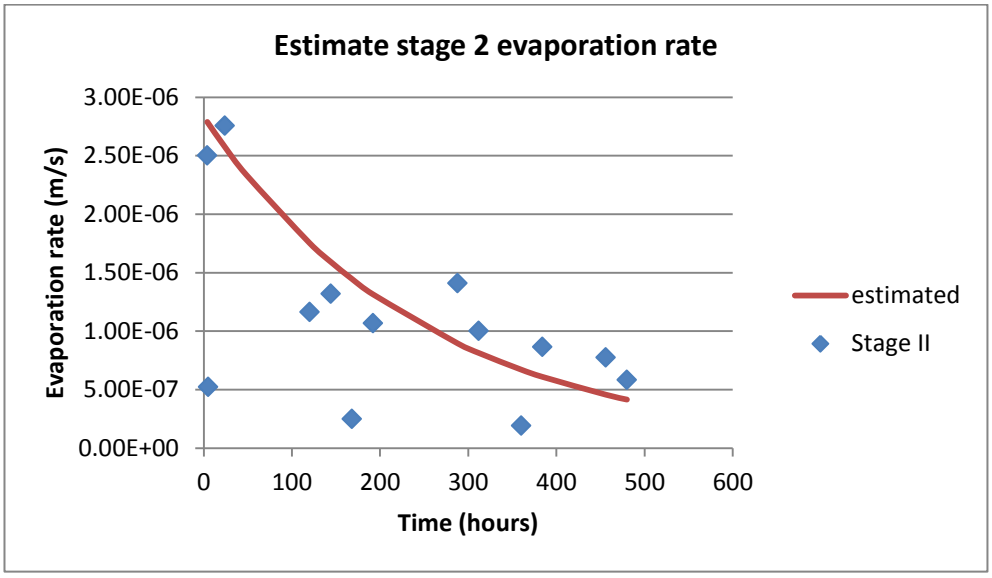

Figure 5.21 Stage 2 evaporation rate of 450 kPa substrate

Although the stage 2 evaporation rate of the 450 kPa green roof substrate seems to fluctuate, this rate decreases with time an exponential decay function is shown.

The exponential decay function in figure 5.21 is shown by equation.

$$r_2 = \left(\frac{r_1}{50}\right) e^{-0.004(t-3)} \tag{5.41}$$

5.6 Evaporation simulation

The green roof substrate evaporation simulation in this section aims to produce the nearest possible moisture content profile prediction at hourly intervals. The simulation starts with the saturated substrate, and then uses evaporation rates obtained from the experiment together with a finite difference flow model, as presented in section 5.3.1 above. The resulting simulation can extend moisture content profiles into hourly intervals instead of daily intervals, which can produce more accuracy in heat conduction simulation.

This simulation will use the 300 kPa green roof specimen as an example. The initial moisture content for the simulation will follow experimental values and the evaporation rate will follow equation 5.40.

However, there is another parameter that is required in this simulation. Due to the large pore spaces in the green roof substrate, the water that moves to the top layer from layer 5 is not fast enough to sustain the evaporation rate. This effect ensures the 5th layer has a much lower moisture content than the top layer. As a result, the flow from layer 5 to layer 6 needs to be verified.

The flow from layer 5, which is now called Q_5, is calculated from the evaporation rate, and the moisture content of layer 6 at current time step and the next time step ($\theta_{6,t}$ and $\theta_{6,t+1}$). From the top layer moisture content balance in equation 5.31, the flow rate from layer 5 can be determined from:

$$\theta_{6,t+\Delta t} = \theta_{6,t} - \frac{r_t \rho A t}{M_{6,t}} + Q_5 \frac{\rho A t}{M_{6,t}}$$

$$\theta_{6,t+\Delta t} - \theta_{6,t} + \frac{r_t \rho A t}{M_{6,t}} = Q_5 \frac{\rho A t}{M_{6,t}}$$

$$\therefore Q_5 = (\theta_{6,t+\Delta t} - \theta_{6,t}) \frac{M_{6,t}}{\rho A t} + r_t \qquad (5.42)$$

From the equation 5.42 and information from the experiment, the flow rate from layer 5 to layer 6 can be calculated and presented in figure 5.22.

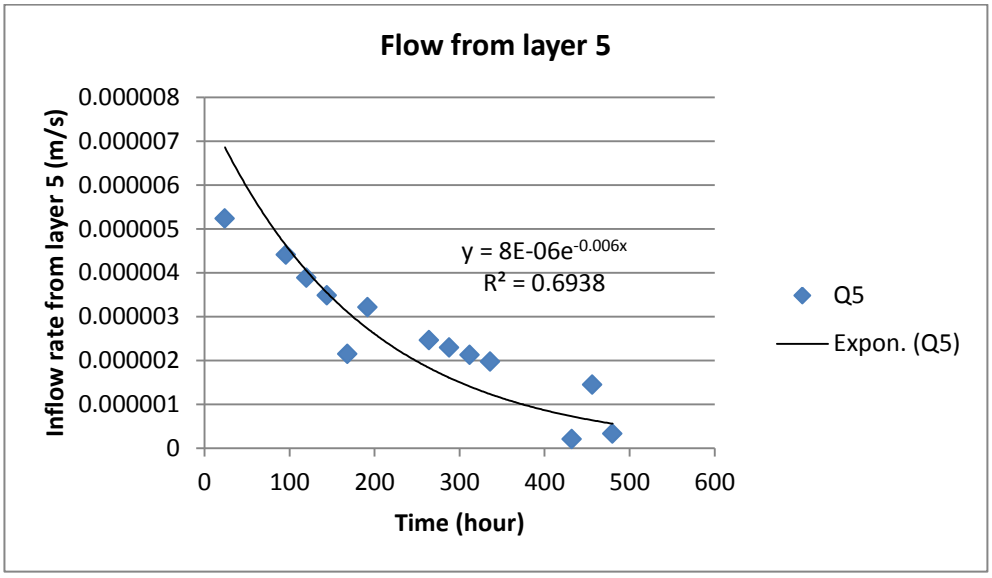

Figure 5.22 Calculated flow rate from layer 5 to layer 6

The flow rate from figure 5.22 is begun at the 4th hour, when the stage 2 evaporation began. The flow rate that is involved in the stage 1 evaporation is 1.67 x 10^{-4} m/s, which applies during the first 3 hours. For the stage 2 evaporation, the flow rate decreases with exponential decay function, which is $(8 \times 10^{-6})e^{-0.006t}$. The next section will compare the simulation with given information and the experimental results recorded from the 300 kPa green roof substrate.

5.6.1 Simulation Result

The simulation result of a 300 kPa green roof substrate is processed by MATLAB, which presents predicted moisture content profiles in 6 layers for the 504 hours simulation duration. The simulation code is presented in the appendix; figure 5.23 presents moisture content profiles of 300 kPa specimens in 6 different layers.

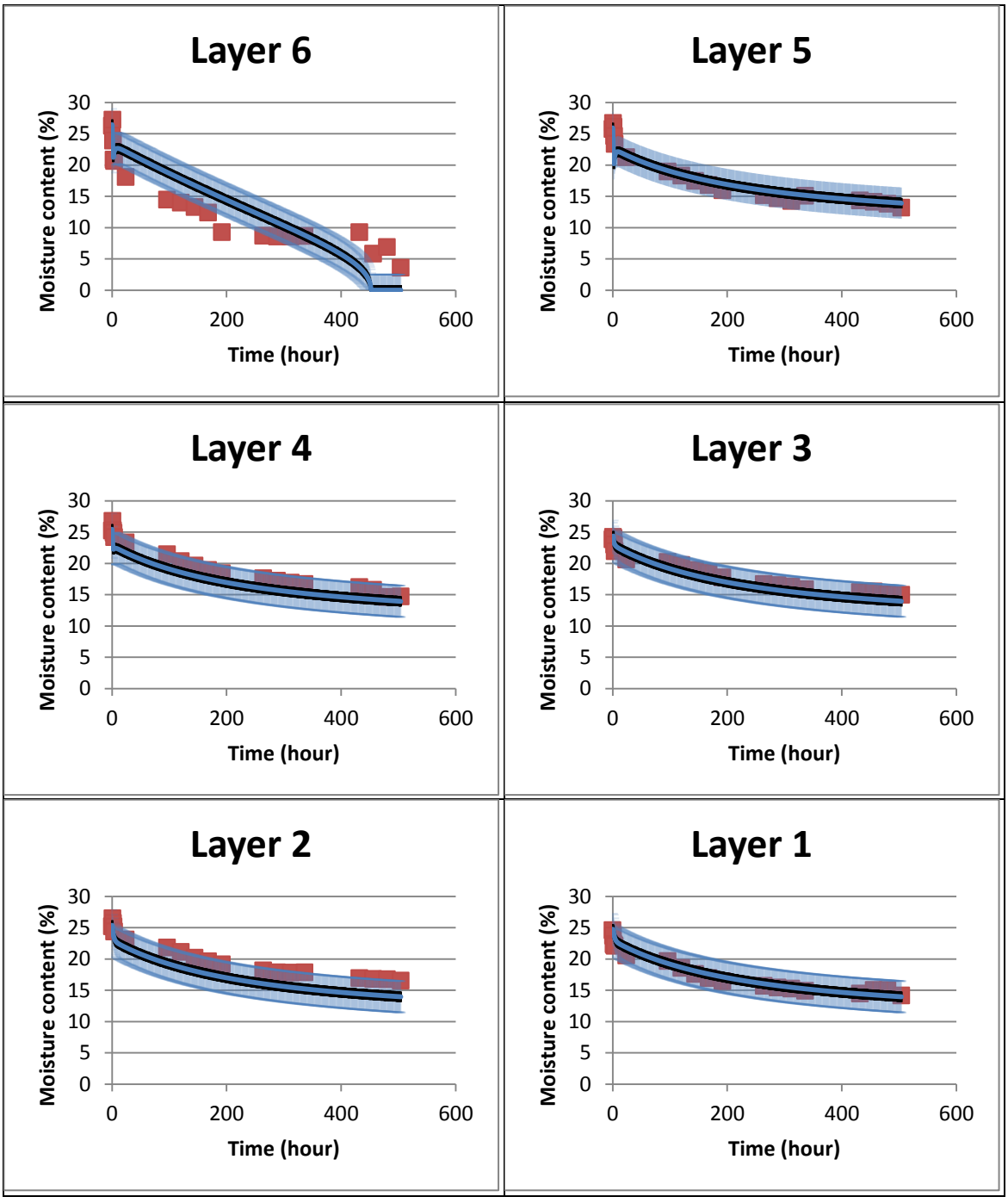

Figure 5.23 The 300 kPa green roof substrate's simulation result of predicted moisture content with 95% prediction interval (Blue line) compared with experimental result (red dots)

The figure 5.23 shows comparisons of 6 layers, where the x-axis indicates time in hours and y-axis indicates the moisture content. Blue lines in each graph indicate the simulation result with ±2.5% mc error bar, and red dots represent the experimental results obtained earlier.

In layer 6, the moisture content profile obtained from simulation shows an accurate result in the stage 1 evaporation, but the moisture content is over-estimated after it reaches the second stage evaporation resulting in a shallower curve. However, half of the experimental data are within the error range. Furthermore, the shape of the moisture profiles of simulated and experimental results follows the same pattern.

For the rest of the layers, simulation results and experimental results are very close together, especially in layer 5 and layer 1, where both results almost coincide. The results from layers 4 and 3 are within the error range. However, the results from layer 2 were under-estimated but 80% of the experimental results are in the ±2.5% mc error range.

With these results, the thermal conduction through the green roof substrate compacted to 300 kPa penetration resistance can be simulated. The next section will link the moisture content results together with the thermal conductivity data to create a thermal simulation due to evaporation.

5.7 Thermal simulation

In this section, the moisture information and the thermal information will be drawn together to produce a thermal conduction simulation with evaporation. The 300 kPa substrate will be used as an example in this section.

The moisture content of each layer in certain time steps from the simulation will be converted back into the thermal conductivity. Table 5.2 presents the thermal conductivity values as a function of moisture content (θ), which is converted from table 5.1.

Table 5.2 Thermal conductivity and moisture content relation

Compaction level	**Thermal conductivity and moisture content relation**
0 kPa	$Thermal\ conductivity = 0.0941e^{0.082\theta}$
150 kPa	$Thermal\ conductivity = 0.2243e^{0.066\theta}$
300 kPa	$Thermal\ conductivity = 0.2613e^{0.069\theta}$
450 kPa	$Thermal\ conductivity = 0.2766e^{0.075\theta}$

The steady state conduction is used in this simulation, during which the hourly effective thermal resistivity is calculated by taking hourly thermal conductivity measures for the 6 layers. Equation 5.43 presents the effective thermal resistivity of whole layers in each time step.

$$\mathrm{R}_{e,t} = \frac{\Delta x_6}{K_{6,t}} + \frac{\Delta x_5}{K_{5,t}} + \frac{\Delta x_4}{K_{4,t}} + \frac{\Delta x_3}{K_{3,t}} + \frac{\Delta x_2}{K_{2,t}} + \frac{\Delta x_1}{K_{1,t}} \tag{5.43}$$

Where; ΔX_{layer} is the thickness of each layer (m),

$K_{layer,t}$ is the thermal conductivity of each layer in that time step (W/m.K), and

$R_{e,t}$ is the effective thermal resistivity of the whole layer (m^2.K/W).

The thickness of each layer was indicated in figure 5.10. The next section will present the thermal simulation results.

5.7.1 Simulation Results

The simulation results in this section are from the 300 kPa green roof substrate with conditions mentioned earlier. This simulated result is an hourly effective thermal resistance, which is presented in figure 5.24.

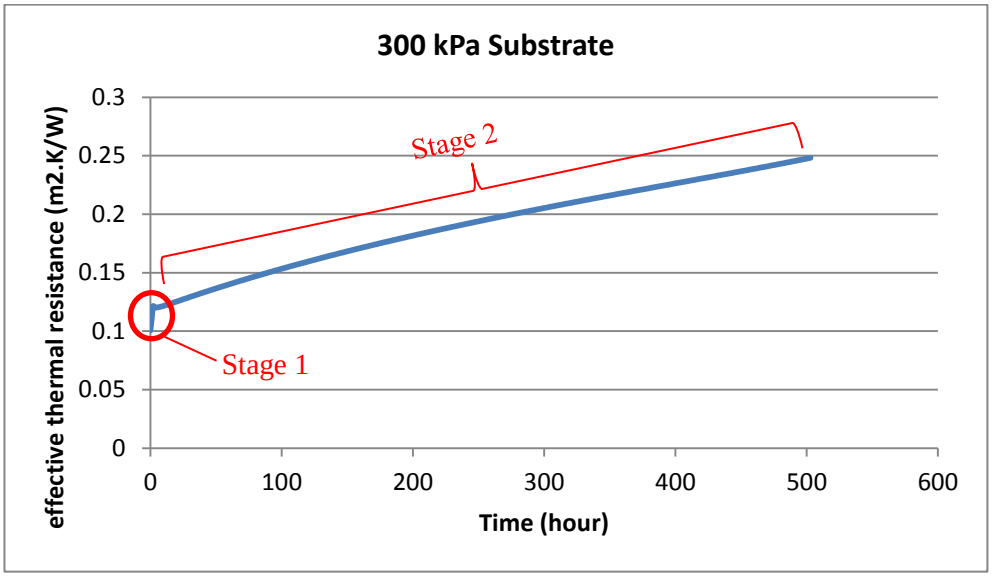

Figure 5.24 Effective thermal resistance of a 300 kPa green roof substrate due to evaporation

The thermal resistance profile in figure 5.24 starts with the lowest resistance (0.10 m^2.K/W) then suddenly rises to 0.125 m^2.K/W. This steep rise is a result from the stage 1 evaporation, which appeared in the first 3 hours. After that, the effective resistance gradually increases at a much slower rate because of the evaporation rate from stage 2. The thermal resistance graph will continue in this manner until the substrate is dried out or there is precipitation to re-wet it.

This thermal resistance information will be applied with the steady state conduction in order to calculate the heat flux through green roof in the following chapter.

5.8 Conclusion

This chapter has introduced the evaporation theory of porous materials, which can be applied to a green roof substrate. Evaporation rates can be divided into two stages, which are stage 1 and stage 2 evaporation. The stage 1 evaporation is the evaporation rate due to the environmental conditions such as wind speed, temperature, and relative humidity, which appear in the early hours of the drying. In contrast, the stage 2 evaporation rate is controlled by properties of the porous material, which is a rate that is much lower than the stage 1 evaporation rate.

The ‘internal flow between layers method’ is defined as the finite difference flow model, but this method did not include the time parameter. For this reason, the adapted finite difference flow model with time step was introduced. This method can predict the

moisture content of each layer in the nearby time step by using the evaporation rate and moisture content information. However, the evaporation rate needs to be determined by experiment.

The experiment of evaporative drying was performed in the environmental chamber, which is controlled for constant temperature, humidity, and wind speed. The green roof specimen was saturated and divided into six layers, before being placed inside the chamber. For the first 5 hours, the thermal conductivity of each layer was measured at hourly intervals in order to determine the stage 1 evaporation rate. After that, the thermal conductivity of each layer was measured at daily intervals. Thermal conductivity data was converted into moisture contents by relations given in table 5.1.

Results from the experiments fluctuated in some samples and some layers, and were calibrated by finding the moisture content with the direct oven dry method. After results were calibrated, the evaporation rate was then calculated and an exponential decay function was fitted.

The thermal simulation uses information obtained from the experiment, such as the initial moisture content of each layer and the evaporation rates. The simulation can predict moisture content profiles at hourly intervals based on given information; the effective thermal resistance can then be calculated by the steady state conduction method. This thermal resistance will be used to calculate the hourly conduction through the green roof substrate. The next chapter will combine the wetting and drying of green roof substrate.

Chapter 6: Absorption and Evaporation Combination

6.1 Introduction

From previous chapters, the absorption and evaporation of green roof substrate have been individually defined through computer simulation. This chapter aims to bring these two mechanisms together and create the wetting to drying thermal property, which leads to the conduction heat flux calculation.

6.2 Simulation process

The focus on theory development will offer theories previously mentioned in chapters 4 and 5, informed by a dynamic flow model. The simulation process is explained in two parts; the absorption cycle and the evaporation cycle.

6.2.1 The absorption simulation process

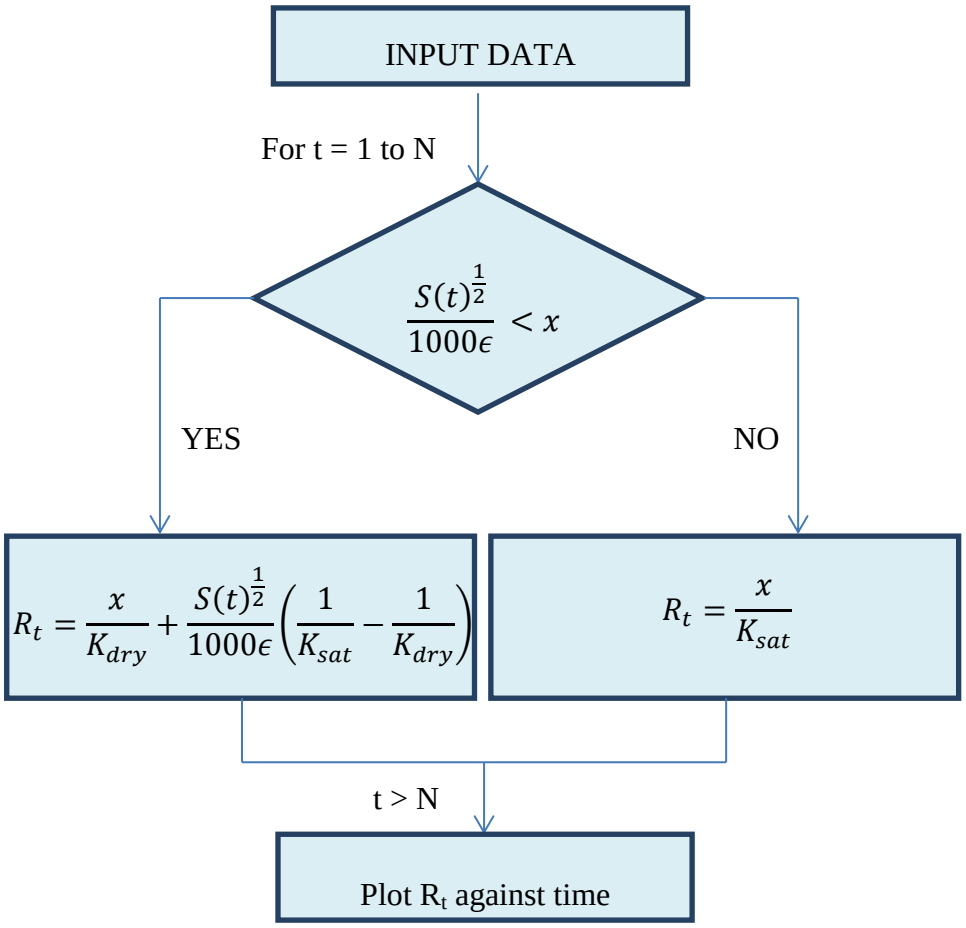

Figure 6.1 The dynamic flow chart of absorption simulation

From figure 6.1, the absorption simulation starts with input data relating to: dry thermal conductivity, saturated thermal conductivity, sorptivity, porosity, thickness of layer, outdoor temperature, and indoor temperature. These data need to be put into the simulation consecutively.

After receiving the input information, the duration of simulation is created, which stretches from 1 to N (N is the last time step). The time step will increase in 1 minute intervals. Furthermore, the boundary condition of this simulation is the depth of the saturated front, which cannot exceed the depth of the substrate. Therefore, the saturated front needs to be calculated before the thermal resistance, where the term $\frac{S(t)^{\frac{1}{2}}}{1000\epsilon}$ is the depth of the saturated front. If the depth of the saturated front is less than the substrate depth (x), the effective thermal resistivity is a combination of dry and saturated layers, which can be determined by $R_t = \frac{x}{K_{dry}} + \frac{S(t)^{\frac{1}{2}}}{1000\epsilon}\left(\frac{1}{K_{sat}} - \frac{1}{K_{dry}}\right)$. On the other hand, when the saturated front reaches the substrate depth, this means the entire layer of substrate is saturated. As a result, the effective thermal resistance is equal to the saturated thermal resistance.

After thermal resistance in every time step is calculated, these data will be stored in array format and can therefore be plotted against time. Finally, these thermal resistances will later be used to calculate the conduction heat flux.

6.2.2 The evaporation simulation process

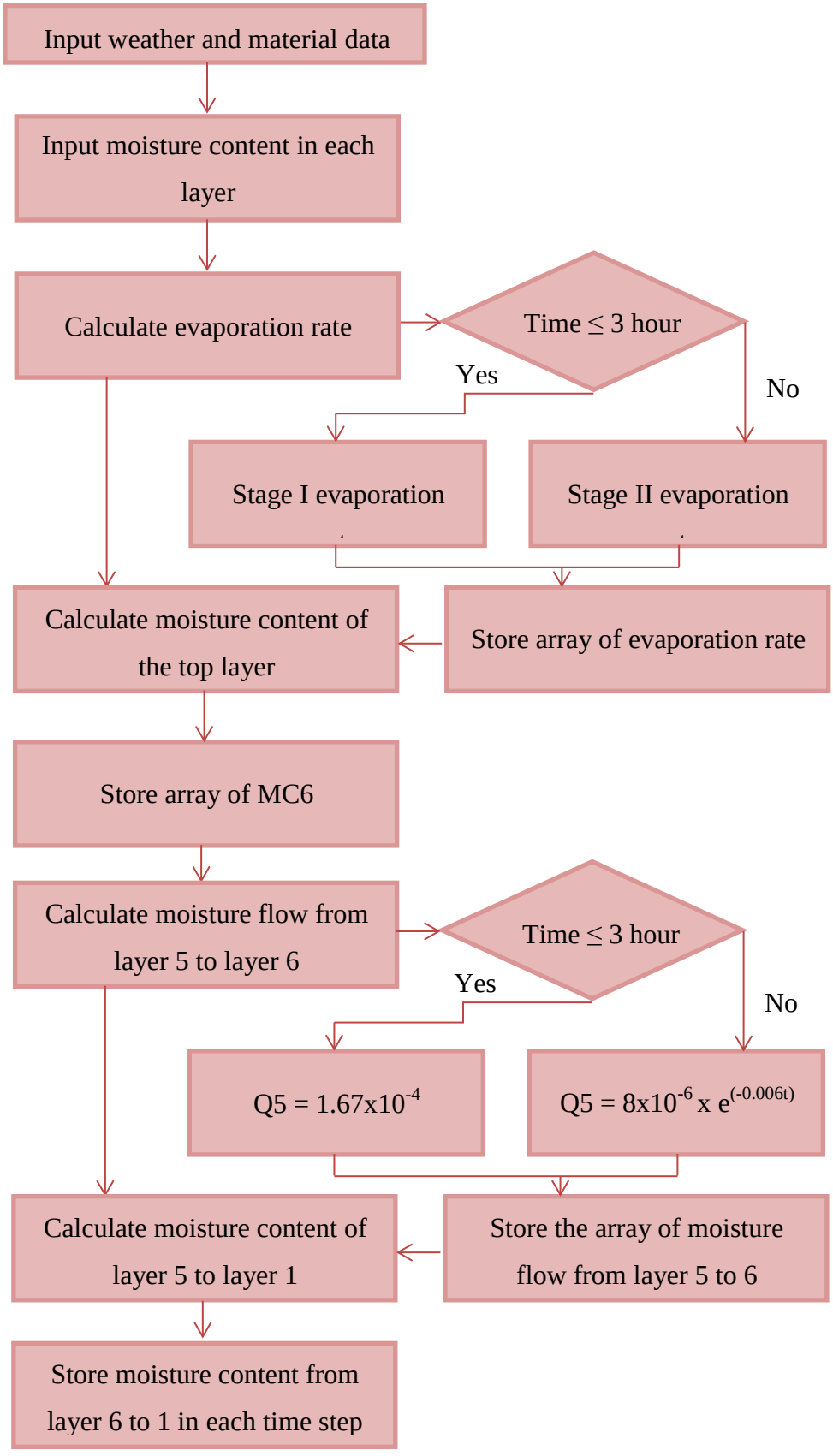

Figure 6.2 The dynamic flow chart of evaporation simulation (1)

From figure 6.2, weather data are made up of the temperature, wind speed, and relative humidity. The required material data are the length of drying plan, cross-sectional area of specimen, density of water, and dry mass of the substrate. However, these aforementioned data are already defined in the simulation code.

On the other hand, the required input data is the initial moisture content of each substrate layer. The next step is to calculate the evaporation rate based on environmental information; a rate that is divided into stage 1 and stage 2. The stage 1 evaporation rate is constant within the first 3 hours, but in stage 2 decays exponentially, recorded every hour after the 3rd hour. This decay rate is determined by experiment, as mentioned in chapter 5. This evaporation rate information will be stored in array format.

Other important information is the flow rate from layer 5 to layer 6; labelled Q_5, which is revealed by experimental determination. Similarly to the evaporation rate, Q_5 is divided into two stages: the maximum flow rate at the first 3 hours and the exponential decay rate after the 3rd hour. This flow rate information is also stored in array format.

The moisture content prediction is considered in two parts: the prediction of moisture content in the top layer (layer 6), and the prediction of moisture content of the other remaining layers (layer 5 to 1). The prediction of moisture content in the top layer is associated with the evaporation rate and the moisture content of layer 5. In contrast, the predicted moisture content of layer 5 is associated with Q_5, and the moisture content of layers 5 and 4. Likewise, moisture contents from layers 6 to 1 are stored in array formation.

The next process is the conversion of moisture content to thermal resistivity, which is presented in figure 6.3.

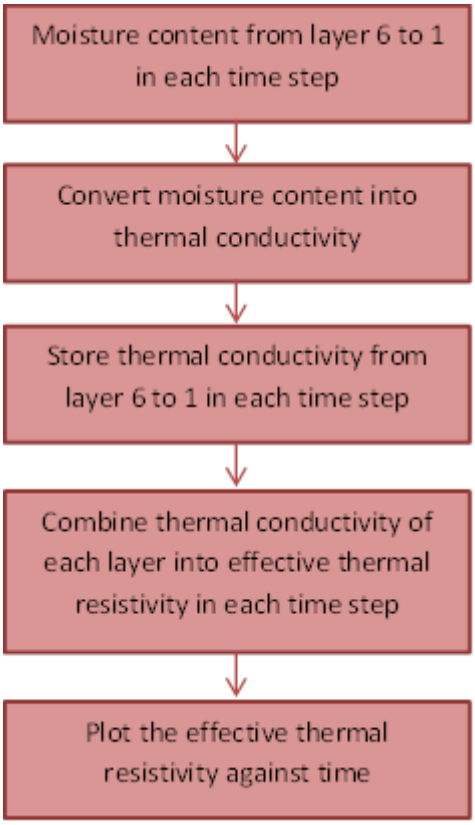

Figure 6.3 The dynamic flow chart of thermal resistivity simulation (2)

From figure 6.3, it can be seen that the moisture content in each time step, from the previous process, is now converted into thermal conductivities of each layer and time step. Relations between moisture content and the thermal conductivity of each compacted substrate can be found in table 5.2 in chapter 5. After thermal conductivities are calculated, the information will be stored in array format with the corresponding time step.

This thermal conductivity information will be combined into the effective thermal resistivity of the whole substrate. The effective thermal resistivity at each corresponding time step can be calculated by using the thermal conductivity and the thickness of each layer, as shown in equation 6.1.

$$\mathrm{R}_{e,t} = \frac{\Delta x_6}{K_{6,t}} + \frac{\Delta x_5}{K_{5,t}} + \frac{\Delta x_4}{K_{4,t}} + \frac{\Delta x_3}{K_{3,t}} + \frac{\Delta x_2}{K_{2,t}} + \frac{\Delta x_1}{K_{1,t}} \tag{6.1}$$

This thermal resistivity will be stored in array formation with the corresponding time step, and then plotted against time. This information is later used in the heat flux calculation.

6.3 Combining absorption and evaporation

Simulation results from previous sections are now combined. By using the effective thermal resistivity of each time step in each hour, the wetting and drying thermal resistivity of the same green roof substrate can be joined in a single graph. For this case, the 300 kPa green roof substrate will be used as an example here and in the case study in next chapter.

Environmental conditions for this wetting and drying cycle are:

- The outdoor temperature is 5^{o}C.
- The relative humidity is 50% Rh.
- The wind speed over the roof is 0.5 m/s.
- The substrate thickness is 162.5 mm.

The time scenario used is as follows. The substrate's moisture content starts in a dry condition (0% mc); then it absorbs water from the precipitation for 60 hours. By this time, the substrate is saturated up to a moisture content equivalent to 26.24%. After the soaking process / 'rain' stops, this substrate is dried under the above mentioned conditions for 3 weeks (504 hours).

Figures 6.4 and 6.5 present the wetting effective thermal resistivity of the green roof substrate and the drying effective thermal resistance respectively.

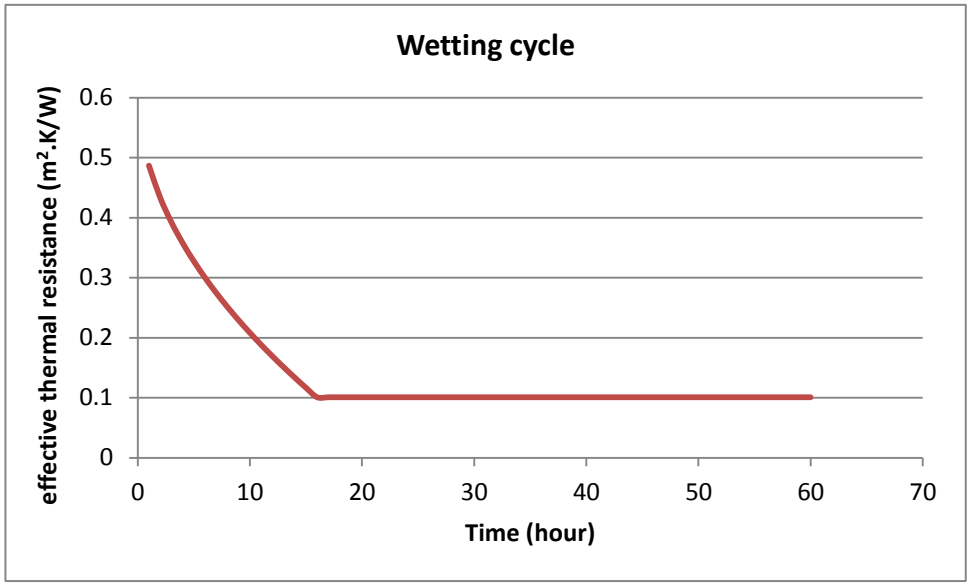

Figure 6.4 The wetting effective thermal resistance of 300 kPa green roof substrate

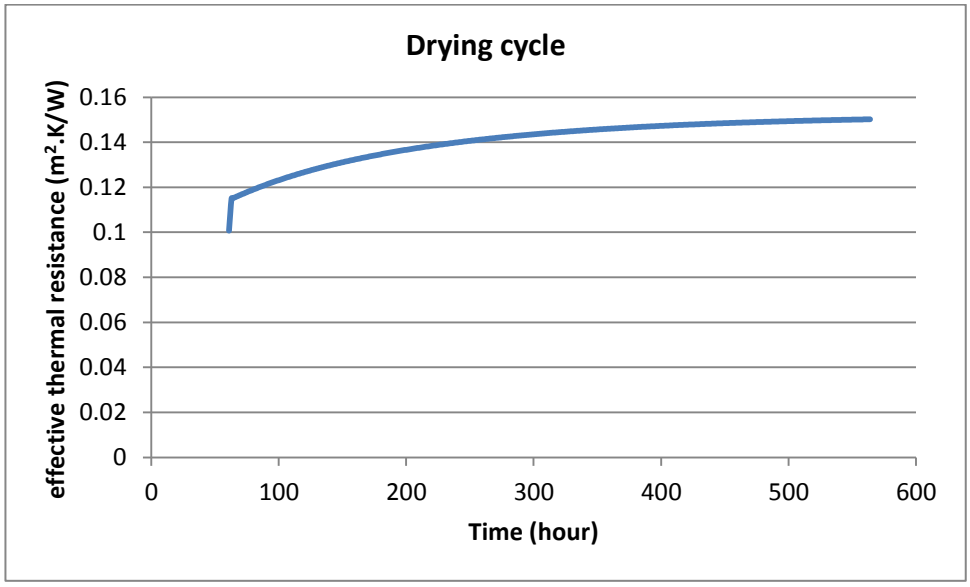

Figure 6.5 The drying effective thermal resistance of 300 kPa green roof substrate

These two cycles can be combined by the corresponding time steps, as shown in figure 6.6.

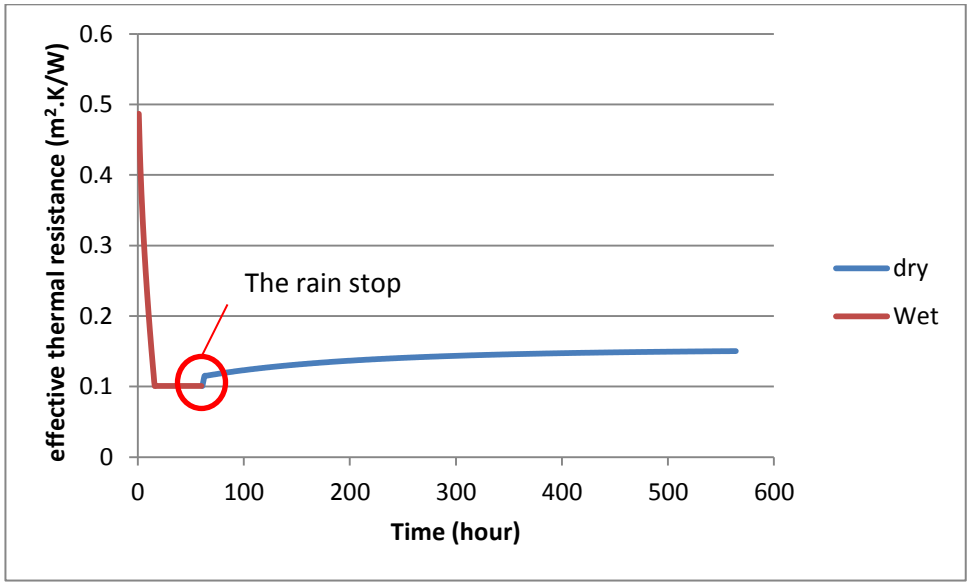

Figure 6.6 The wetting and drying effective thermal resistance of 300 kPa green roof substrate

From figure 6.6, it can be seen the 300 kPa green roof substrate is absorbing water from the start and then reaching the saturated condition with the effective thermal resistance equal to 0.1008 (m^2K/W) after 15 hours of precipitation. This saturated condition will continue for another 45 hours until the rain is stopped. This wetting period is simulated by using the Sharp Front theory (Chapter 4).

After the rain is stopped (the 61st hour), the liquid in the substrate starts to evaporate. From the 61st to 63rd hour, the evaporative drying is in the stage 1, during which thermal resistance rises rapidly. After this stage, the thermal resistivity is slowly increased because water loss is now in the stage 2 evaporation rate.

Figure 6.6 will be applied with thermal conductivity calculations in the next chapter.

6.4 Conclusion

This chapter aims to report details from combining the absorption and evaporation simulation of green roof substrate. Furthermore, this chapter explains the simulation procedures of both cycles.

For the absorption simulation, the required information relates to: dry thermal conductivity, saturated thermal conductivity, sorptivity, a porosity value, thickness of layers, an outdoor temperature, and an indoor temperature. The simulation process is started with a dry substrate then moisture content of each layer will rise until the whole layer is saturated. The effective thermal resistance is calculated, based on the thickness of the saturated and dry layers.

For the evaporation simulation, the process begins with the saturated substrate and then the moisture content of each layer continues dropping. The required information is the initial saturated moisture content of each layer. This simulation calculates two stages of evaporation rate, using this information to calculate the moisture content reduction of each layer in corresponding time steps. After the moisture content is calculated, it is converted into the thermal conductivity; then the effective thermal resistance can be calculated with the available information.

The 300 kPa green roof substrate was used as an example for the absorption and evaporation simulation. The calculated thermal resistance will be used again in the next chapter to discuss and compare the results with literature, and the implications of this simulated data for building examples will be pointed out.

Chapter 7: Model application and discussion of results

7.1 Introduction

This chapter will discuss the results of this research by comparing the findings with previous work on green roof thermal simulation. Furthermore, chapter 7 will consider the limitations of this research, sources of error, and the validation of the underlying assumptions. At the start of this chapter, the results from simulation will be used with an example building in order to see the effect of the green roof at different stages of moisture content.

7.2 Application of the model to a case study building

The implications of this work are made explicit by presenting the case study of a building with different green roof substrate depths, subjected to differing environmental conditions; thereby allowing the researcher to estimate the energy saving without and with the presence of a green roof. Furthermore, the effect of a green roof on the issue of thermal insulation, such as substrate thickness reduction in order to meet the building standard requirement, is also investigated.

The conduction heat loss from a case study building over a defined period is calculated (Ventilation and infiltration heat loss is ignored). The case study building is a shoebox shaped structure with 4 insulated side walls and 8 double glazed windows. The building is initially fitted with three types of flat roof: i) a non-domestic inverted roof, ii) a domestic warm roof, and iii) a sheet metal roof. Initially, the heat transfer via conduction of these roofs is calculated and compared with the other building elements. Then, these roofs will be retrofitted with a green roof system, from which heat conduction is calculated and compared in different situations.

The building geometry and elevations are presented in figures 7.1-7.3.

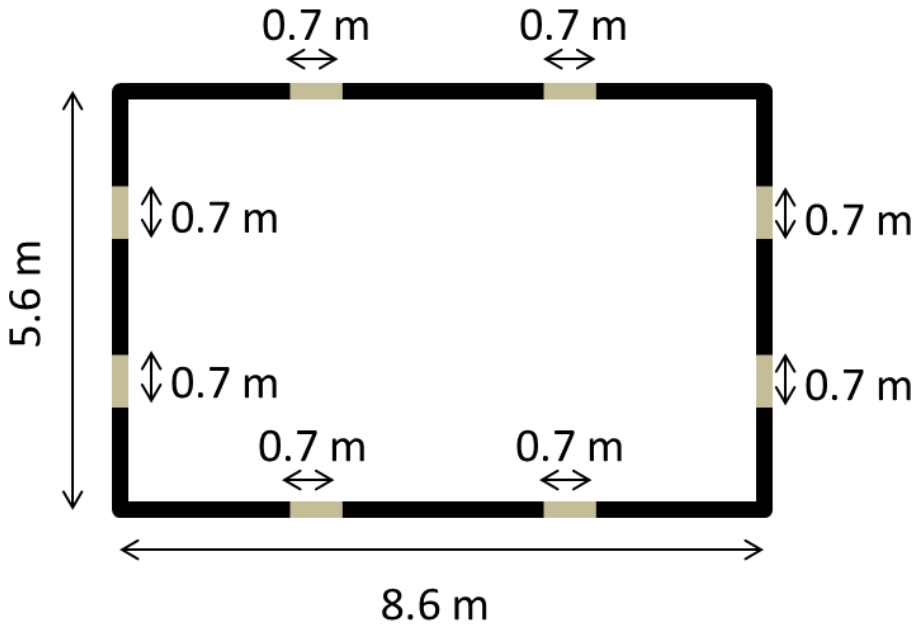

Figure 7.1 Building plan

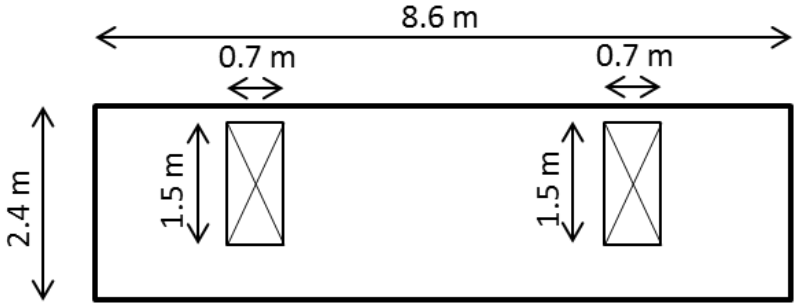

Figure 7.2 First elevation of the building

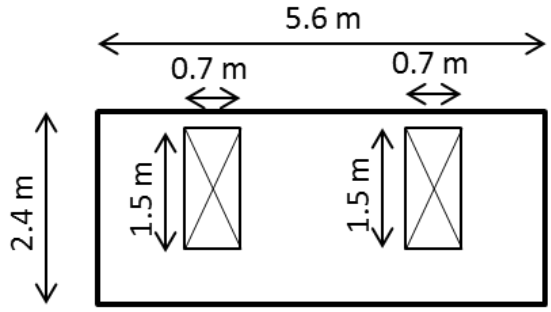

Figure 7.3 Second elevation of the building

The surface area of each building element is summarised in table 7.1.

Table 7.1 Surface area of building elements

Building Element	**Area (m^2)**
Wall	74.16
Window	8.4
Ground floor	48.16
Roof	48.16

The thermal transmittance (U-value) of each building component is informed by the relevant Scottish government building standard (2016).

- U-value of the roof = 0.2 W/m^2K (area average)
- U-value of the wall = 0.27 W/m^2K (area average)
- U-value of the floor = 0.22 W/m^2K (area average)
- U-value of the window = 3.30 W/m^2K (individual)

Values of surface thermal resistance and air space used in calculating the thermal properties of common construction (Chartered Institution of Building Services, 2006) are shown below.

- Thermal resistance of outdoor air film for external wall ($R_{wall,out}$) = 0.04 m^2K/W.
- Thermal resistance of indoor air film for external wall ($R_{wall,in}$) = 0.13 m^2K/W.
- Thermal resistance of outdoor air film for the flat roof ($R_{roof,out}$) = 0.04 m^2K/W.
- Thermal resistance of indoor air film for the flat roof ($R_{roof,in}$) = 0.10 m^2K/W.
- Thermal resistance of airspace for the flat roof ($R_{airspace}$) = 0.16 m^2K/W.

The weather condition is assumed to be rain for the first 60 hours and then constantly dry at 5^oC with 50% Rh for another 504 hours. The indoor temperature of this building is maintained at 20^oC and the outdoor temperature is assumed to be constant at 5^oC and 50% Rh. In addition, the wind speed over the roof is presumed to be constant at 0.5 m/s. The thermal conduction is calculated with three roof types and two substrate depths; a

comparison of the energy saving and thermal insulation thickness reduction is made in a range of different conditions, as shown in the following list.

- Scenario 1: Non-domestic inverted roof
    - 162.5 mm deep green roof substrate on the top
        a) green roof substrate is completely dry throughout
        b) green roof substrate is completely saturated throughout
        c) green roof substrate moisture content varies over time according to the simulation
    - 300 mm deep green roof substrate on the top
        a) green roof substrate is completely dry throughout
        b) green roof substrate is completely saturated throughout
        c) green roof substrate moisture content varies over time according to the simulation
- Scenario 2: Domestic warm roof
    - 162.5 mm deep green roof substrate on the top
        a) green roof substrate is completely dry throughout
        b) green roof substrate is completely saturated throughout
        c) green roof substrate moisture content varies over time according to the simulation
    - 300 mm deep green roof substrate on the top
        a) green roof substrate is completely dry throughout
        b) green roof substrate is completely saturated throughout
        c) green roof substrate moisture content varies over time according to the simulation

- Scenario 3: Non-domestic metal decking
    - 162.5 mm deep green roof substrate on the top
        a) green roof substrate is completely dry throughout
        b) green roof substrate is completely saturated throughout
        c) green roof substrate moisture content varies over time according to the simulation
    - 300 mm deep green roof substrate on the top
        a) green roof substrate is completely dry throughout
        b) green roof substrate is completely saturated throughout
        c) green roof substrate moisture content varies over time according to the simulation

Detailed calculations for each scenario are presented in appendix B. The following section will describe the important findings.

7.2.1 Sensitivity of reference cases

Firstly, three reference cases with no green roof on them need to be verified before progress to the comparison after a green roof is retrofitted. The total heat flow from the building and the percentage of heat flow shared by the roof in three different scenarios is presented in table 7.2.

Table 7.2 Total heat loss and percentage of heat loss through the roof compared in three scenarios

Scenario	Total Q (kWh)	Q from roof (percentage)
1	575.54	14.1
2	576.00	14.2
3	575.47	14.1

From table 7.2, total heat loss in each scenario is around 575.50-576.00 kWh, and the roof shares approximately 14.1-14.2% from the total heat loss. This statement confirms that the reference cases for each scenario are similar. As a result, these reference case scenarios are a good model for the comparison.

7.2.2 Energy saving from green roof

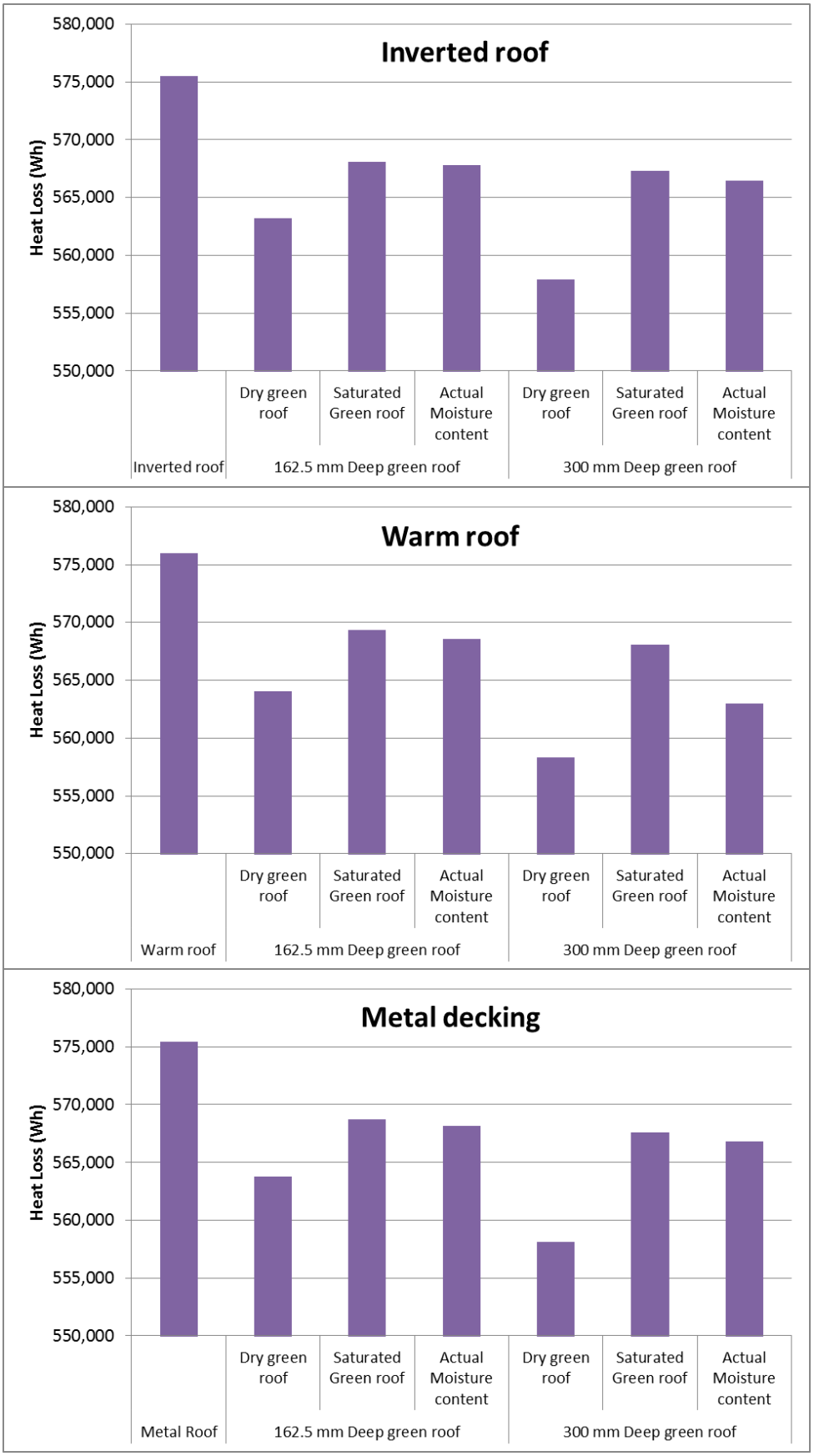

Figure 7.4 Comparison of heat loss of three scenarios with different green roof depths

Figure 7.4 presents the total heat loss from the building (including walls, windows, floor, and roof), in which three scenarios mentioned earlier are compared. As mentioned in the section 7.2.1, the total heat loss of three reference cases is approximately 575 kWh over 564 hours. However, after a green roof is retrofitted, the total heat loss is reduced depending on the green roof substrate moisture condition.

For the dry green roof substrate, the heat loss reduction is approximately 2.03-2.14% and 3.01-3.07% of the total heat loss for the 165.5 mm and 300 mm thick substrate respectively. For the saturated green roof substrate, the heat loss reduction is approximately 1.16-1.29% and 1.37-1.43% of the total heat loss for the 165.5 mm and 300 mm thick substrate respectively. For the simulated moisture content green roof substrate, the heat loss reduction is approximately 1.27-1.34% and 1.50-2.26% of the total heat loss for the 165.5 mm and 300 mm thick substrate respectively.

The heat loss reduction follows the same trend in every scenario, with the highest reduction when the green roof substrate is dry and the lowest reduction with the substrate is saturated. When the substrate moisture content is retrieved from the simulation is the reduction in-between the dry and saturated condition but closer to the saturated condition. This statement applies to both thicknesses of substrate.

7.2.3 Effect of wetting and drying to the heat flow

The moisture content of the green roof substrate influences the heat loss and the hourly heat loss profile is shown in figure 7.5. The profile in figure 7.5 is retrieved from the 162.5 mm thick substrate on the inverted roof, of which the moisture condition was simulated from the weather condition mentioned in section 7.2.

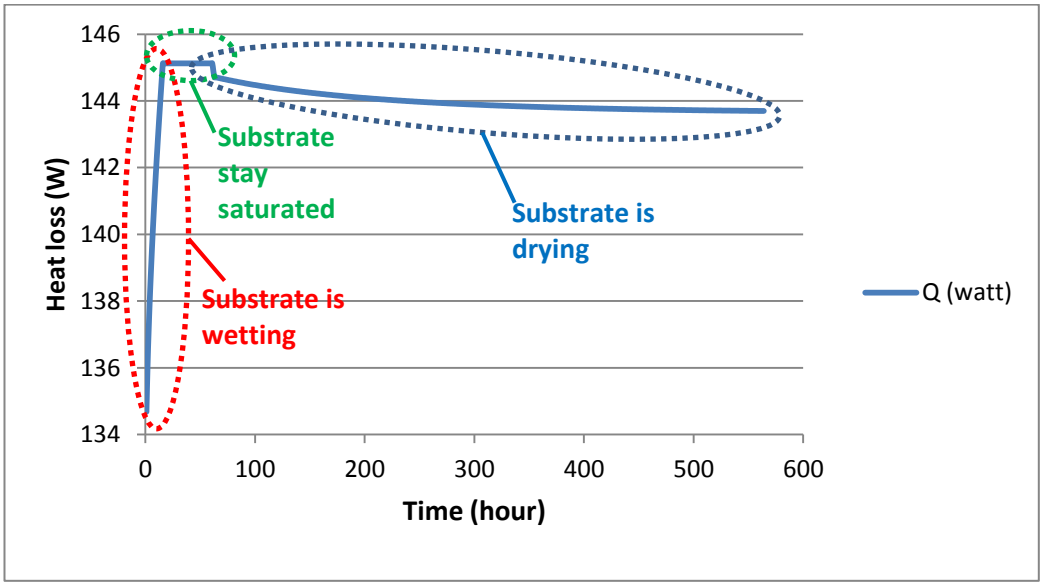

Figure 7.5 Green roof substrate moisture condition and the heat loss

Figure 7.5 shows that in the early hours, substrate starts dry but the rain starts and continues for 60 hours. The substrate absorbs water into its layers and the whole layer is saturated after 15 hours of precipitation. In this absorption process, the effective thermal resistance of substrate is reduced rapidly as water penetrates into the substrate and reaches a minimum when the substrate is saturated. As a result, the hourly heat loss is increased because the substrate is more conductive to the heat, reaching the maximum at 15^{th} hour where it stays until the rain stops (60^{th} hour).

After the rain has stopped, the substrate is drying with mentioned conditions. The effective thermal resistance of the green roof substrate is suddenly increased at the first 3 hour of drying stage because it is in the first stage evaporation. For this reason, there is a sudden drop in the hourly heat loss in the early stage of drying. However, the substrate's effective resistance is slowly increased in the second stage of evaporation; as a result, the hourly heat loss is slowly reduced.

7.2.4 Substitution for thermal insulation

It is clear that the green roof can reduce some amount of heat loss from the building as presented in section 7.2.2. However, those implications were based on the roof that is insulated according to the regulation requirement (U-value = 0.2 W/m^2K) and the green roof was sitting on it, conferring additional thermal resistance. Therefore, the U-value after installing the green roof is much lower than the recommended value.

On the other hand, the roof's U-value does not need to be that low in the design practice. The green roof can substitute for some thermal insulation by reducing its thickness (as shown in table 7.3) and still meet the regulation requirement.

Table 7.3 shows the possible reduction in thermal insulation thickness with the different green roof condition. The dry green roof shows the best result more than twice from the saturated substrate. The saturated substrate can replace approximately 11-17 mm of insulation for 162.5 mm thick substrate, and 13.5-20 mm for 300 mm thick substrate. The thickness reduction calculated from the simulated substrate moisture content is very close to the saturated substrate value but 1-2 mm higher.

Furthermore, the effect of green roof substitution has the most influence on the non-domestic inverted roof, which can substitute thermal insulation thickness by 31 mm in the dry substrate, 17 mm in the saturated substrate, and 18.5 mm in the simulated moisture content substrate for the 162.5 mm thick green roof substrate. This large reduction is caused from the high thermal insulation in the reference case (160 mm). However, the results for the warm roof and the metal decking are similar since the original insulation thickness is close (111 and 117 mm).

Table 7.3 Reduction in thermal insulation thickness possible by installation of a green roof in different conditions

Inverted roof							
Condition	No Green roof	162.5 mm Deep green roof			300 mm Deep green roof		
		Dry green roof	Saturated Green roof	From simulation	Dry green roof	Saturated Green roof	From simulation
Insulation thickness (mm)	160	129	143	141.5	111	140	138
Insulation thickness reduction(mm)	-	31	17	18.5	49	20	22
Warm roof							
Condition	No Green roof	162.5 mm Deep green roof			300 mm Deep green roof		
		Dry green roof	Saturated Green roof	From simulation	Dry green roof	Saturated Green roof	From simulation
Insulation thickness (mm)	111	90	100	99	77	97.5	96.1
Insulation thickness reduction(mm)	-	21	11	12	34	13.5	14.9
Metal decking							
Condition	No Green roof	162.5 mm Deep green roof			300 mm Deep green roof		
		Dry green roof	Saturated Green roof	From simulation	Dry green roof	Saturated Green roof	From simulation
Insulation thickness (mm)	117	95.5	105	104.6	82.5	103	102
Insulation thickness reduction(mm)	-	21.5	12	12.4	34.5	14	15

7.2.5 Summary

The implication of the results summarised here and presented in detail in Appendix A are as follows:

The moisture condition of a green roof has a small but measurable effect on heat loss. As shown in section 7.2.2 and 7.2.3, the green roof can either reduce total heat loss from the building or substitute the thermal insulation thickness to maintain the same total heat loss. This work shows that it is possible to simulate the actual moisture content in the substrate layer with the effects of absorption and evaporation. Therefore, the situation that the green roof substrate is completely dry and completely saturated can be compared with this simulated actual behaviour.

From the comparison with the modelled moisture condition, the effect of moisture condition in a green roof substrate can be summarized as follows.

- Assuming the green roof substrate is dry will overestimate the reduction in heat loss and possible insulation thickness reduction when compared with the actual modelled moisture condition.

- Assuming the green roof substrate is saturated will underestimate the reduction in heat loss and possible insulation thickness reduction when compared with the actual modelled moisture condition.

Comparing the simulated and saturated substrates, the differences in energy saving and thermal insulation thickness reduction are small. However, it is possible to measure this actual moisture content and the small difference can be enlarged with the thicker substrate and when the building is simulated over a long life span. Therefore, the designer must decide if the additional work involved in modelling the actual moisture content is worthwhile if it only achieves such small effects. If it is unnecessary to simulate this moisture condition (e.g. for a small and short life span building), then the recommendation is to assume that the green roof substrate is saturated as this gives results that are very close to the simulated result.

Finally, this research focused on the drying and evaporation of the substrate, and has not modelled the effect of weather on the moisture content of the green roof substrate. It merely provides a simulation method which can evaluate its consequences. These

depend on the intensity and duration of rainfall that affect the absorption process and the factors such as wind speed, temperature and humidity that affect the drying process. This effect is clearly location dependent and must be simulated with defined weather conditions.

7.3 Discussion of findings

This findings discussion section will introduce the limitations of this research; it will also mention the sources of error, which come from the experiment and the theoretical assumptions. Finally, this section confirms whether the assumptions made in the early stages of this research are validated or not.

7.3.1 Limitations of this work

Limitations of this research are divided into four parts, resulting from experimental limitations.

One-dimensional moisture transfer

The green roof moisture content simulation is a one-dimensional finite difference simulation (chapter 5), which means there is no moisture transfer in the horizontal axis of green roof substrate (x and z axes in figure 7.6). The moisture in the substrate will exchange vertically (y-axis in figure 7.6). In the real green roof, liquid is transferred in one direction because the rain falls evenly over the roof and therefore the top surface becomes saturated evenly. This mechanism produces non-transfer in x and z directions because moisture content in these directions is equal.

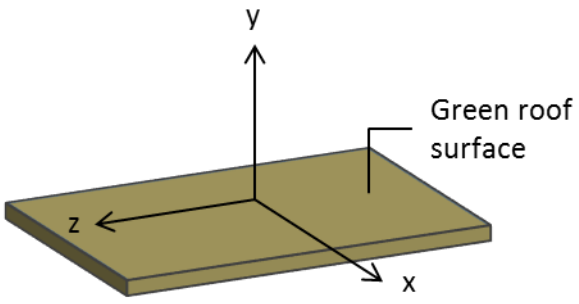

Figure 7.6 Direction of green roof surface

Furthermore, in the real building, the roof extends widely in a horizontal direction. The horizontal variation in moisture content is therefore negligible compared with changes in the vertical moisture transfer, and one-dimensional simulation is acceptable.

Water loss through the surface only

The water that evaporates from the green roof substrate is assumed to move to the top surface only or only in an upward direction. This limitation was made due to the experimental setup, in which the green roof substrate specimen was sealed at the bottom to prevent moisture loss. If liquid is allowed to leave both the top and bottom of the substrate, the evaporation rate cannot be determined.

In addition, with a green roof in a practical situation, the liquid is held by capillary force. This force inside the substrate is normally greater than the gravitational force acting upon it, due to the small pore spaces in the substrate. Furthermore, the bottom of the substrate in real conditions is attached to the drainage layer that is full of liquid or saturated water vapour. As a result, the moisture loss through the bottom layer can be neglected.

No change in compaction level in simulation

The green roof substrate is a dynamic porous material, whose conditions change due to the surrounding environment. Especially, the compaction level of green roof substrate can vary from 150 kPa to 800 kPa. In a newly established green roof, the compaction can be increased by the effect of liquid that pulls particles close together. In addition, the effect from foot traffic on the green roof can increase the compaction level in some of the more frequently trodden areas.

In the evaporation experiment, it can be seen that in some layers of substrate, the compaction can be increased from 0 kPa to 150 kPa (0 kPa green roof substrate, section 5.5.1). This change can be tracked by removing the sample's layer from the container. The moisture content measured by the oven drying method can be compared with the measured moisture content associated with the thermal conductivity. As a result, the compaction level of the substrate can be determined.

However, the created simulation cannot track this compaction change and assumes the compaction level is constant throughout the simulation period, which might affect the

newly established green roof substrate because the compaction can change due to the causes mentioned.

No moisture loss due to solar radiation and plant respiration

In the real green roof evaporation, the moisture content will be lost due to the effects of wind, temperature, solar radiation, and plant respiration; however, the two latter terms have been ignored in this simulation.

The reason to ignore both solar radiation and plant respiration is the limitation of an environmental chamber. The chamber cannot simulate solar radiation and there is no solar radiation sensor inside. Furthermore, the green roof plant cannot grow in the chamber since it needs to be stored in the chamber for three weeks without sunlight and irrigation. As a result, the evaporation rate that includes the solar radiation and the plant respiration cannot be included in this simulation, and the simulated heat loss is likely to be lower because the substrate will dry more quickly and its thermal resistance will be higher.

7.3.2 Sources of error

The main errors in this research come from the equipment. Sources of error are separated into three parts: i) the errors from thermal conductivity and moisture content measurement, ii) errors from weighing equipment, and iii) errors caused by the environmental chamber. These errors are individually explained.

Thermal conductivity and moisture content error

The error caused from the thermal conductivity and moisture content relationship has already been described in chapter 3. The fitted linear equation of green roof substrates in four different compaction levels (0, 150, 300, and 450 kPa) is positioned within a 95% prediction interval (see figures 3.22, 3.24, 3.26, 3.28).

As a result, this error factors in the green roof substrate evaporation test, which causes an error in moisture content calculation equivalent to ±2.5% mc. This error can be expanded when the moisture content is used in any evaporation rate calculations, which can be expanded from 10% to 40% in evaporation rates. This expansion results from the time factor that multiplies this error.

Weighing error

The error from the weighing process can affect the sorptivity measurement and values. The recommended scale for the sorptivity measurement is rated at five decimals of precision (Hall and Hoff, 2009) in order to be sufficiently sensitive to capture weight change over a one minute interval of water absorption.

In this research, the available scale only had the precision of three decimals, which does not achieve the above mentioned requirement. This can cause a minor error in sorptivity values of green roof substrates. However, points of measurement are extended to 60 minutes (measured at 1, 2, 5, 10, 20, 30, and 60 minutes). The last five points of measurement do not require the most sensitive scale because the weight of absorbed water is large enough to negate the need for this five decimal precision. As a result, this error can be ignored in the latter points of measurement; the results of the sorptivity values show a good coefficient of determination, which is almost 1 in every test.

In addition, the absorption from the filter layer that holds the green roof substrate at the bottom of the container is another source of error. In the early minutes of the sorptivity test, the dry filter layer also absorbs water into its pores, which raises the overall sample weight. Nevertheless, this error makes only a very small contribution due to the small amount of absorption involved, when compared with the overall weight of the sample.

Error from chamber condition

The error caused by the environmental chamber is a main error in the substrate evaporation test, which comes from fluctuations in the chamber itself. Fluctuations include the unstable temperature, relative humidity, and wind speed. Because of these fluctuations, the evaporation rate determination can be outside of the predicted value, which can be seen as a sudden drop or rise rather than the smooth exponential decay curve in the calculated evaporation rate graph.

These fluctuations seem to appear instantaneously because the chamber tries to adjust itself by tuning the temperature and humidity into the required setup conditions. This adjustment is around 3 out of 18 points of measurement, equivalent to 17% total measured points.

This error can be observed and recorded during the experiment, but sometimes it happens during out-of-hours working time. For this reason, any sudden rises and drops

from the exponential decay curve were removed from the evaporation rate determination.

7.4 Comparing this work with the published literature

The findings from this current work will be compared with previous works on green roof thermal simulation with a focus on result validation. Furthermore, proposed theories for simulation improvement (the Sharp Front theory and the porous medium evaporation principle) will be compared with previous works, involving other material than green roofing, in the context of validating the assumptions.

7.4.1 Assumption validation

Assumptions that were stated in the introduction chapter will be validated in this section; in particular the application of the Sharp Front theory in the green roof substrate and the porous medium evaporation principle in the green roof substrate.

Sharp Front theory in green roof substrate

The Sharp Front theory that was applied to porous construction materials such as concrete, limestone, or bricks, is used to explain the absorption behaviour of the green roof substrate. Because the substrate involves capillary absorption, as do the construction materials named in the previous sentence, this theory is assumed to apply to a green roof.

From the sorptivity measurement in chapter 4, points of absorbed water distance are fitted with the linear line and the best fit linear equation is determined, as shown in figure 7.7. From figure 7.7, the coefficient of determination (R^2) is very close to 1, which represents a near perfect fit linear line. Furthermore, when compared with the measurement of the clay brick by Hall and Hoff (2009), as presented in figure 7.8, the water increment against the square root of time ($min^{1/2}$) is increased with the linear relationship. These two figures confirm that the green roof has absorption behaviour and has a single value of a sorptivity similar to the other construction material. For this reason, the application of the Sharp Front theory with the green roof substrate can be validated.

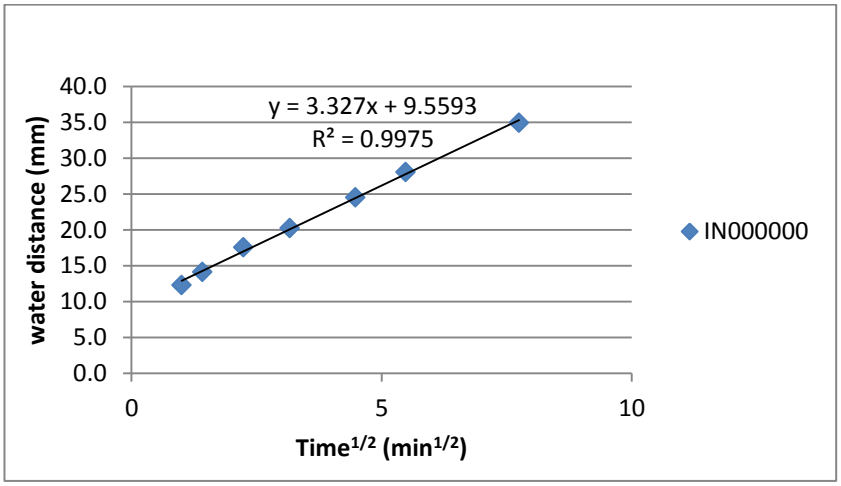

Figure 7.7 The sorptivity measurement of dry and uncompact green roof substrate

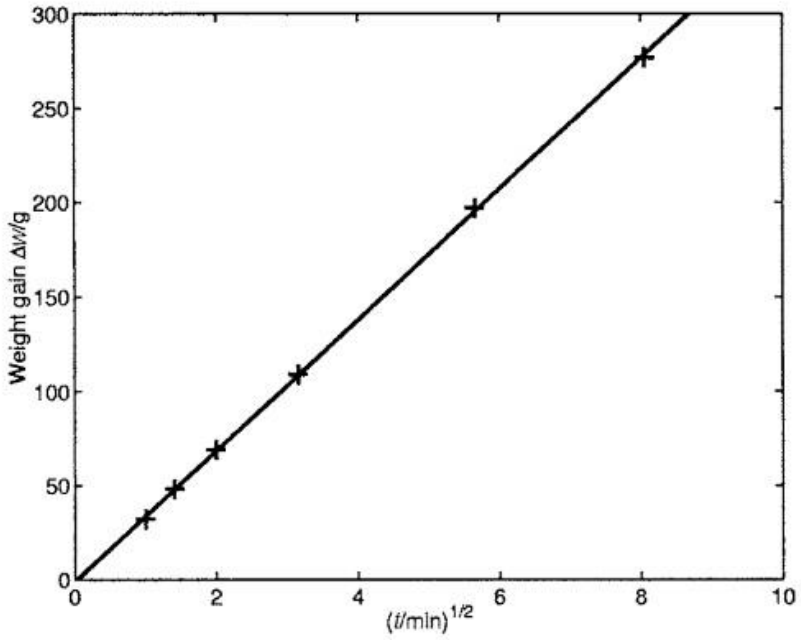

Figure 7.8 The sorptivity measurement of whole clay brick (Hall and Hoff, 2009)

Another assumption relating to green roof substrate behaviour is the effect of compaction levels, which are assumed to affect the roof's sorptivity value. From the experiment on substrate, with various compaction levels, the compaction can affect the absorption by decreasing the sorptivity value when the compaction is increased. This reduction is demonstrated in figure 7.9.

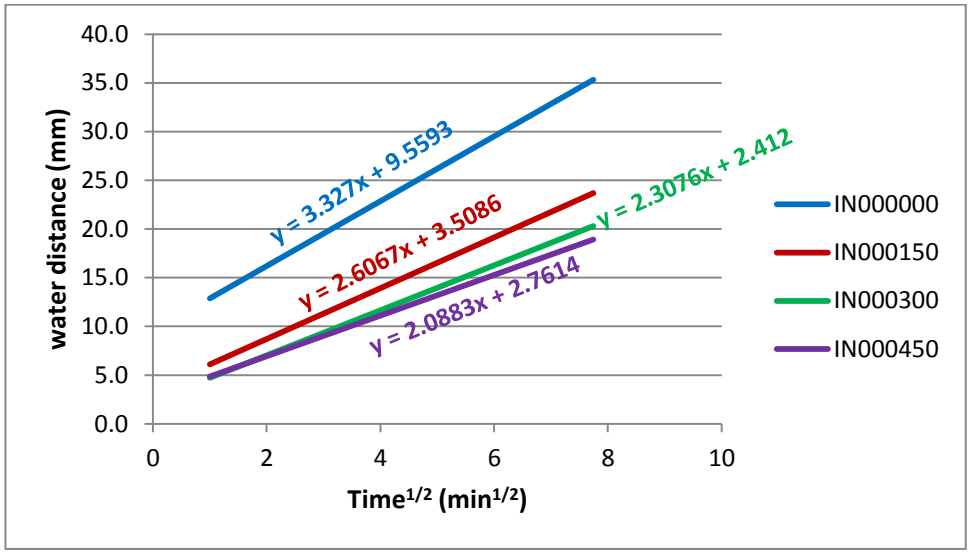

Figure 7.9 The effect of compaction on the sorptivity value of dry green roof substrates

Table 7.4 presents the sorptivity of common construction materials, where both their density and porosity are shown.

Table 7.4 The sorptivity of some construction materials (Hall and Hoff, 2009)

Material	**Density (kg/m^3)**	**Porosity**	**Sorptivity (mm/min$^{1/2}$)**
Clay brick			
Pressed semi-dry	1727	0.357	1.32
Hand-moulded facing	1784	0.334	2.21
Extruded facing	1567	0.461	2.53
Engineering	2210	0.065	0.09
Building stone			
Brauvilliers limestone	1930	0.25	0.60
Cleris limestone	1890	0.29	1.49
Jaumont limestone	2010	0.21	0.45
Lepine limestone	2080	0.239	1.00
Lepine limestone	2010	0.245	0.99
Portland limestone	2340	0.19	0.30
Richemont limestone	1900	0.26	0.90
St. Maximin fine	1590	0.39	4.60
Baumberger sandstone	1980	0.23	0.34
Kerridge sandstone	-	-	0.03
Obernkirkchner sandstone	2150	0.14	0.36
Ruthener sandstone	1950	0.24	2.33
Gypsum/sand plaster			
1 water:0.45 plaster	1390	0.42	1.62
1 water:0.45 plaster	1480	0.39	1.44
1 water:0.45 plaster	1590	0.35	1.31
1 water:0.40 plaster	1490	0.37	0.83

Figure 7.9 indicates that the green roof substrate's sorptivity is at maximum value when there is no compaction applied. However, this value decreases when compaction is added. This increment in sorptivity due to compaction corresponds to the construction material. For example, the sand plaster in table 7.4 (1 water: 0.45 plaster) that has density and porosity equal to 1390 kg/m^3 and 0.42 respectively, has sorptivity equal to 1.62 $mm/min^{1/2}$. On the other hand, when compaction increased, as in the sand plaster that has density and porosity equal to 1590 kg/m^3 and 0.35 respectively (compaction increases density and reduces porosity), the sorptivity is reduced to 1.31 $mm/min^{1/2}$. These data confirm that the sorptivity level is reduced as compaction is increased.

As a consequence, both the assumptions cited above are validated by the stated reasons and proofs from the experiment.

Two stages of evaporation rate

From Platten's (1985) thesis, the evaporation has three stages, which are the evaporation rate due to the surrounding condition (stage 1), the evaporation rate controlled by the internal moisture flow (stage 2), and the evaporation rate caused from the moisture vapour (stage 3). His thesis studied the evaporation from common construction materials (concrete, stone, and limestone). However, the theory from his thesis might be assumed to apply to the green roof substrate, because it has a fine porous structure similar to several construction materials.

From the experiment on evaporation of green roof substrate, as described in chapter 5, the substrate showed signs of two distinct stages of evaporation rates. However, the value of the stage 1 evaporation rate is not equal to the calculated rate from wind speed, temperature, and relative humidity data. The measured stage 1 evaporation is within a 40% error range (the measure value is 1.78×10^{-4} m/s to 2.02×10^{-4} m/s and the calculated value is 1.40×10^{-4} m/s), which is mentioned in the 'source of error' section. Furthermore, the duration of stage 1 evaporation of the green roof substrate is significantly shorter than the construction material; the substrate involved 3 hours but the duration was 9 hours for the limestone construction material. This difference in duration might come from the loosely packed particles in the top surface and the low compaction between the green roof's layers (compared with limestone) that allow liquid to leave the substrate's surface more quickly.

For stage 2 evaporation, the evaporation rate in the green roof substrate is significantly lower than the common construction material. In the construction material, the stage 2 evaporation rate is the decay rate from stage 1. On the other hand, in the green roof substrate, the stage 2 evaporation rate is the decay rate from the stage 1 evaporation rate multiplied by a constant (around 0.02 to 0.05).

The substantial difference in this stage 2 evaporation rate, between the green roof substrate and the other porous building material, may come from the discontinuous moisture flow between the top layer and the underneath layer, due to the low compaction, and the large pore spaces. In the porous construction materials, such as bricks or stones, the compaction levels of these materials are much higher than the level in the green roof substrate, because it was compacted by natural process (consolidation) and physical process (fired brick). This compaction process makes the whole layer of the porous material become homogenous and packs pore spaces closer together. As a result the water movement between layers continues.

On the other hand, in the green roof substrate, the discontinuity between layers disrupts the moisture supply to the top layer (from layer 5 to layer 6). This problem creates the sudden drop in evaporation rate after the top layer passed the stage 1 evaporation phase. As a result, the stage 2 evaporation rate of the green roof substrate is much lower than in stage 1.

From this discontinuity in the top layer of the green roof substrate, the moisture flow rate to the top layer (Q_5) needs to be introduced (see section 5.6). This flow rate stabilises the moisture content prediction in those substrate layers located below the top layer.

For the reasons mentioned, the evaporation rate of the green roof substrate might present a much different range from the other porous construction materials. However, the substrate has the same distinct features, particularly two stages of the evaporation rate, with the rate being reduced through an exponential decay function. As a consequence, the use of a theory of porous medium evaporation (Platten, 1985) with a green roof substrate is validated.

7.4.2 Result validation

The results from the experiments and simulations, as presented in previous chapters, will be compared with green roof investigations from other researchers.

Moisture content profile in evaporation process

In the evaporation process, the moisture content profile is different from the profile in the absorption process. The profile will have a greater drop in moisture content at the top of the evaporative surface than in the bottom because conditions are dryer at the top. Platten (1985) observed the moisture content profile of porous building material, such as a common brick bar, over a duration of 51 hours (see figure 7.10).

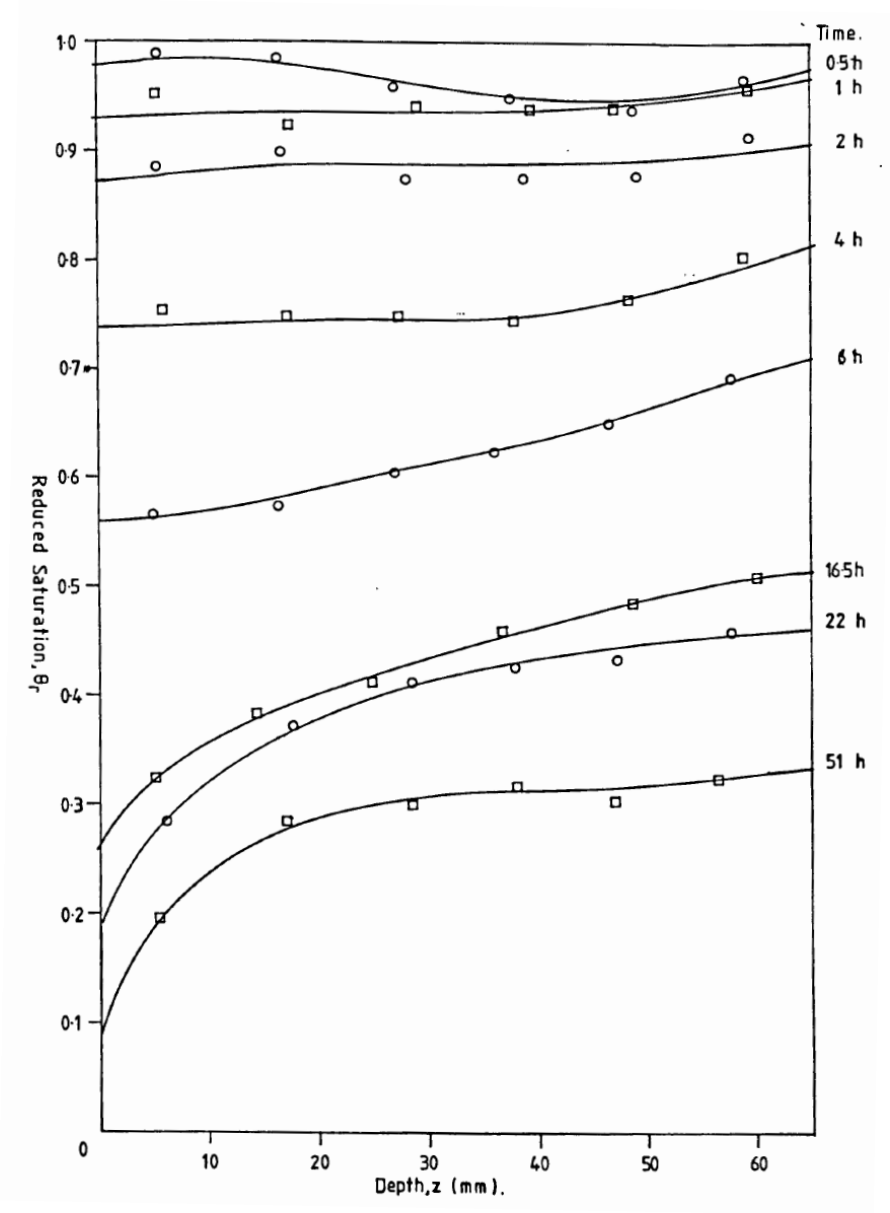

Figure 7.10 The moisture content profile of a 10 x 10 x 65 mm common brick bar (Platten, 1985)

Figure 7.10 indicates the moisture content is reduced linearly in the first four hours, which can be seen by the constant drop of moisture content in each position. Nevertheless, there is a significant drop in moisture content at the top layer of the brick's surface after 16.5 hours. This profile continues over 51 hours.

This moisture content profile is similar to the green roof substrate evaporation behaviour, which is demonstrated in figure 7.11.

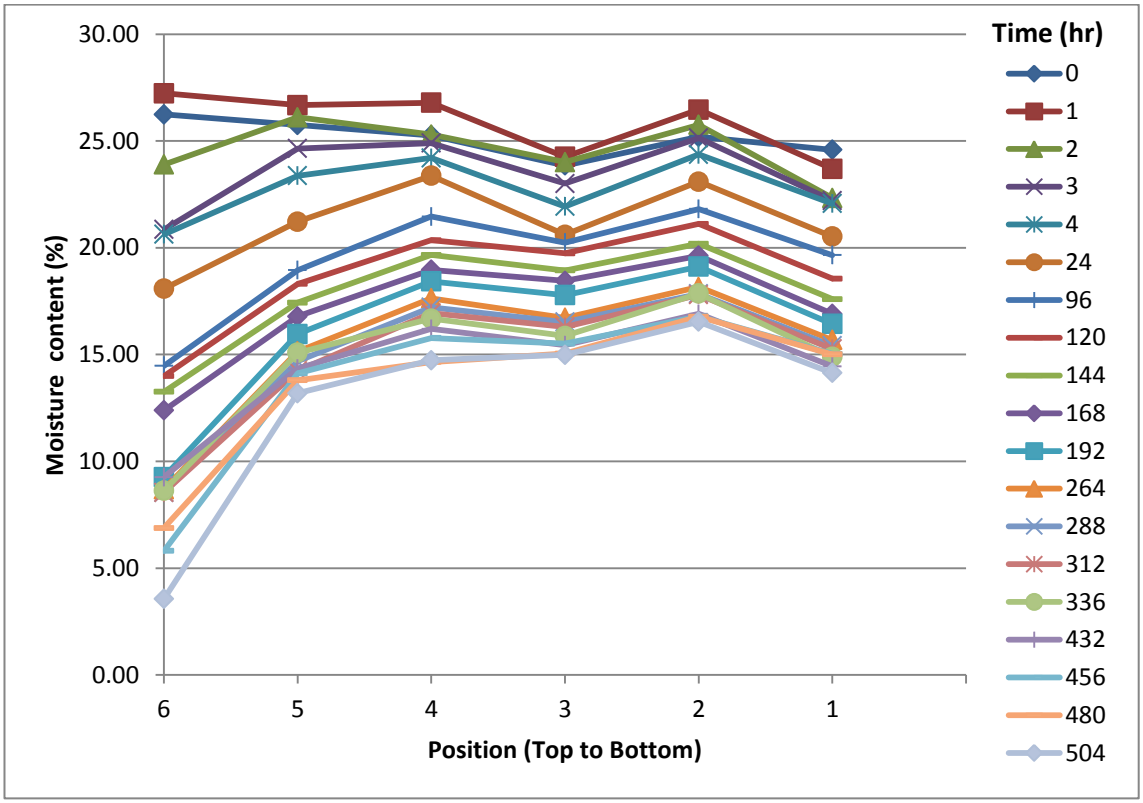

Figure 7.11 The moisture content profile of 300kPa green roof substrate

From figure 7.11 it can be seen the substrate moisture content profile is dropping linearly, almost as if it were another porous material, during the first three hours. However, after the fifth hour, the substrate shows a significant reduction at the top surface (position 6), while there are small reductions in the other layers. This profile continues until the top surface reaches a dry condition at the 504th hour.

These two figures and two materials share common evaporation behaviour, thereby allowing the conclusion that the green roof substrate moisture content profile corresponds to the evaporative moisture content profile in porous materials.

Thermal property of green roof substrate

In this study, the important thermal property that affects the overall green roof performance is the thermal conductivity of the substrate. The thermal conductivity is observed by varying the compaction level and moisture content of the green roof substrate, as described in chapter 3 of this thesis.

Firstly, the work from Sailor *et al*. (2008) observed eight 'eco-roof' soils in western USA and found that the thermal conductivity was increased as a function of fractional moisture saturation. The evidence is presented in figure 7.12.

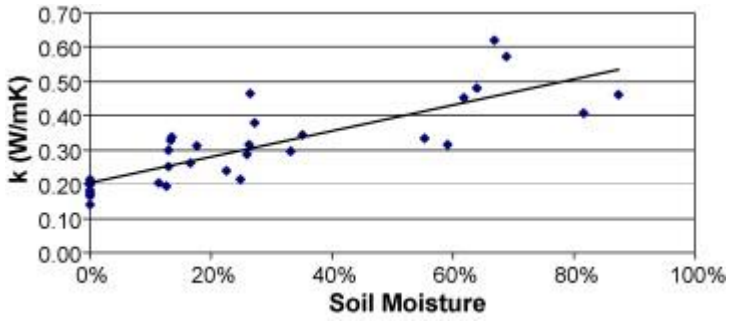

Figure 7.12 Soil thermal conductivity as a function of fractional moisture saturation level for all eight soil samples tested (Sailor *et al*., 2008)

Subsequently, Sailor and Hagos (2011) investigated the thermal conductivity of the green roof substrate. However, this time, they included the effect of compaction level observed in the real green roof. The results are shown in figure 7.13.

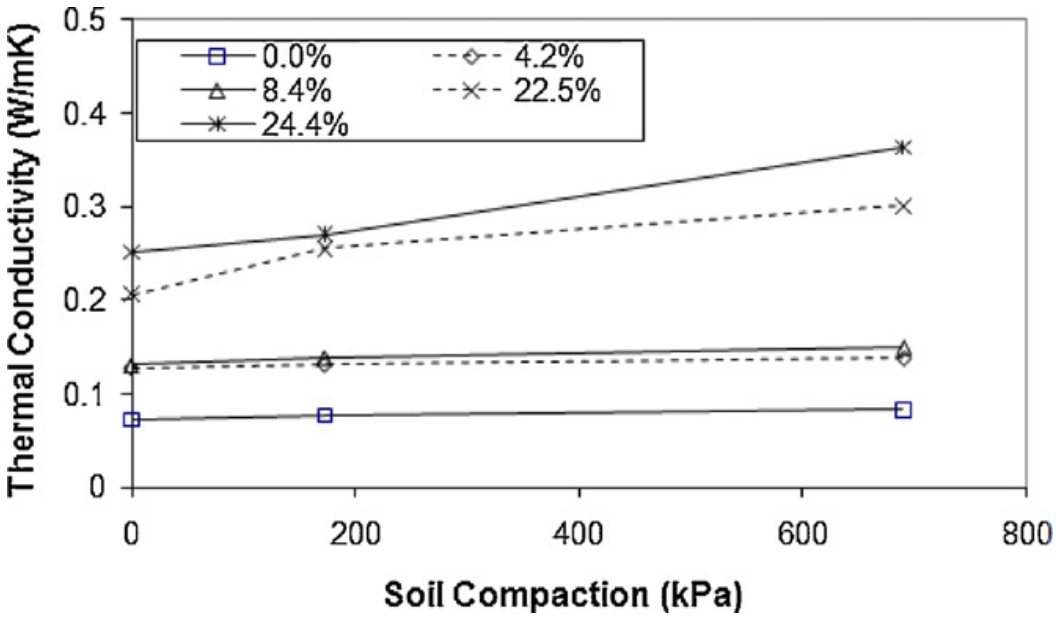

Figure 7.13 Thermal conductivity of green roof soil as a function of compaction for moisture levels ranging from 0.0 to 24.4% by volume (Sailor and Hagos, 2011)

As illustrated in figure 7.13, the researchers concluded that compaction affects the green roof substrate by increasing its thermal conductivity. In addition, the compaction significantly affects substrate with a high moisture level; this outcome can be seen by the high slope in substrate samples that have moisture levels of more than 20%.

In this study, the green roof substrate thermal conductivity was also observed with different ranges of compaction and moisture content. The result presentation is informed by figure 7.13, and the experimented results in this study are presented in figure 7.14.

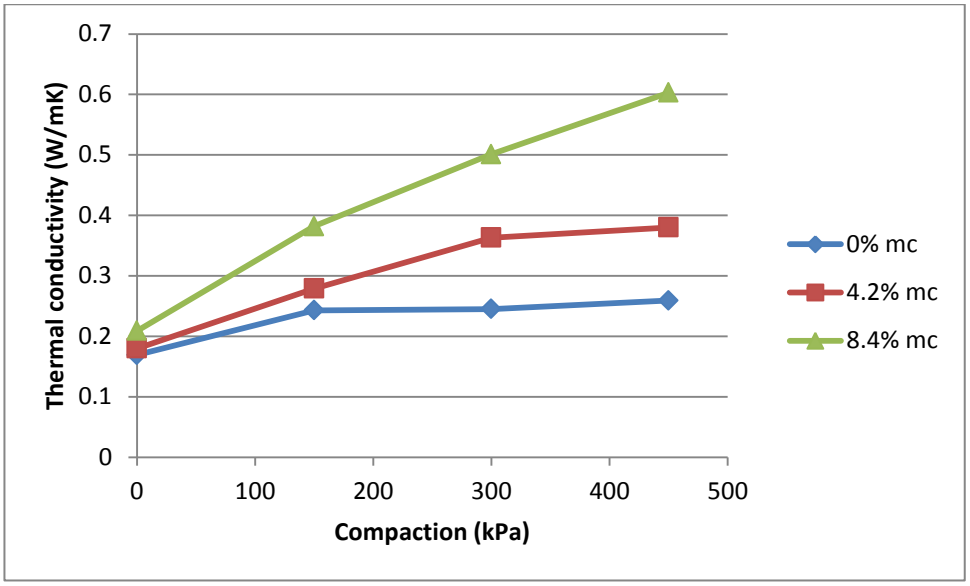

Figure 7.14 Thermal conductivity of green roof substrate as a function of compaction for moisture content ranging from 0.0 to 8.4% by mass

From figure 7.14, the substrate used in this study shares the same behaviour with the green roof substrate data offered by Sailor and Hagos (2011). Compaction of the substrate also increases the thermal conductivity and the effect is more pronounced at higher moisture contents. However, the thermal conductivity range in figure 7.14 (0.2 to 0.6 W/mK) is slightly higher than that in figure 7.13 (0.08 to 0.55 W/mK). This difference might come from the low percentage of organic matter in the substrate used in this experiment compared to that of Sailor and Hagos (2011). As a result, the low level of organic matter increased the thermal conductivity of the green roof substrate, based on the premise that the higher the percentage of organic matter, the lower the substrate's thermal conductivity.

7.5 Conclusion

The green roof simulation was applied to the case study building with a range of three different roof structures: i) the non-domestic inverted roof, ii) the domestic warm roof, and iii) the metal decking. Two green roof substrate thicknesses of 162.5 mm and 300 mm were studied in this context, which represented the semi-intensive and intensive green roofs. Furthermore, these green roofs were simulated with three moisture

conditions, which were: i) the green in a totally dry condition, ii) the green roof in a totally saturated condition, and iii) the green roof with moisture content obtained from the simulation. The green roof substrate with moisture content obtained from the simulation produced the highest energy saving and insulation thickness reduction, when compared with the green roof that was simulated with a totally saturated substrate condition. The energy saving was by approximately 1% and the insulation thickness reduction was 2 mm.

This chapter has also discussed the limitations of this work and the possible sources of error. In addition, this research was compared to other literature informed by two validations: assumptions and results. The next chapter will summarise the work and findings of this thesis, as well as offering suggestions for future research initiatives.

Chapter 8: Conclusion

8.1 Introduction

This chapter will conclude this thesis on green roof substrate thermal simulation, from the start of identifying the research gaps to the development of theories, which led to the research's originality. The aims and objectives of this study, which were defined in section 1.2, will be readdressed and discussed. Finally, recommendations for future studies will be suggested.

8.2 The research's originality

This research aims to improve the (understanding of the) thermal simulation of a green roof system by focusing on the substrate layer, as this layer plays an important role in the thermal insulation of the roof since it mostly dominates the thickness of a green roof system. However, previous work in green roof simulations mainly focused on the foliage layer, where the substrate layer was considered as a single layer and the moisture in this layer was treated as a single layer. The liquid movement within this layer had been ignored; discounting in practical terms that liquid (water) requires some time to move from point to point (time dependent). This problem was not considered in previous work on green roof thermal simulation.

This current research tries to fill this knowledge gap by studying the moisture changes in the substrate layer. Two mechanisms of liquid movement have been considered in this research: i) the absorption of liquid into the substrate layer and ii) the phase during which liquid leaves the substrate layer (evaporation). For the absorption mechanism, this research adapted the 'Sharp Front theory' in porous medium, from the work of Hall and Hoff (2009), which can predict the thickness of a saturated layer of the substrate over a time change. For an understanding of the evaporation mechanism, this study uses the 'evaporation of porous medium theory' from Platten (1985) to predict the moisture content change in each layer, over time.

8.3 Main findings in substrate properties

Referring to the objectives (section 1.2.1), the substrate has a crucial role in the issue of heat transfer, so some properties of the green roof substrate need to be clarified and related together. The thermal property is affected by some external factors, such as

moisture content, compaction level and porosity. Therefore, this research has tried to unite these properties in order to understand their influences on the thermal properties of a green roof.

Similar to other porous materials, moisture content and compaction are related parameters. Therefore, this research measures these data because they are the sensitive parameters, which can directly affect the green roof's conduction heat transfer.

The moisture content in this study uses the percentage of liquid by mass, and the compaction level is measured by the penetration resistance encountered by a needle probe, measured in kilo Pascal (kPa) (sections 3.2 and 3.3). Varying the number of blows applied to the sample by the compactor produced different levels of penetration resistance.

The results (section 3.3) show that the more moisture content in the substrate the easier it is to achieve the value required of penetration resistance. This relationship enabled the green roof substrate of the desired properties to be produced.

The other parameter that affects the wetting process in the green roof substrate is the porosity; a value which depends on both the substrate's compaction level and moisture content. The result (section 3.4.2) show that porosity decreases significantly with compaction but is relatively unaffected by moisture content. Therefore, the porosity information was used in the absorption calculation by the Sharp Front theory with the sorptivity equation (equation 4.22).

Furthermore, the influence of moisture content and compaction level on the roof's thermal conductivity was established using a needle type soil thermal conductivity meter (section 3.6.1). The results show that the thermal conductivity of the green roof substrate is increased, through an exponential function, when the moisture content is increased. Additionally, the thermal conductivity can be further increased by increasing the degree of compaction. Prediction equations were developed and applied in the subsequent analysis.

8.4 Main finding in absorption

Referring to the objectives (section 1.2.2), the absorption process, this study adapted the Sharp Front theory from Hall and Hoff (2009) in order to predict the liquid penetration distance from the absorption surface into the green roof substrate over time. The key parameter is sorptivity (S) and the investigation relates it to two parameters: i) moisture content and ii) compaction level. Section 4.3 shows that sorptivity has a maximum value when the substrate is dry and this value is reduced by the increment of moisture content. In addition, section 4.3 also confirms that sorptivity is decreased by increasing compaction.

Finally, a model was developed (section 4.5) to connect the Sharp Front theory with the conduction heat transfer; as a result, the time dependent conduction heat flux change can be calculated during the absorption process. The model separates the substrate into two layers: the wetted part and the dry part, which have different thermal conductivities. From this variation of wetted layer thickness, the heat flux in each time step was determined (section 4.5).

The results show that substrate samples with different moisture content and degree of compaction start with different heat flux, but when they reach the saturated condition substrates that have the same compaction levels will also have the same heat flux. However, time required for samples with the same compaction levels to reach the saturation heat flux depends on the original moisture content; the higher moisture content sample will reach its saturation point more slowly than the sample with the lower moisture content.

8.5 Main finding in evaporation

Referring to the objectives (section 1.2.3), after the green roof substrate absorbs water until it reaches saturation, it will dry out (desorb) provided there are no irrigation or precipitation events. The evaporation mechanism of the green roof substrate was treated by using the porous medium drying theory, investigated by Platten (1985) and applicable to porous construction materials.

From an investigation of one-directional evaporation from the green roof substrate surface in a controlled environment, the moisture content of each layer and hence the evaporation rate can be determined. The results confirmed the two-stage evaporation

process: a constant rate in stage 1 and an exponentially decreasing rate in stage 2, which is restricted by water migration below.

Having divided the green roof substrate into 6 layers, the results (section 5.5) correspond to those of other porous construction materials, which were previously investigated by Platten (1985).

Finally, a model linking evaporation and the conduction heat transfer was developed (section 5.7) using the thermal conductivity and moisture content relationship that was observed and reported in chapter 3. As a result, the time-dependent effective thermal resistance of the whole substrate can be obtained, as can the conduction heat flux. The results show a steep rise in the first three hours followed by a much lower rate of increase. The overall variation in thermal resistance and conduction heat flux in a green roof was modelled in chapter 6 and discussed in chapter 7.

Applying the simulation method to a model green roof (chapter 7) shows that the moisture condition of a green roof substrate has a small but measurable effect on the heat loss from a building. Having the ability to simulate the actual moisture content in the substrate as it changes with the weather enables a more realistic estimate of heat loss to be made. Existing thermal simulations assume the substrate is either constantly dry or constantly saturated compared to the absence of a green roof, assuming the substrate is dry will overestimate the improvement in thermal performance, whereas assuming it is saturated will underestimate the improvement. The simulation method developed have improved the accuracy of the heat loss estimate but if a designer considers the extra work involved to be unjustified then it is recommended that the substrate is assumed to be saturated. This will give a conservative estimate of heat loss, which is still close to the simulation result.

8.6 Recommendation for future study

Taking everything into account, this study explored the problem evident in previous green roof substrate research models and answered this problem by proposing some theories. However, there are other problems, which have already been mentioned in the literature review chapter. These problems, which have not as yet been addressed, are the heat conduction in the drainage layer and the heat convection from the drainage water under the green roof.

These problems are outside the scope of the work described in this thesis, but a possible approach to them will be presented in this section.

8.6.1 Conduction in a drainage layer

Unlike a substrate layer, a drainage layer (including both the gravel type and profiled plastic type) does not involve tightly packed particles, which means such a layer has no capillary force. For this reason, the Sharp Front theory cannot be applied. However, this layer is still considered as a porous material, but the thermal conductivity is changed according the thermal properties of solid and fluid phase.

In general porous materials, the thermal conductivity of the solid (k_s) phase is greater than the fluid phase (k_f). Nevertheless, the behaviour of the solid that interconnects with liquid significantly influences the heat conduction. The effective thermal conductivity (k_e) is defined to estimate conduction heat transfer of a porous material, but this transfer depends on the thermal conductivity of each phase (solid and fluid), the structure of the solid matrix, and the contact resistance between the nonconsolidated particle (Kaviany, 1991). This value has been studied by many researchers and those theories were compared with experimental data by Nozad *et al*. (1985), as shown in figure 8.1.

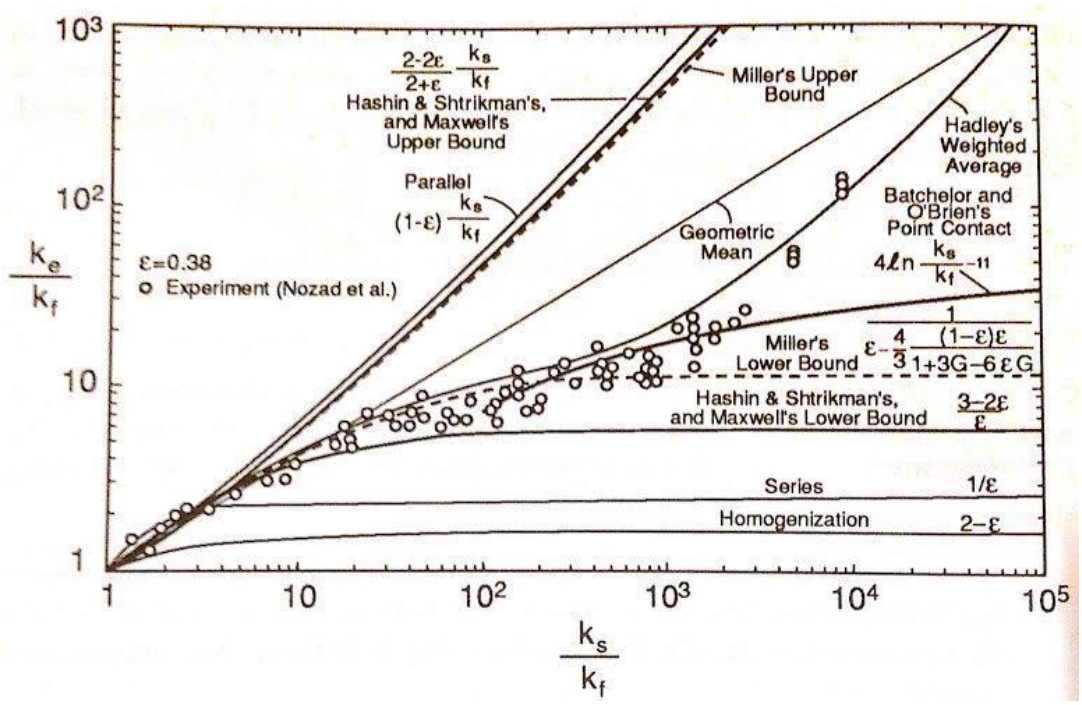

Figure 8.1 Effective thermal conductivity of beds of spherical particles predicted by various theories compared with experimental data (Nozad *et al*., 1985)

From figure 8.1, the method that is closest to the experimental data is Hadley's weighted average of Maxwell's upper bound method. This uses thermal diffusivity (α_o) with an expression obtained by the introduction of an adjustable function (f_o) into a weighted averaged expression (Kaviany, 1991). The effective thermal conductivity can be calculated by equations 8.1.

$$\frac{k_e}{k_f} = (1-\alpha_o)\frac{\epsilon f_o + K_s/K_f(1-\epsilon f_o)}{1-\epsilon(1-f_o)+K_s/K_f[\epsilon(1-f_o)]} + \alpha_o \frac{2(K_s/K_f)^2(1-\epsilon)+(1+2\epsilon)K_s/K_f}{(2+\epsilon)K_s/K_f+1-\epsilon} \quad (8.1)$$

Where; ϵ is porosity,

K_s is the thermal conductivity of the solid (W/m.K),

K_f is the thermal conductivity of the fluid (W/m.K),

f_0 is the adjustable function, which calculate from $f_o = 0.8 + 0.1\epsilon$,

α_o is the thermal diffusivity (m^2/sec).

The thermal diffusivity (α_o) can be obtained by the porosity of the porous material (drainage layer), which is calculated by a logarithmic function as follows:

$log\alpha_o = -4.898\epsilon$, if $0 \leq \epsilon \leq 0.0827$,
$log\alpha_o = -0.405 - 3.158(\epsilon - 0.0827)$, if $0.0827 \leq \epsilon \leq 0.298$,
$log\alpha_o = -1.084 - 6.778(\epsilon - 0.298)$, if $0.298 \leq \epsilon \leq 0.580$.

The effective thermal conductivity is mainly influenced by porosity, which is a ratio of the void space volume to the total volume of porous material. The porosity in a drainage layer is varied by the amount of inflow of drained water from the substrate layer and the outflow from the drainage layer. Because porosity varies with time, the effective thermal conductivity is considered to be a dynamic value. For this reason, the time dependent effective conductivity of a drainage layer could be calculated by using this theory.

8.6.2 Convection under a drainage layer

The other heat transfer parameter that is suggested to be worthy of study in future research is the convection from the drained water under the drainage layer (above the waterproof membrane). The convection levels under a green roof system had been ignored in previous research because most green roofs were installed over a flat roof,

and this heat flow parameter makes a very small contribution, when compared with the conduction heat flow, because the velocity of the drained water is extremely low. Therefore, this convective heat transfer is considered to be negligible.

However, the green roof system nowadays can be installed over a pitched roof, with a slope of 20^o to 35^o. With this slope configuration, the velocity of the drained liquid is much higher than with a flat roof. Therefore, the convection heat transfer becomes more significant and needs to be included in the simulation when a pitched roof building is thermally modelled.

If this convection heat transfer is considered as a laminar flow over a flat plate, the challenge for solving the convection heat transfer under the drainage layer is the determination of the critical distance that is used in the Reynolds number (Re_x) and the Nusselt number (Nu_x). The critical distance in this case is not the length of the roof (L) but it is the distance between the bottoms of each "dimple" (x) in a drainage module. Consider the profiled plastic type drainage layer, as shown in figure 8.2.

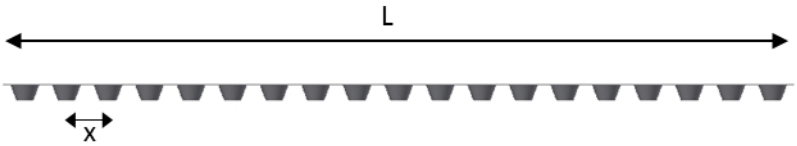

Figure 8.2 The drainage module critical distance

After the critical distance is considered, the heat transfer coefficient (h) can be calculated by using the Nusselt number and the Reynolds number, and then putting them into Newton's Law of Cooling equation. Therefore, the convection heat transfer from the drained water under the drainage layer could be determined.

8.7 Conclusion

This chapter has addressed and summarised the originality of this research, together with its objectives, as mentioned in this document's introduction chapter. Answers to the objectives include the findings relating to a substrate's properties, findings relating to a substrate's absorption mechanism, and findings relating to evaporation in a substrate. In addition, recommendations for future studies in green roof simulation are mentioned, including the conduction and convection processes that occur in the drainage layer.

Appendix A: Effect of substrate moisture content on the accuracy of thermal simulation

These examples will consider the effect of substrate layer on the overall thermal resistivity of a green roof. Three substrate thicknesses (100, 200, 300 mm) will be considered with three substrate conditions, which are (i) the substrate is homogeneously saturated, (ii) the substrate is homogeneously dry, (iii) and the moisture content in the substrate is distributed into 4 layers.

The green roof in this example consists of the foliage layer (turf) and the substrate layer. For the foliage layer, the turf layer has a thermal resistance of 0.360 m^2K/W as suggested by Wong *et al*. (2003). For the substrate thermal conductivity, this example will use the information from Sailor and Hagos (2011), in which the substrate is ES50C00 (50% expanded slate, 50% sand, Dry density is 1.49 kg/m^3, and moisture capacity is 0.25 m^3/m^3). The thermal conductivity of this substrate at different moisture contents follows the table A.1.

Table A.1 The thermal conductivity against the volumetric water content of the ES50C00 substrate (Sailor and Hagos, 2011)

Volumetric water content (m^3/m^3)	Thermal conductivity (W/mK)
0	0.21
0.04	0.45
0.08	0.55
0.23	0.75

The following section will calculate the effect of moisture content on the overall thermal resistivity of the green roof substrate.

A.1 Substrate 100 mm thick

The total thermal resistance of 100 mm green roof substrate in a saturated condition is shown in table A.2.

Table A.2 Thermal resistance of green roof when 100 mm substrate layer is saturated

Saturated substrate (23% water content)				
R turf (m^2K/W)	Substrate thickness (mm)	Thermal conductivity (W/mK)	R substrate (m^2K/W)	R total (m^2K/W)
0.36	100	0.75	0.133	0.493

From table 2.12, the thermal resistance of the 100 mm thick saturated substrate is only 37% of the foliage layer. For the extreme condition, which the substrate is completely dry, the thermal resistance of the green roof is shown in the table A.3.

Table A.3 Thermal resistance of green roof when 100 mm substrate layer is dry

Dry substrate				
R turf (m^2K/W)	Substrate thickness (mm)	Thermal conductivity (W/mK)	R substrate (m^2K/W)	R total (m^2K/W)
0.36	100	0.21	0.476	0.836

From table A.3, the dry substrate thermal resistance is 32% higher than the foliage layer resistance. Using a more realistic approach of dividing the substrate into four layers (25 mm thick), of which the top layer is dry but the bottom layer is saturated (moisture content profile is 0%, 4%, 8%, and 23% from the top respectively) produces table A.4.

Table A.4 Thermal resistance of green roof when 100 mm substrate layer is divided into 4 layers

Divide substrate into 4 layer					
R turf (m^2K/W)	Substrate thickness (mm)	Water content (%)	Thermal conductivity (W/mK)	R substrate (m^2K/W)	R total (m^2K/W)
0.36	25	0	0.21	0.119	0.613
	25	4	0.45	0.056	
	25	8	0.55	0.045	
	25	23	0.75	0.033	

From table A.4, the total thermal resistance of the substrate is 0.253 m^2K/W, almost twice that of the saturated substrate (0.133 m^2K/W). However, it is still only 70% of the thermal resistance of the foliage layer. Figure A.1 compares these three substrate conditions graphically.

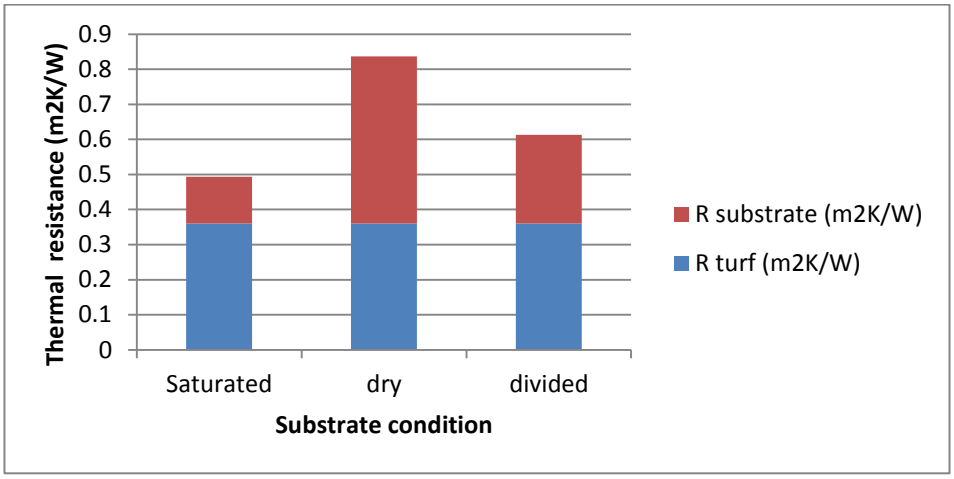

Figure A.1 Comparison between foliage and substrate thermal resistance of different substrate condition for 100 mm depth green roof substrate

Figure A.1 shows that the substrate makes a small contribution to the overall thermal resistance compared with the foliage layer resistance for the saturated substrate condition. On the other hand, when the substrate layer is assumed to be dry, the thermal resistance of the substrate layer makes a significant contribution to the overall resistance and is larger than the foliage resistance, but this situation is unreal in practice. Modelling the substrate in layers can increase the thermal resistance from that in the saturated condition, but the effect from the foliage thermal resistance is still greater than the substrate layer.

This can explain the fact that studies of extensive green roof, such as Sailor (2008), Chan and Chow (2013), Djedjig et al. (2012), give a good result in thermal modelling because the effect of the substrate is small when compare with the foliage layer. Considering thicker green roof substrates will show the effect of substrate thickness and the method of modelling this layer.

A.2 Substrate 200 mm thick

Repeating the calculation for a 200 mm green roof gives table A.5, A.6, and A.7 and the summary graph in figure A.2.

Table A.5 Thermal resistance of green roof when 200 mm substrate layer is saturated

Saturated substrate (23% water content)				
R turf (m^2K/W)	Substrate thickness (mm)	Thermal conductivity (W/mK)	R substrate (m^2K/W)	R total (m^2K/W)
0.36	200	0.75	0.267	0.627

Table A.6 Thermal resistance of green roof when 200 mm substrate layer is dry

Dry substrate				
R turf (m^2K/W)	Substrate thickness (mm)	Thermal conductivity (W/mK)	R substrate (m^2K/W)	R total (m^2K/W)
0.36	200	0.21	0.952	1.312

Table A.7 Thermal resistance of green roof when 200 mm substrate layer is divided into 4 layers

Divide substrate into 4 layer					
R turf (m^2K/W)	Substrate thickness (mm)	Water content (%)	Thermal conductivity (W/mK)	R substrate (m^2K/W)	R total (m^2K/W)
0.36	50	0	0.21	0.238	0.867
	50	4	0.45	0.111	
	50	8	0.55	0.091	
	50	23	0.75	0.067	

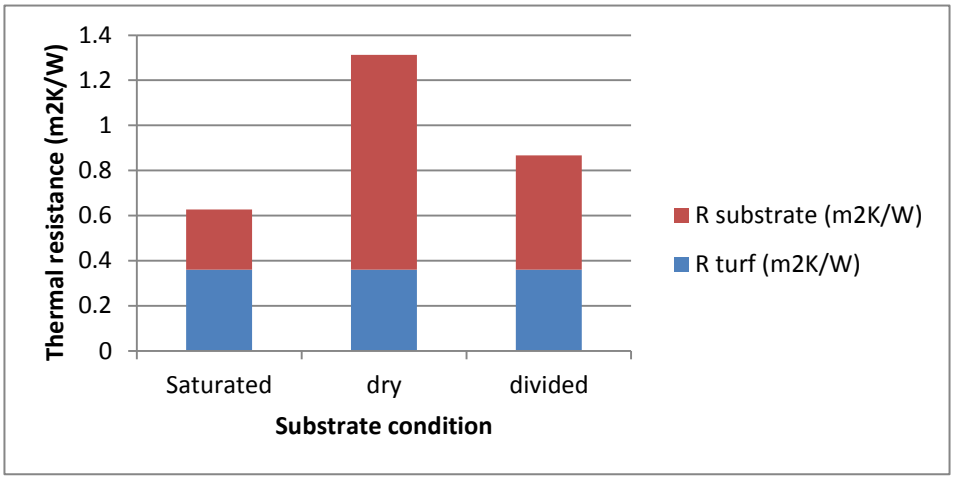

Figure A.2 Comparison between foliage and substrate thermal resistance of different substrate condition for 200 mm depth green roof substrate

A.3 Substrate 300 mm thick

Repeating the calculation for a 300 mm green roof substrate gives table A.8, A.9, and A.10 and the summary graph in figure A.3.

Table A.8 Thermal resistance of green roof when 300 mm substrate layer is saturated

Saturated substrate (23% water content)				
R turf (m^2K/W)	Substrate thickness (mm)	Thermal conductivity (W/mK)	R substrate (m^2K/W)	R total (m^2K/W)
0.36	300	0.75	0.400	0.760

Table A.9 Thermal resistance of green roof when 300 mm substrate layer is dry

Dry substrate				
R turf (m^2K/W)	Substrate thickness (mm)	Thermal conductivity (W/mK)	R substrate (m^2K/W)	R total (m^2K/W)
0.36	300	0.21	1.429	1.789

Table A.10 Thermal resistance of green roof when 300 mm substrate layer is divided into 4 layers

Divide substrate into 4 layer					
R turf (m^2K/W)	Substrate thickness (mm)	Water content (%)	Thermal conductivity (W/mK)	R substrate (m^2K/W)	R total (m^2K/W)
0.36	75	0	0.21	0.357	1.120
	75	4	0.45	0.167	
	75	8	0.55	0.136	
	75	23	0.75	0.100	

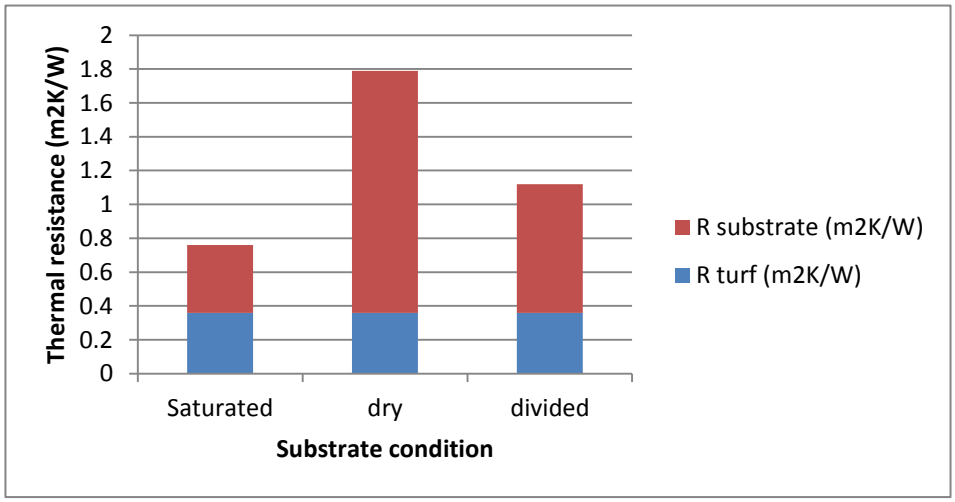

Figure A.3 Comparison between foliage and substrate thermal resistance of different substrate condition for 300 mm depth green roof substrate

Clearly the influence of the substrate layer on the overall thermal resistance of a green roof increases as the substrate increases in thickness and, furthermore, the overall thermal resistance is critically dependent on the moisture condition of the substrate.

Appendix B: Application of the model to a case study building

B.1 Introduction

This appendix details the calculations summarised in the implication section in chapter 7, which presents the effect of a green roof on the shoebox building (section 7.2) to the energy saving and thermal insulation replacement. Two green roof thicknesses will be retrofitted with three common roof types (non-domestic inverted roof, domestic warm roof and metal decking). In addition, three different moisture scenarios will be discussed and calculated, which are: (i) the green substrate is dry all the time, (ii) the green roof substrate is saturated all time, and (iii) the green roof substrate moisture behaviour is obtained from the simulation (actual moisture content). The environmental conditions are all defined in section 7.2.

B.2 The building with non-domestic inverted roof

Scenario 1 is the shoebox-shaped building, with non-domestic inverted roof over the concrete structure. According to the Scottish government building standards for non-domestic buildings (2016), the inverted roof is a roof that offers external protective covering; it has low permeability insulation laid on a waterproof membrane between the roof structure and the external covering (Scottish_Building, 2016b). Details of this roof construction are shown in figure B.1 below.

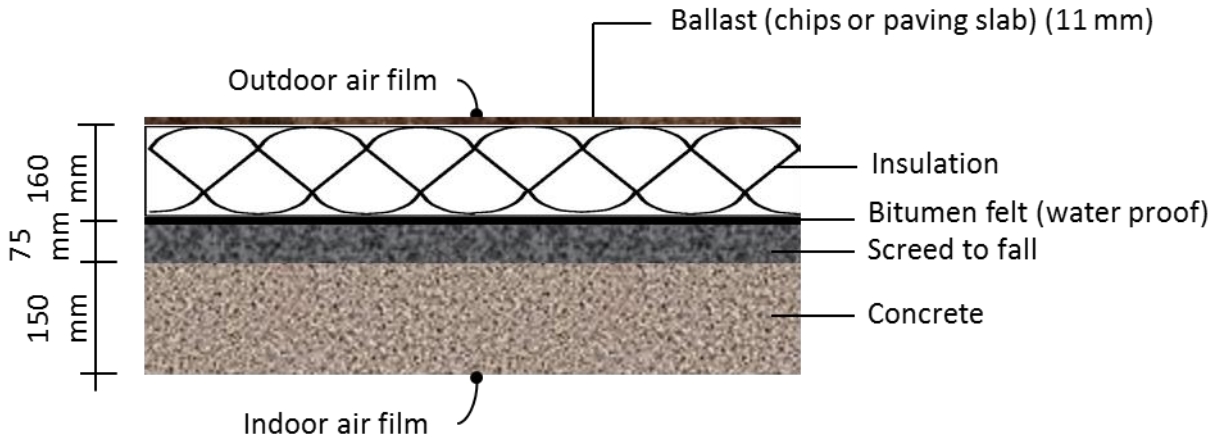

Figure B.1 Non-domestic inverted roof construction details

The thermal properties of some building materials are presented in table B.1 (Chartered Institution of Building Services, 2006).

Table B.1 Thermal conductivities of materials in an inverted roof

Material	**Thermal conductivity, k (W/m.K)**	**Thickness (mm)**
Ballast (chips or paving slab)	1.10	11
Extruded polystyrene	0.035	160
Bitumen layer (water proof)	0.23	5
Screed	0.46	75
Cast concrete (2000 kg/m^3)	1.33	150

The thermal resistance of each building element can be calculated by using the equation B.1.

$$R = \frac{Thickness}{Thermal\ conductivity} \tag{B.1}$$

The total thermal resistance (R_{roof}) of the concrete roof can be calculated by equation B.2.

$$R_{roof} = R_{roof,out} + R_{ballast} + R_{insulation} + R_{bitumen} + R_{screed} + R_{concrete} + R_{roof,in} \tag{B.2}$$

R_{roof} = 0.04 + (0.011/1.10) + (0.15/0.035) + (0.005/0.23) + (0.075/0.40) + (0.15/1.33) + 0.10

R_{roof} = 5.02 m^{2}K/W

This R-value is equivalent to the U-value of 0.20 W/m^{2}K, which is equivalent to the Scottish standard.

Total heat flow (Q) can be calculated by equation B.3.

$$Q = U \times Area \times (T_{in} - T_{out}) \times Time \tag{B.3}$$

The heat flow through each building component from the information given earlier in chapter 7 and table B.1 will be calculated and summarised in table B.2.

Table B.2 Heat loss through inverted roof and other building components

Element	U-value (m^2K/W)	Area (m^2)	Tin-Tout (^oC)	Time (hour)	Q (kWh)	Percentage (%)
Wall	0.270	74.16	15	564	169,396.3	29.43
Window	3.300	8.4	15	564	234,511.2	40.75
Floor	0.220	48.6	15	564	90,454.32	15.72
Roof	0.199	48.16	15	564	81,178.35	14.10
Total					**575,540.1**	**100**

The total heat loss of the building is 575,540 kWh. An inverted roof has approximately 81,178 kWh of heat loss, which are equivalent to 14.10% of the total loss.

B.2.1 The non-domestic inverted roof with 162.5 mm green roof substrate on top

The inverted roof is now retrofitted with a 162.5 mm semi-intensive green roof system. The ballast layer is now replaced with a waterproof layer and the green roof system; a drainage layer, filter layer, and 162.5 mm green roof substrate are now involved, as show in figure B.2.

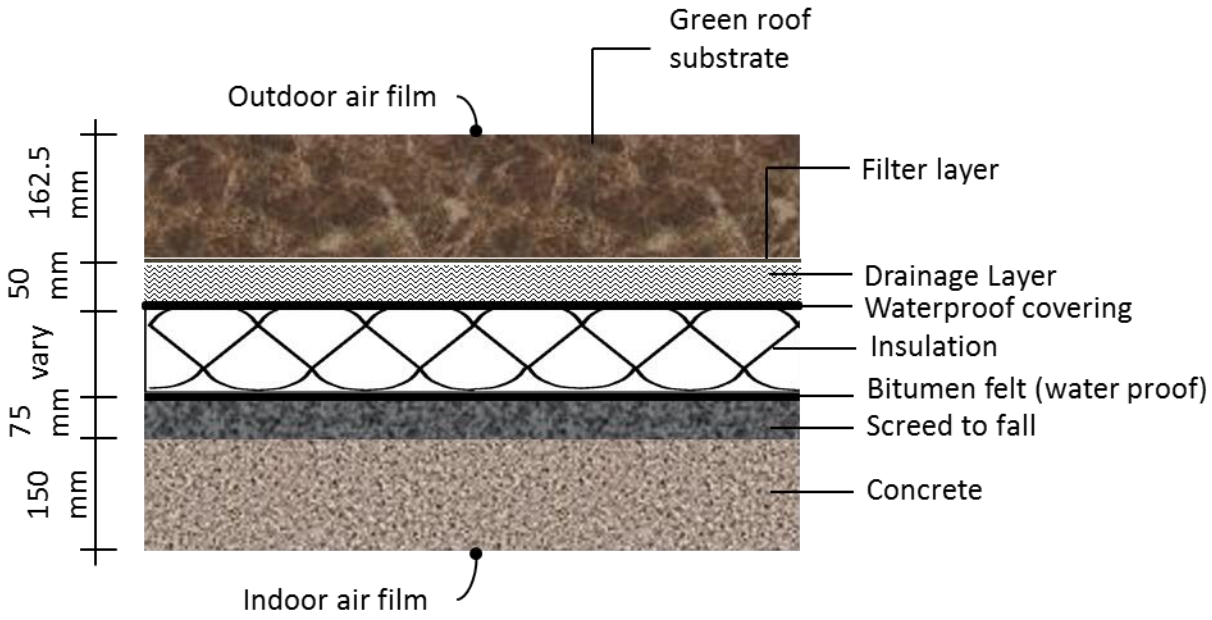

Figure B.2 Inverted roof and 162.5 mm deep green roof system on top

The total heat loss from this roof will be calculated informed by three substrate conditions: i) the dry substrate, ii) the saturated substrate, and iii) the substrate with varying moisture content from wet to dry. In addition, some thermal properties of such a green roof system are presented in table B.3.

Table B.3 Thermal property of green roof material

Material	Thermal conductivity, k (W/m.K)	Thickness (mm)
Drainage layer	0.14	50
Waterproof covering	0.23	10

a) Green roof is completely dry all the time

The inverted roof in this example is fitted with green roof substrate in the dry condition throughout the whole 564 hours. The thermal resistance of dry green roof substrate ($R_{substrate}$) is 0.487 m^2K/W. The heat loss of this building will be calculated over the period of 564 hours.

By using the thermal properties of some building materials that are declared in chapter 7 and table B.3, the concrete roof's total thermal resistance ($R_{roof,dry}$) can be calculated from equation B.4.

$$R_{roof,dry} = R_{roof,out} + R_{substrate,\ dry} + R_{drainage} + R_{waterproof} + R_{insulation} + R_{bitumen} + R_{screed} + R_{concrete} + R_{roof,in} \quad (A.4)$$

$$R_{roof} = 0.04 + 0.487 + (0.05/0.14) + (0.01/0.23) + (0.16/0.035) + (0.005/0.23) + (0.075/0.40) + (0.15/1.33) + 0.10$$

$$R_{roof} = 5.90\ m^2K/W$$

This R-value is equivalent to the U-value of 0.169 W/m^2K, which is lower than the Scottish standard (0.2 W/m^2K).

The heat flow through each building component from the information given earlier will be calculated and summarised in table B.4.

Table B.4 Heat loss through inverted roof with dry 162.5 mm green roof and other building components

Element	U-value (m^2K/W)	Area (m^2)	Tin-Tout (^oC)	Time (hour)	Q (kWh)	Percentage (%)
Wall	0.270	74.16	15	564	169.396	30.08
Window	3.300	8.4	15	564	234.511	41.64
Floor	0.220	48.6	15	564	90.454	16.06
Roof	0.169	48.16	15	564	68.856	12.23
Total					**563.218**	**100**

The total heat loss of the building in this scenario is 563.218 kWh. An inverted roof with dry substrate gives approximately 68.856 kWh of heat loss; equivalent to 12.23% of the total heat loss.

b) Green roof is saturated all the time

The inverted roof in this example is fitted with a green roof substrate that is in a saturated condition throughout the whole 564 hours. The thermal resistance of saturated green roof substrate ($R_{substrate}$) is 0.1007 m^2K/W. The heat loss of this building was calculated over the period of 564 hours.

By using the thermal properties of some building materials, as declared in chapter 7 and B.3, the total thermal resistance ($R_{roof,sat}$) of the concrete roof can be calculated from equation B.5.

$$R_{roof,sat} = R_{roof,out} + R_{substrate,\ sat} + R_{drainage} + R_{waterproof} + R_{insulation} + R_{bitumen} + R_{screed} + R_{concrete} + R_{roof,in} \quad \text{(B.5)}$$

$$R_{roof,sat} = 0.04 + 0.1007 + (0.05/0.14) + (0.01/0.23) + (0.16/0.035) + (0.005/0.23) + (0.075/0.40) + (0.15/1.33) + 0.10$$

$$R_{roof} = 5.51\ m^2K/W$$

This R-value is equivalent to the U-value of 0.181 W/m^2K, which is lower than the Scottish standard (0.2 W/m^2K).

The heat flow through each building component from the information given earlier will be calculated and summarised in the table B.5.

Table B.5 Heat loss through inverted roof with saturated 162.5 mm green roof and other building components

Element	**U-value (m^2K/W)**	**Area (m^2)**	**Tin-Tout (^oC)**	**Time (hour)**	**Q (kWh)**	**Percentage (%)**
Wall	0.270	74.16	15	564	169.396	29.82
Window	3.300	8.4	15	564	234.511	41.28
Floor	0.220	48.6	15	564	90.454	15.92
Roof	0.181	48.16	15	564	73.745	12.98
Total					**568.107**	**100**

The total heat loss of the building in this scenario is 568.107 kWh. An inverted roof with saturated substrate gives approximately 73.745 kWh of heat loss, which is equivalent to 12.98% of the total heat loss.

c) *Green roof with the actual moisture content (from simulation)*

The inverted roof in this example is now fitted with a 162.5 mm green roof substrate, but the moisture condition is archived from the 564 hours green roof substrate evaporation simulation. The thermal resistance of the green roof substrate over 564 hours (*with outdoor temperature 5^{o}C, indoor temperature 20^{o}C, 50% relative humidity, and 0.5 m/s wind speed*) is shown in figure B.3.

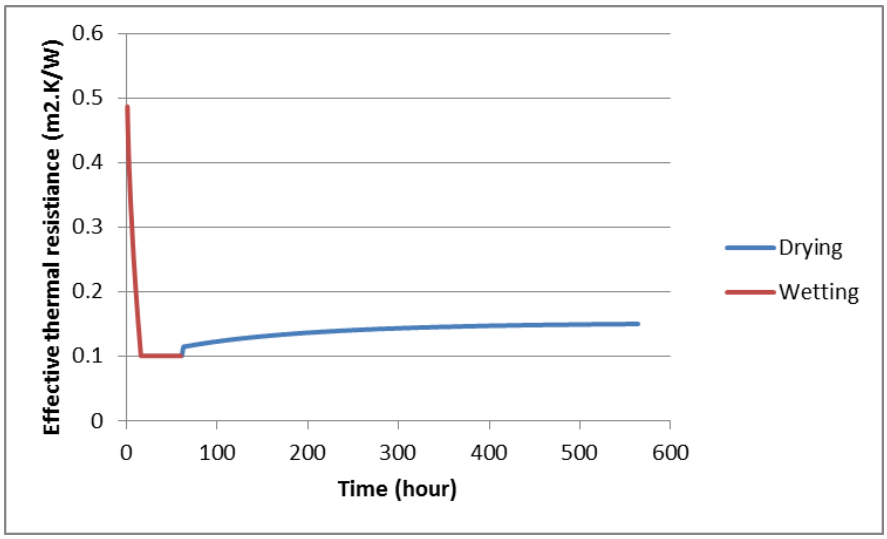

Figure B.3 Thermal resistance of 162.5 mm green roof substrate over 564 hours

The hourly thermal resistance of this roof (green roof and inverted roof combined) over the period of 564 hours is presented in figure B.4.

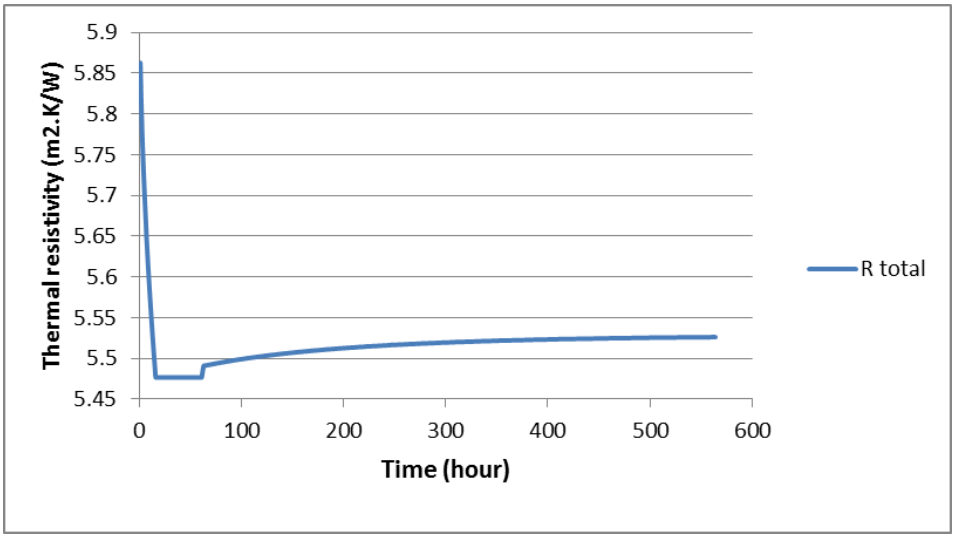

Figure B.4 Hourly thermal resistance of inverted roof with 162.5 mm green roof

The hourly heat flow through this roof, with the given information, can be calculated and summarised in figure B.5

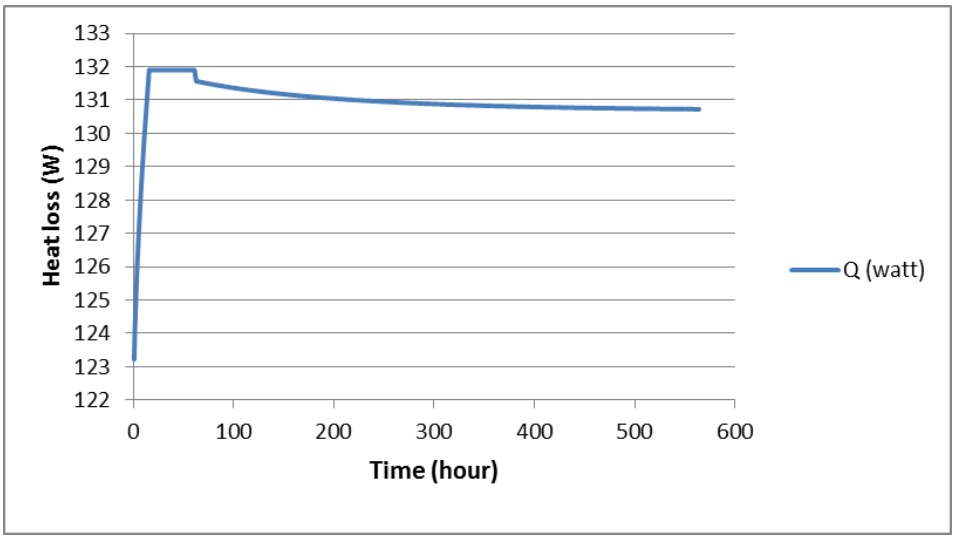

Figure B.5 Heat flow through inverted roof with 162.5 mm green roof in hourly basis

The heat flow through each building component from the information given earlier will be calculated and summarised in the table B.6.

Table B.6 Heat loss through inverted roof with 162.5 mm green roof (actual moisture content) and another building component

Element	**U-value (m^2K/W)**	**Area (m^2)**	**Tin-Tout (^oC)**	**Time (hour)**	**Q (kWh)**	**Percentage (%)**
Wall	0.270	74.16	15	564	169.396	29.83
Window	3.300	8.4	15	564	234.511	41.30
Floor	0.220	48.6	15	564	90.454	15.93
Roof	Vary	48.16	15	564	73.442	12.93
Total					**567.804**	**100**

The total heat loss of the building in this scenario is 567.804 kWh. An inverted roof with simulated moisture content substrate on the top produces approximately 73.443 kWh of heat loss, which is equivalent to 12.93% of the total loss.

B.2.2 The non-domestic inverted roof with 300 mm green roof substrate on top

The inverted roof is now retrofitted with a 300 mm semi-intensive green roof system. The ballast layer is replaced with a waterproof layer and the green roof system. This new construction involves a drainage layer, filter layer, and 300 mm green roof substrate, with the latter standing on the top as show in figure B.6.

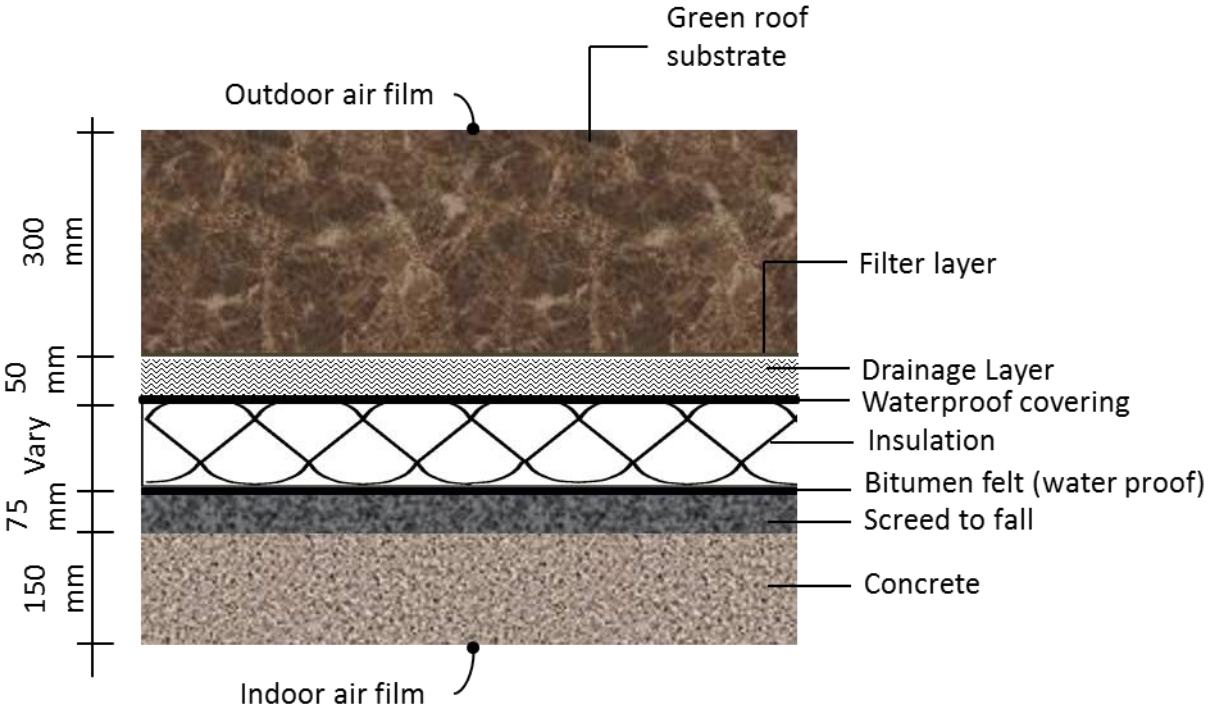

Figure B.6 Inverted roof and 300 mm deep green roof system on top

The conduction heat transfer of this roof will be calculated with three substrate conditions: i) the dry substrate, ii) saturated substrate, and iii) substrate with varying moisture content from wet to dry. In addition, the thermal properties of the green roof system are using the tables 7.1 in chapter 7 and B.3 as it uses same materials.

a) <u>The green roof is completely dry all the time</u>

The inverted roof in this example is fitted with a green roof substrate in the dry condition throughout the 564 hours. The thermal resistance of the dry green roof substrate ($R_{substrate}$) is 1.008 m^2K/W. The heat loss of this building is calculated over the period of 564 hours.

By using the thermal properties of some building materials, as presented in tables 7.1 and B.3, the concrete roof's total thermal resistance ($R_{roof,dry}$) can be calculated from equation B.6.

$$R_{roof,dry} = R_{roof,out} + R_{substrate,\ dry} + R_{drainage} + R_{waterproof} + R_{insulation} + R_{bitumen} + R_{screed} + R_{concrete} + R_{roof,in} \quad \text{(B.6)}$$

$$R_{roof,dry} = 0.04 + 1.008 + (0.05/0.14) + (0.01/0.23) + (0.15/0.035) + (0.005/0.23) + (0.075/0.40) + (0.15/1.33) + 0.10$$

$$R_{roof,dry} = 6.42\ m^2K/W$$

This R-value is equivalent to the U-value of 0.156 W/m^2K, which is lower than the Scottish standard (0.2 W/m^2K).

The heat flow through each building component from the information given earlier will be calculated and summarised in the table B.7.

Table B.7 Heat loss through inverted roof with dry 300 mm green roof and another building component

Element	**U-value (m^2K/W)**	**Area (m^2)**	**Tin-Tout (^oC)**	**Time (hour)**	**Q (kWh)**	**Percentage (%)**
Wall	0.270	74.16	15	564	169.396	30.36
Window	3.300	8.4	15	564	234.511	42.03
Floor	0.220	48.6	15	564	90.454	16.21
Roof	0.156	48.16	15	564	63.559	11.39
Total					**557.921**	**100**

The total heat loss of the building in this scenario is 557.921 kWh. An inverted roof with 300 mm dry green roof on the top produces approximately 63.560 kWh of heat loss, which are equivalent to 11.39% of the total heat loss.

b) The green roof is saturated all the time

The inverted roof in this example is fitted with a green roof substrate in a constantly saturated condition throughout the whole 564 hours. The thermal resistance of the saturated green roof substrate ($R_{substrate}$) is 0.186 m^2K/W. The heat loss of this building was calculated over the period of 564 hours.

By using the thermal properties of some building materials, as declared in tables B.1 and B.3, the concrete roof's total thermal resistance ($R_{roof,sat}$) can be calculated from equation B.7.

$$R_{roof} = R_{roof,out} + R_{substrate,\ sat} + R_{drainage} + R_{waterproof} + R_{insulation} + R_{bitumen} + R_{screed} + R_{concrete} + R_{roof,in} \quad \text{(B.7)}$$

$$R_{roof} = 0.04 + 0.186 + (0.05/0.14) + (0.01/0.23) + (0.15/0.035) + (0.005/0.23) + (0.075/0.40) + (0.15/1.33) + 0.10$$

$$R_{roof} = 5.60\ m^2K/W$$

This R-value is equivalent to the U-value of 0.179 W/m^2K, which is lower than the Scottish standard (0.2 W/m^2K).

The heat flow through each building component from the information given earlier will be calculated and summarised in the table B.8.

Table B.8 Heat loss through inverted roof with saturated 300 mm green roof and another building component

Element	**U-value (m^2K/W)**	**Area (m^2)**	**Tin-Tout (^oC)**	**Time (hour)**	**Q (kWh)**	**Percentage (%)**
Wall	0.270	74.16	15	564	169.396	29.86
Window	3.300	8.4	15	564	234.511	41.34
Floor	0.220	48.6	15	564	90.454	15.94
Roof	0.179	48.16	15	564	72.930	12.86
Total					**567.292**	**100**

The total heat loss of the building in this scenario is 567.292 kWh. An inverted roof with 300 mm saturated green roof on the top produces approximately 72.931 kWh of heat loss, which is the equivalent to 12.86% of the total heat loss.

c) A green roof with the actual moisture content

The inverted roof in this example is now fitted with 300 mm deep green roof substrate, but the moisture condition is archived from the 564 hours green roof substrate evaporation simulation. The thermal resistance of green roof substrate over 564 hours (*with outdoor temperature 5^{o}C, indoor temperature 20^{o}C, 50% relative humidity, and 0.5 m/s wind speed*) is shown in figure B.7.

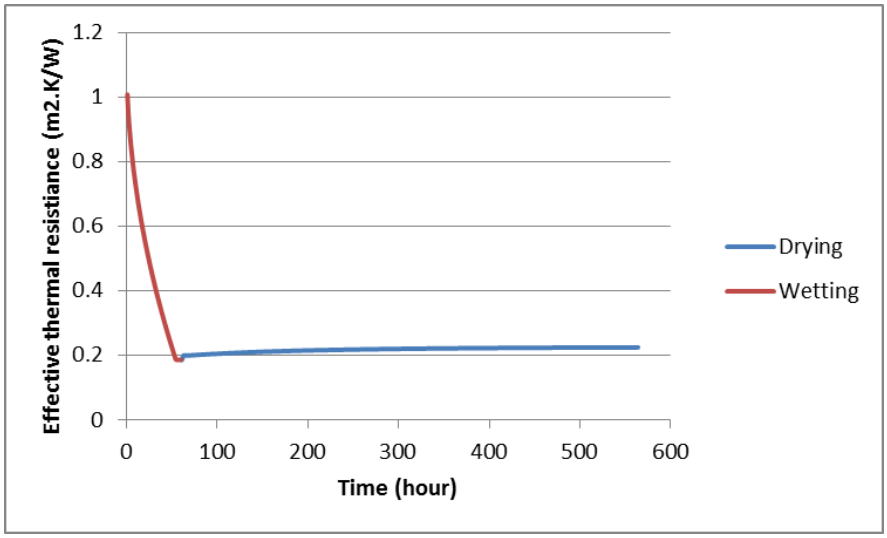

Figure B.7 Thermal resistance of 300 mm green roof substrate over 564 hours

The hourly thermal resistance of this roof (green roof and inverted roof combined) over the period of 564 hours is presented in figure B.8.

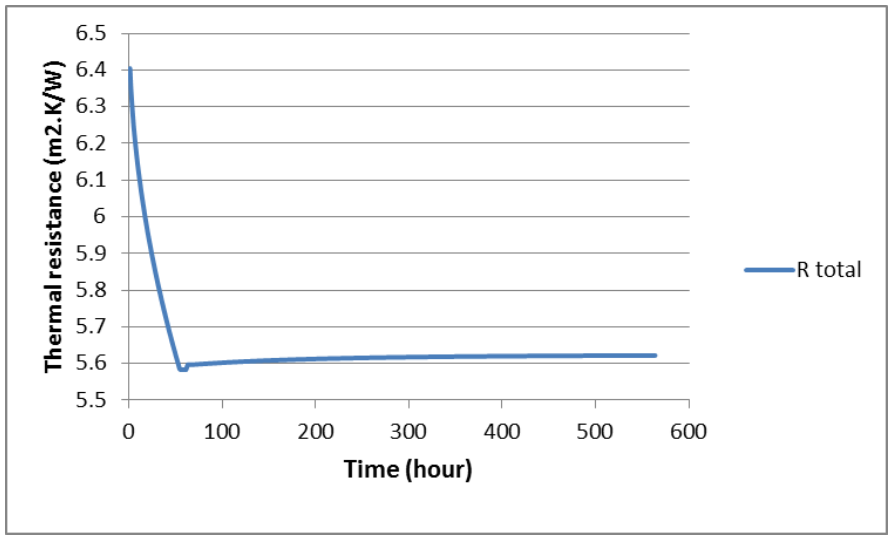

Figure B.8 Hourly thermal resistance of inverted roof with 300 mm green roof

The hourly heat flow through this roof can be calculated from the given information and is summarised in figure B.9.

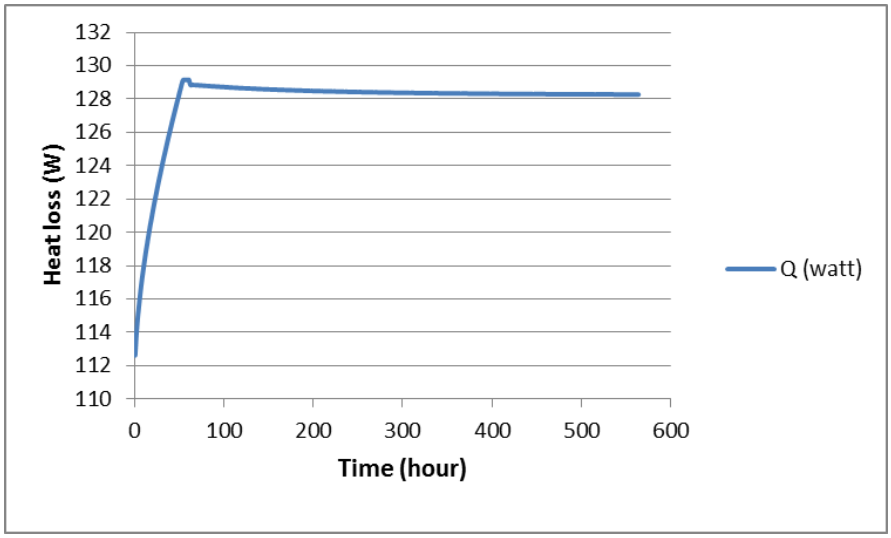

Figure B.9 Heat flow through the inverted roof with 300 mm green roof in hourly basis

The heat flow through each building component from the information given earlier will be calculated and summarised in the table B.9.

Table B.9 Heat loss through an inverted roof with 300 mm green roof (actual moisture content) and another building component

Element	**U-value (m^2K/W)**	**Area (m^2)**	**Tin-Tout (^oC)**	**Time (hour)**	**Q (kWh)**	**Percentage (%)**
Wall	0.270	74.16	15	564	169.396	29.90
Window	3.300	8.4	15	564	234.511	41.40
Floor	0.220	48.6	15	564	90.454	15.97
Roof	Vary	48.16	15	564	72.119	12.73
Total					**566.481**	**100**

The total heat loss of the building in this scenario is 566.482 kWh. An inverted roof with simulated moisture content (300 mm substrate) produces approximately 72.120 kWh of heat loss, which is equivalent to 12.73% of the total loss.

Energy saving comparisons

In order to compare the heating energy saving from green roof installation, six examples from two green roof substrate depths are compared by using the inverted roof with no green roof system as a base case. The percentages of heating energy savings for each scenario are shown in figure B.10 and table B.10.

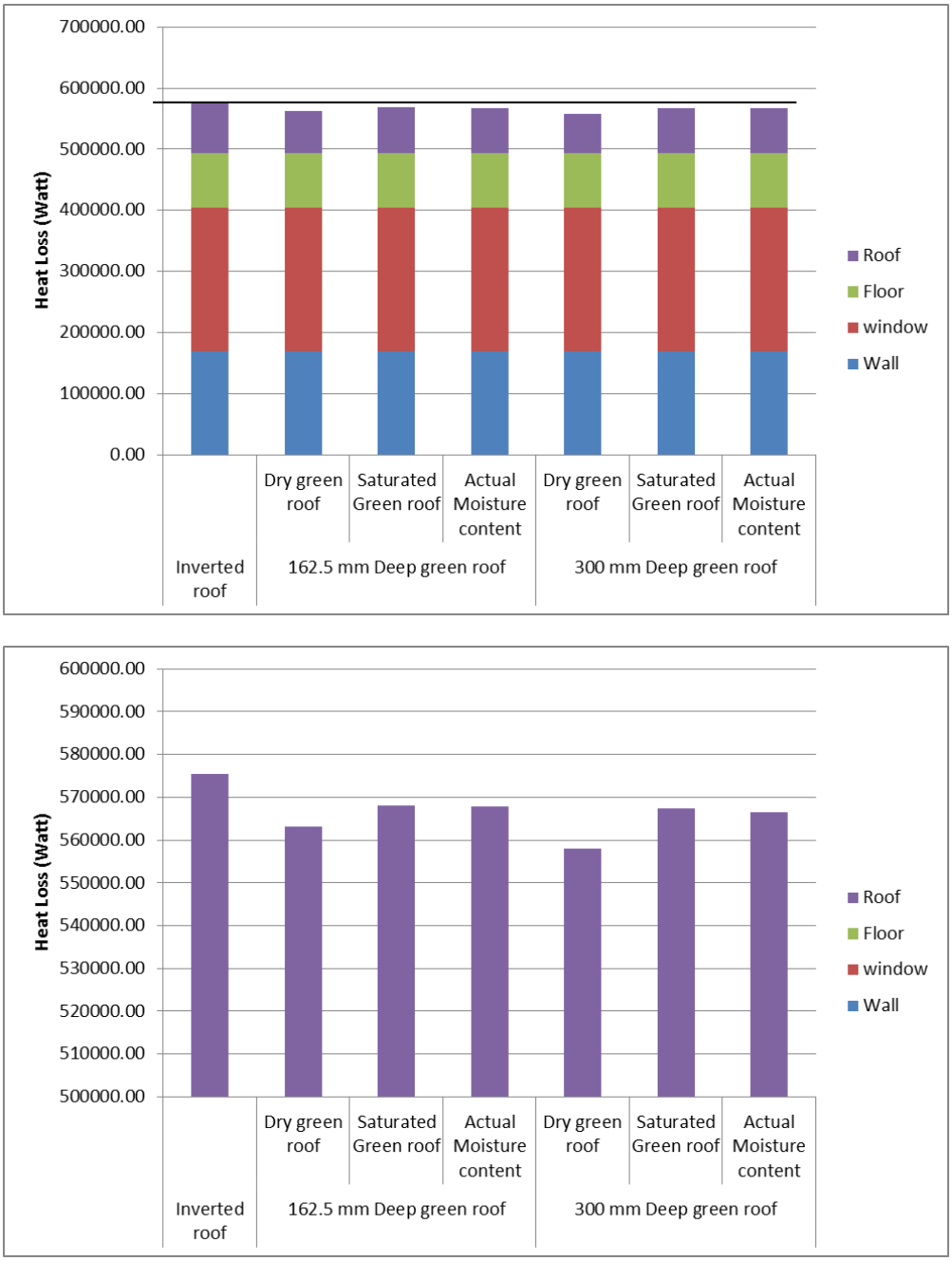

Figure B.10 Energy saving from green roof over the inverted roof, with enlarged heat loss scale below

Table B.10 Heat loss comparison of 162.5 mm and 300 mm green roof substrate over the non-domestic inverted roof in different conditions

	Heat loss (kWh)						
Element	**Inverted roof**	**162.5 mm deep green roof**			**300 mm deep green roof**		
		Dry green roof	**Saturated green roof**	**Actual moisture content**	**Dry green roof**	**Saturated green roof**	**Actual moisture content**
Wall	169.396	169.396	169.396	169.396	169.396	169.396	169.396
Window	234.511	234.511	234.511	234.511	234.511	234.511	234.511
Floor	90.454	90.454	90.454	90.454	90.454	90.454	90.454
Roof	81.178	68.856	73.745	73.442	63.559	72.930	72.119
Total	575.540	563.218	568.107	567.804	557.921	567.292	566.481
Saving (%)		**2.14**	**1.29**	**1.34**	**3.06**	**1.43**	**1.57**

Thermal insulation thickness reduction

In this section, the effect of heating energy saving from green roof installation on the non-domestic inverted roof is now replaced with the insulation thickness reduction. The original insulation thickness of this roof (extruded polystyrene) is 160 mm, which brings the total U-value of this roof close to the U-value that is required in the regulation (0.2 $W/m^2.K$). Therefore, the insulation thickness needs to be revised after a green roof is installed.

The insulation reduction can be calculated from the thermal transmittance equation B.8.

$$1/U = R_{roof,out} + R_{substrate} + R_{drainage} + R_{waterproof} + R_{insulation} + R_{bitumen} + R_{screed} + R_{concrete} + R_{roof,in} \quad \text{(B.8)}$$

By using information given in the previous section, the $R_{substrate}$ is changed according to the substrate condition and the $R_{insulation}$ is now replaced with $thickness/k_{insulation}$. In order to archive the certain U-value, the thickness of insulation can be determined by equation B.9.

$$Thickness = k_{insulation}\,(1/U - (R_{roof,out} + R_{substrate} + R_{drainage} + R_{waterproof} + R_{bitumen} + R_{screed} + R_{concrete} + R_{roof,in})) \quad \text{(B.9)}$$

Thicknesses of the inverted roof's insulation, in different green roof substrate conditions, are calculated and shown in table B.11.

Table B.11 Thermal insulation thickness reduction of inverted roof (1)

Condition	Inverted roof	162.5 mm deep green roof		300 mm deep green roof	
		Dry green roof	Saturated green roof	Dry green roof	Saturated green roof
Insulation thickness (mm)	160	129	143	111	140
Insulation thickness reduction (mm)	-	31	17	49	20

The green roof with simulated moisture content, on the other hand, cannot be calculated directly, as has been achieved in previous scenarios. The thickness of insulation in this current scenario is revised from the total hourly heat loss with the purely inverted roof system over the simulation time. The thickness of insulation can be found by using the

trial and error method, in order to get to the nearest value of the total heat loss through the roof.

The total heat loss from the inverted roof over 564 hours is 81,178 kWh. The purely inverted roof thermal resistance (excepting a green roof system) required to reach that amount of heat loss is 4.42m^2K/W, after the green roof was simulated with actual moisture content. This value can be converted into the thickness of insulation, which is equivalent to 141.5mm and 138mm (162.5 mm and 300 mm substrate depth). For this reason, the thickness of thermal insulation and its reduction in each scenario can be represented again in table B.12.

Table B.12 Thermal insulation thickness reduction of inverted roof (2)

Condition	Inverted roof	162.5 mm deep green roof			300 mm deep green roof		
		Dry green roof	Saturated green roof	Actual moisture content	Dry green roof	Saturated green roof	Actual moisture content
Insulation thickness (mm)	160	129	143	141.5	111	140	138
Insulation thickness reduction (mm)	-	31	17	18.5	49	20	22

From table B.12, the roof with dry substrate yields the maximum thermal insulation thickness reduction in every case, and the saturated substrate and simulated moisture content substrate produce very close thickness reductions when compared.

B.3 The building with a domestic warm roof

Scenario 2 is the shoebox shape building with a domestic warm flat roof over the timber structure. According to Scottish government building standards for domestic buildings (2016), the warm flat roof is a flat roof structure of timber or metal-framed construction with a board decking 19 mm thick; with or without a ceiling or soffit. Externally there is a weatherproof covering, an insulation and a vapour control layer (Scottish_Building, 2016a). This roof construction detail is shown in figure B.11.

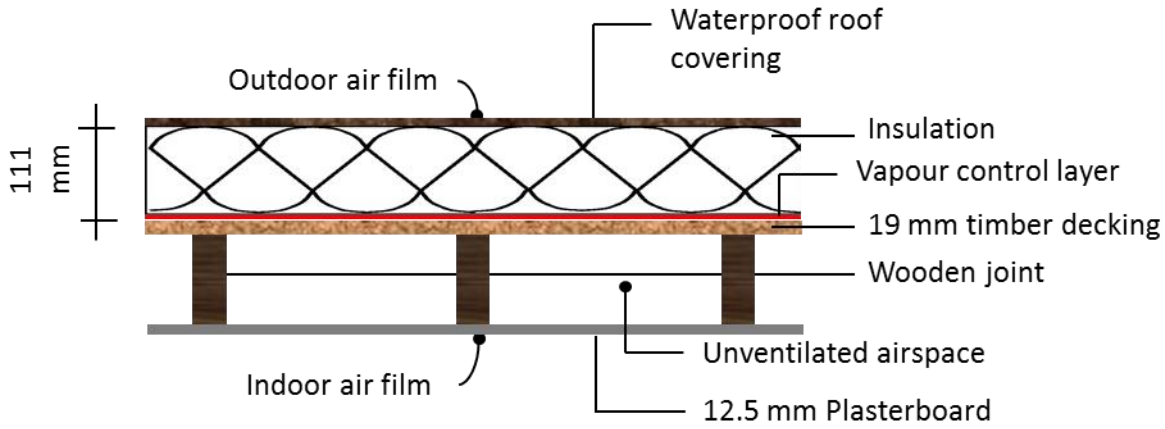

Figure B.11 Domestic warm roof construction detail

The thermal properties of some building materials constructed into this roof are shown in table B.13 (Chartered Institution of Building Services, 2006).

Table B.13 Thermal conductivities of materials in a warm roof

Material	**Thermal conductivity, k (W/m.K)**	**Thickness (mm)**
Waterproof covering	0.23	10
Polyurethane insulation	0.025	111
Timber decking	0.13	19
Plasterboard (standard)	0.21	12.5

The warm roof's total thermal resistance (R_{roof}) can be calculated from equation B.10.

$$R_{roof} = R_{roof,out} + R_{waterproof} + R_{insulation} + R_{deck} + R_{airspace} + R_{plasterboard} + R_{roof,in} \quad (B.10)$$

$$R_{roof} = 0.04 + (0.01/0.23) + (0.111/0.025) + (0.019/0.13) + 0.16 + (0.0125/0.21) + 0.10$$

$$R_{roof} = 4.99\ m^2K/W$$

This R-value is equivalent to the U-value of 0.20 W/m^{2}K, which exactly equivalent to the Scottish standard (0.2 W/m^{2}K). As a result, the heat flow through each building component from the information given earlier (table B.13) will be calculated and summarised in the table B.14.

Table B.14 Heat loss through inverted roof and another building component

Element	U-value (m^{2}K/W)	Area (m^2)	Tin-Tout (^{o}C)	Time (hour)	Q (kWh)	Percentage (%)
Wall	0.270	74.16	15	564	169.396	29.41
Window	3.300	8.4	15	564	234.511	40.71
Floor	0.220	48.6	15	564	90.454	15.70
Roof	0.200	48.16	15	564	81.663	14.18
Total					**576.025**	**100**

The total heat loss of the building in this scenario is 576.026 kWh. An inverted roof produces approximately 81.664 kWh of heat loss, which are equivalent to 14.18% of the total loss.

B.3.1 The domestic warm roof with 162.5 mm green roof substrate on top

The warm roof in the second scenario is now retrofitted with a 162.5 mm semi-intensive green roof system, as show in figure B.12.

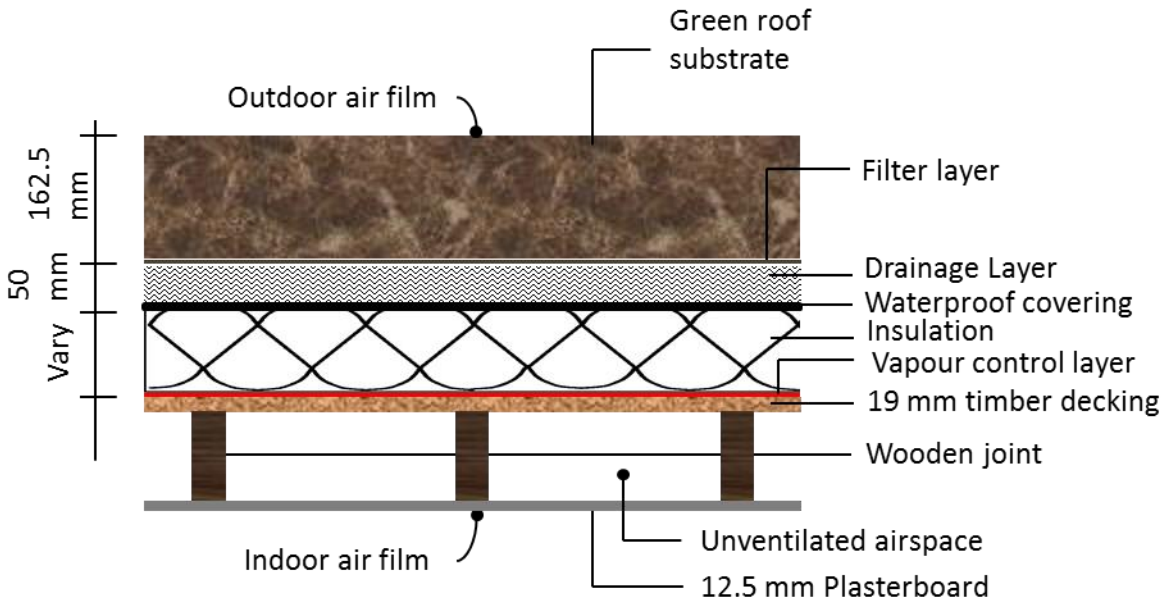

Figure B.12 The domestic warm roof with a 162.5 mm green roof system

The total heat loss for this roof will be calculated with three substrate conditions: i) the dry substrate, ii) saturated substrate, and iii) substrate with varying moisture content from wet to dry.

a) Green roof is completely dry all the time

The warm roof in this example is fitted with green roof substrate in the dry condition throughout the whole 564 hours. The thermal resistance of the dry green roof substrate ($R_{substrate}$) is 0.487m^2K/W. The heat loss of this building over the period of 564 hours can be calculated by using the information given in tables B.3 and B.13.

The concrete roof's total thermal resistance (R_{roof}) can be calculated from equation B.11.

$$R_{roof} = R_{roof,out} + R_{substrate,\ dry} + R_{drainage} + R_{waterproof} + R_{insulation} + R_{deck} + R_{airspace} + R_{plasterboard} + R_{roof,in} \quad \text{(B.11)}$$

$$R_{roof} = 0.04 + 0.487 + (0.05/0.14) + (0.01/0.23) + (0.111/0.025) + (0.019/0.13) + 0.16 + (0.0125/0.21) + 0.10$$

$$R_{roof} = 5.83\ m^2K/W$$

This R-value is equivalent to the U-value of 0.171 W/m^2K, which is lower than the Scottish standard (0.2 W/m^2K). As a result, the heat flow through each building component from the information given earlier will be calculated and summarised in the table B.15.

Table B.15 Heat loss through warm roof with dry 162.5 mm green roof and another building component

Element	**U-value (m^2K/W)**	**Area (m^2)**	**Tin-Tout (^{o}C)**	**Time (hour)**	**Q (kWh)**	**Percentage (%)**
Wall	0.270	74.16	15	564	169.396	30.03
Window	3.300	8.4	15	564	234.511	41.58
Floor	0.220	48.6	15	564	90.454	16.04
Roof	0.171	48.16	15	564	69.671	12.35
Total					**564.032**	**100**

The total heat loss of the building in this scenario is 564.033 kWh. A warm roof with 162.5 mm dry substrate produces approximately 69.671 kWh of heat loss, which are equivalent to 12.35% of the total loss.

b) <u>The green roof is saturated all the time</u>

The warm roof in this example is fitted with a green roof substrate in the saturated condition throughout the whole 564 hours. The thermal resistance of saturated green roof substrate ($R_{substrate}$) is 0.1007 m^2K/W. The heat loss of this building over the period of 564 hours can be calculated by using material properties outlined in tables B.3 and B.13. Consequently, the warm roof with saturated substrate's total thermal resistance ($R_{roof,sat}$) can be calculated from equation B.12.

$$R_{roof,sat} = R_{roof,out} + R_{substrate,\ sat} + R_{drainage} + R_{waterproof} + R_{insulation} + R_{deck} + R_{airspace} + R_{plasterboard} + R_{roof,in} \quad \text{(B.12)}$$

$R_{roof,sat}$ = 0.04 + 0.1007 + (0.05/0.14) + (0.01/0.23) + (0.111/0.025) + ((0.019/0.13) + 0.16 + (0.0125/0.21) + 0.10

$R_{roof,sat}$ = 5.44 m^2K/W

This R-value is equivalent to the U-value of 0.184 W/m^2K, which is lower than the Scottish standard (0.2 W/m^2K). As a result, the heat flow through each building component from the information given earlier will be calculated and summarised in the table B.16.

Table B.16 Heat loss through a warm roof with saturated 162.5 mm green roof and another building component

Element	**U-value (m^2K/W)**	**Area (m^2)**	**Tin-Tout (^oC)**	**Time (hour)**	**Q (kWh)**	**Percentage (%)**
Wall	0.270	74.16	15	564	169.396	29.75
Window	3.300	8.4	15	564	234.511	41.19
Floor	0.220	48.6	15	564	90.454	15.89
Roof	0.184	48.16	15	564	74.967	13.17
Total					**569.329**	**100**

The total heat loss of the building in this scenario is 569.330 kWh. A warm roof with 162.5 mm saturated substrate produces approximately 74.968 kWh of heat loss, which is equivalent to 13.17% of the total loss.

c) <u>Green roof with the actual moisture content</u>

The warm roof in this example is now fitted with a green roof substrate. However, the moisture condition is achieved from the 564 hours green roof substrate evaporation simulation. Thermal resistance of the green roof substrate over 564 hours (*with outdoor*

temperature 5°C, indoor temperature 20°C, 50% relative humidity, and 0.5 m/s wind speed) is shown in figure B.13.

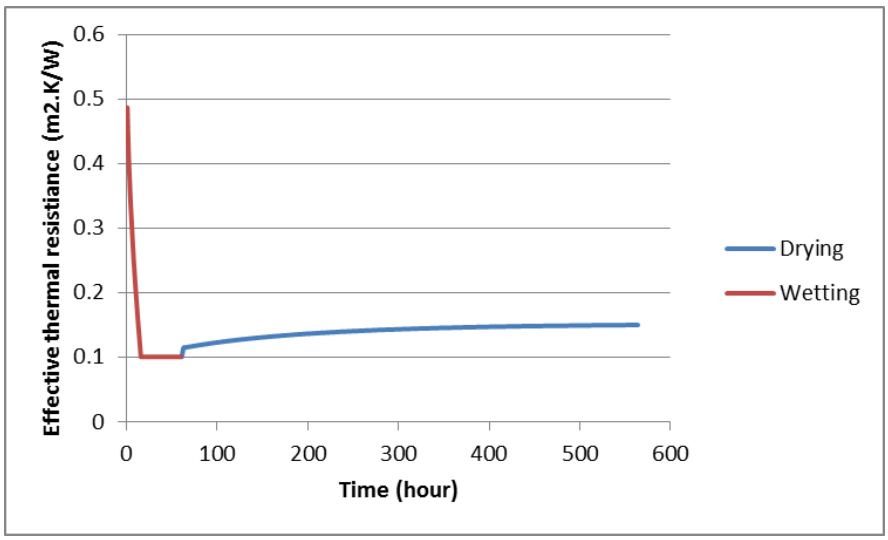

Figure B.13 Thermal resistance of 162.5 mm green roof substrate over 564 hours

The total thermal resistance of this roof (green roof and warm roof combined) over the period of 564 hours is presented in figure B.14.

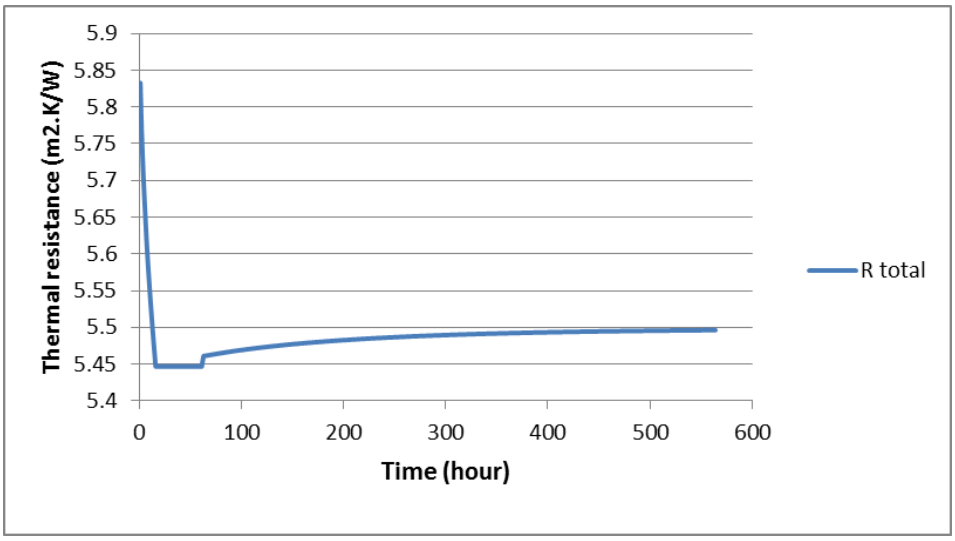

Figure B.14 Total thermal resistance of warm roof with 162.5 mm green roof

The hourly heat flow through this roof, with the given information, can be calculated and summarised in figure B.15.

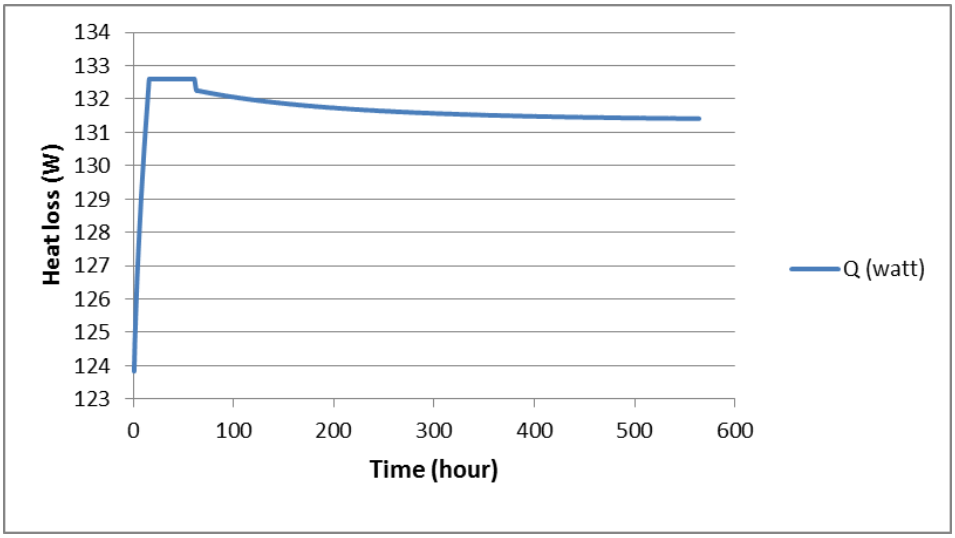

Figure B.15 Heat flow through the warm roof with 162.5 mm green roof in hourly basis

As a result, the heat flow through each building component from the information given earlier will be calculated and summarised in the table B.17.

Table B.17 Heat loss through warm roof with actual 162.5 mm green roof moisture content and another building component

Element	**U-value (m^2K/W)**	**Area (m^2)**	**Tin-Tout (^oC)**	**Time (hour)**	**Q (kWh)**	**Percentage (%)**
Wall	0.270	74.16	15	564	169.396	29.79
Window	3.300	8.4	15	564	234.511	41.24
Floor	0.220	48.6	15	564	90.454	15.91
Roof	vary	48.16	15	564	74.245	13.06
Total					**568.607**	**100**

The total heat loss of the building in this scenario is 568.607 kWh. A warm roof with 162.5 mm substrate (simulated moisture content) produces approximately 74.246 kWh of heat loss, which is equivalent to 13.06% of the total loss.

B.3.2 The building with a domestic warm roof and 300 mm green roof substrate on top

The warm roof is now retrofitted with a 300mm intensive green roof system, as show in figure B.16.

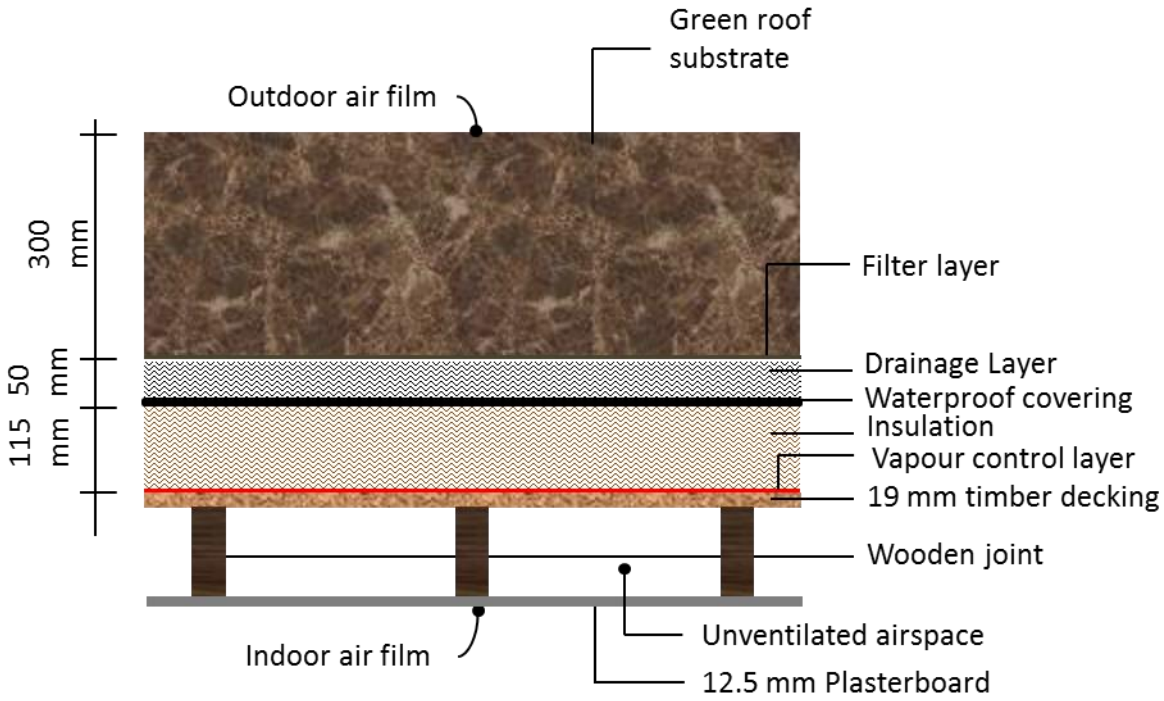

Figure B.16 The warm roof with 300 mm green roof substrate

The total heat loss for this roof will be calculated for three substrate conditions: i) the dry substrate, ii) saturated substrate, and iii) substrate with varying levels of moisture content from wet to dry.

a) <u>The green roof is completely dry all the time</u>

The warm roof in this example is fitted with a 300 mm green roof substrate in the dry condition throughout 564 hours, for which the thermal resistance of substrate ($R_{substrate}$) is 1.008m^2K/W. The heat loss of this building is calculated over the period of 564 hours by using the thermal properties of some building materials, as shown in tables B.3 and B.13.

The roof's total thermal resistance ($R_{roof,dry}$) can be calculated from equation B.13.

$$R_{roof,dry} = R_{roof,out} + R_{substrate,\ dry} + R_{drainage} + R_{waterproof} + R_{insulation} + R_{deck} + R_{airspace} + R_{plasterboard} + R_{roof,in} \quad (B.13)$$

$R_{roof,dry}$ = 0.04 + 1.008 + (0.05/0.14) + (0.01/0.23) + (0.115/0.025) + (0.019/0.13) + 0.16 + (0.0125/0.21) + 0.10

R_{roof} = 6.35 m^2K/W

This R-value is equivalent to the U-value of 0.157 W/m^2K, which is much lower than the Scottish standard (0.2 W/m^2K). With the given information, the heat flow through each element can be calculated, and is summarised in table B.18.

Table B.18 Heat loss through a warm roof with dry 300 mm green roof and another building component

Element	U-value (m^2K/W)	Area (m^2)	Tin-Tout (^oC)	Time (hour)	Q (kWh)	Percentage (%)
Wall	0.270	74.16	15	564	169.396	30.34
Window	3.300	8.4	15	564	234.511	42.00
Floor	0.220	48.6	15	564	90.454	16.20
Roof	0.157	48.16	15	564	63.967	11.46
Total					**558.328**	**100**

The total heat loss of the building in this scenario is 558.329 kWh. A warm roof with 300 mm dry substrate produces approximately 63.967 kWh of heat loss, which are equivalent to 11.46% of the total heat loss.

b) Green roof is completely saturated all the time

The warm roof in this example is now fitted with a green roof substrate in the saturated condition throughout the whole 564 hours. The thermal resistance of saturated 300 mm substrate ($R_{substrate}$) is 0.186m^2K/W. The heat loss of this building was calculated over the period of 564 hours.

By using the thermal conductivity data given in tables B.3 and B.13, the warm roof with 300 mm saturated substrate's total thermal resistance ($R_{roof,sat}$) can be calculated from equation B.14.

$R_{roof,sat} = R_{roof,out} + R_{substrate,\ sat} + R_{drainage} + R_{waterproof} + R_{insulation} + R_{deck} + R_{airspace} + R_{plasterboard} + R_{roof,in}$ (B.14)

$R_{roof,sat}$ = 0.04 + 0.186 + (0.05/0.14) + (0.01/0.23) + (0.115/0.025) + (0.019/0.13) + 0.16 + (0.0125/0.21) + 0.10

$R_{roof,sat}$ = 5.53 m^2K/W

This R-value is equivalent to the U-value of 0.181 W/m^{2}K, which is lower than the Scottish standard (0.2 W/m^{2}K). As a result, the heat flow through each building component from the information given earlier will be calculated and summarised in the table B.19.

Table B.19 Heat loss through warm roof with saturated 300 mm green roof and another building component

Element	**U-value (m^{2}K/W)**	**Area (m^2)**	**Tin-Tout (^{o}C)**	**Time (hour)**	**Q (kWh)**	**Percentage (%)**
Wall	0.270	74.16	15	564	169.396	29.82
Window	3.300	8.4	15	564	234.511	41.28
Floor	0.220	48.6	15	564	90.454	15.92
Roof	0.181	48.16	15	564	73.745	12.98
Total					**568.107**	**100**

The total heat loss of the building in this scenario is 568.107 kWh. A warm roof with a 300 mm saturated green roof substrate produces approximately 73.745 kWh of heat loss, which is equivalent to 12.98% of the total heat loss.

c) A green roof with the actual moisture content

The warm roof in this example is now fitted with a green roof substrate, but the moisture condition is archived from the 564 hours green roof substrate evaporation simulation. Thermal resistance of green roof substrate over 564 hours (*with outdoor temperature 5^{o}C, indoor temperature 20^{o}C, 50% relative humidity, and 0.5 m/s wind speed*) is presented in figure B.17.

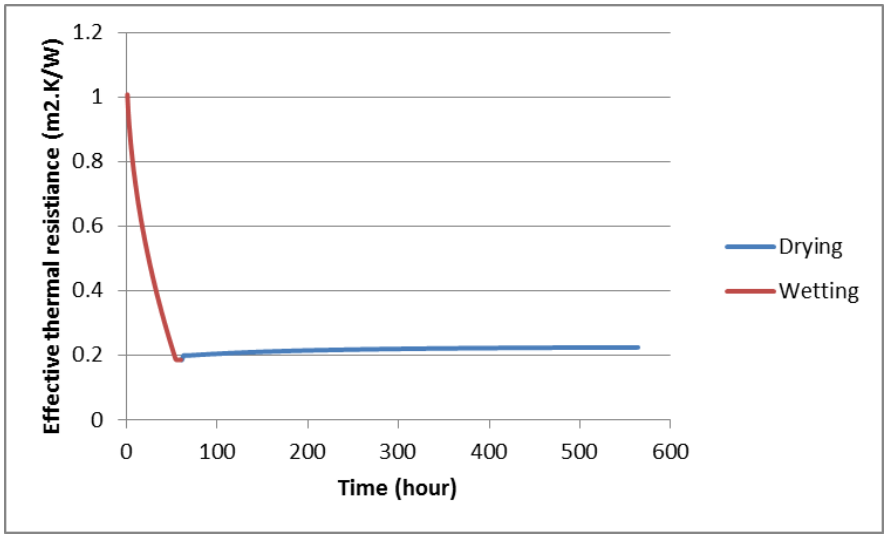

Figure B.17 Thermal resistance of 300 mm green roof substrate over 564 hours

The hourly thermal resistance of this roof (green roof and warm roof combined) over the period of 564 hours is presented in figure B.18.

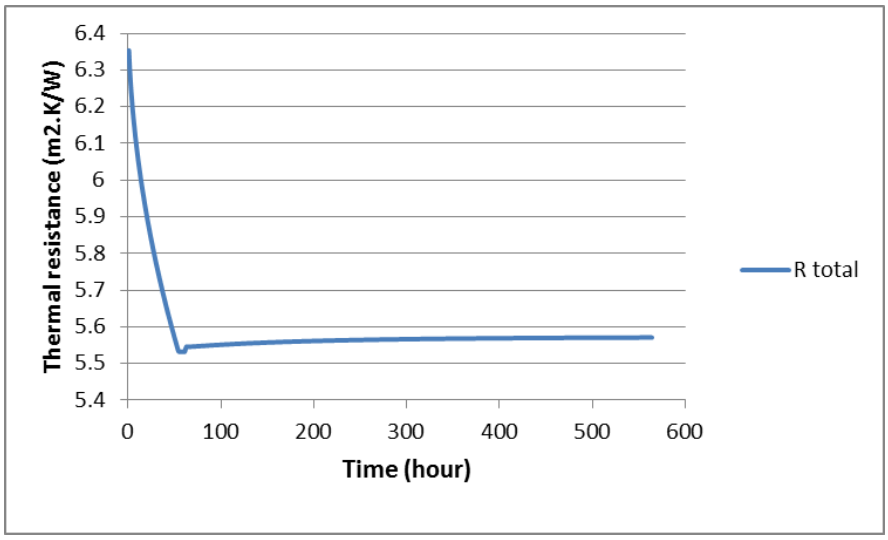

Figure B.18 Hourly thermal resistance of warm roof with 300 mm substrate

The hourly heat flow through this roof, with the given information, can be calculated and is summarised in figure B.19.

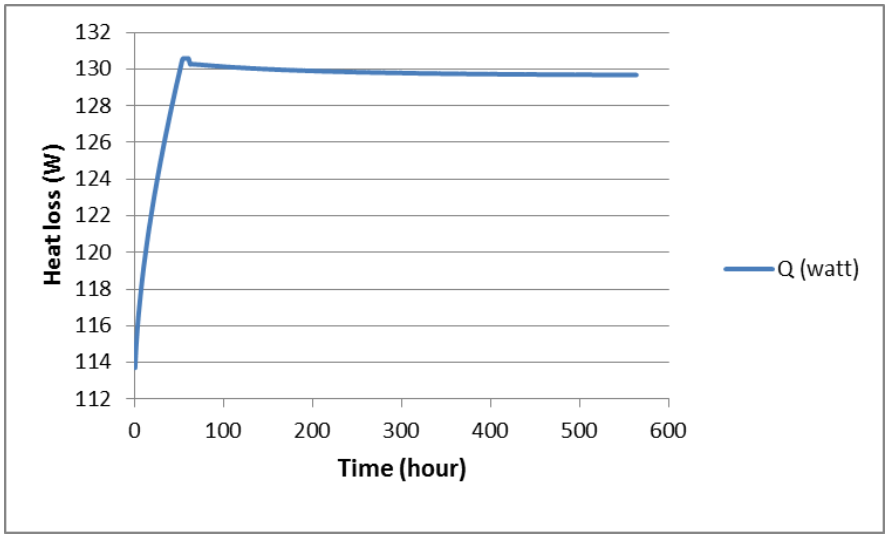

Figure B.19 Heat flow through the warm roof with 300 mm green roof in hourly basis

As a result, the heat flow through each building component from the information given earlier will be calculated and summarised in the table B.20.

Table B.20 Heat loss through warm roof with actual 300 mm green roof moisture content and another building component

Element	**U-value (m^2K/W)**	**Area (m^2)**	**Tin-Tout (^oC)**	**Time (hour)**	**Q (kWh)**	**Percentage (%)**
Wall	0.270	74.16	15	564	169.396	30.09
Window	3.300	8.4	15	564	234.511	41.65
Floor	0.220	48.6	15	564	90.454	16.07
Roof	Vary	48.16	15	564	68.667	12.20
Total					**563.028**	**100**

The total heat loss of the building in this scenario is 563.028 kWh. A warm roof with 300 mm substrate (simulated moisture content) produces approximately 68.667 kWh of heat loss; the equivalent to 12.20% of the total loss.

Energy saving comparisons

In order to compare the heat energy saving from green roof installation, six examples from two green roof substrate depths are compared by using the warm roof with no green roof system. The percentages of heating energy saving of each scenario are showing in the figure B.20 and table B.21.

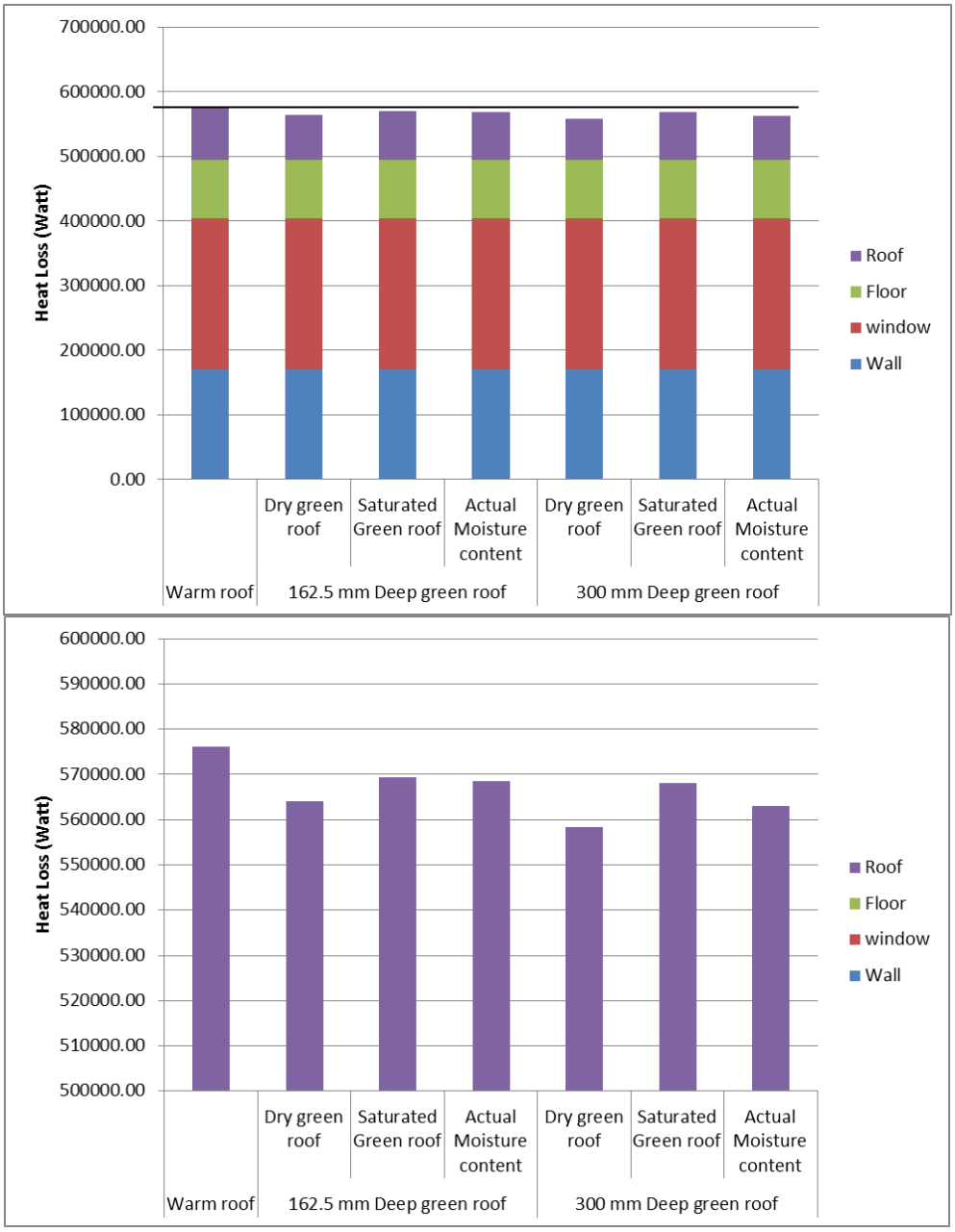

Figure B.20 Energy saving from green roof on the warm roof, with enlarged heat loss scale below

Table B.21 Comparison of heat loss of 162.5 mm and 300 mm green roof substrate over the domestic warm roof in different condition

	Heat loss (kWh)						
Element	**Warm roof**	**162.5 mm deep green roof**			**300 mm deep green roof**		
		Dry green roof	**Saturated green roof**	**Actual moisture content**	**Dry green roof**	**Saturated green roof**	**Actual moisture content**
Wall	169.396	169.396	169.396	169.396	169.396	169.396	169.396
Window	234.511	234.511	234.511	234.511	234.511	234.511	234.511
Floor	90.454	90.454	90.454	90.454	90.454	90.454	90.454
Roof	81.663	69.671	74.967	74.245	63.967	73.745	68.667
Total	576.025	564.032	569.329	568.607	558.328	568.107	563.028
Saving (%)		**2.08**	**1.16**	**1.29**	**3.07**	**1.37**	**2.26**

Thermal insulation thickness reduction

In this section, the effect of heating energy saving from green roof installation on the domestic warm roof is now replaced with the insulation thickness reduction. The original thickness of the polyurethane insulation in this roof is 111 mm, which brings the total U-value of this roof close to the U-value that is required in the regulations (0.2 $W/m^2.K$). As a result, the insulation thickness needs to be revised after a green roof is installed.

The insulation reduction can be calculated from the thermal transmittance equation B.15.

$$1/U = R_{roof,out} + R_{substrate} + R_{drainage} + R_{waterproof} + R_{insulation} + R_{bitumen} + R_{screed} + R_{concrete} + R_{roof,in} \quad \text{(B.15)}$$

By using information given in the previous section, the $R_{substrate}$ is changed according to the substrate condition and the $R_{insulation}$ is now replaced with $thickness/k_{insulation}$. In order to archive the certain value of U-value, the thickness of insulation can be determined by equation B.16.

$$Thickness = k_{insulation}\,(1/U - (R_{roof,out} + R_{substrate} + R_{drainage} + R_{waterproof} + R_{bitumen} + R_{screed} + R_{concrete} + R_{roof,in})) \quad \text{(B.16)}$$

Thicknesses of the inverted roof's insulation in different green roof substrate conditions are calculated and shown in table B.22.

Table B.22 Thermal insulation thickness reduction of warm roof (1)

Condition	Inverted roof	162.5 mm deep green roof		300 mm deep green roof	
		Dry green roof	Saturated green roof	Dry green roof	Saturated green roof
Insulation thickness (mm)	111	90	100	77	97.5
Insulation thickness reduction (mm)	-	21	11	34	13.5

The green roof with simulated moisture content, on the other hand, cannot be calculated directly as previous scenarios. The thickness of insulation in this scenario is revised from the total hourly heat loss from the purely inverted roof system over the simulation

time. The thickness of insulation can be found by using the trial and error method, in order to get the nearest value of the total heat loss through the roof.

The total heat loss from warm roof over 564 hours is 81.664 kWh. The purely inverted roof thermal resistance (except green roof system) required to reach that amount of heat loss is approximately 4.40 m^2K/W, after the green roof was simulated with actual moisture content. This value can be converted into the thickness of insulation, which is equivalent to 99 and 96.1 mm (162.5 mm and 300 mm substrate depth). For this reason, the thickness of thermal insulation and its reduction in each scenario can be represented again in table B.23.

Table B.23 Thermal insulation thickness reduction of warm roof (2)

Condition	Warm roof	162.5 mm deep green roof			300 mm deep green roof		
		Dry green roof	Saturated green roof	Actual moisture content	Dry green roof	Saturated green roof	Actual moisture content
Insulation thickness (mm)	111	90	100	99	77	97.5	96.1
Insulation thickness reduction (mm)	-	21	11	12	34	13.5	14.9

From the table B.23, the roof with dry substrate yields the maximum thermal insulation thickness reduction in every case, and the saturated substrate and simulated moisture content substrate produce very similar thickness reduction when compared.

B.4 The building with metal decking

Scenario 3 is the shoebox-shaped building with a metal decking warm roof over the steel structure. According to Scottish government building standards for domestic building section 3.10.7 (2016), the metal decking warm roof is a flat roof structure of metal-framed construction with a troughed metal decking; with or without a ceiling or soffit. Externally there is a weatherproof covering, insulation and a vapour control layer. This roof construction detail is shown in figure B.21.

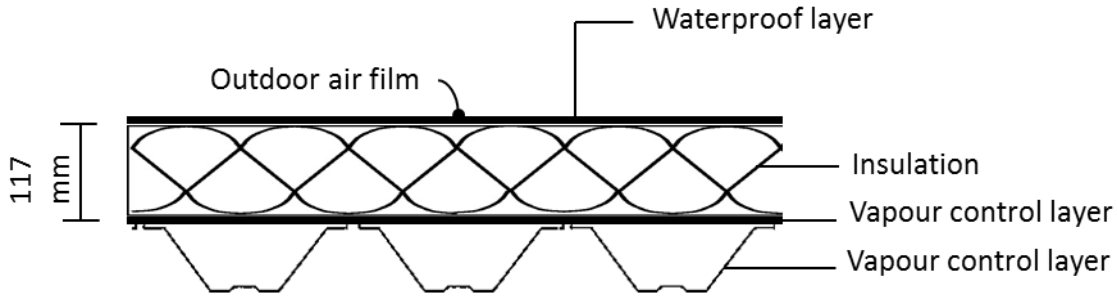

Figure B.21 Metal decking warm roof construction detail

The thermal properties of some building materials constructed into this roof are shown in the table B.24 (Chartered Institution of Building Services, 2006).

Table B.24 Thermal conductivities of materials in metal decking

Material	**Thermal conductivity, k (W/m.K)**	**Thickness (mm)**
Waterproof covering	0.23	10
Polyurethane insulation	0.025	117

The metal roof's total thermal resistance (R_{roof}) can be calculated from equation B.17.

$$R_{roof} = R_{roof,out} + R_{waterproof} + R_{insulation} + R_{airspace} + R_{roof,in} \quad \text{(B.17)}$$

$$R_{roof} = 0.04 + (0.01/0.23) + (0.117/0.025) + 0.16 + 0.10$$

$$R_{roof} = 5.023\ m^2K/W$$

This R-value is equivalent to the U-value of 0.199W/m^2K, which is exactly equivalent to the Scottish standard (0.2 W/m^2K). Therefore, the heat flow through each building component from the information given earlier (table B.24) will be calculated and summarised in the table B.25.

Table B.25 Heat loss through metal decking roof and another building component

Element	U-value (m^2K/W)	Area (m^2)	Tin-Tout (^oC)	Time (hour)	Q (kWh)	Percentage (%)
Wall	0.270	74.16	15	564	169.396	29.41
Window	3.300	8.4	15	564	234.511	40.71
Floor	0.220	48.6	15	564	90.454	15.70
Roof	0.199	48.16	15	564	81.105	14.09
Total					**575.467**	**100**

The total heat loss from the building in this scenario is 575.468 kWh. A metal roof yields approximately 81.106 kWh of heat loss, which is equivalent to 14.09% of the total heat loss.

B.4.1 The metal roof with 162.5 mm green roof substrate on top

The metal roof is now retrofitted with 162.5 mm semi-intensive green roof system, as show in figure B.22.

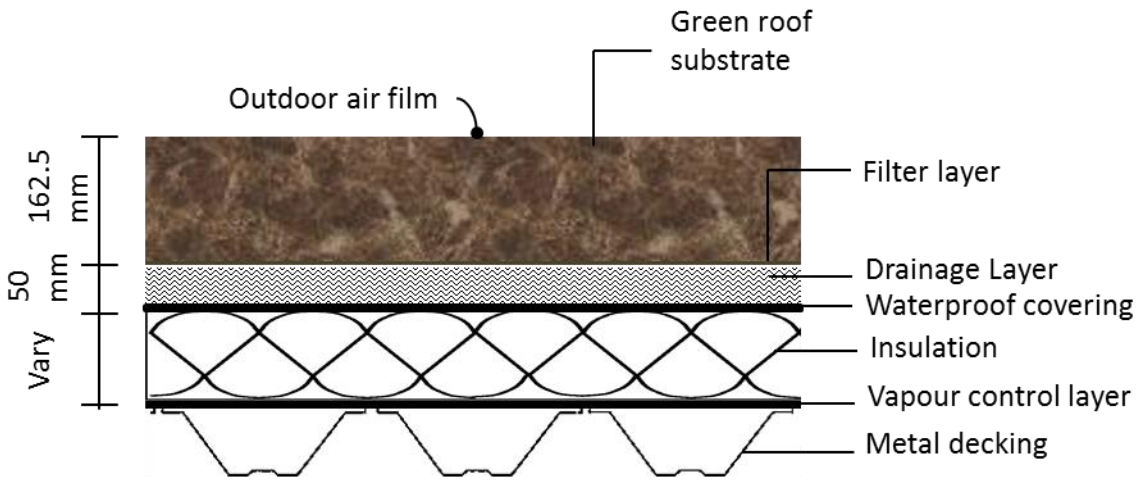

Figure B.22 The domestic warm roof with 162.5 mm green roof system

The total heat loss from this roof will be calculated for three substrate conditions: i) the dry substrate, ii) saturated substrate, and iii) substrate with varying moisture content from wet to dry.

a) <u>The green roof is completely dry all the time</u>

The metal decking roof in this example is fitted with green roof substrate in the dry condition throughout the whole 564 hours. The thermal resistance of dry green roof

substrate ($R_{substrate}$) is 0.487m^2K/W. The heat loss of this building over the period of 564 hours can be calculated by using the information given in tables B.3 and B.24.

The metal roof's total thermal resistance (R_{roof}) can be calculated from equation B.18.

$$R_{roof} = R_{roof,out} + R_{substrate,\ dry} + R_{drainage} + R_{waterproof} + R_{insulation} + R_{airspace} ++ R_{roof,in} \quad (B.18)$$

$$R_{roof} = 0.04 + 0.487 + (0.05/0.14) + (0.01/0.23) + (0.117/0.025) + 0.16 + 0.10$$

$$R_{roof} = 5.87\ m^2K/W$$

This R-value is equivalent to the U-value of 0.17 W/m^2K, which is lower than the Scottish standard (0.2W/m^2K). Therefore, the heat flow through each building component from the information given earlier will be calculated and summarised in the table B.26.

Table B.26 Heat loss through metal roof with dry 162.5 mm green roof and another building component

Element	**U-value (m^2K/W)**	**Area (m^2)**	**Tin-Tout (^oC)**	**Time (hour)**	**Q (kWh)**	**Percentage (%)**
Wall	0.270	74.16	15	564	169.396	30.03
Window	3.300	8.4	15	564	234.511	41.58
Floor	0.220	48.6	15	564	90.454	16.04
Roof	0.170	48.16	15	564	69.437	12.32
Total					**563.799**	**100**

The total heat loss of the building in this scenario is 563.799 kWh. A metal roof with 162.5 mm dry substrate yields approximately 69.437 kWh of heat loss, which is equivalent to 12.32% of the total loss.

b) <u>The green roof is saturated all the time</u>

The metal decking roof in this example is fitted with green roof substrate in the saturated condition throughout the whole 564 hours. The thermal resistance of saturated green roof substrate ($R_{substrate}$) is 0.1007m^2K/W. The heat loss of this building, over the period of 564 hours, can be calculated by using the material properties in tables B.3 and B.24. Consequently, the total thermal resistance ($R_{roof,sat}$) of the roof with a saturated substrate can be calculated from equation B.19.

$$R_{roof,sat} = R_{roof,out} + R_{substrate,sat} + R_{drainage} + R_{waterproof} + R_{insulation} + R_{airspace} + \quad (B.19)$$

$R_{roof,in}$

$R_{roof,sat} = 0.04 + 0.1007 + (0.05/0.14) + (0.01/0.23) + (0.117/0.025) + 0.16 + 0.10$

$R_{roof,sat} = 5.48\ m^2K/W$

This R-value is equivalent to the U-value of $0.182 W/m^2K$, which is lower than the Scottish standard ($0.2\ W/m^2K$). Therefore, the heat flow through each building component from the information given earlier will be calculated and summarised in the table B.27.

Table B.27 Heat loss through warm roof with saturated 162.5 mm green roof and another building component

Element	**U-value (m^2K/W)**	**Area (m^2)**	**Tin-Tout (^oC)**	**Time (hour)**	**Q (kWh)**	**Percentage (%)**
Wall	0.270	74.16	15	564	169.396	29.75
Window	3.300	8.4	15	564	234.511	41.19
Floor	0.220	48.6	15	564	90.454	15.89
Roof	0.182	48.16	15	564	74.331	13.07
Total					**568.693**	**100**

The total heat loss of the building in this scenario is 568.693 kWh. A metal roof with 162.5 mm saturated substrate yields approximately 74.331 kWh of heat loss, which are the equivalent to 13.07% of the total heat loss.

c) A green roof with the actual moisture content

The metal roof in this case is now fitted with a green roof substrate. However, the moisture condition is achieved from the 564 hour green roof substrate evaporation simulation. Thermal resistance of the green roof substrate over 564 hours (*with outdoor temperature 5^oC, indoor temperature 20^oC, 50% relative humidity, and 0.5 m/s wind speed*) is shown in figure B.23.

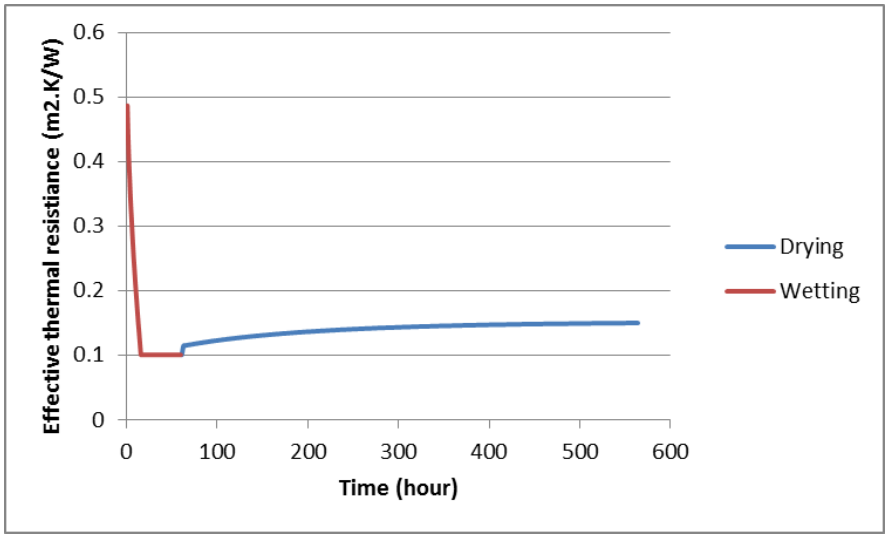

Figure B.23 Thermal resistance of 162.5 mm green roof substrate over 564 hours

The total thermal resistance of this roof (green roof and inverted roof combined) over the period of 564 hours is presented in figure B.24.

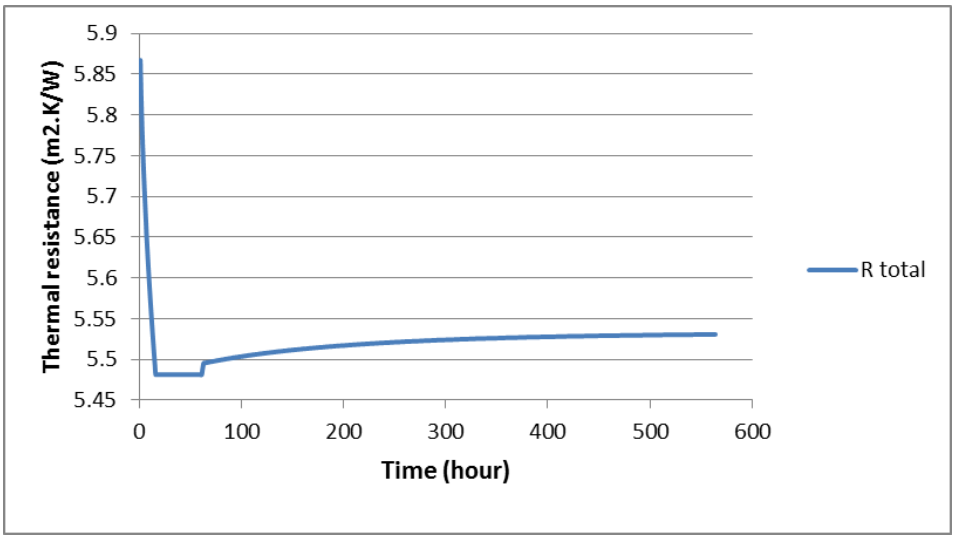

Figure B.24 Total thermal resistance of metal roof with 162.5 mm green roof

The hourly heat flow through this roof with the given information can be calculated and is summarised in figure B.25.

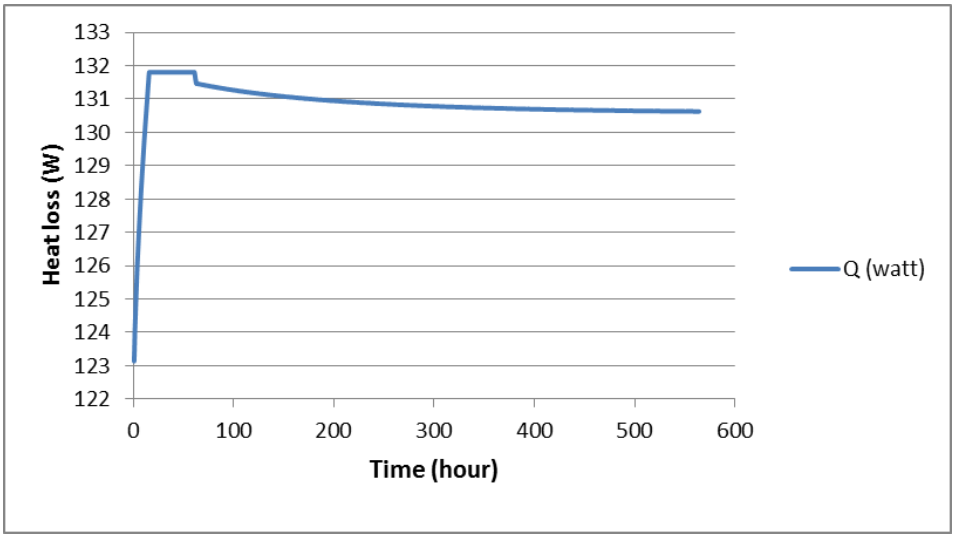

Figure B.25 Heat flow through the metal roof with 162.5 mm green roof in hourly basis

Therefore, the heat flow through each building component from the information given earlier will be calculated and summarised in the table B.28.

Table B.28 Heat loss through metal roof with actual 162.5 mm green roof moisture content and another building component

Element	**U-value (m^2K/W)**	**Area (m^2)**	**Tin-Tout (^oC)**	**Time (hour)**	**Q (kWh)**	**Percentage (%)**
Wall	0.270	74.16	15	564	169.396	29.79
Window	3.300	8.4	15	564	234.511	41.24
Floor	0.220	48.6	15	564	90.454	15.91
Roof	vary	48.16	15	564	73.801	12.99
Total					**568.163**	**100**

The total heat loss of the building in this scenario is 568.164 kWh. A metal roof with 162.5 mm substrate (simulated moisture content) yields approximately 73.802 kWh of heat loss, which are equivalent to 12.99% of the total heat loss.

B.4.2 The metal roof with a 300 mm green roof substrate on top

The metal roof in section B.4 is now retrofitted with 300mm an intensive green roof system, as show in figure B.26.

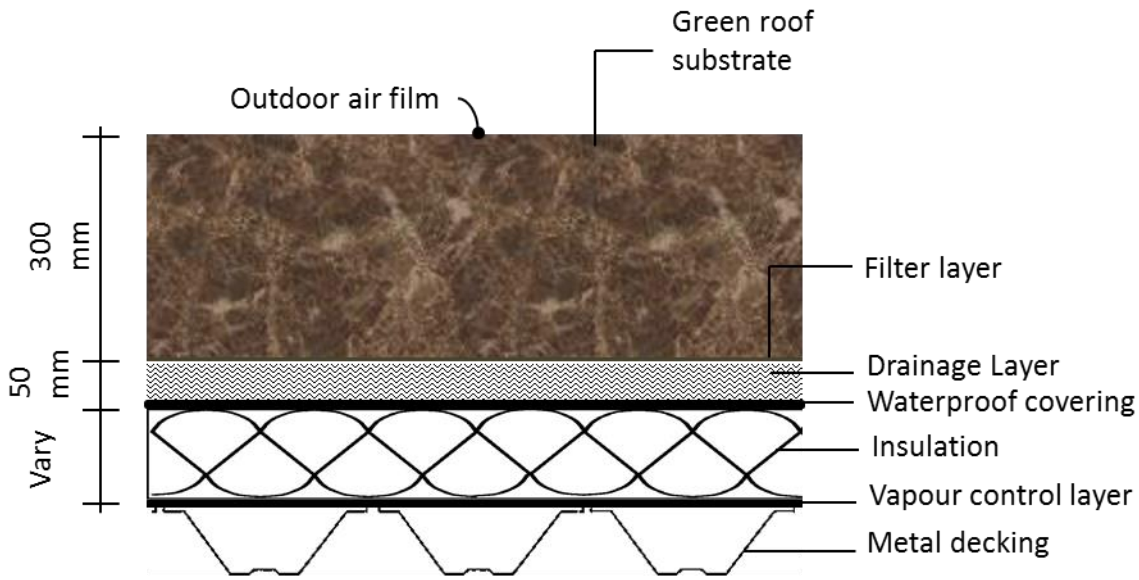

Figure B.26 The metal roof with a 300 mm green roof substrate

The total heat loss of this roof will be calculated with three different substrate conditions: i) dry substrate, ii) saturated substrate, and iii) substrate with varying moisture levels from wet to dry.

a) <u>Green roof is completely dry all the time</u>

The metal decking roof in this example is fitted with a 300mm green roof substrate in the dry condition throughout 564 hours; the thermal resistance of the substrate ($R_{substrate}$) being 1.008m^2K/W. The heat loss of this building is calculated over the period of 564 hours by using the thermal properties of some building materials, as noted in tables B.3 and B.24.

The roof's total thermal resistance ($R_{roof,dry}$) can be calculated from equation B.20.

$$R_{roof,dry} = R_{roof,out} + R_{substrate,\ dry} + R_{drainage} + R_{waterproof} + R_{insulation} + R_{airspace} + R_{roof,in} \quad \text{(B.20)}$$

$$R_{roof,dry} = 0.04 + 1.008 + (0.05/0.14) + (0.01/0.23) + (0.117/0.025) + 0.16 + 0.10$$

$$R_{roof} = 6.39\ m^2K/W$$

This R-value is equivalent to the U-value of 0.157 W/m^2K, which is significantly lower than the Scottish standard (0.2 W/m^2K). With the given information, the heat flow through each element can be calculated and is summarised in table B.29.

Table B.29 Heat loss through metal roof with dry 300 mm green roof and another building component

Element	U-value (m^2K/W)	Area (m^2)	Tin-Tout (^oC)	Time (hour)	Q (kWh)	Percentage (%)
Wall	0.270	74.16	15	564	169.396	30.35
Window	3.300	8.4	15	564	234.511	42.02
Floor	0.220	48.6	15	564	90.454	16.21
Roof	0.157	48.16	15	564	63.774	11.43
Total					**558.136**	**100**

The total heat loss of the building in this scenario is 558.137 kWh. A metal roof with dry substrate yields approximately 63.775 kWh of heat loss, which is equivalent to 11.43% of the total.

b) Green roof is completely saturated all the time

The metal roof in this example is now fitted with a green roof substrate in the saturated condition throughout the whole 564 hours. The thermal resistance of 300mm saturated substrate ($R_{substrate}$) is 0.186m^2K/W, with the heat loss of this building being calculated over the period of 564 hours.

By using thermal conductivity data given in tables B.3 and B.24, the total thermal resistance ($R_{roof,sat}$) of the metal roof with its 300 mm saturated substrate can be calculated from equation B.21.

$$R_{roof,sat} = R_{roof,out} + R_{substrate,\ sat} + R_{drainage} + R_{waterproof} + R_{insulation} + R_{airspace} + R_{roof,in} \quad \text{(B.21)}$$

$R_{roof,sat} = 0.04 + 0.186 + (0.05/0.14) + (0.01/0.23) + (0.117/0.025) + 0.16 + 0.10$

$R_{roof,sat} = 5.57\ m^2K/W$

This R-value is equivalent to the U-value of 0.180W/m^2K, which is lower than the Scottish standard (0.2 W/m^2K). Therefore, the heat flow through each building component from the information given earlier will be calculated and summarised in the table B.30.

Table B.30 Heat loss through metal roof with saturated 300 mm green roof and another building component

Element	U-value (m^2K/W)	Area (m^2)	Tin-Tout (^oC)	Time (hour)	Q (kWh)	Percentage (%)
Wall	0.270	74.16	15	564	169.396	29.85
Window	3.300	8.4	15	564	234.511	41.32
Floor	0.220	48.6	15	564	90.454	15.94
Roof	0.180	48.16	15	564	73.192	12.90
Total					**567.554**	**100**

The total heat loss of the building in this scenario is 567.554 kWh. A metal roof with 300 mm saturated green roof substrate yields approximately 73.192 kWh of heat loss, which is equivalent to 12.90% of the total heat loss.

c) Green roof with the actual moisture content

The metal roof in this example is now fitted with a green roof substrate, but the moisture condition is archived from the 564 hours green roof substrate evaporation simulation. The thermal resistance of a green roof substrate over 564 hours (*with outdoor temperature 5^{o}C, indoor temperature 20^{o}C, 50% relative humidity, and 0.5 m/s wind speed*) is shown in figure B.27.

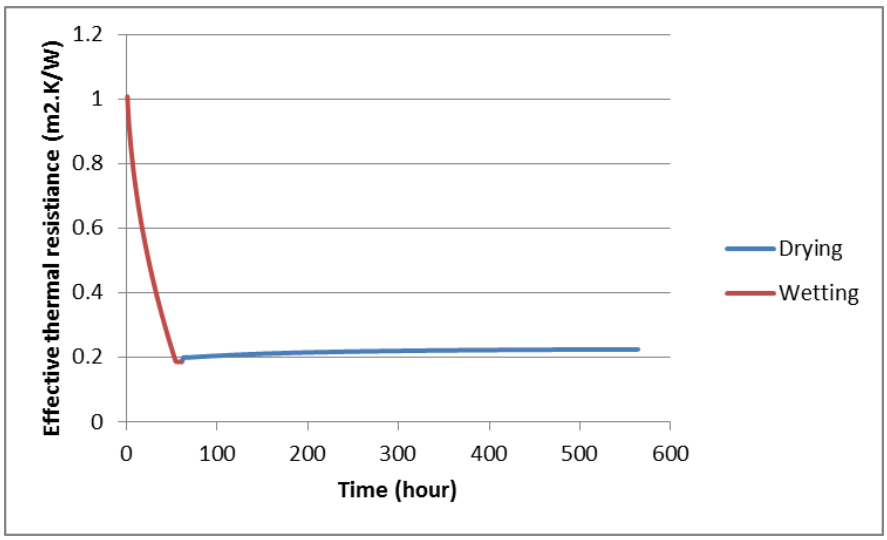

Figure B.27 Thermal resistance of 300 mm green roof substrate over 564 hours

The hourly thermal resistance of this roof (green roof and metal roof combined) over the period of 564 hours is presented in figure B.28.

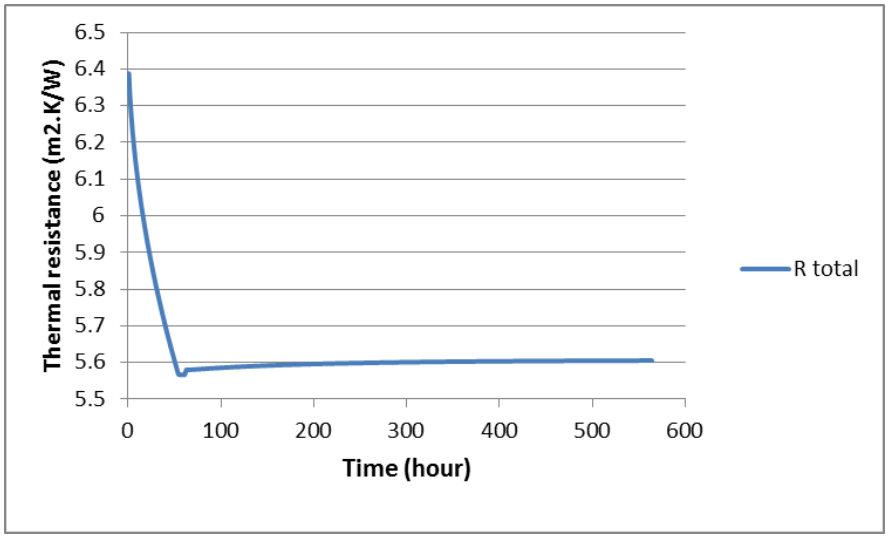

Figure B.28 Hourly thermal resistance of metal roof with 300 mm substrate

The hourly heat flow through this roof with the given information can be calculated and is summarised in figure B.29.

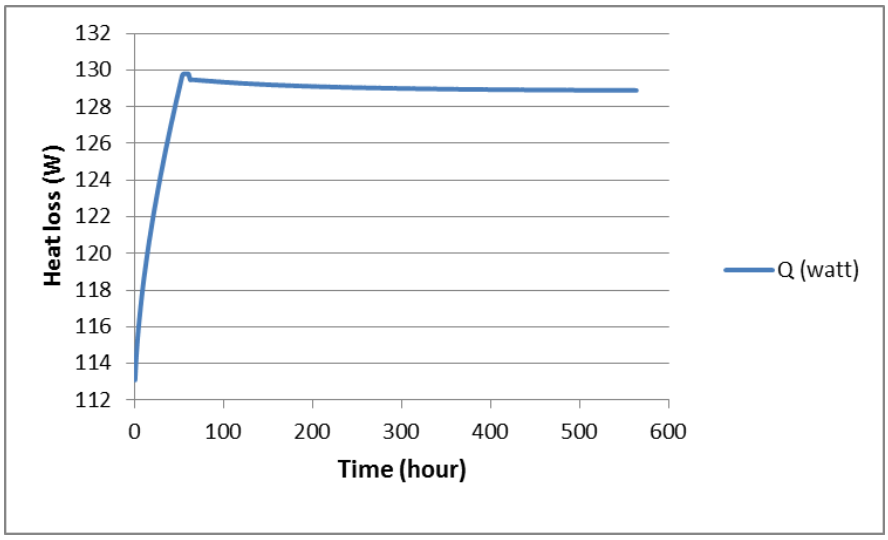

Figure B.29 Heat flow through the metal roof with 300 mm green roof in hourly basis

Therefore, the heat flow through each building component from the information given earlier will be calculated and summarised in the table B.31.

Table B.31 Heat loss through metal roof with actual 300 mm green roof moisture content and another building component

Element	**U-value (m^2K/W)**	**Area (m^2)**	**Tin-Tout (^oC)**	**Time (hour)**	**Q (kWh)**	**Percentage (%)**
Wall	0.270	74.16	15	564	169.396	29.88
Window	3.300	8.4	15	564	234.511	41.37
Floor	0.220	48.6	15	564	90.454	15.96
Roof	vary	48.16	15	564	72.466	12.78
Total					**566.828**	**100**

The total heat loss of the building in this scenario is 566.828 kWh. A metal roof with 300 mm substrate (simulated moisture content) yields approximately 72.466 kWh of heat loss, which are equivalent to 12.78% of the total.

Energy saving comparisons

In order to compare the saving from green roof installation, six examples from two green roof substrate depths are compared, by using the metal decking roof with no green roof system as a reference. The percentages of heating energy saving of each scenario are shown in figure B.30 and table B.32.

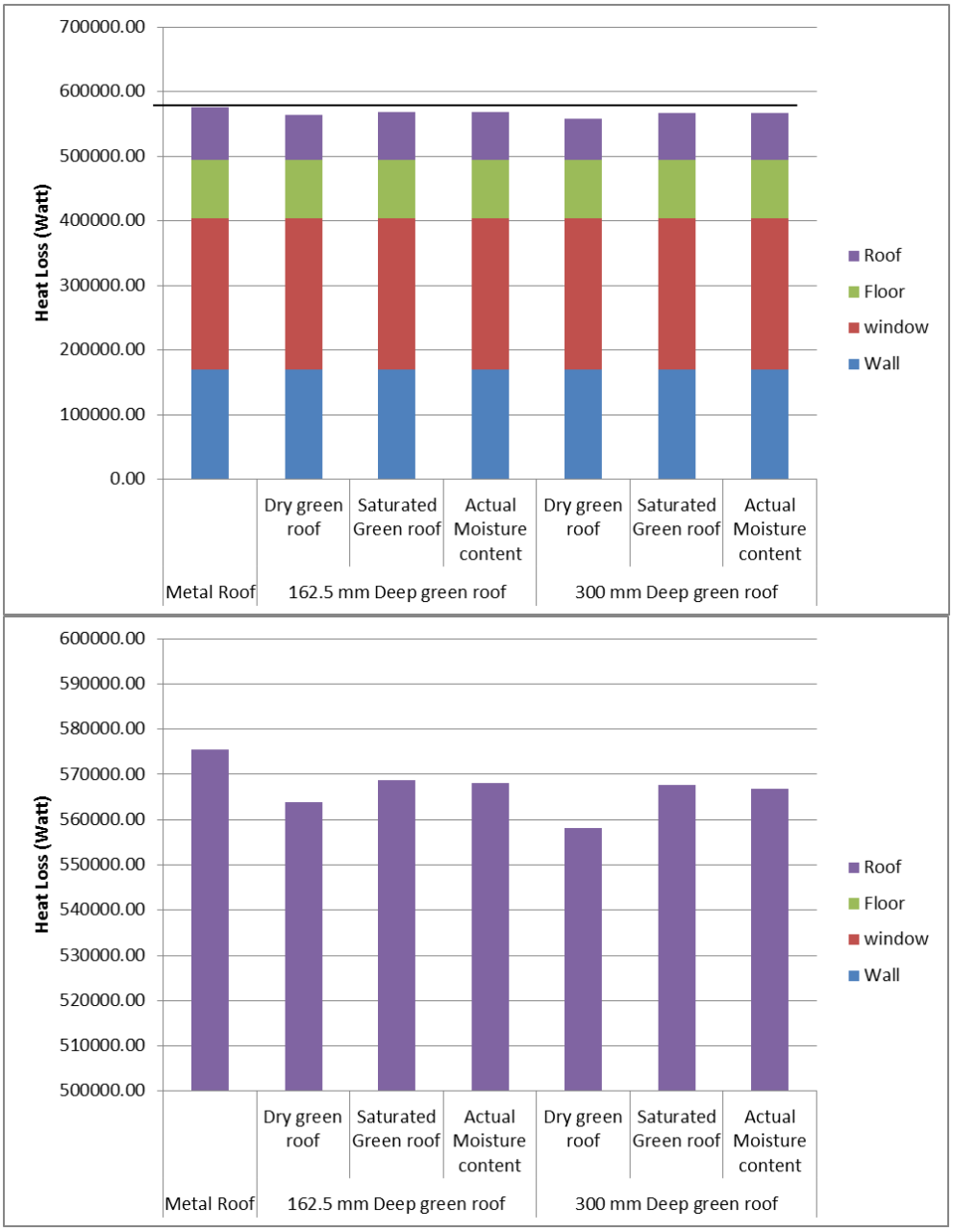

Figure B.30 Energy saving from green roof on the metal roof, with enlarged heat loss scale below

Table B.32 Comparison of heat loss of 162.5 mm and 300 mm green roof substrates over metal decking in different conditions

	Heat loss (kWh)						
Element	**Metal roof**	**162.5 mm deep green roof**			**300 mm deep green roof**		
		Dry green roof	**Saturated green roof**	**Actual moisture content**	**Dry green roof**	**Saturated green roof**	**Actual moisture content**
Wall	169.396	169.396	169.396	169.396	169.396	169.396	169.396
Window	234.511	234.511	234.511	234.511	234.511	234.511	234.511
Floor	90.454	90.454	90.454	90.454	90.454	90.454	90.454
Roof	81.105	69.437	74.331	73.801	63.774	73.192	72.466
Total	575.467	563.799	568.693	568.163	558.136	567.554	566.828
Saving (%)		**2.03**	**1.18**	**1.27**	**3.01**	**1.38**	**1.50**

Thermal insulation thickness reduction

In this section, the effect of heating energy saving from a green roof installation on the metal roof is now replaced with insulation thickness reduction. The original insulation thickness of this roof (polyurethane) is 117 mm, which brings the total U-value of this roof close to the U-value requirement (0.2 $W/m^2.K$). Therefore, the insulation thickness needs to be revised after a green roof is installed.

The insulation reduction can be calculated from the thermal transmittance equation B.22.

$$1/U = R_{roof,out} + R_{substrate} + R_{drainage} + R_{waterproof} + R_{insulation} + R_{airspace} + R_{roof,in} \quad \text{(B.22)}$$

By using information given in the previous section, the $R_{substrate}$ is changed according to the substrate condition and the $R_{insulation}$ is now replaced with $thickness/k_{insulation}$. In order to archive the certain value of U-value, the thickness of insulation can be determined by equation B.23.

$$Thickness = k_{insulation}\,(1/U - (R_{roof,out} + R_{substrate} + R_{drainage} + R_{waterproof} + R_{airspace} + R_{roof,in})) \quad \text{(B.23)}$$

Thicknesses of the inverted roof's insulation in different green roof substrate conditions are calculated and shown in table B.33.

Table B.33 Thermal insulation thickness reduction of metal roof (1)

Condition	Metal roof	162.5 mm deep green roof		300 mm deep green roof	
		Dry green roof	Saturated green roof	Dry green roof	Saturated green roof
Insulation thickness (mm)	117	95.5	105	77	97.5
Insulation thickness reduction (mm)	-	21.5	12	34	13.5

The green roof with simulated moisture content, on the other hand, cannot be calculated directly, as done in previous scenarios. The thickness of insulation in this scenario is informed by the total hourly heat loss from the purely inverted roof system over the simulation time. The thickness of insulation can be found by using a trial and error method, in order to establish the nearest value of the total heat loss through the roof.

The total heat loss from the warm roof over 564 hours is 81.106 kWh. The purely inverted roof thermal resistance (except green roof system) required to reach that amount of heat loss is approximately 4.40 m^2K/W, after the green roof was simulated with actual moisture content. This value can be converted into the thickness of insulation, which is equivalent to 104.6 and 102 mm (162.5 mm and 300 mm substrate depth). For this reason, the thickness of thermal insulation and its reduction in each scenario can be presented again in table B.34.

Table B.34 Thermal insulation thickness reduction of metal roof (2)

Condition	Metal roof	162.5 mm deep green roof			300 mm deep green roof		
		Dry green roof	Saturated green roof	Actual moisture content	Dry green roof	Saturated green roof	Actual moisture content
Insulation thickness (mm)	117	95.5	105	99	77	97.5	96.1
Insulation thickness reduction (mm)	-	21.5	12	12	34	13.5	14.9

From table B.34, it can be seen that the roof with dry substrate yields the maximum thermal insulation thickness reduction in every case, and the saturated substrate and simulated moisture content substrate produce the very similar thickness reduction when compared.

Appendix C: Simulation code

C.1 Introduction

This appendix presents the simulation code of the absorption and evaporation in a green roof substrate. The code is written by the MATLAB R2014b, which simulation codes include the absorption simulation, the evaporation simulation of 162.5 mm thick substrate, and the evaporation simulation of 300 mm thick substrate.

C.2 Absorption simulation code

```
function u = scond(kdry, ksat, s, e, x, tout, tin)
%calculate conduction heat flux with sorptivity value
%input data
%kdry = thermal conductivity of dry green roof substrate (W/m.K)
%ksat = thermal conductivity of saturated green roof substrate (W/m.K)
%s = sorptivity value (mm/min^1/2)
%e = porosity of green roof substrate
%x = thickness of green roof substrate (m)
%tout = outdoor temperature (Celsius)
%tin = indoor temperature (Celsius)
t = (0:1:1440); %time in minute in one day
N = length(t); %number of time step
dt = mean(diff(t)); %length of time step (min)
R = zeros(1,1440);
for i=1:N
   if x>((s*sqrt(i*dt))/(e*1000))
      R(i) = (x/kdry)+(((s*sqrt(i*dt))/(e*1000))*((1/ksat)-(1/kdry)));
      %R(n) = thermal resistivity
   else
      R(i) = (x/kdry)+(x*((1/ksat)-(1/kdry))); %the entire material is saturated (x/ksat)
```

```
    end
    q(i) = -(tout-tin)/R(i);
end
R(1306);
sum(q)
plot(t,q)
xlabel('Time (min)');
ylabel('Thermal Conduction (W/m2)');
end
```

C.3 Evaporation simulation code for 162.5 mm substrate

```
function D = Desorption(m6, m5, m4, m3, m2, m1)
%calculate moisture content change in each layer due to the evaporation
%input
%mc6 is initial moisture contents at layer 6
%mc5 is initial moisture contents at layer 5
%mc4 is initial moisture contents at layer 4
%mc3 is initial moisture contents at layer 3
%mc2 is initial moisture contents at layer 2
%mc1 is initial moisture contents at layer 1

%evaporation rate calculation (stage I)
temp = 5; %temperature at evaporation period (Celsius)
u = 0.5; %air velocity over the evaporation surface (m/s)
rh = 50; %relative humidity (%)
l = 100; %length of drying plane (mm)
R = exp(-5390/(temp+273))*(u^(1/2))*(7*10^6)/((l/1000)^(1/2))*(1-(rh/100));
%evaporation rate (kg/m2.sec)
rate1 = R/1000 %evaporation rate at stage I (m/sec)
```

```
%material property
A = 0.007854; %crossectional area (m2)
rho = 1000000; %density of water (g/m3)
deltat = 3600; %consideration time step (second)
m = 2200; %sample dry mass (g)
C = rho*A*deltat; %factor C
Ttotal = 504; %total simulation time (hour in 3 weeks)
%set 0 array of real moisture content for each layer
mc6 = zeros(1,Ttotal+1);
mc5 = zeros(1,Ttotal+1);
mc4 = zeros(1,Ttotal+1);
mc3 = zeros(1,Ttotal+1);
mc2 = zeros(1,Ttotal+1);
mc1 = zeros(1,Ttotal+1);
%set 0 array of imaginary moisture content for each layer
mc6img = zeros(1,Ttotal+1);
mc5img = zeros(1,Ttotal+1);
mc4img = zeros(1,Ttotal+1);
mc3img = zeros(1,Ttotal+1);
mc2img = zeros(1,Ttotal+1);
%set 0 array of mass of water of each layer
Mass6 = zeros(1,Ttotal+1);
Mass5 = zeros(1,Ttotal+1);
Mass4 = zeros(1,Ttotal+1);

t = (1:1:Ttotal+1);
%set initial moisture content condition
```

```
mc6(1) = m6; %moisture content at layer 6 when time is 0 sec
mc5(1) = m5; %moisture content at layer 5 when time is 0 sec
mc4(1) = m4; %moisture content at layer 4 when time is 0 sec
mc3(1) = m3; %moisture content at layer 3 when time is 0 sec
mc2(1) = m2; %moisture content at layer 2 when time is 0 sec
mc1(1) = m1; %moisture content at layer 1 when time is 0 sec

%exponential decay of evaporation rate
r1 = zeros(1,Ttotal+1);
for i=1:Ttotal+1
   if i<3
      r1(i)=rate1;
   elseif i>=3
      r1(i)=(rate1/20)*exp(-0.0038*(i-3)); %evaporation rate of 300 kPa sample
   end
end
%plot(t,r1)
%flow from layer 5 loop
Q5 = zeros(1,Ttotal+1);
for i=1:Ttotal+1
   if i<3
      Q5(i)= 1.67*10^(-4);
   end
   if i>=3
      %Q5(i)= (7*10^(-8)*i)-1.75*10^(-5);
      %Q5(i)= (5*10^(-6))-(1*10^(-8)*i);
      Q5(i)= (8*10^(-6))*exp(-0.006*i);
   end
```

```
end

%plot(t,Q5)

%seperate top layer

mcx6 = zeros(1,Ttotal+1);

mcx5 = zeros(1,Ttotal+1);

mcx4 = zeros(1,Ttotal+1);

mcx3 = zeros(1,Ttotal+1);

mcx2 = zeros(1,Ttotal+1);

mcx1 = zeros(1,Ttotal+1);

mcx6(1)= m6;

mcx5(1)= m5;

mcx4(1)= m4;

mcx3(1)= m3;

mcx2(1)= m2;

mcx1(1)= m1;

loop = 1;

for i=1:Ttotal

   if mcx6(i)>0

   %layer 6

   Mass6(i) = mcx6(i)*m/(100-mcx6(i)); %mass of water of layer 6 at time i sec

   mc6img(i) = mcx6(i)-(r1(i)*C/Mass6(i)); %imaginary moisture content of layer 6

   mcx6(i+1) = mc6img(i)/2+mcx5(i)/2; %moisture content of layer 6 at the next time step

   %layer 5

   mc5img(i) = mcx6(i+1); %imaginary moisture content of layer 5

   mcx5(i+1) = (mc5img(i)+mcx4(i))/2; %moisture content of layer 5 at the next time step

   %layer 4

   mc4img(i) = mcx5(i+1); %imaginary moisture content of layer 4
```

```
    mcx4(i+1) = (mc4img(i)+mcx3(i))/2; %moisture content of layer 4 at the next time
step

    %layer 3

    mc3img(i) = mcx4(i+1); %imaginary moisture content of layer 3

    mcx3(i+1) = (mc3img(i)+mcx2(i))/2; %moisture content of layer 3 at the next time
step

    %layer 2

    mc2img(i) = mcx3(i+1); %imaginary moisture content of layer 2

    mcx2(i+1) = (mc2img(i)+mcx1(i))/2; %moisture content of layer 2 at the next time
step

    %layer 1

    mcx1(i+1) = mcx2(i+1); %moisture content of layer 1 at the next time step

    loop = loop + 1;

    end

end

mcx6(loop) = 0;

loopcount = 1;

%moisture content prediction when layer 6 is more than 0

for i=1:Ttotal

    if mc6(i)>0

    %layer 6

    Mass6(i) = mc6(i)*m/(100-mc6(i)); %mass of water of layer 6 at time i sec

    %mc6img(i) = mc6(i)-(r1(i)*C/Mass6(i)); %imaginary moisture content of layer 6

    %mc6(i+1) = mc6img(i)/2+mc5(i)/2; %moisture content of layer 6 at the next time
step

    mc6(i+1) = mc6(i)-((r1(i)-Q5(i))*C/Mass6(i));

    %layer 5

    %mc5img(i) = mc6(i+1); %imaginary moisture content of layer 5

    %mc5(i+1) = (mc5img(i)+mc4(i))/2; %moisture content of layer 5 at the next time
step
```

```
    mc5(i+1) = (mc5(i)+mc4(i))/2 - (Q5(i)*C/Mass6(i))/2;
    %layer 4
    mc4img(i) = mc5(i+1); %imaginary moisture content of layer 4
    mc4(i+1) = (mc4img(i)+mc3(i))/2; %moisture content of layer 4 at the next time step
    %layer 3
    mc3img(i) = mc4(i+1); %imaginary moisture content of layer 3
    mc3(i+1) = (mc3img(i)+mc2(i))/2; %moisture content of layer 3 at the next time step
    %layer 2
    mc2img(i) = mc3(i+1); %imaginary moisture content of layer 2
    mc2(i+1) = (mc2img(i)+mc1(i))/2; %moisture content of layer 2 at the next time step
    %layer 1
    mc1(i+1) = mc2(i+1); %moisture content of layer 1 at the next time step
    loopcount = loopcount+1;
    end
end
mc6(loopcount)=0; %avoid last mc6 to be lower than 0
loopcount2 = loopcount-1; %2nd loop count
for i=loopcount2:Ttotal
    if mc5(i)>0
    %layer 5
    Mass5(i) = mc5(i)*m/(100-mc5(i)); %mass of water of layer 5 at time i sec
    mc5img(i) = mc5(i)-(r1(i)*C/Mass5(i)); %imaginary moisture content of layer 5
    mc5(i+1) = (mc5img(i)+mc4(i))/2; %moisture content of layer 5 at the next time step
    %layer 4
    mc4img(i) = mc5(i+1); %imaginary moisture content of layer 4
    mc4(i+1) = (mc4img(i)+mc3(i))/2; %moisture content of layer 4 at the next time step
    %layer 3
    mc3img(i) = mc4(i+1); %imaginary moisture content of layer 3
```

```
    mc3(i+1) = (mc3img(i)+mc2(i))/2; %moisture content of layer 3 at the next time step
    %layer 2
    mc2img(i) = mc3(i+1); %imaginary moisture content of layer 2
    mc2(i+1) = (mc2img(i)+mc1(i))/2; %moisture content of layer 2 at the next time step
    %layer 1
    mc1(i+1) = mc2(i+1); %moisture content of layer 1 at the next time step
    loopcount2 = loopcount2+1;
    end
end
%plot(t,mcx6,t,mc5,t,mc4,t,mc3,t,mc2,t,mc1)
%300 kPa edited.xlsx';
%xlswrite(filename,mcx6,'mc6','A1')
%xlswrite(filename,mc5,'mc5','A1')
%xlswrite(filename,mc4,'mc4','A1')
%xlswrite(filename,mc3,'mc3','A1')
%xlswrite(filename,mc2,'mc2','A1')
%xlswrite(filename,mc1,'mc1','A1')
%Thermal Resistivity calculation
%convert moisture content into thermal conductivity
%For 300 kPa sample only
%K = 0.2639*exp(0.069*mc)
delta_x_6 = 0.025; %thickness of layer 6 (m)
delta_x_5 = 0.025; %thickness of layer 5 (m)
delta_x_4 = 0.025; %thickness of layer 4 (m)
delta_x_3 = 0.025; %thickness of layer 3 (m)
delta_x_2 = 0.025; %thickness of layer 2 (m)
delta_x_1 = 0.0375; %thickness of layer 1 (m)
%K is thermal conductivity (W/m.K)
```

```
%Set 0 array for thermal conductivity in each layer

K6 = zeros(1,Ttotal+1);

K5 = zeros(1,Ttotal+1);

K4 = zeros(1,Ttotal+1);

K3 = zeros(1,Ttotal+1);

K2 = zeros(1,Ttotal+1);

K1 = zeros(1,Ttotal+1);

%calculate thermal conductivity in each layer

for i = 1:Ttotal+1

   K6(i) = 0.2639*exp(0.069*mcx6(i));

   K5(i) = 0.2639*exp(0.069*mc5(i));

   K4(i) = 0.2639*exp(0.069*mc4(i));

   K3(i) = 0.2639*exp(0.069*mc3(i));

   K2(i) = 0.2639*exp(0.069*mc2(i));

   K1(i) = 0.2639*exp(0.069*mc1(i));

end

%plot(t,K6,t,K5,t,K4,t,K3,t,K2,t,K1)

%calculate effective thermal resistivity (Re)

Re = zeros(1,Ttotal+1); %effective thermal resistivity (m2.K/W)

for i = 1:Ttotal+1

   Re(i) = (delta_x_6/K6(i))+(delta_x_5/K5(i))+(delta_x_4/K4(i))+(delta_x_3/K3(i))+(delta_x_2/K2(i))+(delta_x_1/K1(i));

end

plot(t,Re)

filename = '300 kPa at 5 degree dry Resistant.xlsx';

xlswrite(filename,Re,'Thermal resistant','A1')

end
```

C.4 Evaporation simulation code for 300 mm substrate

```
function D = Desorption300mm(m12, m11, m10, m9, m8, m7, m6, m5, m4, m3, m2, m1)

%calculate moisture content change in each layer due to the evaporation

%input

%mc6 is initial moisture contents at layer 6

%mc5 is initial moisture contents at layer 5

%mc4 is initial moisture contents at layer 4

%mc3 is initial moisture contents at layer 3

%mc2 is initial moisture contents at layer 2

%mc1 is initial moisture contents at layer 1


%evaporation rate calculation (stage I)

temp = 5; %temperature at evaporation period (Celsius)

u = 0.5; %air velocity over the evaporation surface (m/s)

rh = 50; %relative humidity (%)

l = 100; %length of drying plane (mm)

R = exp(-5390/(temp+273))*(u^(1/2))*(7*10^6)/((l/1000)^(1/2))*(1-(rh/100));

%evaporation rate (kg/m2.sec)

rate1 = R/1000 %evaporation rate at stage I (m/sec)


%material property

A = 0.007854; %crossectional area (m2)

rho = 1000000; %density of water (g/m3)

deltat = 3600; %consideration time step (second)

m = 2200; %sample dry mass (g)

C = rho*A*deltat; %factor C

Ttotal = 504; %total simulation time (hour in 3 weeks)
```

```
%set 0 array of real moisture content for each layer
mc12 = zeros(1,Ttotal+1);
mc11 = zeros(1,Ttotal+1);
mc10 = zeros(1,Ttotal+1);
mc9 = zeros(1,Ttotal+1);
mc8 = zeros(1,Ttotal+1);
mc7 = zeros(1,Ttotal+1);
mc6 = zeros(1,Ttotal+1);
mc5 = zeros(1,Ttotal+1);
mc4 = zeros(1,Ttotal+1);
mc3 = zeros(1,Ttotal+1);
mc2 = zeros(1,Ttotal+1);
mc1 = zeros(1,Ttotal+1);
%set 0 array of imaginary moisture content for each layer
mc12img = zeros(1,Ttotal+1);
mc11img = zeros(1,Ttotal+1);
mc10img = zeros(1,Ttotal+1);
mc9img = zeros(1,Ttotal+1);
mc8img = zeros(1,Ttotal+1);
mc7img = zeros(1,Ttotal+1);
mc6img = zeros(1,Ttotal+1);
mc5img = zeros(1,Ttotal+1);
mc4img = zeros(1,Ttotal+1);
mc3img = zeros(1,Ttotal+1);
mc2img = zeros(1,Ttotal+1);
%set 0 array of mass of water of each layer
Mass12 = zeros(1,Ttotal+1);
Mass11 = zeros(1,Ttotal+1);
```

```
Mass10 = zeros(1,Ttotal+1);

Mass9 = zeros(1,Ttotal+1);

Mass8 = zeros(1,Ttotal+1);

Mass7 = zeros(1,Ttotal+1);

Mass6 = zeros(1,Ttotal+1);

Mass5 = zeros(1,Ttotal+1);

Mass4 = zeros(1,Ttotal+1);

Mass3 = zeros(1,Ttotal+1);

Mass2 = zeros(1,Ttotal+1);

Mass1 = zeros(1,Ttotal+1);


t = (1:1:Ttotal+1);

%set initial moisture content condition

mc12(1) = m12; %moisture content at layer 12 when time is 0 sec

mc11(1) = m11; %moisture content at layer 11 when time is 0 sec

mc10(1) = m10; %moisture content at layer 10 when time is 0 sec

mc9(1) = m9; %moisture content at layer 9 when time is 0 sec

mc8(1) = m8; %moisture content at layer 8 when time is 0 sec

mc7(1) = m7; %moiture content at layer 7 when time is 0 sec

mc6(1) = m6; %moisture content at layer 6 when time is 0 sec

mc5(1) = m5; %moisture content at layer 5 when time is 0 sec

mc4(1) = m4; %moisture content at layer 4 when time is 0 sec

mc3(1) = m3; %moisture content at layer 3 when time is 0 sec

mc2(1) = m2; %moisture content at layer 2 when time is 0 sec

mc1(1) = m1; %moisture content at layer 1 when time is 0 sec


%exponential decay of evaporation rate

r1 = zeros(1,Ttotal+1);
```

```
for i=1:Ttotal+1
   if i<3
      r1(i)=rate1;
   elseif i>=3
      r1(i)=(rate1/20)*exp(-0.0038*(i-3)); %evaporation rate of 300 kPa sample
   end
end
%plot(t,r1)
%flow from layer 11 loop
Q11 = zeros(1,Ttotal+1);
for i=1:Ttotal+1
   if i<3
      Q11(i)= 1.67*10^(-4);
   end
   if i>=3
      %Q5(i)= (7*10^(-8)*i)-1.75*10^(-5);
      %Q5(i)= (5*10^(-6))-(1*10^(-8)*i);
      Q11(i)= (8*10^(-6))*exp(-0.006*i);
   end
end
%plot(t,Q5)
%separate top layer
mcx12 = zeros(1,Ttotal+1);
mcx11 = zeros(1,Ttotal+1);
mcx10 = zeros(1,Ttotal+1);
mcx9 = zeros(1,Ttotal+1);
mcx8 = zeros(1,Ttotal+1);
mcx7 = zeros(1,Ttotal+1);
```

```
mcx6 = zeros(1,Ttotal+1);

mcx5 = zeros(1,Ttotal+1);

mcx4 = zeros(1,Ttotal+1);

mcx3 = zeros(1,Ttotal+1);

mcx2 = zeros(1,Ttotal+1);

mcx1 = zeros(1,Ttotal+1);

%assign value

mcx12(1)= m12;

mcx11(1)= m11;

mcx10(1)= m10;

mcx9(1)= m9;

mcx8(1)= m8;

mcx7(1)= m7;

mcx6(1)= m6;

mcx5(1)= m5;

mcx4(1)= m4;

mcx3(1)= m3;

mcx2(1)= m2;

mcx1(1)= m1;

loop = 1;

for i=1:Ttotal

   if mcx12(i)>0

   %layer 12

   Mass12(i) = mcx12(i)*m/(100-mcx12(i)); %mass of water of layer 12 at time i sec

   mc12img(i) = mcx12(i)-(r1(i)*C/Mass12(i)); %imaginary moisture content of layer
12

   mcx12(i+1) = mc12img(i)/2+mcx11(i)/2; %moisture content of layer 12 at the next
time step

   %layer 11
```

```
mc11img(i) = mcx12(i+1); %imaginary moisture content of layer 11

mcx11(i+1) = (mc11img(i)+mcx10(i))/2; %moisture content of layer 11 at the next time step

%layer 10

mc10img(i) = mcx11(i+1); %imaginary moisture content of layer 10

mcx10(i+1) = (mc10img(i)+mcx9(i))/2; %moisture content of layer 10 at the next time step

%layer 9

mc9img(i) = mcx10(i+1); %imaginary moisture content of layer 9

mcx9(i+1) = (mc9img(i)+mcx8(i))/2; %moisture content of layer 9 at the next time step

%layer 8

mc8img(i) = mcx9(i+1); %imaginary moisture content of layer 8

mcx8(i+1) = (mc8img(i)+mcx7(i))/2; %moisture content of layer 8 at the next time step

%layer 7

mc7img(i) = mcx8(i+1); %imaginary moisture content of layer 7

mcx7(i+1) = (mc7img(i)+mcx6(i))/2; %moisture content of layer 7 at the next time step

%layer 6

mc6img(i) = mcx7(i+1); %imaginary moisture content of layer 6

mcx6(i+1) = (mc6img(i)+mcx5(i))/2; %moisture content of layer 6 at the next time step

%layer 5

mc5img(i) = mcx6(i+1); %imaginary moisture content of layer 5

mcx5(i+1) = (mc5img(i)+mcx4(i))/2; %moisture content of layer 5 at the next time step

%layer 4

mc4img(i) = mcx5(i+1); %imaginary moisture content of layer 4

mcx4(i+1) = (mc4img(i)+mcx3(i))/2; %moisture content of layer 4 at the next time step
```

```
    %layer 3

    mc3img(i) = mcx4(i+1); %imaginary moisture content of layer 3

    mcx3(i+1) = (mc3img(i)+mcx2(i))/2; %moisture content of layer 3 at the next time step

    %layer 2

    mc2img(i) = mcx3(i+1); %imaginary moisture content of layer 2

    mcx2(i+1) = (mc2img(i)+mcx1(i))/2; %moisture content of layer 2 at the next time step

    %layer 1

    mcx1(i+1) = mcx2(i+1); %moisture content of layer 1 at the next time step

    loop = loop + 1;

    end

end

mcx12(loop) = 0;

loopcount = 1;

%moisture content prediction when layer 6 is more than 0

for i=1:Ttotal

    if mc12(i)>0

    %layer 12

    Mass12(i) = mc12(i)*m/(100-mc12(i)); %mass of water of layer 12 at time i sec

    %mc6img(i) = mc6(i)-(r1(i)*C/Mass6(i)); %imaginary moisture content of layer 6

    %mc6(i+1) = mc6img(i)/2+mc5(i)/2; %moisture content of layer 6 at the next time step

    mc12(i+1) = mc12(i)-((r1(i)-Q11(i))*C/Mass12(i));

    %layer 11

    %mc5img(i) = mc6(i+1); %imaginary moisture content of layer 11

    %mc5(i+1) = (mc5img(i)+mc4(i))/2; %moisture content of layer 11 at the next time step

    mc11(i+1) = (mc11(i)+mc10(i))/2 - (Q11(i)*C/Mass12(i))/2;

    %layer 10
```

```
mc10img(i) = mc11(i+1); %imaginary moisture content of layer 10

mc10(i+1) = (mc10img(i)+mc9(i))/2; %moisture content of layer 4 at the next time step

%layer 9

mc9img(i) = mc10(i+1); %imaginary moisture content of layer 9

mc9(i+1) = (mc9img(i)+mc8(i))/2; %moisture content of layer 3 at the next time step

%layer 8

mc8img(i) = mc9(i+1); %imaginary moisture content of layer 8

mc8(i+1) = (mc8img(i)+mc7(i))/2; %moisture content of layer 2 at the next time step

%layer 7

mc7img(i) = mc8(i+1); %imaginary moisture content of layer 7

mc7(i+1) = (mc7img(i)+mc6(i))/2; %moisture content of layer 2 at the next time step

%layer 6

mc6img(i) = mc7(i+1); %imaginary moisture content of layer 6

mc6(i+1) = (mc6img(i)+mc5(i))/2; %moisture content of layer 2 at the next time step

%layer 5

mc5img(i) = mc6(i+1); %imaginary moisture content of layer 5

mc5(i+1) = (mc5img(i)+mc4(i))/2; %moisture content of layer 2 at the next time step

%layer 4

mc4img(i) = mc5(i+1); %imaginary moisture content of layer 4

mc4(i+1) = (mc4img(i)+mc3(i))/2; %moisture content of layer 2 at the next time step

%layer 3

mc3img(i) = mc4(i+1); %imaginary moisture content of layer 3

mc3(i+1) = (mc3img(i)+mc2(i))/2; %moisture content of layer 2 at the next time step

%layer 2

mc2img(i) = mc3(i+1); %imaginary moisture content of layer 2

mc2(i+1) = (mc2img(i)+mc1(i))/2; %moisture content of layer 2 at the next time step

%layer 1
```

```
    mc1(i+1) = mc2(i+1); %moisture content of layer 1 at the next time step

    loopcount = loopcount+1;

    end

end

mc12(loopcount)=0; %avoid last mc6 to be lower than 0

loopcount2 = loopcount-1; %2nd loop count

for i=loopcount2:Ttotal

    if mc11(i)>0

    %layer 11

    Mass11(i) = mc11(i)*m/(100-mc11(i)); %mass of water of layer 5 at time i sec

    mc11img(i) = mc11(i)-(r1(i)*C/Mass11(i)); %imaginary moisture content of layer 5

    mc11(i+1) = (mc11img(i)+mc10(i))/2; %moisture content of layer 5 at the next time
step

    %layer 10

    mc10img(i) = mc11(i+1); %imaginary moisture content of layer 4

    mc10(i+1) = (mc10img(i)+mc9(i))/2; %moisture content of layer 4 at the next time
step

    %layer 9

    mc9img(i) = mc10(i+1); %imaginary moisture content of layer 3

    mc9(i+1) = (mc9img(i)+mc8(i))/2; %moisture content of layer 3 at the next time step

    %layer 8

    mc8img(i) = mc9(i+1); %imaginary moisture content of layer 2

    mc8(i+1) = (mc8img(i)+mc7(i))/2; %moisture content of layer 2 at the next time step

    %layer 7

    mc7img(i) = mc8(i+1); %imaginary moisture content of layer 2

    mc7(i+1) = (mc7img(i)+mc6(i))/2; %moisture content of layer 2 at the next time step

    %layer 6

    mc6img(i) = mc7(i+1); %imaginary moisture content of layer 2

    mc6(i+1) = (mc6img(i)+mc5(i))/2; %moisture content of layer 2 at the next time step
```

```
    %layer 5
    mc5img(i) = mc6(i+1); %imaginary moisture content of layer 2
    mc5(i+1) = (mc5img(i)+mc4(i))/2; %moisture content of layer 2 at the next time step
    %layer 4
    mc4img(i) = mc5(i+1); %imaginary moisture content of layer 2
    mc4(i+1) = (mc4img(i)+mc3(i))/2; %moisture content of layer 2 at the next time step
    %layer 3
    mc3img(i) = mc4(i+1); %imaginary moisture content of layer 2
    mc3(i+1) = (mc3img(i)+mc2(i))/2; %moisture content of layer 2 at the next time step
    %layer 2
    mc2img(i) = mc3(i+1); %imaginary moisture content of layer 2
    mc2(i+1) = (mc2img(i)+mc1(i))/2; %moisture content of layer 2 at the next time step
    %layer 1
    mc1(i+1) = mc2(i+1); %moisture content of layer 1 at the next time step
    loopcount2 = loopcount2+1;
    end
end
%plot(t,mcx6,t,mc5,t,mc4,t,mc3,t,mc2,t,mc1)
%300 kPa edited.xlsx';
%xlswrite(filename,mcx6,'mc6','A1')
%xlswrite(filename,mc5,'mc5','A1')
%xlswrite(filename,mc4,'mc4','A1')
%xlswrite(filename,mc3,'mc3','A1')
%xlswrite(filename,mc2,'mc2','A1')
%xlswrite(filename,mc1,'mc1','A1')

%Thermal Resistivity calculation
%convert moisture content into thermal conductivity
```

```
%For 300 kPa sample only
%K = 0.2639*exp(0.069*mc)
delta_x_12 = 0.025; %thickness of layer 12 (m)
delta_x_11 = 0.025; %thickness of layer 11 (m)
delta_x_10 = 0.025; %thickness of layer 10 (m)
delta_x_9 = 0.025; %thickness of layer 9 (m)
delta_x_8 = 0.025; %thickness of layer 8 (m)
delta_x_7 = 0.025; %thickness of layer 7 (m)
delta_x_6 = 0.025; %thickness of layer 6 (m)
delta_x_5 = 0.025; %thickness of layer 5 (m)
delta_x_4 = 0.025; %thickness of layer 4 (m)
delta_x_3 = 0.025; %thickness of layer 3 (m)
delta_x_2 = 0.025; %thickness of layer 2 (m)
delta_x_1 = 0.025; %thickness of layer 1 (m)
%K is thermal conductivity (W/m.K)
%Set 0 array for thermal conductivity in each layer
K12 = zeros(1,Ttotal+1);
K11 = zeros(1,Ttotal+1);
K10 = zeros(1,Ttotal+1);
K9 = zeros(1,Ttotal+1);
K8 = zeros(1,Ttotal+1);
K7 = zeros(1,Ttotal+1);
K6 = zeros(1,Ttotal+1);
K5 = zeros(1,Ttotal+1);
K4 = zeros(1,Ttotal+1);
K3 = zeros(1,Ttotal+1);
K2 = zeros(1,Ttotal+1);
K1 = zeros(1,Ttotal+1);
```

```
%calculate thermal conductivity in each layer

for i = 1:Ttotal+1

   K12(i) = 0.2639*exp(0.069*mcx12(i));

   K11(i) = 0.2639*exp(0.069*mc11(i));

   K10(i) = 0.2639*exp(0.069*mc10(i));

   K9(i) = 0.2639*exp(0.069*mc9(i));

   K8(i) = 0.2639*exp(0.069*mc8(i));

   K7(i) = 0.2639*exp(0.069*mc7(i));

   K6(i) = 0.2639*exp(0.069*mc6(i));

   K5(i) = 0.2639*exp(0.069*mc5(i));

   K4(i) = 0.2639*exp(0.069*mc4(i));

   K3(i) = 0.2639*exp(0.069*mc3(i));

   K2(i) = 0.2639*exp(0.069*mc2(i));

   K1(i) = 0.2639*exp(0.069*mc1(i));

end

%plot(t,K6,t,K5,t,K4,t,K3,t,K2,t,K1)

%calculate effective thermal resistivity (Re)

Re = zeros(1,Ttotal+1); %effective thermal resistivity (m2.K/W)

for i = 1:Ttotal+1

   Re(i) = (delta_x_12/K12(i))+(delta_x_11/K11(i))+(delta_x_10/K10(i))+(delta_x_9/K9(i))+(delta_x_8/K8(i))+(delta_x_7/K7(i))+(delta_x_6/K6(i))+(delta_x_5/K5(i))+(delta_x_4/K4(i))+(delta_x_3/K3(i))+(delta_x_2/K2(i))+(delta_x_1/K1(i));

end

plot(t,Re)

filename = '300 kPa 300mm at 5 degree dry Resistant.xlsx';

xlswrite(filename,Re,'Thermal resistant','A1')

end
```

Appendix D: Conference paper

Present problems with building performance simulation of green roofs

Kantitut Tubsuwan[1] and Phil Banfill[1]

[1]Centre of Excellence in Sustainable Building Design, School of the Built Environment, Heriot-Watt University, Edinburgh, United Kingdom

Abstract

Green roofs are increasingly popular with designers and performance simulation is necessary to ensure a building's energy efficiency but there are some problems with present theories that support green roof modelling. For example, it is assumed that a substrate layer is continuously saturated, which is not true in practice. Most models ignore the drainage layer, which is an important service layer integrated with current green roof systems. Where included, models have used an inappropriate mechanism. In a substrate layer, the liquid absorbs into the soil by capillary attraction, and the contact surface is saturated first, while soil underneath remains dry and requires some time to reach saturation. Sharp Front Theory can be used to understand this situation and the rate of liquid absorption by the material is called its sorptivity. This can be used with the one-dimensional conduction heat transfer. In the drainage layer, the theory of conduction of porous material is applied by using Hadley's weighted average of Maxwell upper bound method to estimate the effective thermal conductivity. This varies with porosity and can be used to calculate the transient conduction heat transfer. A concept for improved performance simulation models is presented.

Introduction

Green roofs are a sustainable construction that satisfies the current world energy and thermal crisis. With a history dating back to Babylon's hanging gardens ([2], Ascione et al., 2013), it was used for energy considerations by German engineers during the 19th century ([3], Newton, 2007). The modern green roof can withstand various climates and has increased durability resulting from its service layers such as waterproofing and drainage layers.

The environmental benefits of green roofs include improved storm water management, reduced noise and air pollution, and reduced carbon footprint from the land used ([3], Newton, 2007). However, the unique feature of green roofs is enhanced building energy saving from heat transfer through the roof. It reduces solar heat gain by shading the roof structure from sunlight with the foliage canopy, and also provides passive cooling from transpiration. In addition, increased roof thermal mass due to the soil layer reduces heat loss in winter.

Most large buildings are subjected to a building performance simulation, using appropriate software, at the design stage, usually to confirm compliance with performance criteria, but simulation of green roof thermal behaviour is complex and some important factors have been ignored in the interests of simplicity. However, this may result in an inaccuracy in some situations. Furthermore, due to developments in the technology of green roofs, some service layers have been added, but are not included in the simulation. This paper will discuss alternative solutions to improve the thermal simulation of a green roof.

Literature review

Research investigations into the thermal performance of green roofs can be divided into three types: experimental measurements in laboratory or field, theoretical analysis, and combination of the two. Despite their relative advantages and disadvantages there are some problems.

At first, experimental thermal performance was measured by heat flux reduction from the reference roof (normally a bare concrete roof) compared with the green roof in a same situation. As a result, the thermal resistance (R-value) was calculated by deducing the green roof's R-value from the layers in another roof assembly ([4], Sonne, 2006, [5], Wonget al., 2003). In Wonget al. (2003) [5] study, they found that the green roof with higher Leaf Area Index (LAI) reduced the cooling energy required and this factor became important for green roof simulation. The growing substrate is also important because they found that a green roof with wet soil had lower cooling efficiency than dry soil because it has a lower R-value ([5], Wonget al., 2003). However, this model did not consider the effect of evaporation from wet soil, which could result in more heat loss from the roof. For this reason, researchers have been studying this important phenomenon and trying to explain it by numerical methods.

The plant respiration and soil evaporation are unique features of a green roof which affect thermal transfer by latent heat removal on foliage and substrate surfaces. It was studied by Balicket al. (1981) [6] and Deardorff (1978) [7] to evaluate ground surface temperature when vegetation is present. These models were developed by Frankenstein and Koenig (2004) [8] into the FASST soil and vegetation model using the energy balance method. After the development of building energy simulation software, those theories were applied in EnergyPlus simulation software, and included effects of short and long-wave solar radiation, interlayer long-wave emission, sensible heat flux from wind, and finally latent heat flux from plant respiration in an unsteady state condition ([9], Sailor, 2008).

The evapotranspiration calculation in former green roof models were calculated by using the Bowen ratio or a convective mass transfer coefficient ignoring stomata and substrate resistance ([10], Nayaket al., 1982, [11], Gaffinet al., 2005, [12], Gaffinet al., 2006, [13], He and Jim, 2010). This ratio is very convenient to use in any green roofs model, but it is useable only if evapotranspiration is not directly related to water content. To satisfy this requirement it is assumed that the green roof is well irrigated ([1], Tabares-Velasco, 2009).

On the other hand, most modern evapotranspiration models use the Vapour Pressure Deficit (VPD) method ([9], Sailor, 2008, [14], Barrio, 1998, [15], Lazzarinet al., 2005, [16], Alexandri and Jones, 2007). This takes the difference between the moisture present in the air and the amount that the air can hold when saturated. Nevertheless, each model uses a different function of the resistance in order to calculate evapotranspiration of a plant layer, such as wind correlation and vapour resistance. This method was applied to the latent heat flux calculation.

In order to calculate thermal transfer in unsteady state condition of green roofs, some assumptions are needed to reduce difficulties in modelling ([1], Tabares-Velasco, 2009).

- A green roof vegetation and growing medium layer are horizontally homogeneous
- The horizontal length of green roof is much greater than its vertical depth and horizontal heat transfer is negligible in order to simplify the models into one-dimensional heat transfer
- The air under the stomata (vegetation layer) is always saturated
- Any heat flux during biochemical photosynthesis reactions is negligible
- Conduction heat transfer does not occur in the foliage layer
- A vegetation layer is irrigated, fully grown and completely covers the substrate layer
- There is homogenous distribution of water in the canopy
- A green roof is free from mulch

These assumptions were applied to most of green roof simulations to simplify the equations and computer processing. Furthermore, some assumptions such as photosynthetic reaction and green roof mulch are difficult to estimate due to their complicated behaviour, but the energy used can be ignored. However, the assumption of well irrigated plants means that the substrate, as a result, is always saturated, which does not correspond to reality.

Tabares-Velasco (2009) [1] summarised the theories in heat flux calculation for the models applied in different building performance simulations (Table 1). All of these models are using heat and mass transfer functions.

Table 1. Comparison of heat and mass transfer functions used in green roof models ([1], Tabares-Velasco, 2009)

	Sailor (2008) [9]	**Alexandri and Jones (2007) [16]**	**Lazzarinet al. (2005) [15]**	**Barrio (1998) [14]**
Short-wave Radiation	Beer's Law	Beer's Law	Beer's Law	Beer's Law
Long-wave Radiation	Plant-Sky Substrate-Sky Substrate-Plants (infinite plates)	Plant-Sky Substrate-Sky Substrate-Plants (Plants surrounding substrate)	Adduction coefficient	Plant-Sky Substrate-Sky Substrate-Plants (Plants surrounding substrate)
Convection	1.1 factor + Logarithmic profile + instability factors + LAI	Logarithmic profile	Adduction coefficient	2 Factor + Empirical equation for aerodynamic resistance based on plant characteristics +LAI
Evapotranspiration	VPD for plants and soil covered/uncovered	VPD for plants and soil covered	Penman Equation	VPD for plants and soil covered
Stomata Resistance to atmosphere	a function of moisture content, Sun (multiplicative)	A function of moisture content, Sun (additive)	Empirical wind equation	A function of moisture content, Sun, Temperature and CO_2 (additive)
Substrate Resistance to atmosphere	Alpha method	A function of moisture content, moisture content at saturation	Not considered	Not considered
Substrate Thermal Conductivity	Not considered	Exponential function depending on moisture content	Not considered	Power + Exponential function depending on moisture content and density

Some green roof models, such as Sailor (2008) [9] and Lazzarinet al. (2005) [15], are already integrated with building simulation software, - EnergyPlus and TRNSYS, respectively. However, these models have ignored important features of some green roof layers, the soil and drainage layers.

Problems found in green roof modelling

From the literature review the four main problems with thermal simulation models for green roofs are:

- The soil in the growing medium or substrate layer is assumed to be saturated at all times but this is not necessarily so in practice because of the variability in weather over time in arid and semi-arid regions. Also with climate change northern regions are expected to experience more extreme weather events in the future, so soil moisture content will vary with time. The thermal conductivity of soil varies by a factor of ten between dry and saturated.
- The dynamics of variations in soil moisture content are not considered in the models.
- The thermal conductivity of the drainage layer is not considered in any model.
- The effect of convection heat transfer as water flows through the drainage layer is not considered.

Problems in substrate layer

Most of the assumptions made for green roof modellings aim to reduce complication in the heat and mass transfer calculation. Others have very small energy contributions compared to overall thermal transfer energy, but there is one key assumption about roof moisture and irrigation behaviour. It assumed that a green roof vegetation layer is always well irrigated, and consequently, a substrate layer (beneath the vegetation) is also always saturated.I In reality, a roof can be well irrigated only in the pre-installation period in order to allow the plant to settle down. In service period, it is almost impossible to maintain saturation on a roof.

The problem is that the properties of the green roof substrate or soil are influenced by water content. According to Johansen and the De Vries methods, the thermal conductivity of soil depends on its density, porosity, degree of saturation, quartz content, and thermal conductivity of contained minerals ([17], Farouki, 1986). Whilst quartz content and thermal conductivity of minerals are constant, density and porosity can be controlled and measured. In contrast, the degree of saturation depends only on the amount of water absorbed from irrigation or precipitation. As a result, the effect of moisture changes in soil is very important for thermal conductivity and overall heat transfer.

However, the green roof growing medium is different from ordinary soil. It is designed to be lightweight, lower density, and has various organic content, so it is difficult to classify into any soil types. In regular soil thermal conductivity varies from 0.2 to 2.0 W/mK from dry to wet. In green roof growing mediums, in contrast, thermal conductivities vary from 0.18 to 0.22 W/mK for dry substrate, and 0.5 to 1.0 W/mK for saturated ([1], Tabares-Velasco, 2009). See figure 1.

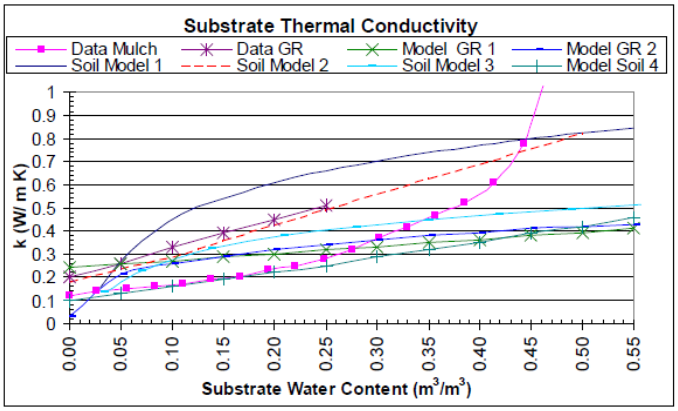

Figure 1 Green roof substrate thermal conductivity at different water content ([1], Tabares-Velasco, 2009)

In figure 1, the soil models 1, 2, 3 and 4 are Johansen's correlation for a crushed rock (a solid conductivity of 1.5 W/mK, 0.70 porosity, 0.15 quartz content, and substrate density of 800 kg/m^3), De Vries' correlation for a soil (a solid conductivity of 1.5 W/mK and 0.7 porosity), Kersten's model for a soil (density 800 kg/m^3), and experimental correlation from Barrio (1998) [14] on a large soil sample (density from 1100 kg/m^3 to 1500 kg/m^3 and volumetric water content from 4-25 percent) respectively

([17], Farouki, 1986). For green roof substrates, the data GR, GR-1, and GR-2 are plotted beneath ordinary substrates conductivity. It confirms that substrate water content significantly affects thermal conductivity, and that the assumption of constant thermal conductivity is unjustified.

When water is absorbed by unsaturated soil, the contact surface is wetted first but points underneath remain dry. Capillary attraction brings a moisture front into the soil until it is completely saturated. This mechanism is similar to absorption of water in concrete or brick, which can be described by "Sharp Front Theory" ([18], Hall and Hoff, 2009), as described later.

Thermal conductivity of the drainage layer

The drainage layer is used to retain moisture inside the green roof, but also provide drainage for excess water in case of heavy rainfall. It uses either granular material or plastic drainage modules ([19], Dunnett and Kingsbury, 2004). Despite becoming increasingly common, this service layer has been ignored in building performance simulation models. As a result, an appropriate model for thermal conduction is needed.

Only ([2], Ascione et al., 2013, [15], Lazzarinet al., 2005) included a drainage layer in their calculation but used a constant R-value for the materials in the drainage layer in order to calculate heat conduction. However, this assumption cannot be true for a porous material. Its thermal conductivity depends on the porosity, which varies by the inflow and drained water. For this reason, the thermal conductivity value requires a dynamic calculation, based on porous material conduction theory.

Convection in the drainage layer

The drainage layer facilitates flow of excess water which removes some heat by convection. This mechanism is not mentioned in any green roof models.

The convection of water drained on a roof surface and its coefficient depend on the flow mechanism and velocity of liquid. In a flat green roof, convection does not have a significant effect on heat removal since the flow velocity is low, but on a sloping green roof the higher velocity increases convection heat transfer. This may be significant in a large building and for this reason, it should be included in any green roof model.

Suggestions for improvement

Substrate layer

Water transport in the soil must be better quantified. The Sharp Front Theory, according to Hall and Hoff (2009) [18], explains the liquid absorption into an unsaturated porous solid over time. The moisture content versus distance profile maintains a constant shape and advances in proportion to $t^{1/2}$. The sorptivity is the proportionality constant, the tendency of a material to absorb and transmit water or other liquid by capillarity. It depends on the microscopic structure of the material, and is influenced by the capillary suction and hydraulic conductivity. It is readily determined experimentally.

Soil and Sharp Front Theory

Water transport in porous materials is mainly caused by capillary forces. Consequently, a porous material is able to absorb the liquid in contact with capillaries in its surface. According to Hall and Hoff (2009) [18], the capillary rise in a capillary tube in contact with a liquid reservoir caused by surface tension (σ) creates a pressure deficit arising from meniscus curvature. This pressure is balanced by the hydrostatic pressure of the liquid column (Figure 2).

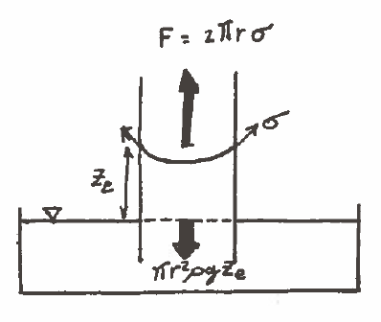

Figure 1 Force balance in a capillary tube

$$2\pi r\sigma = \pi r^2 \rho g Z_e \quad (1)$$

Then,

$$Z_e = \frac{2\sigma}{r\rho g} \quad (2)$$

Equation 2 shows that the radius of the capillary tube has a significant effect on the capillary rise. It can be applied to porous media where a smaller particle size, such as clay, can raise water higher than larger particles like sand. This basic theory of capillary rise does not explain the rate of absorption: this requires unsaturated flow theory.

When the porous material dries in the initial state, after exposure to liquid, liquid is drawn to the material's surface by capillary forces. This flow is described by extended Darcy equation (3) ([18], Hall and Hoff, 2009).

$$\mathbf{u} = K(\theta)\mathbf{F} \quad (3)$$

Where **u** is a vector flow velocity, θ is a ratio of liquid volume to bulk volume (volume fraction saturation), $K(\theta)$ is an unsaturated permeability at given liquid content (θ), and **F** is the capillary force that can be identified with the negative gradient of capillary potential Ψ. Thus, the extended Darcy equation is transformed to equation 4.

$$\mathbf{u} = -K(\theta)\nabla\Psi \quad (4)$$

Ψ is the capillary potential per unit weight of liquid has dimension (L), which is the energy required to transfer unit weight of liquid from the porous material to a reservoir of the same liquid at the same temperature and elevation ([18], Hall and Hoff, 2009). This unsaturated flow mechanism is depicted in figure 3.

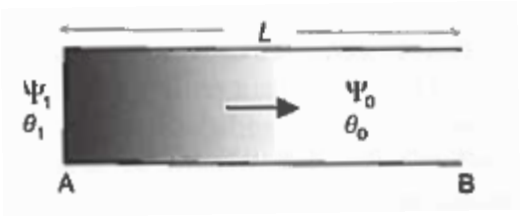

Figure 2. Unsaturated flow in porous materials ([18], Hall and Hoff, 2009)

However, the function of velocity is not suitable for determining moisture gradient so this equation is converted by combining with the continuity equation and transformed by Boltzmann transformation

$$x(\theta, t) = \emptyset(\theta) t^{1/2} \quad (5)$$

This equation shows a key point of unsaturated flow theory. As liquid is absorbed into a porous material, the liquid content against distance profile advances as $t^{1/2}$ and maintains a constant shape $\emptyset(\theta)$. In other words, at $t > 0$, the liquid content at a distance x from the liquid entrance is θ_x, whereas beyond this point, the liquid content remains dry θ_d. This concept is fundamental for the Sharp Front Theory.

The Sharp Front Theory has been confirmed by many experiments for inorganic construction materials, such as gypsum plaster, Portland limestone, and cement mortar ([18], Hall and Hoff, 2009). The typical water content profiles of these materials are shown in figure 4. Sorptivity can be used to estimate the time taken for the substrate to achieve saturation.

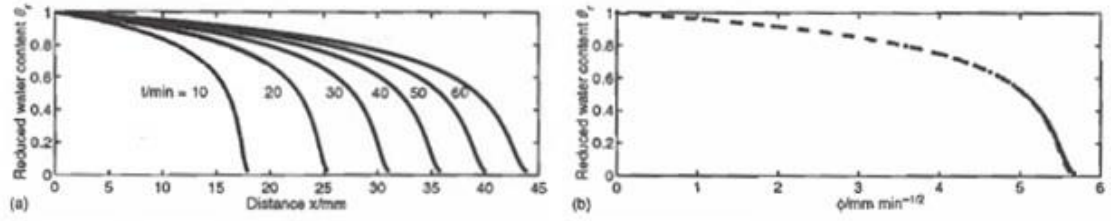

Figure 1. (a) Water content profiles according to time and distance (b) Master curve $\emptyset(\boldsymbol{\theta})_{\boldsymbol{r}}$ for the same material ([18], Hall and Hoff, 2009)

If the unsaturated flow equation is integrated, the total amount of liquid absorbed in time t is given by equation 6.

$$\int_{\theta_d}^{\theta_s} x d\theta = t^{1/2} \int_{\theta_d}^{\theta_s} \emptyset(\theta) d\theta = S t^{1/2} \quad (6)$$

In this equation, Sorptivity (S), which is the most important property of unsaturated flow in porous material, is defined. It was first introduced by Philip in the field of soil physics and hydrology ([20], Philip, 1957).

The sorptivity is the property which expresses the tendency of a material to absorb and transmit water and other liquids by capillarity. In contrast to saturated permeability (K_s), it is sensitive both to the hydraulic conductivity (K) and the suction characteristic of a material ([18], Hall and Hoff, 2009).

Sharp Front Theory is suitable to estimate the thickness of the saturated layer according to the time $t^{1/2}$. This layer has a known thermal conductivity. Additionally, the thermal conductivity of the dry layer beneath is known, so it is possible to combine Sharp Front Theory and these thermal conductivities to calculate the overall thermal conductivity at each time step. Sorptivity is easily measured for the growing medium and the overall soil thermal conductivity simply depends on the relative thickness of the two layers (dry and saturated), each of which is known.

Drainage layer

The drainage layer differs from a substrate layer because there is no capillary suction. For this reason, the Sharp Front Theory cannot be applied here. In general porous materials, the thermal conductivity of the solid (k_s) phase is greater than the liquid (k_f). Nevertheless, the behaviour of the solid that interconnects with liquid influences the heat conduction significantly. The effective thermal conductivity is defined to estimate conduction heat transfer of a porous material, but this depends on the thermal conductivity of each phase (solid and fluid), the structure of solid matrix, and the contact resistance between the nonconsolidated particle ([21], Kaviany, 1991). This value had been studied by many researchers and those theories were compared with experimental data by Nozad et al. (1985) [22], which is shown in figure 5.

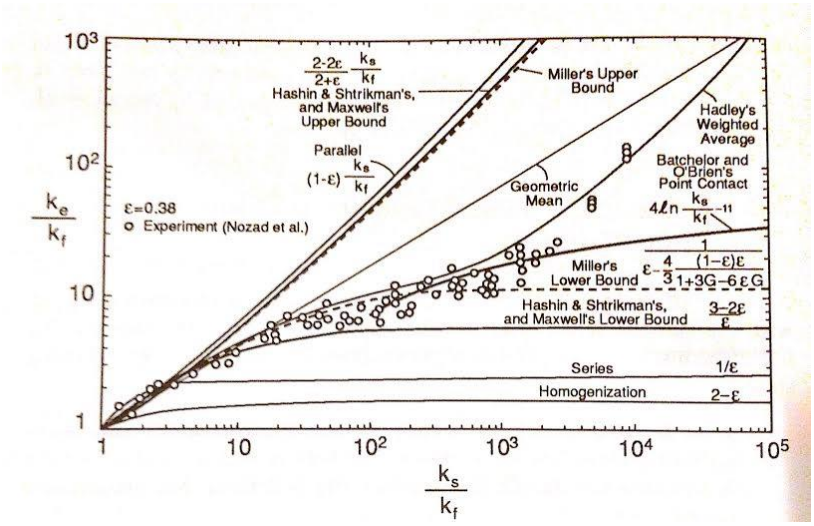

Figure 1. Effective thermal conductivity of beds of spherical particles predicted by various theories compared with experimental data ([22], Nozad et al., 1985)

From figure 5, the method that is closest to the experimental data is Hadley's weighted average of Maxwell upper bound method. This uses thermal diffusivity (α_o) with an expression obtained by introduction of an adjustable function (f_o) into a weighted averaged expression ([21], Kaviany, 1991). The effective thermal conductivity can be calculated by equation 7.

$$\frac{k_e}{k_f} = (1-\alpha_o)\frac{\epsilon f_o + K_s/K_f(1-\epsilon f_o)}{1-\epsilon(1-f_o)+K_s/K_f[\epsilon(1-f_o)]} + \alpha_o \frac{2(K_s/K_f)^2(1-\epsilon)+(1+2\epsilon)K_s/K_f}{(2+\epsilon)K_s/K_f+1-\epsilon} \quad (7)$$

Where;

$$log\alpha_o = -4.898\epsilon, 0 \le \epsilon \le 0.0827$$
$$log\alpha_o = -0.405 - 3.158(\epsilon - 0.0827), 0.0827 \le \epsilon \le 0.298$$

$$\epsilon = porosity$$
$$K_s = thermal\ conductivity\ of\ solid$$
$$K_f = thermal\ conductivity\ of\ fluid$$
$$K_e = effective\ thermal\ conductivity$$
$$f_o = 0.8 + 0.1\epsilon$$

From the equation 5, the thermal conductivity of both liquid and solid is constant, and as a result, the equation is influenced by porosity, which is a ratio of the void space volume to the total volume of porous material. In a drainage layer, the void space volume is varied by the amount of drained water from a substrate layer. That directly affects the porosity and the effective thermal conductivity. Because porosity varies with time, the effective thermal conductivity is considered to be a dynamic value. For this reason, the transient conduction of a drainage layer must be calculated by using the theory of porous material conductivity.

Discussion

From these suggestions, the research will combine these theories to create a complete green roof thermal model. This could be then be integrated with building energy simulation software. However, before going to that stage, the concept of this model must be verified.

surface temperature on a substrate layer, the conduction of a substrate layer will calculated by using a one-dimensional finite difference calculation with time variation with saturated and unsaturated thermal conductivity values. The transient conduction model will be incorporated with Sharp Front Theory by dividing a substrate layer into two layers, one saturated with a saturated thermal conductivity and one unsaturated layer with a different thermal conductivity. This calculation will continue until the substrate is fully saturated after which a normal conduction calculation can be used.

For the drainage layer, it is important to define the value of porosity since it contributes to an effective thermal conductivity, which the weighted average of the Maxwell upper bound is used to calculate. At each time step a single value of porosity is calculated from the amount of water transported into the layer from which an effective conductivity is calculated. Finally, the conduction through drainage layer is evaluated by knowing the temperature at the top of drainage layer, thermal conductivity, then temperature at the bottom of drainage layer can be estimated.

Conclusion

Previous green roof models and theories have dealt with radiation heat transfer in foliage layer, sensible heat gain or loss by convection between foliage and substrate layer, latent heat from evapotranspiration of vegetation and soil, and conduction through substrate into the room beneath. However, those theories share similar assumptions to simplify calculations and this results in some errors.

The assumption that vegetation is well irrigated requires that saturated thermal conductivity is used for a simulation. In reality, this is not so and the Sharp Front Theory presented in this paper offers an alternative approach by dividing the substrate layer into one saturated and one dry layer with appropriate thermal conductivities. By this means it is anticipated that green roof thermal models will be improved.

References

[1] Tabares-Velasco PC.(2009). Predictive heat and mass transfer model of plant-based roofing materials for assessment of energy savings: The Pennsylvania State University.

[2] Ascione F, Bianco N, de'Rossi F, Turni G, Vanoli GP.(2013). Green roofs in European climates. Are effective solutions for the energy savings in air-conditioning? Applied Energy. 104, 845-59.

[3] Newton J.(2007). Building Greener: Guidance on the Use of Green Roofs, Greens Walls and Complementary Features on Buildings. Construction Industry Research & Information Association (CIRIA).

[4] Sonne J.(2006). Evaluating Green Roof Energy Performance. ASHRAE Journal. 48, 59-61.

[5] Wong NH, Cheong DKW, Yan H, Soh J, Ong CL, Sia A.(2003). The effects of rooftop garden on energy consumption of a commercial building in Singapore. Energ Buildings. 35, 353-64.

[6] Balick LK, Scoggins RK, Link LE.(1981). Inclusion of a Simple Vegetation Layer in Terrain Temperature Models for Thermal IR Signature Prediction. Geoscience and Remote Sensing, IEEE Transactions on. GE-19, 143-52.

[7] Deardorff J.(1978). Efficient prediction of ground surface temperature and moisture, with inclusion of a layer of vegetation. J geophys Res. 83, 1889-903.

[8] Frankenstein S, Koenig G. (2004). FASST vegetation models. ENGINEER RESEARCH AND DEVELOPMENT CENTER HANOVER NH COLD REGIONS RESEARCH AND ENGINEERING LAB: DTIC Document; p.

[9] Sailor DJ.(2008). A green roof model for building energy simulation programs. Energ Buildings. 40, 1466-78.

[10] Nayak J, Srivastava A, Singh U, Sodha M.(1982). The relative performance of different approaches to the passive cooling of roofs. Building and Environment. 17, 145-61.

[11] Gaffin S, Rosenzweig C, Parshall L, Beattie D, Berghage R, O'Keefe G, et al. (2005). Energy balance modeling applied to a comparison of white and green roof cooling efficiency. Presentation at Greening Rooftops for Sustainable Communities. Third Annual International Conference.

[12] Gaffin S, Rosenzweig C, Parshall L, Hillel D, Eichenbaum-Pikser J, Greenbaum A, et al. (2006). Quantifying evaporative cooling from green roofs and comparison to other land surfaces. Fourth Annual Greening Rooftops for Sustainable Communities Conference, Awards and Trade Show11-2.

[13] He HM, Jim CY.(2010). Simulation of thermodynamic transmission in green roof ecosystem. Ecol Model. 221, 2949-58.

[14] Barrio EPD.(1998). Analysis of the green roofs cooling potential in buildings. Energ Buildings. 27, 179-93.

[15] Lazzarin RM, Castellotti F, Busato F.(2005). Experimental measurements and numerical modelling of a green roof. Energ Buildings. 37, 1260-7.

[16] Alexandri E, Jones P.(2007). Developing a one-dimensional heat and mass transfer algorithm for describing the effect of green roofs on the built environment: Comparison with experimental results. Building and Environment. 42, 2835-49.

[17] Farouki O.(1986). Thermal Properties of Soils (Series on Rock and Soil Mechanics vol 11)(Clausthal-Zellerfeld, Germany. Trans Tech Publications.

[18] Hall C, Hoff WD.(2009). Water transport in brick, stone and concrete. CRC PressI Llc.

[19] Dunnett N, Kingsbury N.(2004). Planting green roofs and living walls. Timber, Portland, OR [etc.].

[20] Philip JR.(1957). The theory of infiltration: 4. Sorptivity and algebraic infiltration equations. Soil science. 84, 257-64.

[21] Kaviany.(1991). Principles of heat transfer in porous media / by M. Kaviany. Springer, 1991.

[22] Nozad I, Carbonell R, Whitaker S.(1985). Heat conduction in multiphase systems—I: theory and experiment for two-phase systems. Chemical Engineering Science. 40, 843-55.

References

ALEXANDRI, E. & JONES, P. 2007. Developing a one-dimensional heat and mass transfer algorithm for describing the effect of green roofs on the built environment: Comparison with experimental results. *Building and Environment,* 42**,** 2835-2849.

ASCIONE, F., BIANCO, N., DE'ROSSI, F., TURNI, G. & VANOLI, G. P. 2013. Green roofs in European climates. Are they effective solutions for the energy savings in air-conditioning? *Applied Energy,* 104**,** 845-859.

BALICK, L. K., SCOGGINS, R. K. & LINK, L. E. 1981. Inclusion of a Simple Vegetation Layer in Terrain Temperature Models for Thermal IR Signature Prediction. *Geoscience and Remote Sensing, IEEE Transactions on,* GE-19**,** 143-152.

BARRIO, E. P. D. 1998. Analysis of the green roofs cooling potential in buildings. *Energy and Buildings,* 27**,** 179-193.

BIANCHINI, F. & HEWAGE, K. 2012. How "green" are the green roofs? Lifecycle analysis of green roof materials. *Building and Environment,* 48**,** 57-65.

BUCKINGHAM, E. 1907. *Studies on the movement of soil moisture,* Washington, Govt. Print. Off.

CASTLETON, H., STOVIN, V., BECK, S. & DAVISON, J. 2010. Green roofs; building energy savings and the potential for retrofit. *Energy and Buildings,* 42**,** 1582-1591.

CHAN, A. L. S. & CHOW, T. T. 2013. Evaluation of Overall Thermal Transfer Value (OTTV) for commercial buildings constructed with green roof. *Applied Energy,* 107**,** 10-24.

CHARTERED INSTITUTION OF BUILDING SERVICES, E. 2006. *Environmental design : CIBSE guide A,* London, CIBSE.

CHEN, F., MITCHELL, K., SCHAAKE, J., XUE, Y., PAN, H.-L., KOREN, V., DUAN, Q. Y., EK, M. & BETTS, A. 1996. Modeling of land surface evaporation by four schemes and comparison with FIFE observations. *Journal of Geophysical Research: Atmospheres,* 101**,** 7251-7268.

CONNELLY, M. & HODGSON, M. 2008. Sound transmission loss of green roofs. *Canadian Acoustics,* 36**,** 74-75.

CONNELLY, M. & HODGSON, M. 2015. Experimental investigation of the sound absorption characteristics of vegetated roofs. *Building and Environment,* 92**,** 335-346.

DEARDORFF, J. 1978. Efficient prediction of ground surface temperature and moisture, with inclusion of a layer of vegetation. *J. Geophys. Res,* 83**,** 1889-1903.

DECRUZ, A., KOKOGIANNAKIS, G., DARKWA, J., STRACHAN, P. & HONG, J. 2012. *A Theoretical Framework for The Integration of a Green Roof Model in ESP-r* [Online]. Available: http://www.ibpsa.org/proceedings/asim2012/0081.pdf.

DJEDJIG, R., OULDBOUKHITINE, S.-E., BELARBI, R. & BOZONNET, E. 2012. Development and validation of a coupled heat and mass transfer model for green roofs. *International Communications in Heat and Mass Transfer,* 39**,** 752-761.

DUNNETT, N. & KINGSBURY, N. 2004. *Planting green roofs and living walls,* Portland, OR, USA, Timber Press.

FENG, C., MENG, Q. & ZHANG, Y. 2010. Theoretical and experimental analysis of the energy balance of extensive green roofs. *Energy and Buildings,* 42**,** 959-965.

FRANKENSTEIN, S. & KOENIG, G. 2004a. FASST vegetation models. *Engineer research and development center handover nh cold regions research and engineering lab.*: DTIC Document.

FRANKENSTEIN, S. & KOENIG, G. G. 2004b. Fast all-season soil strength (FASST). *Engineer research and development center handover nh cold regions research and engineering lab.*: DTIC Document.

GAFFIN, S., ROSENZWEIG, C., PARSHALL, L., BEATTIE, D., BERGHAGE, R., O'KEEFFE, G. & BRAMAN, D. Energy balance modeling applied to a comparison of white and green roof cooling efficiency. Proceedings of the 3rd Annual Greening Rooftops for Sustainable Cities Conference, May 4-6 2005 Washington, DC.

GETTER, K. L. & ROWE, D. B. 2006. The role of extensive green roofs in sustainable development. *HortScience,* 41**,** 1276-1285.

GRANT, G. 2006. Extensive green roofs in London. *Urban Habitats,* 4**,** 51-65.

GRANT, G., ENGLEBACK, L., NICHOLSON, B., GEDGE, D., FRITH, M. & HARVEY, P. 2003. Green roofs: their existing status and potential for conserving biodiversity in urban areas. *English Nature Reports.* Northminster House, Peterborough: English Nature.

GRO 2011. The GRO Green Roof Code: Green Roof Code for Best Practice for the UK 2011. *Groundwork, Sheffield, UK*.

HALL, C. & HOFF, W. D. 2009. *Water transport in brick, stone and concrete,* CRC PressI Llc.

HALL, C., HOFF, W. D. & NIXON, M. R. 1984. Water movement in porous building materials—VI. Evaporation and drying in brick and block materials. *Building and Environment,* 19**,** 13-20.

HE, H. M. & JIM, C. Y. 2010. Simulation of thermodynamic transmission in green roof ecosystem. *Ecological Modelling,* 221**,** 2949-2958.

HO, D. W. S. & LEWIS, R. K. 1984. Concrete quality as measured by water sorptivity. *Institution of Engineers (Australia) Civ Eng Trans,* CE 26**,** 306-313.

HUI, S. C. & CHAN, H.-M. Development of modular green roofs for high-density urban cities. World Green Roof Congress, 17–18 September 2008 London.

JIM, C. Y. & TSANG, S. W. 2011. Modeling the heat diffusion process in the abiotic layers of green roofs. *Energy and Buildings,* 43**,** 1341-1350.

JOHNSTON, J. & NEWTON, J. 2004. *Building Green, A guide to using plants on roofs, walls and pavements,* London, Greater London Authority.

KAVIANY 1991. *Principles of heat transfer in porous media*, Springer, 1991.

KNAPPETT J & CRAIG R.F 2012. *Craig's soil mechanics*, Spon, 8th ed.

KÖHLER, M. 2006. Long-term vegetation research on two extensive green roofs in Berlin. *Urban Habitats,* 4**,** 3-26.

KOTSIRIS, G., ANDROUTSOPOULOS, A., POLYCHRONI, E. & NEKTARIOS, P. A. 2012. Dynamic U-value estimation and energy simulation for green roofs. *Energy and Buildings,* 45**,** 240-249.

LAZZARIN, R. M., CASTELLOTTI, F. & BUSATO, F. 2005. Experimental measurements and numerical modelling of a green roof. *Energy and Buildings,* 37**,** 1260-1267.

LIU, K. & MINOR, J. 2005. Performance evaluation of an extensive green roof. *Presentation at Green Rooftops for Sustainable Communities, Washington DC***,** 1-11.

NEWTON, J., GEDGE, D., EARLY, P. & WILSON, S. 2007. *Building Greener: Guidance on the Use of Green Roofs, Greens Walls and Complementary Features on Buildings,* Construction Industry Research & Information Association (CIRIA).

NOZAD, I., CARBONELL, R. & WHITAKER, S. 1985. Heat conduction in multiphase systems—I: theory and experiment for two-phase systems. *Chemical Engineering Science,* 40**,** 843-855.

OBERNDORFER, E., LUNDHOLM, J., BASS, B., COFFMAN, R. R., DOSHI, H., DUNNETT, N., GAFFIN, S., KÖHLER, M., LIU, K. K. Y. & ROWE, B. 2007. Green Roofs as Urban Ecosystems: Ecological Structures, Functions, and Services. *BioScience,* 57**,** 823-833.

OLDHAM, D. J., EGAN, C. A. & COOKSON, R. D. 2011. Sustainable acoustic absorbers from the biomass. *Applied Acoustics,* 72**,** 350-363.

OSMUNDSON, T. 1999. *Roof gardens: history, design, and construction,* New York, WW Norton & Company.

OULDBOUKHITINE, S.-E., BELARBI, R. & DJEDJIG, R. 2012. Characterization of green roof components: Measurements of thermal and hydrological properties. *Building and Environment,* 56**,** 78-85.

PECK, S. W. & KUHN, M. 2003. *Design guidelines for green roofs,* Ontario Association of Architects.

PHILIP, J. R. 1957. The theory of infiltration: 4. Sorptivity and algebraic infiltration equations. *Soil science,* 84**,** 257-264.

PITTALUGA, I., SCHENONE, C. & BORELLI, D. Sound absorption of different green roof systems. Proceedings of Meetings on Acoustics, 2012. 015005.

PLATTEN, A. K. 1985. *A study of evaporation and drying in porous building materials (PhD thesis).* University of Manchester Institute of Science and Technology (UMIST).

POË, S., STOVIN, V. & DUNSIGER, Z. The Impact of Green Roof Configuration on Hydrological Performance. 12th Int. Conf on Urban Drainage, 2011.

RAMÍREZ, J. A. & SENARATH, S. U. 2000. A statistical-dynamical parameterization of interception and land surface-atmosphere interactions. *Journal of climate,* 13**,** 4050-4063.

SAILOR, D. J. 2008. A green roof model for building energy simulation programs. *Energy and Buildings,* 40**,** 1466-1478.

SAILOR, D. J. & HAGOS, M. 2011. An updated and expanded set of thermal property data for green roof growing media. *Energy and Buildings,* 43**,** 2298-2303.

SAILOR, D. J., HUTCHINSON, D. & BOKOVOY, L. 2008. Thermal property measurements for ecoroof soils common in the western U.S. *Energy and Buildings,* 40**,** 1246-1251.

SANTAMOURIS, M. 2014. Cooling the cities – A review of reflective and green roof mitigation technologies to fight heat island and improve comfort in urban environments. *Solar Energy,* 103**,** 682-703.

SCHOLZ-BARTH, K. & TANNER, S. 2004. Green roofs: federal energy management (FEMP) federal technology alert. Washington: U. S. DOE.

SCOTTISH_BUILDING 2016a. Domestic Handbook 2016 Complete.

SCOTTISH_BUILDING 2016b. Non-Domestic Handbook 2016 Complete.

SENNETT, A. R. 1905. *Garden cities in theory and practice,* London, Bemrose and Sons.

SKELLAND, A. H. P. 1974. *Diffusional mass transfer [by] A. H. P. Skelland,* New York, Wiley.

SONNE, J. 2006. Evaluating Green Roof Energy Performance. *ASHRAE Journal,* 48**,** 59-61.

SUN, T., BOU-ZEID, E., WANG, Z.-H., ZERBA, E. & NI, G.-H. 2013. Hydrometeorological determinants of green roof performance via a vertically-resolved model for heat and water transport. *Building and Environment,* 60**,** 211-224.

TABARES-VELASCO, P. C. 2009. *Predictive heat and mass transfer model of plant-based roofing materials for assessment of energy savings.* Doctor of Philosophy, Pennsylvania State University.

TABARES-VELASCO, P. C. & SREBRIC, J. 2012. A heat transfer model for assessment of plant based roofing systems in summer conditions. *Building and Environment,* 49**,** 310-323.

TANNER, S. & SCHOLZ-BARTH, K. 2004. Green Roofs. Federal Technology Alert DOE/EE-0298. Federal Energy Management Program (FEMP), US Department of Energy.

WARK, C. G. & WARK, W. W. 2003. Green roof specifications and standards Establishing an Emerging Technology. *The Construction Specifier,* 56**,** 76-82.

WONG, N. H., CHEONG, D. K. W., YAN, H., SOH, J., ONG, C. L. & SIA, A. 2003. The effects of rooftop garden on energy consumption of a commercial building in Singapore. *Energy and Buildings,* 35**,** 353-364.

WONG, N. H., KWANG TAN, A. Y., TAN, P. Y., CHIANG, K. & WONG, N. C. 2010. Acoustics evaluation of vertical greenery systems for building walls. *Building and Environment,* 45**,** 411-420.

YANG, H. S., KANG, J. & CHOI, M. S. 2012. Acoustic effects of green roof systems on a low-profiled structure at street level. *Building and Environment,* 50**,** 44-55.

YANG, Z.-L., DICKINSON, R. E., SHUTTLEWORTH, W. J. & SHAIKH, M. 1998. Treatment of soil, vegetation and snow in land surface models: a test of the Biosphere–Atmosphere Transfer Scheme with the HAPEX-MOBILHY, ABRACOS and Russian data. *Journal of Hydrology,* 212–213**,** 109-127.